Investigating the Relationship between Chinese Hamster Ovary Cellular Stress Responses, Culture Harvest Day and Formulated mAb Stability

Natalie Elizabeth Talbot

Supervisor: Professor Mark Smales

This thesis is submitted to the University of Kent for the degree of Doctor of Philosophy

2019

Declaration

I hereby declare that no part of this thesis has been submitted in support of an application for any degree or other qualification of the University of Kent, or any other university or institution of learning. I declare that the contents of this dissertation are original, and consist of my own work, along with collaborators who have been specified in the text.

Natalie Talbot August 2019

Abstract

Establishing an appropriate formulation is a crucial step in development of therapeutic monoclonal antibodies (mAbs). The drug product formulation is designed to minimise formation of product instabilities including sub-visible particles (SVPs), aggregates and fragments, and impacts the mode of delivery, dosage, drug format, storage conditions and expiration date. The production of a mAb using Chinese hamster ovary (CHO) cells can be considered as a three phase process; upstream cell culture, downstream purification and formulation/fill-finish activities. Throughout each phase, a therapeutic mAb may be exposed to many stresses, both intracellular during the synthesis of the protein, and extracellular; including pH changes, shear stresses, temperature and concentration changes, all of which can impact on the molecule's susceptibility to aggregation and SVP formation. Specifically, during culture, cells can be placed under increased endoplasmic reticulum (ER) and oxidative stresses due to cell culture conditions and recombinant protein loads on the cell, which may result in compromised mAb yield and quality. Although much work has been undertaken to investigate how such intracellular stresses impact mAb titres and quality, there are no published studies investigating how cellular stresses change across culture and how such stress may impact formulated mAb stability. The work presented in this thesis explores the relationship between intracellular stress, cell culture processes, culture harvest day and formulated mAb stability of three model therapeutic mAbs (denoted 109, 4212 and 184) by profiling ER stress throughout culture at the transcript and protein level, and by comparing the stability profile of purified mAb material from an 'early' and 'late' harvest of 400 mL roller bottle cultures (day 9 and 13 respectively) and 10 L disposable bioreactors (days 8 and 13 respectively). Furthermore, the use of ER and oxidative stress reporter constructs to monitor these stresses in real time during mAb production was also investigated.

Overall, harvest day was shown to impact mAb stability, as assessed by the propensity of formulated material to form SVPs. Interestingly, the intracellular ratio of mAb heavy chain (HC) to light chain (LC) mRNA also impacted on the stability of harvested mAb material from 400 mL cultures when formulated in different buffer compositions. Furthermore, studies on mAb material generated using 400 mL roller bottle cultures also showed inherent molecular differences between cell lines cultured under fed-batch and batch conditions, where cell lines 4212 and 184 displayed similar titre, growth and biomarker profiles under batch culture; but under fed-batch behaved differently. Stability studies of both 400 mL roller bottle and 10 L disposable bioreactor material showed a cell line and/or mAb and/or culture process specific relationship between harvest day and SVP formation. Formulated 4212 mAb material harvested on day 9 of roller bottle culture produced fewer SVPs than that from day 13 indicating a relationship between day of harvest and mAb stability, whereas mAb 184 showed no harvest day trend. When cultured in 10 L disposable bioreactors, however, cell line/mAb 184 showed a strong harvest day trend, with mAb 184 material from day 8 of culture producing fewer SVPs and appearing more opalescent than that from day 13. Furthermore, CD spectroscopy highlighted conformational differences between mAb 184 material from the two harvest days, with RNAseq revealing differences between cellular transcript profiles on days 6, 8 and 13 of culture for cell line 184. Finally, reporter constructs to monitor ER and oxidative stress during fed-batch culture showed varying levels of sensitivity. During validation studies, the ER stress response element (ERSE) proved unresponsive to chemical induction of ER stress, however, the antioxidant response element (ARE) responded to chemically induced oxidative stress across a range of drug concentrations, however there was insufficient oxidative stress perceived by cells during culture to activate the reporter during mAb synthesis. Collectively the data presented in this thesis provides novel insights into the impact of bioprocessing on formulated mAb stability, and shows how harvest day can impact on the stability of formulated mAbs and demonstrates that the relationship between upstream cell culture and the stability of an expressed therapeutic is complex and dynamic.

Acknowledgements

Firstly, I would like to thank Professor Mark Smales for his help and guidance throughout this project; and for taking the time to painstakingly proof read this thesis! Thanks also to Dr Stephanie Davies and Mr Shahid Uddin for their supervision; to the BBSRC for funding this project and to AstraZeneca and the University of Kent for hosting me.

I would like say a huge thank you to Gary Pettman and Emma Tyzack for their help with disposable bioreactor culturing. Trips to AstraZeneca were not always enjoyable, however working with Gary's team offered me a confidence boost during a challenging time, and I will always be very grateful for their help with a particularly intense workload. I would also like to say a huge thank you to Karen Dickson, Aled Charles, Faisal Uddin, Niel Birkett and Silvia Cicerano for all of their help with purification and buffer exchange of my material; but more-so for always being approachable and for giving me their time even when snowed under with their own work.

I would like to thank Dr Wei-feng, Mr Ian Brown, Mr Kevin Howland, Dr Emma Hargreaves, Dr Tanya Knight, Dr James Budge, Dr Anne Roobol, Sarah 'Smash' Martin, J Roobs and Dr Davide Vito at the University of Kent for their help with AFM, CD spectroscopy, RNA work, FACS, cloning and RNA-seq analysis. This work would not have been possible without their assistance, time and patience. I am also grateful for the help, support and friendship from all members of the Smales lab and School of Biosciences – past and present. I would especially like to thank Sarah 'Smash' Martin, Andy Martin (not for his puns though), Dr Emilie De La Nougerede, Dr Cat Hogwood, Dr Emma Hargreaves, J Roobs, Dr Jane Povey, Dr Charlotte Godfrey, Dr Aline Guimaraes and Dr Alex Brown - thank you for always checking in on me during my time away and for injecting some fun into the PhD experience! I would also like to say a special thank you to Eva Pekle for always being a friendly face during my trips to Cambridge - thank you for your friendship and, most importantly, for the regular gossip updates.

I would also like to thank all of the lovely people in the BBSRC Communications and Engagement team, who I worked with during a 6-week internship. Thank you for showing me that life exists outside of the Kent/AstraZeneca bubble, and for giving me the experience and confidence to pursue an alternative career.

I would like to say a huge thank you to my family - Mark, Manuela and Emily - for their unconditional love and support. Thank you for putting up with my moaning and for helping to push me through the past four years... you will probably be even more relieved than I am when this is all done!

I would also like to thank Jane and David Lee for having me to stay during my trips to Cambridge. Thank you for welcoming me into your family and for giving me a home away from home - especially when rescuing me from that landlord who accused me of moving all of the locks onto different doors.

My biggest thank you however, has to go to Dr Matthew Lee. Without your love, care, patience, support and encouragement I would have quit this PhD within my first year (then the second, third and fourth…). Thank you for pushing me to see this through, for surprising me during the never-ending stays in Cambridge and for helping me to grow as a person, and as a scientist. Thank you for believing in me and for listening to the twists and turns of this project over and over again. You have effectively been my own personal cheerleader throughout this PhD and I will be forever grateful for that.

In a truly millennial fashion, I would also like to thank myself. This PhD has been challenging in ways I never expected, and has pushed me beyond my limits both mentally and physically. From this experience, however, I take forward with me a new found sense of self-worth, determination and resilience.

Finally, I would like to acknowledge Beyoncé for providing the soundtrack to this PhD, Travelodge for providing just about adequate accommodation, and Nandos for fueling the majority of my work in Cambridge.

This thesis is dedicated to Milo
2005 - 2018

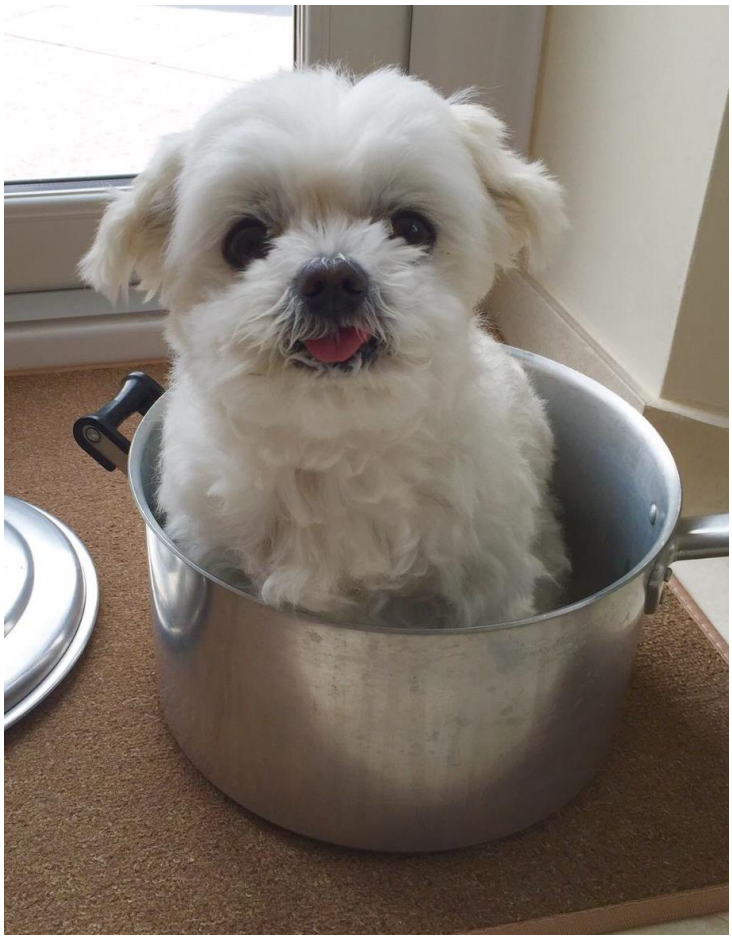

Contents

Abstract ii

Acknowledgements iii

List of Figures xiii

List of Tables xviii

Abbreviations xx

Chapter 1 Introduction 1

1.1 The Biotherapeutic Market and Challenges in mAb Development 2

1.2 Structure and Function of Antibodies 3

1.3 Cell Line Development for mAb Production 5

1.4 Industrial Production of Monoclonal Antibodies 8

1.4.1 Upstream Cell Culture 9

1.4.1.1 Cellular Stress During Over-Grow Culture 9

1.4.1.1.1 Nutrient Deprivation 9

1.4.1.1.2 Oxidative Stress 10

1.4.1.1.3 Endoplasmic Reticulum Stress 10

1.4.1.1.3.1 The Unfolded Protein Response 11

1.4.1.1.3.2 Endoplasmic Reticulum Associated Degradation 12

1.4.2 Downstream Purification of Recombinant mAbs from Cell Culture Harvests 13

1.4.3 Formulation Development and Fill Finish Activities 14

1.4.4 Degradation of mAbs 15

1.4.4.1 Mechanisms of Aggregation 15

1.4.4.1.1 Sub-Visible Particle Formation 17

1.4.4.2 Visual Appearance 17

1.4.4.2.1 Opalescence and Phase Separation 18

1.5 Assessing mAb Stability 19

1.5.1 Official Guidelines on Product Stability 19

1.5.2 Methods to Assess mAb Stability 20

1.5.2.1 Visual Inspection 21
1.5.2.2 Assessing Aggregation 22
1.5.2.2.1 Light Obscuration Methods 22
1.5.2.2.2 Flow Microscopy 22
1.5.2.2.3 Size Exclusion High Performance Liquid Chromatography 22

1.6 Excipients for Biotherapeutic Protein Formulation 23
1.6.1.1 Buffering Agents; Histidine 24
1.6.1.2 Stabilisers; Arginine and Sucrose 25

1.7 The Impact of Bioprocessing on Formulated mAb Stability 25

1.8 Aims of this Project 26

Chapter 2 Materials and Methods 28

2.1 Generation of Monoclonal Antibody Material 29
2.1.1 Roller Bottle Culture 29
2.1.1.1 Cell Lines and Maintenance 29
2.1.1.2 Over-Grow Cultures 29
2.1.1.3 Harvesting of Material 29
2.1.2 10L Disposable Bioreactor Culture 30
2.1.2.1 Cell Lines and Maintenance 30
2.1.2.2 Over-Grow Culturing 30
2.1.2.3 Harvesting of Cell Culture Material 30
2.1.3 Sampling 31
2.1.3.1 Cell Concentration and Culture Viability 31
2.1.3.2 Cell Pellet and Supernatant Collection 31
2.1.3.3 Titre Determination 31
2.1.3.4 Metabolite Analysis (10 L Bioreactor Only) 31

2.2 Purification of mAb Material from Harvested Supernatant 32
2.2.1 Protein A Purification 32
2.2.2 pH Adjustment of Eluates 32

2.3 Buffer Exchange 32
2.3.1 Roller bottle Material 32
2.3.2 10 L Disposable Bioreactor Material 32

2.4 Vial Filling 33

2.5 Stability Study Outline: Buffers and Time-Points 33
2.5.1 Roller Bottle Material 33
2.5.2 10 L Disposable Bioreactor Material 33

2.6 mAb Stability Analysis 34
2.6.1 Visual Inspection 34
2.6.2 Analysis of Soluble Aggregates and Monomeric Species 34
2.6.2.1 Size Exclusion HPLC 34
2.6.2.2 Sample Preparation and Standards 34
2.6.2.2.1 Data Analysis 35
2.6.3 Analysis of Sub-Visible Particle Formation 35
2.6.3.1 Micro-Flow Imaging 35
2.6.3.2 Data Analysis 35

2.7 Atomic Force Microscopy 35
2.7.1 Preparation of Samples 35
2.7.2 Image Acquisition Parameters and Processing 36

2.8 Intracellular Protein Analysis 36
2.8.1 Cell Lysis 36
2.8.2 Lysate Preparation for SDS-PAGE Analysis 37
2.8.3 SDS-PAGE Gel Composition and Running Conditions 37
2.8.4 Coomassie Staining of SDS-PAGE Gels 38
2.8.5 Western Blotting 38
2.8.5.1 Densitometry Analysis 39

2.9 Gene Expression Analysis 40
2.9.1 RNA Extraction and DNAse Treatment 40
2.9.2 qRT-PCR Analysis 40
2.9.3 Generation of Standard Curves for Relative HC and LC Copy Number Analysis 43
2.9.4 Data Analysis 43
2.9.4.1 $\Delta\Delta C_t$ and Fold Change Calculation 43
2.9.4.2 Linear Regression Analysis 45
2.9.4.3 Establishing Relative HC and LC Copy Number per Cell 45
2.9.5 RNA Sequencing 45
2.9.5.1 RNA Sequencing Quality Check and Gene Assignment 45
2.9.5.2 Differential Expression Analysis and Pathway Enrichment 45

2.10 Molecular Biology Techniques to Create Stress Reporter Constructs 45
2.10.1 Preparation of Calcium Competent DH5α Cells 46

2.10.2 Transformation of DNA into Competent DH5α Cells 46
2.10.3 Purification of Plasmid DNA 46
2.10.4 Amplification of Target Sequences using Polymerase Chain Reaction 47
2.10.5 Agarose Gel Electrophoresis 47
2.10.5.1 Purification of DNA from Agarose Gels 47
2.10.6 Restriction Digest of DNA 47
2.10.7 Dephosphorylation of DNA 48
2.10.8 DNA Ligation 48
2.10.9 Primer and Oligonucleotide Design 48
2.10.10 Oligonucleotide Phosphorylation and Annealing 49

2.11 Utilising Stress Reporter Constructs 49
2.11.1 Initial Stress Reporter Construct Testing 49
2.11.1.1 Transient Transfection of CHO-S Cells using Electroporation 50
2.11.1.2 Initial Reporter Construct Testing using Tunicamycin and t-BHQ 50
2.11.1.3 Flow Cytometry Analysis of Transfected Samples 50
2.11.2 Utilising Stress Reporter Constructs During Fed-Batch Overgrow Culture 50
2.11.2.1 Transient Transfection of mAb Producing CHO Cell Lines Using PEI 51
2.11.2.2 Flow Cytometry Analysis of Transfected Samples 51

2.12 Assessing Oxidative Stress During Fed-Batch Overgrow Culture Using a Commercial Cell Staining Kit 51

2.13 Sample and Buffer Labelling Throughout this Thesis 52

Chapter 3 Application of ER Stress Biomarkers to Predict Formulated Monoclonal Antibody Stability 53

3.1 Declaration of Contribution 54

3.2 Abstract 54

3.3 Introduction 54

3.4 Materials and Methods 56
3.4.1 Cell Culture 56
3.4.2 Determination of Monoclonal Antibody Concentrations 57
3.4.3 Sampling of Cells for mRNA and Protein Analysis 57
3.4.4 Purification of Monoclonal Antibody from Cell Culture Supernatant 57
3.4.5 Formulation of Protein A Purified mAb Material 57

3.4.6 Sub-Visible Particle Counting 58
3.4.7 Analysis of Aggregate, Fragment and Monomeric Species 58
3.4.8 Total RNA Extraction and DNAse Treatment 58
3.4.9 mRNA Expression Analysis by qRT-PCR 58
3.4.10 Western Blotting to Determine Intracellular HC and LC Protein Expression 59

3.5 Results 59
3.5.1 Analysis of mAb Producing CHO Cell Line Growth and Productivity Characteristics 60
3.5.2 Profiling of ER Stress mRNA Transcript Biomarkers 62
3.5.3 Analysis of mAb Heavy and Light Chain Expression at the Transcript and Protein Level 64
3.5.4 Effect of Harvest Day during Fed-Batch Culture on Monoclonal Antibody Stability 66

3.6 Discussion 68

3.7 Acknowledgements: 71

3.8 Supplementary Tables and Figures 71
3.8.1 Limitations 75

Chapter 4 Investigating the Relationship Between Culture Harvest Day, ER Stress and Formulated mAb Stability in 10 L Disposable Bioreactors 76

4.1 Introduction 78

4.2 Aims of this Chapter 78

4.3 Growth Profiles and Productivity of Cell Lines Cultured in 10 L Disposable Bioreactors Under Fed-Batch Conditions 78
4.3.1 Growth and Productivity of Cell Line 109 79
4.3.2 Growth and Productivity of Cell Line 4212 80
4.3.3 Growth and Productivity of Cell Line 184 82

4.4 Extracellular Metabolite Analysis of 10 L Disposable Bioreactors Under Fed-Batch Conditions 84
4.4.1 Cell Line 109 Metabolite Profiles 84
4.4.2 Cell Line 4212 Metabolite Profiles 86
4.4.3 Cell Line 184 Metabolite Profiles 88

4.5 mRNA Biomarker Profling 90

4.6 Western Blot Analysis for Markers of ER Stress 91

4.6.1 Western Blot Analysis of eIf2α and eEF2 Expression Throughout Fed-Batch Culture of Cell Line 109 91
4.6.2 Western Blot Analysis of eIf2α and eEF2 Expression Throughout Fed-Batch Culture of Cell Line 4212 92
4.6.3 Western Blot Analysis of eIf2α and eEF2 Expression Throughout Fed-Batch Culture of Cell Line 184 93

4.7 Intracellular Heavy Chain and Light Chain mRNA and Polypeptide Expression Throughout Culture..... 94
4.7.1 Heavy Chain and Light Chain mRNA and Polypeptide Analysis for Cell Line 109 94
4.7.2 Heavy Chain and Light Chain mRNA and Polypeptide Analysis for Cell Line 4212 97
4.7.3 Heavy Chain and Light Chain mRNA and Polypeptide Analysis for Cell Line 184 99

4.8 Stability of Purified mAbs from Different Harvest Days of 10L Disposable Bioreactor Cultures 101
4.8.1 Stability of mAb 109 Material from Day 8 and Day 13 Harvests Under Accelerated Stability Conditions at 40°C 101
4.8.2 Stability of mAb 4212 Material from Day 8 and Day 13 Harvests Under Accelerated Stability Conditions at 40°C 105
4.8.3 Stability of mAb 184 Material from Day 8 and Day 13 Harvests Under Accelerated Stability Conditions at 40°C 111
4.8.4 SEC-HPLC Analysis of all mAbs 115

4.9 Analysis of Aggregate and Particle Formation in mAb Samples using Atomic Force Microscopy 116

4.10 Conformation Characterisation of Formulated mAb Samples using Near-UV CD Spectroscopy 119
4.10.1 Near-UV CD Spectroscopy Analysis of mAb 109 Samples 119
4.10.2 Near-UV CD Spectroscopy Analysis of mAb 4212 Samples 121
4.10.3 Near-UV CD Spectroscopy Analysis of mAb 184 Samples 124

4.11 Summary of Results and Discussion 126
4.11.1 Limitations 131

Chapter 5 Mapping the Cellular Response of Cell Line 184 Throughout Culture and Between Harvest days using RNA Sequencing..... 133

5.1 Introduction 134
5.1.1 Aims of this Chapter 135

5.2 Quality Assessment of RNA Sequencing Data 135

5.3 Comparison of RNASeq Gene Expression Between Sample Days and Biological Replicates of Cell Line 184 Samples 137

5.4 Differential Gene Expression Analysis 139

5.5 Pathway Enrichment Analysis 142

5.5.1 KEGG Pathway Enrichment 142

5.5.2 GO Pathway Enrichment 144

5.6 Validation of RNA Sequencing Data by qRT-PCR 145

5.7 Comparison of RNASeq Analysis to the Original Panel of Genes Relating to ER Stress Response Pathways Analysed by qRT-PCR 148

5.8 Discussion 150

5.8.1 Limitations 153

Chapter 6 Investigating the Use of Stress Reporter Constructs to Assess ER and Oxidative Stresses During Fed-Batch Culture of CHO Cells 155

6.1 Introduction 156

6.1.1 Aims of this Chapter 156

6.1.2 Basic Design and Principle of Stress Reporter Constructs 157

6.1.2.1 The ER Stress Response Element (ERSE) 157

6.1.2.2 The Antioxidant Response Element (ARE) 158

6.2 Construction of Stress Reporter Constructs 159

6.3 Initial Validation of Reporter Gene Constructs 165

6.3.1 Validation of the ERSE-SV40 and ERSE-TATA Reporter Constructs 165

6.3.2 Validation of the ARE-SV40 and ARE-TATA Reporter Constructs 168

6.4 Application of the ARE-TATA Oxidative Stress Responsive Reporter Construct in Fed-Batch Over-Grow Culture 171

6.4.1 Cell Growth and Productivity Characteristics of the Cell Lines during Fed-Batch Culture 171

6.4.1.1 Cell Line 109 171

6.4.1.2 Cell Line AB001 173

6.4.1.3 Cell Lines 2223 and 2491 175

6.4.2 Comparing Oxidative Stress Responses Between Culture Time Points and Cell Lines Using the ARE-TATA GFP Stress Reporter Construct 179
6.4.3 Comparing Oxidative Stress Responses Between Culture Time Points and Cell Lines Using a Commercial Cell Staining Kit 187

6.5 Discussion 190
6.5.1 Limitations 193

Chapter 7 Discussion 195

7.1 Overall Discussion 196

7.2 Future Work 201

7.3 Conclusions 203

References 205

Appendix A 215

Appendix B 230

List of Figures

Figure 1.1: Simplified general structure of an IgG molecule depicting heavy and light chains (HC/LC), variable (V) and constant (C) domains, and the Fab and Fc regions.

Figure 1.2: Comparison of the hinge region between IgG subclasses, depicting the number of disulphide bonds and amino acids.

Figure 1.3: Schematic outlining the stages of typical therapeutic mAb production.

Figure 1.4: Schematic depicting the activation of PERK, ATF6 and IRE1 pathways within the unfolded protein response.

Figure 1.5: Example of (A) opalescence and (B) liquid-liquid phase separation of a mAb.

Figure 1.6: Schematic showing the size range detection of analytical techniques routinely used for the quantification of aggregates in biotherapeutics.

Figure 1.7: Example SEC-HPLC Chromatogram.

Figure 2.1: 'Sandwich' assembly for wet transfer of proteins from a SDS gel to nitrocellulose membrane.

Figure 2.2: Equation used to establish plasmid copy number.

Figure 2.3: Equation used to establish relative difference in transcript expression per cell.

Figure 2.4: Thermocycler Parameters for Three-step PCR Amplification of Target DNA.

Figure 3.1. Growth Characteristics of Cell Lines Under Fed-Batch and Batch Conditions.

Figure 3.2. HC and LC Transcript Copy Numbers Produced in Cells Under Fed-batch and Batch Conditions.

Figure 3.3. Intracellular HC and LC Polypeptide Expression.

Figure 3.4. Sub-Visible Particle Formation of Formulated mAb Determined by MFI Analysis.

Supplementary Figure 3.1: Linear Regression Analysis of qRT-PCR Data to Assess the Statistical Significance ($P<0.05$) of the Relationship Between Day of Culture and Fold Change in Expression for Each Gene of Interest for (A) Cell line A and (B) Cell Line B.

Supplementary Figure 3.2: Fold Change in Expression of (A) *bip,* (B), *hsp90b,* and (C) *derl3* Genes Under Fed-Batch Conditions Relative to Day 3 Expression, Determined Using qRT-PCR.

Supplementary Figure 3.3: Coomassie Stained SDS-PAGE Gels for Cell Lysate Samples Collected from (A) Cell Line A and (B) Cell Line B.

Figure 4.1: Viable cell concentration (VCC) per mL of culture, and the percentage of cells that were viable (culture viability) on each day of culture for cultures 109A, 109B and 109C grown in 10 L disposable wave bag bioreactors.

Figure 4.2: Viable cell concentration (VCC) per mL of culture, and the percentage of cells that were viable (culture viability) on each day of culture for cultures 4212A, 4212B and 4212C grown in 10 L disposable wave bag bioreactors.

Figure 4.3: Viable cell concentration (VCC) per mL of culture, and the percentage of cells that were viable (culture viability) on each day of culture for cultures 184A and 184B grown in 10 L disposable wave bag bioreactors.

Figure 4.4: Offline metabolite data for 10 L wave bag cultures 109A, 109B and 109C collected using a BioProfile Flex

Figure 4.5: Online dissolved oxygen (DO) and pH readings for cultures 109A, 109B and 109C collected throughout culture using probes within the 10 L WAVE25 system.

Figure 4.6: Offline metabolite data for 10 L wave bag cultures 4212A, 4212B and 4212C collected using a BioProfile Flex.

Figure 4.7: Online dissolved oxygen (DO) and pH readings for cultures 4212A, 4212B and 4212C collected throughout culture using probes within the 10 L WAVE25 system.

Figure 4.8: Offline metabolite data for 10 L wave bag cultures 184A and 184B collected using a BioProfile Flex.

Figure 4.9: Online dissolved oxygen (DO) and pH readings for cultures 4212A, 4212B and 4212C collected throughout culture using probes within the 10 L WAVE25 system.

Figure 4.10: Western blot analysis of total eEF2, eEF2-P, total eIF2α and eIF2α-P intracellular expression in cell lysates from cultures 109A, 109B and 109C.

Figure 4.11: Western blot analysis of total eEF2, eEF2-P, total eIF2α and eIF2α-P intracellular expression in cell lysates from cultures 4212A, 4212B and 4212C

Figure 4.12: Western blot analysis of total eEF2, eEF2-P, total eIF2α and eIF2α-P intracellular expression in cell lysates from cultures 184A and 184B.

Figure 4.13: Relative HC and LC mRNA transcript copy number per cell for cultures 109A, 109B and 109C.

Figure 4.14: Intracellular HC (upper panel), LC (middle panel) and beta actin (lower panel) polypeptide expression in cultures 109A, 109B and 109C.

Figure 4.15: Relative HC and LC mRNA transcript copy number per cell for cultures 4212A, 4212B and 4212C.

Figure 4.16: Intracellular HC (upper panel), LC (middle panel) and beta actin (lower panel) polypeptide expression in cultures 4212A, 4212B and 4212C.

Figure 4.17: Relative HC and LC mRNA transcript copy number per cell for cultures 184A and 184B

Figure 4.18: Intracellular HC (upper panel), LC (middle panel) and beta actin (lower panel) expression in cultures 184A and 184B

Figure 4.19: Analysis of SVP count per mL of mAb 109 material harvested at day 8 and day 13 from cultures 109A, 109B and 109C formulated in (A) 80 mM arginine-HCl, 120 mM sucrose and 20 mM histidine or (B) 190 mM arginine-HCl and 20 mM histidine.

Figure 4.20: Images of mAb 109 material on white and black backgrounds after incubation at 40oC for 3 months.

Figure 4.21: Analysis of SVP numbers per mL of mAb 4212 material and visual inspection of material harvested on day 8 and day 13 from cultures 4212A, 4212B and 4212C formulated in 80 mM arginine-HCl, 120 mM sucrose and 20 mM histidine.

Figure 4.22: Analysis of SVP numbers per mL of mAb 4212 material and visual inspection of material harvested on day 8 and day 13 from cultures 4212A, 4212B and 4212C formulated in 190 mM arginine-HCl and 20 mM histidine.

Figure 4.23A and 4.23B: Visual inspection and SVP count per mL of (A) mAB 184A and (B) mAb 184B material harvested at day 8 and day 13 of culture formulated in 80 mM arginine-HCl, 120 mM sucrose and 20 mM histidine.

Figure 4.24A and 4.24B: Visual inspection and SVP count per mL of (A) mAB 184A and (B) mAb 184B material harvested at day 8 and day 13 of culture formulated in 190 mM arginine-HCl and 20 mM histidine.

Figure 4.25: AFM analysis of mAb 4212 material from samples formulated in 80 mM arginine-HCl, 120 mM sucrose and 20 mM histidine at T=0

Figure 4.26: AFM analysis of mAb 4212 material from samples formulated in 80 mM arginine-HCl, 120 mM sucrose and 20 mM histidine and incubated at 40oC for 3 months.

Figure 4.27: Near-UV CD spectra of mAb 109 samples harvested on day 8 and day 13 of 109A (A), 109B (B) and 109C (C) cultures, formulated in 80 mM arginine-HCl, 120 mM sucrose and 20 mM histidine at T=0 and after incubation at 40oC for 3 months

Figure 4.28: Near-UV CD spectra of mAb 109 samples harvested on day 8 and day 13 of 109A (A), 109B (B) and 109C (C) cultures formulated in 190 mM arginine-HCl and 20 mM histidine, at T=0 and after incubation at 40oC for 3 months.

Figure 4.29A, 4.29B and 4.29C: Near-UV CD spectra of mAb 4212 samples harvested on day 8 and day 13 of 4212A (A), 4212B (B) and 4212C (C) cultures, formulated in 80 mM arginine-HCl, 120 mM sucrose and 20 mM histidine at T=0 and after incubation at 40oC for 3 months

Figure 4.30A, 4.30B and 4.30C: Near-UV CD spectra of mAb 4212samples harvested on day 8 and day 13 of 4212A (A), 4212B (B) and 4212C (C) cultures, formulated in 190 mM arginine-HCl, and 20 mM histidine at T=0 and after incubation at 40oC for 3 months.

Figure 4.31A, 4.31B, 4.31C and 4.31D: Near-UV CD spectra of mAb 184 samples harvested on day 8 and day 13 of culture, formulated in (A and B) 80 mM arginine-HCl, 120 mM sucrose and 20 mM histidine and (B and C) 190 mM arginine-HCl and 20 mM histidine, at T=0 and after incubation at 40oC for 3 months.

Figure 5.1: Mean quality scores for Illumina RNA sequencing output at each nucleotide position along the 100 bp sequences for all cell line 184 samples (from days 6, 8 and 13 of culture).

Figure 5.2: Mean Phred quality scores per 100 bp sequence for all cell line 184 samples from days 6, 8 and 13 of culture.

Figure 5.3: Scatter Plots of the log-fold Change in Expression of all Genes Present in RNA Seq data of Cell Line 184 Samples, Where Sample day and Biological Replicates are Compared.

Figure 5.4: Heat Map with Dendrogram Depicting the Relationship of Culture Sample day and Biological Replicate RNAseq datasets.

Figure 5.5: Volcano plots of differentially expressed genes between days 6 and 8, days 6 and 13 and days 8 and 13 of fed-batch culture of cell line 184 as determined by RNAseq analysis.

Figure 5.6: Principle Component Analysis (PCA) of differentially expressed genes on Days 6,8 and 13 of culture for samples from cultures 184A and 184B.

Figure 5.8 KEGG Pathway Enrichment Analysis of Differentially Expressed Genes Between Samples of Cell Line 184 Cultures on Days 6 and 13, and Days 8 and 13.

Figure 5.9: GO Pathway Enrichment Analysis of Differentially Expressed Genes Between Samples of Cell Line 184 Cultures on Days 6 and 13, and Days 8 and 13.

Figure 5.10: Validation of RNASeq Data Using qRT-PCR.

Figure 5.11: Transcript Copy Numbers for the Original Panel of 11 Genes Relating to ER Stress Response Pathways Determined by RNASeq for Cell Line 184 Samples.

Figure 6.1: Schematic showing the sequence and design of the erse with a tata box downstream to drive GFP expression.

Figure 6.2: ARE Sequence with mluI and xmaI restriction sites for subsequent cloning.

Figure 6.3: Schematic showing construction of the PGL3P-ERSE-GFP-mCh stress reporter vector.

Figure 6.4: Schematic showing construction of the PGL3-ERSE-TATA-GFP-mCh stress reporter vector.

Figure 6.5: Schematic showing construction of PGL3P-ARE-GFP-mCh and PGL3-ARE-TATA-GFP-mCh stress reporter vectors.

Figure 6.6: DNA agarose gel showing test digest of PGL3P-ERSE-GFP-mCh and PGL3P-ARE-GFP-mCh constructs with *HindIII*.

Figure 6.7: DNA agarose gel showing test digest of PGL3-ERSE-TATA-GFP-mCh and PGL3-ARE-TATA-GFP-mCh constructs with *HindIII*.

Figure 6.8: Histograms generated from flow cytometry data showing GFP and mCherry fluorescence in CHO-S cells transiently transfected with the ERSE-SV40 stress reporter construct and treated with different concentrations of tunicamycin.

Figure 6.9: Histograms generated from flow cytometry data showing GFP and mCherry fluorescence of CHO-S cells transiently transfected with the ERSE-TATA stress reporter construct and treated with different concentrations of tunicamycin

Figure 6.10: Histograms generated from flow cytometry data showing GFP and mCherry fluorescence in CHO-S cells transiently transfected with the ARE-SV40 stress reporter construct and treated with different concentrations of t-BHQ

Figure 6.11: Histograms generated from flow cytometry data showing GFP and mCherry fluorescence of CHO-S cells transiently transfected with the ARE-TATA stress reporter construct and treated with t-BHQ.

Figure 6.12: Viable cell concentration and percentage culture viability of cell line 109 fed-batch cultures.

Figure 6.13: Viable cell concentration and percentage culture viability of cell line AB001 during fed-batch cultures.

Figure 6.14: Viable cell concentration and culture viability of cell line 2223 fed-batch cultures.

Figure 6.15: Viable cell concentration and culture viability of cell line 2491 fed-batch cultures.

Figure 6.16: Histograms showing fluorescence of CHO cells, as determined by flow cytometry, as a result of GFP expression in samples from cell lines 109, AB001, 2223 and 2491 transfected with the ARE-TATA stress reporter construct.

Figure 6.17: Histograms showing fluorescence of CHO cells, as determined by flow cytometry, as a result of mCherry expression in samples from cell lines 109, AB001, 2223 and 2491 transfected with the ARE-TATA stress reporter construct.

Figure 6.18: Scatter plots showing GFP and mCherry expression, as determined by flow cytometry on days 4, 7 and 12 in triplicate cultures for cell lines 109, AB001, 2223 and 2491.

Figure 6.19: Histograms showing fluorescence representing GFP expression within samples +/- TBHP from Cell Lines 109, AB001, 2223 and 2491 transfected with the ARE-TATA Stress reporter construct.

Figure 6.20: Scatter plots showing fluorescence as a result of GFP and mCherry expression on days 4, 7 and 12 in transfected Cultures +/- TBHP for cell lines 109, AB001, 2223 and 2491.

Figure 6.21: Histograms showing fluorescence as determined by flow cytometry within samples from cell lines 109, AB001, 2223 and 2491 assayed using a commercial cell staining kit.

Figure 6.22: Histograms showing fluorescence as determined by flow cytometry within samples +/- TBHP for cell lines 109, AB001, 2223 and 2491 assayed using a commercial cell staining kit.

List of Tables

Table 1.1: ICH general recommendations for stability study parameters to assess the stability of a drug product.

Table 1.2: Summary of excipient types and effects on biotherapeutic protein formulations with a selection of example compounds.

Table 2.1: Parameters for AFM image acquisition using 'tapping mode'.

Table 2.2: Component volumes to make four 12% and 8% acrylamide resolving gels, and 5% stacking gels.

Table 2.3: Details of primary and secondary antibodies used in western blotting.

Table 2.4: Thermocycler programme used to run all qRT-PCR plates.

Table 2.5: Primer sequences for amplification of genes of interest analysed by qRT-PCR to assess ER stress in Chapters 3 and 4.

Table 2.6: Primer sequences used for validation of RNA sequencing data by qRT-PCR in Chapter 5.

Table 2.7: Sizes of each plasmid encoding either the HC or LC for mAbs 109, 4212 and 184.

Table 2.8: Primer and oligonucleotide sequences with incorporated restriction sites

Table 3.1: Summary of Linear Regression Analysis for each gene of interest (GOI) and function of the corresponding proteins.

Supplementary Table 3.1: qRT-PCR Primer Sequences used to Determine Transcript Fold Change in Expression Relative to GAPDH.

Supplementary Table 3.2: Cell Productivity Under Fed-Batch and Batch Conditions.

Supplementary Table 3.3: HC to LC Transcript Ratios for Fed-Batch Samples.

Supplementary Table 3.4: Rate of Soluble Monomer Loss, Aggregate Gain and Fragment Gain per Month.

Table 4.1A, 4.1B and 4.1C: Titre and Specific Productivity Data for mAb 109 Producing Cultures.

Table 4.2A, 4.2B and 4.2C: Titre and Specific Productivity Data for mAb 4212 Producing Cultures

Table 4.3A, 4.3B and 4.3C: Titre and Specific Productivity Data for mAb 184 Producing Cultures

Table 4.4: Average relative HC:LC mRNA transcript copy number ratios for the three cell line 109 cultures.

Table 4.5: Average relative HC:LC mRNA transcript copy number ratios for cell line 4212 cultures.

Table 4.5: Average relative HC:LC mRNA transcript copy number ratios for cell line 184 cultures

Table 4.6: Percentage of total SVP counts which fall within 1 – 10 µm and 10 – 100 µm size ranges mAb 109 samples incubated at 40oC for up to three months.

Table 4.7: Percentage of total SVP counts which fall within 1 – 10 µm and 10 – 100 µm size ranges mAb 4212 samples incubated at 40oC for up to three months

Table 4.8: Percentage of total SVP counts which fall within 1 – 10 µm and 10 – 100 µm size ranges mAb 184 samples incubated at 40oC for up to three months.

Table 4.9: Rate of monomer loss and aggregate/fragment generation per month, as determined by size exclusion HPLC analysis for all mAb samples incubated at 40oC for 3 months.

Table 5.1: Number of Differentially Expressed Genes (DE) Between Sample Days in Cell Line 184 RNAseq Data Sets.

Table 5.2: List of Genes Randomly Selected for Validation of RNASeq Data using qRT-PCR.

Table 6.1: List of vectors used to construct ERSE and ARE stress reporter constructs.

Table 6.2: Specific productivity (Qp) for cell line 109 cultures fed-batch cultures.

Table 6.3: mAb Titre Data for Each Cell Line 109 Culture.

Table 6.4: Specific productivity (Qp) for cell line AB001 cultures.

Table 6.5: mAb titre data for each cell Line AB001 culture.

Table 6.6: Specific productivity (Qp) for cell line 2223 cultures.

Table 6.7: Specific productivity (Qp) for cell line 2491 cultures.

Table 6.8A and 6.8B: mAb titre data for each cell line (A) 2223 and (B) 2491 during fed-batch culture.

Table 6.9: Percentage of events which fall into each quadrant for scatter plots presented in Figure 6.18, comparing GFP and mCherry fluorescence of ARE-TATA construct transfected samples over time.

Table 6.10: Percentage of events which fall into each quadrant for scatter plots presented in Figure 6.20, plotting GFP and mCherry fluorescence of ARE-TATA construct transfected samples +/- TBHP.

Abbreviations

AFM – Atomic force microscopy

ARE – Antioxidant response element

Arg – Arginine-HCl

ATF4 – Activating Transcription Factor 4

BiP – Binding Immunoglobulin Protein

CD – circular dichroism

Chac1 – ChaC Glutathione Specific Gamma-Glutamylcyclotransferase

CHO – Chinese hamster ovary

C_L – Constant light chain region

C_H – constant heavy chain region

Derl3 – Derlin 3

DMSO – Dimethyl Sulfoxide

ER – endoplasmic reticulum

ERAD – Endoplasmic associated degradation

ERSE – ER stress response element

FDA – food and drug administration

GO – Gene Ontology

GS – glutamine synthetase

HC – heavy chain

HCP – host cell protein

Hspa9 – Heat Shock Protein Family A Member 9

Hsp90b – Heat Shock Protein 90

HERPUD1 – Homocysteine Inducible ER Protein with Ubiquitin-like Domain 1

ICH - The International Council for Harmonisation of Technical Requirements for Pharmaceuticals for Human Use

Ig – immunoglobulin

KEGG – Kyto Encyclopaedia of Genes and Genomes

LC – light chain

mAb – monoclonal antibody

MFI – micro-flow imaging

mth - month

PBS – Phosphate buffered saline

Pfdn2 – Prefoldin Subunit 2

pI – isoelectric point

Qp – Specific productivity

qRT-PCR – quantitative real time polymerase chain reaction

RagC - Ras-related GTP-binding Protein C

RNA seq – RNA sequencing

Rpn1 – Ribophorin 1

SEC-HPLC – size exclusion chromatography high performance liquid chromatography

SDS-PAGE - Sodium dodecyl sulfate polyacrylamide gel electrophoresis

SVP – sub-visible particles

TBHP – tert-Butyl Hydroperoxide

t-BHQ – Tert-Butylhydroquinone

TRIS - Tris(hydroxymethyl)aminomethane

UPR – unfolded protein response

V_L – Variable light chain region

V_H – Variable heavy chain region

XBP1 – X-box binding protein 1

Chapter 1

Introduction

1.1 The Biotherapeutic Market and Challenges in mAb Development

In 2017 the FDA approved 49 new drugs, 19 of which were classed as biologics. Of these biologics 10 were monoclonal antibodies (mAbs), typically IgGs, with the mAb market in the USA valued at $120-200 billion. The mAb production/manufacturing process is generally well-established and, in the majority of cases, uses *in vitro* cultured Chinese hamster ovary (CHO) cell lines as the host (Grilo and Mantalaris, 2019; Morrison, 2018). The dominance of CHO cells for the manufacture of mAbs is due to their ability to undertake human-like post-translational modifications (e.g. glycosylation, disulphide bond formation), proven regulatory acceptance, ability to deliver g/L of appropriate quality material and robustness in manufacturing processes. Despite the ability of CHO cells to produce g/L of mAb material, developing a therapeutic mAb can take several years to decades, and requires substantial investment, with project failure rates high. In 2015 it was estimated that 20.5% of mAb research and development programmes were discontinued, with just 2.6% of projects making it to market (Geng *et al.*, 2015).

mAb projects can fail for a variety of reasons, initially based around the biology of the drug and this not showing the desired biological effect(s), all the way through to manufacturing issues such as scalability, low productivity titres, poor product quality, drug format issues or lack of efficacy and side-affects during clinical trials. Research to improve therapeutic mAb manufacturing has attracted much attention over the last 20-30 years, with industry and academia seeking to minimise the costs associated with manufacturing bioprocesses, and to further understand how each stage of production can be optimised. As a result, significant progress has been made in the upstream production and downstream purification of mAbs, with titres exceeding 10 g/L reported (Huang *et al.*, 2010).

The end of the manufacturing process, and the final step before the drug is fill/finished and enters the patient, is formulation of the mAb.. Formulation development can also pose a bottleneck in developing mAbs, with an inability to formulate a mAb at an appropriate concentration and stability potentially resulting in the failure of a mAb product (Daugherty and Mrsny, 2006). Formulation development aims to provide the mAb in a state suitable to maintain product stability, and for delivery to the patient. As such, one of the goals of formulation is to mitigate potential stability issues, such as aggregation, through the use of excipients to ensure a product is safe and efficacious; but can also determine drug concentration, the mode of delivery, dosage and storage conditions. If formulation scientists cannot address product stability issues or achieve concentrations suitable for the desired delivery format a promising drug candidate could fail at this late stage of development. It is therefore essential to understand

the impact of the bioprocess as a whole on the stability of mAbs and how this might impact on the stability of the formulated product.

1.2 Structure and Function of Antibodies

Antibodies, also termed immunoglobulins (Ig), are 'Y' shaped glycoproteins (see Figure 1.1) mostly produced in the body by B cells, that have differentiated into plasma cells, and function to neutralise pathogens through binding specific antigens. Five classes of Ig exist (IgA, IgD, IgE IgG and IgM) which are each defined by the type of heavy chain (HC) they possess (Vidarsson *et al.*, 2014). The work in this thesis focuses on IgGs, which possess a y heavy chain and are further divided into subclasses denoted as IgG1s, IgG2s, IgG3s and IgG4s. For the purpose of this thesis, only IgG1 and IgG2 subclasses are discussed, however Figure 1.2 shows a representation of the hinge region variation between all four subclasses.

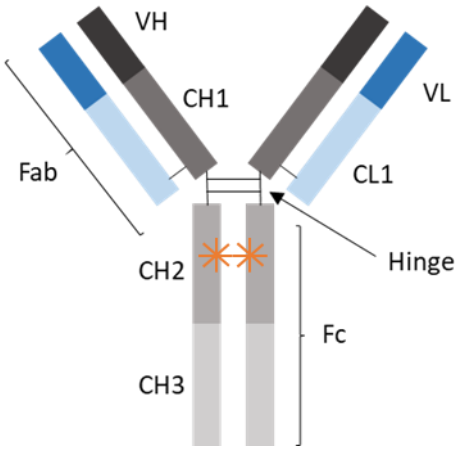

Figure 1.1: Simplified general structure of an IgG molecule depicting heavy and light chains (HC/LC), variable (V) and constant (C) domains, and the Fab and Fc regions. Orange stars indicate the conserved N-glycosylation site at N297 of the C_H2 domains, and black lines show disulphide bonding.

IgGs are the most abundant class of immunoglobulins circulating in serum in humans, and are composed of two identical HCs at the amino acid level and two identical light chains (LC), 50 and 25 kDa in size respectively. These are linked by disulphide bonds, as outlined in Figure 1.1. In humans the LC can be present as a kappa (κ) or lambda (λ) type, both of which are present in all IgG classes (Feige *et al.*, 2010a). Both the HC and LC are divided into constant and variable domains, denoted C_H/C_L and V_H/V_L respectively.

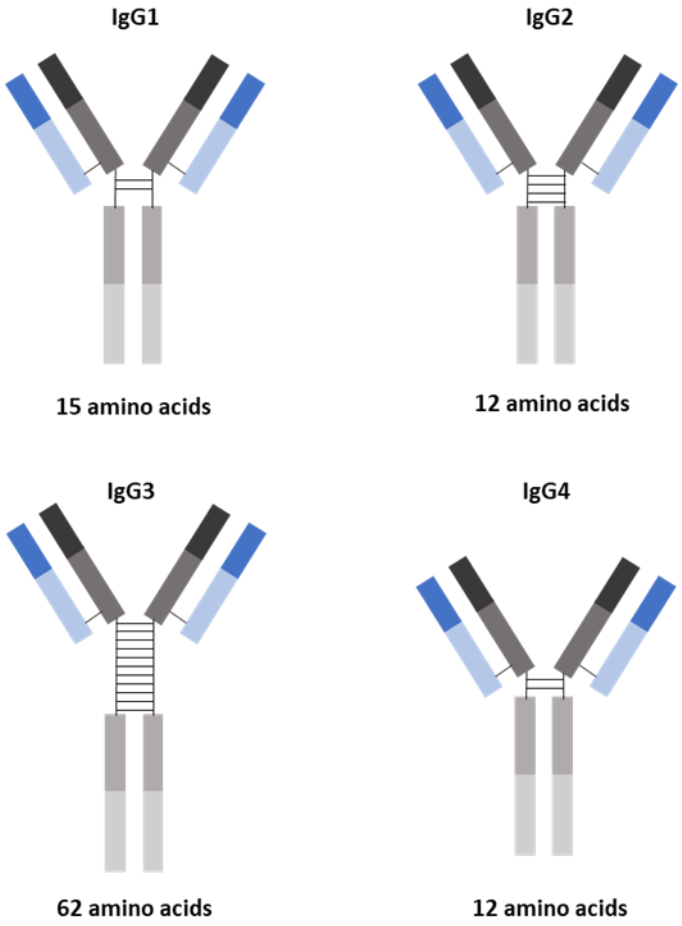

Figure 1.2: Comparison of the hinge region between IgG subclasses, depicting the number of disulphide bonds and amino acids. Note that the IgG2 representation corresponds to the IgG2A form which possesses a lambda (λ) light chain. Back lines represent disulphide bonds between polypeptide chains within the IgG.

The HC is composed of three C_H domains, termed C_H1, C_H2 and C_H3, while the LC contains just one C_L1 domain. Both the HC and LC contain a single variable domain. Constant regions are well conserved between immunoglobulin subclasses although there are subtle, yet important differences around the hinge region of the heavy chain constant domains, whilst the variable regions are different in each antibody and are specific to the antigen for which an IgG is designed/adapted to bind to, and has a diverse amino acid sequence (Feige *et al.*, 2010a; Irani *et al.*, 2015).

Based on the domain structure, IgG molecules are broadly divided into two portions termed the Fab and Fc fragments. The Fab fragment is the 'fragment antigen binding' portion and refers to the V_H, V_L, C_H1 and C_L1 regions and functions in antigen binding. The Fc fragment ('fragment crystallisable') consists of the C_H2 and C_H3 domains and is important for antibody effector functions once an antigen is bound, for example recruiting other immune cells such as

phagocytes to facilitate phagocytosis. (Feige and Buchner, 2014; Feige *et al.*, 2010a; Vidarsson *et al.*, 2014; Irani *et al.*, 2015).

C_H1 and C_H2 domains are connected through a hinge region where disulphide bonds form between heavy chains, as seen in Figure 1.2. This hinge region varies between IgG subclasses (Feige *et al.*, 2010a; Wang *et al.*, 2007). Aside from functioning to connect the C_H1 and C_H2 domains, the length and flexibility of the hinge region can impact on the conformation of the Fab 'arms' relative to the Fc domain (Liu and May, 2012; Vidarsson *et al.*, 2014). The hinge region of IgG1s consists of 15 amino acids and two disulfide bonds, and is therefore very flexible, allowing a good range of movement in the Fab 'arms'. IgG2s however, have a comparatively restricted hinge region, consisting of fewer amino acids (12) and 4 disulphide bonds (Figure 1.2). Furthermore, the IgG2 hinge also forms a poly-proline helix due to repeating proline residues which further contributes to the rigidity of the IgG2 hinge (Irani *et al.*, 2015; Liu and May, 2012; Vidarsson *et al.*, 2014).

Another important aspect of IgG function and structure is N-glycosylation. All IgGs have a conserved N-glycosylation site at N297 within the C_H2 domain (Figure 1.1) which contributes to the overall conformation of the Fc region. This glycosylation site can also impact on antibody effector functions through effecting Fc receptor binding (Irani *et al.*, 2015; Jefferis, 2007).

The majority of therapeutic mAbs on the market are IgG1s, with 79% of all mAbs approved between 2012 and 2017 being IgG1s with a kappa light chain (Grilo and Mantalaris, 2019). So termed next generation antibody formats have now been developed for use in the clinic (Sedykh *et al.*, 2018), with formats such as bi-specifics, antibody fusion proteins and Fc fusion proteins in development or in the clinic. Whilst some of these new formats are yet to be applied extensively in the clinic, two bi-specifics have been approved by the FDA (Grilo and Mantalaris, 2019), and represent a promising tangent to traditional therapeutic mAbs with over 50 bi-specifics reported to be in clinical trials in 2017 (Krishnamurthy and Jimeno, 2018). A number of Fc-fusion proteins are also on the market, with one of the biggest selling biotherapeutic molecules, Etanercept, being such an Fc-fusion protein of an Fc fragment (Schumock *et al.*, 2019).

1.3 Cell Line Development for mAb Production

Once a therapeutic mAb is identified with appropriate biological activity and the sequence of the chains determined, genes for the heavy and light chain are usually cloned into a suitable plasmid, and the constructed DNA used to drive expression of the two recombinant genes. The plasmid, which contains a selection marker to isolate those cells that have stably integrated the

plasmid into their genome, is then transfected into host cells to create polyclonal cell lines as part of the cell line construction process. During this process, monoclonal cell lines producing the molecule at an appropriate yield and quality (whilst able to maintain good cell growth and culture viability) are isolated from polyclonal populations and then tested for their scalability and robustness.

CHO cells can be transfected with plasmid DNA to give transient or stable expression of the genes of interest. Transient transfection, and hence transient expression of a mAb, can be carried out using chemical (such as lipofectamine) or electroporation techniques to facilitate the uptake of plasmid DNA through the cell membrane and into the nucleus. During this process, the vector DNA is not integrated into the host cells genome, and as a result, the transfected DNA is diluted over time, resulting in fewer cells in a population possessing the vector over time and therefore decreased product titre. Furthermore, the amount of DNA which is successfully transfected into each cell within a population varies. Despite these limitations, transient methods are utilised in product development to enable rapid production of material without the need to generate stably expressing cell lines, which is a more costly and time consuming process (Daramola *et al.*, 2014; Dyson, 2016; Rajendra *et al.*, 2016).

Stable transfection of plasmid DNA enables long term production of a target recombinant protein through integration of recombinant DNA with the genomic DNA of the host cell. As with transient expression, cells can be stably transfected using chemical and electroporation methods, however in the case of stable cell line development, the plasmid DNA is usually linearized prior to transfection and a selection marker is used (Kim and Eberwine, 2010). Incorporation of recombinant DNA into that of the host cell is a rare event, hence selection pressure must be applied, for example glutamine synthetase (GS), to ensure that only cells with integrated genomic DNA are isolated during the cell line selection process. GS is an enzyme which functions in producing glutamine from glutamate and ammonium ions. The GS system is one of the most commonly used selection markers in recombinant protein production using CHO cells, and works on the basis that CHO cells endogenously express low levels of GS; which is required for cell survival during culture. Plasmid DNA encoding the desired recombinant protein can therefore be engineered to contain genes for GS expression, hence only cells containing the desired plasmid DNA are able to produce glutamine and survive during cell culture. Methionine sulfoximine (MSX) is a suppressor of GS may be added to cultures as a further layer of selection, to select for cells expressing high amounts of GS (Dhara *et al.*, 2018).

Following selection, cells can then be cultured as either polyclonal pools, and/or individual cells/populations achieving an appropriate titre and growth rate which are in turn isolated using limiting dilution techniques or single cell sorting. Following this, monoclonal cell lines (derived from a single cell) are grown in larger volume cultures and further evaluated for growth and productivity attributes. Clonal cell lines are eventually selected to express the product of interest for process development or manufacturing, where cell lines chosen for manufacturing must have expression, stability and product characteristics to meet regulatory requirements. Stably expressing cell lines are more time-consuming and costlier to make than generating material by transient expression, however the long-term production, and greater yields associated with this, makes stable cell lines the method of choice for industry when producing material for manufacturing. Furthermore, through selecting clonal cell lines with appropriate growth profiles and high titres, cells which are tolerant of stresses that might be encountered during culture, and which may arise as a result of recombinant protein production, are also selected for.

1.4 Industrial Production of Monoclonal Antibodies

Typical commercial production of a mAb involves a multi-step process with various stages, as depicted in Figure 1.3. Many of these steps are adapted on a molecule and/or cell line and scale specific basis. The process can be broadly divided into three stages; upstream cell culture, downstream purification and formulation/fill finish activities.

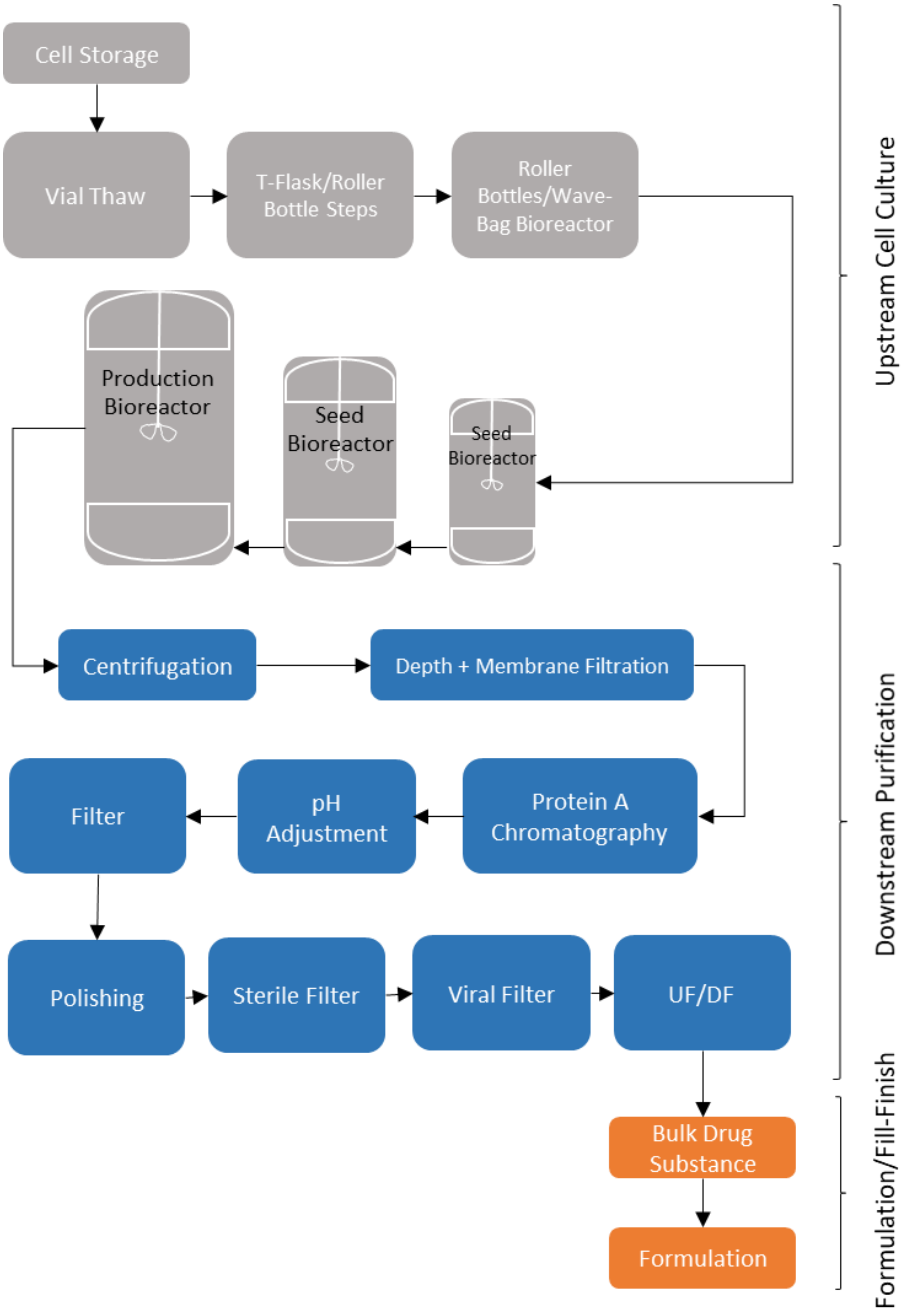

Figure 1.3: Schematic outlining the stages of typical therapeutic mAb production. The bioprocess can be broadly split into three steps; upstream cell culture, downstream purification and formulation/fill finish activities.

1.4.1 Upstream Cell Culture

Once a cell line has been established, a seed train is developed through different scales of culture to obtain the required cell numbers to inoculate a manufacturing culture to produce the large amounts of recombinant protein required for the market under batch or, more usually, fed-batch conditions. During batch culture, cells are seeded in media containing the nutrients required for the duration of the culture. During fed-batch culture, cells are supplemented with commercial or proprietary feeds, and glucose to replenish nutrients lost from the media as cultures progress. Key nutrients in media and feed include amino acids, glucose, vitamins, trace metals, lipids and growth factors (Dhara *et al.*, 2018; Ritacco *et al.*, 2018). The volume of supplements added is usually dictated by the cell concentration over the preceding period of time and metabolite analysis of lactate and glucose levels present in the media. The precise details of a feeding regime are often company and/or product and cell line specific, with proprietary media and feed compositions being used. For both batch and fed-batch fermentations, cultures are either allowed to run until a certain culture viability is reached or for a set number of days; whichever comes first. When producing material for process development, CHO cells are generally cultured under fed-batch over-grow conditions, as this is the format most frequently used for large scale mAb production (Fan *et al.*, 2018).

1.4.1.1 Cellular Stress During Over-Grow Culture

During over-grow cultures, cells are exposed to, and potentially experience, a number of extra- and intracellular stresses, such as pH changes, shear stresses, nutrient deprivation, toxins as a result of metabolism, oxidative stresses, and endoplasmic reticulum (ER) stress; all of which can impact on cell growth, productivity and product quality.

1.4.1.1.1 Nutrient Deprivation

All cell cultures require basic nutrients to sustain growth and productivity. Water and sources of carbon, nitrogen, phosphate, amino acids, fatty acids, vitamins, trace elements and salts are all supplied in culture media and feeds to replenish essential nutrients as cultures progress (Ritacco *et al.*, 2018). As such, there have been extensive efforts to develop media and feed compositions that support rapid growth and high recombinant protein production. Nevertheless, nutrient deprivation can still remain a limitation, particularly during batch, but also fed-batch, culture, and can lead to an accumulation of waste products, generation of reactive oxygen species and hydrodynamic stress (Kim *et al.*, 2013). Such stress can result in autophagy, which in turn can reduce cellular growth and productivity. For example, glucose deprivation has been shown to

promote autophagy in CHO cultures, as cells resort to recycling components for alternative energy sources (Lee and Lee, 2012). Sugars, such as glucose and galactose, are also essential for correct glycosylation, and have been shown to impact on mAb quality and function (Ritacco *et al.*, 2018). Amino acid deprivation has also been reported to impact on mAb glycosylation and cell growth, with glutamine levels in culture being linked to the presence of Man5 glycans, and regulation of leucine and arginine levels reported to extend culture duration (Fan *et al.*, 2015).

1.4.1.1.2 Oxidative Stress

Oxidative stress has been shown to have a negative impact on CHO cell growth and mAb production, is linked to ER stress (Ha *et al.*, 2018; Halliwell, 2014), and can result in cell death in the event of unresolvable stress (Birben *et al.*, 2012; Ha *et al.*, 2018). Reactive oxygen species (ROS) are continuously generated by aerobic metabolism during cell culture and are detoxified through enzymatic antioxidant pathways to maintain homeostasis (Gille and Joenje, 1992). An abundance of ROS can result from a variety of factors such as the presence of oxidants, infection, shear stress and cell density; and can be detrimental to the cell through damaging DNA, lipids and proteins (Birben *et al.*, 2012). ROS have been shown to cleave chaperones in the ER such as Hsp90 (Beck *et al.*, 2012), and to prevent such chaperones from aiding the folding of polypeptides in the ER. Furthermore, studies in CHO cells have shown that chemically induced oxidative stress reduced mAb production in a dose dependent manner, and that such stress also reduced product quality through decreasing the proportion of the correctly galactosylated form of the model mAb (Ha *et al.*, 2018).

1.4.1.1.3 Endoplasmic Reticulum Stress

CHO cells are capable of producing grams per litre of recombinant mAb material, with titres as high as 10 g/L (Huang *et al.*, 2010) and beyond reported. Producing such high quantities of protein can, however, place the ER under considerable stress, resulting in an accumulation of mis- or un-folded proteins and, in cases of unresolvable stress, cell death (Cudna and Dickson, 2003; Chakrabarti *et al.*, 2011; Schroder, 2008). The ER has quality control mechanisms in place to maintain cellular homeostasis and to ensure correct protein folding. Specifically, the unfolded protein response (UPR) and ER associated degradation (ERAD) serve as quality control pathways and are triggered during times of ER stress which can result from factors such as nutrient deprivation, hypoxia, viral infection, cellular ageing, a high protein load on the ER and accumulation of mis-folded proteins in the ER (Chakrabarti *et al.*, 2011; Naidoo, 2009).

1.4.1.1.3.1 The Unfolded Protein Response

The UPR functions to reduce protein load and increase the folding capacity of the ER. Three resident ER transmembrane proteins have been identified as sensors of ER stress within the UPR; inositol-requiring enzyme 1 (IRE1), protein kinase R endoplasmic reticulum kinase (PERK) and activation transcription factor 6 (ATF6). These molecules become activated in response to an accumulation of unfolded proteins, which results in the upregulation of genes involved in folding in the ER, such as chaperones, and proteins involved in ERAD; and downregulation of protein synthesis to reduce the intake of nascent proteins into the ER as outlined in Figure 1.4 (Rutkowski and Kaufman, 2004; Schroder, 2008).

All three of the transmembrane proteins are bound on the ER lumen side by the chaperone BiP during normal ER conditions, however during an accumulation of mis- or un-folded proteins, Bip is released from these sensors and binds to hydrophobic areas of mis or unfolded proteins to prevent them from aggregating (Chakrabarti *et al.*, 2011; Rutkowski and Kaufman, 2004; Schroder, 2008). Upon BiP release, PERK dimerises and functions to reduce the protein load on the ER through directly phosphorylating the translation factor eIF2α, to halt global mRNA translation. Whilst mRNA translation is attenuated by phosphorylation of eIF2α, translation of ATF4 mRNA is actually promoted, which subsequently acts to upregulate the transcription of downstream targets that can act to alleviate the source of ER stress (Rutkowski and Kaufman, 2004).

ATF6 is localised to the ER membrane, translocating to the Golgi upon activation, where it is then cleaved. Once cleaved, ATF6 moves to the nucleus where it binds to ERSEs (ER stress element sequences) upstream of target genes and promotes the transcription of such genes which typically function as chaperones, therefore increasing the folding capacity of the ER in an effort to clear the accumulated mis- or un-folded proteins. Cleaved ATF6 also upregulates the expression of *XBP1* mRNA, and therefore interacts with the IRE1 pathway, as discussed below.

IRE1 is also activated upon ER by dissociation from BiP. IRE1 binds *XBP1* mRNA directly and splices the gene to give *XBP1*s, which, when translated generates a transcription factor that in turn functions to upregulate the transcription of genes involved in folding and degradation pathways. The IRE1 pathway takes longer to initiate than those associated with PERK and ATF6 due to its dependence on the presence of *XBP1* mRNA. IRE1-dependent transcription is therefore reliant on the action of ATF6 to upregulate *XBP1* mRNA production to provide enough mRNA for splicing (Cudna and Dickson, 2003; Rutkowski and Kaufman, 2004).

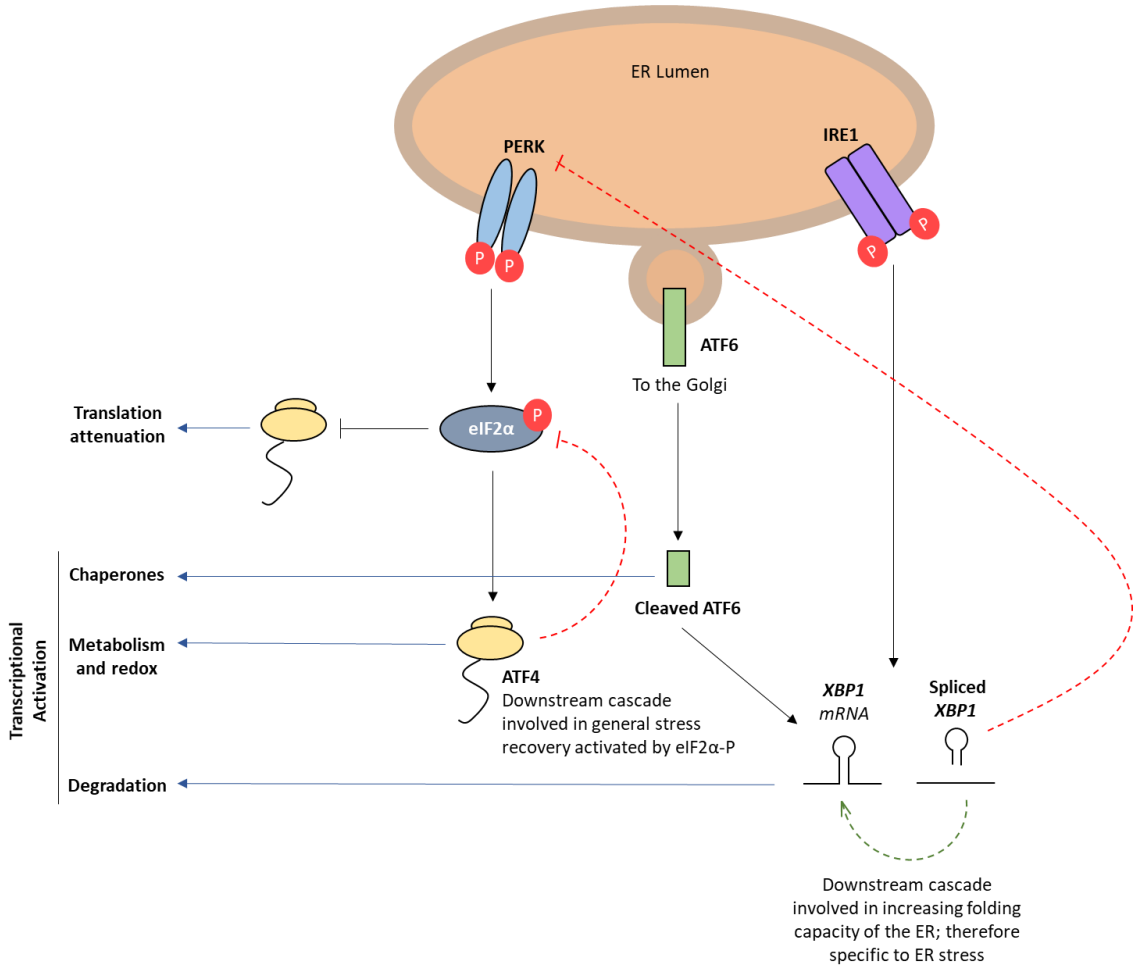

Figure 1.4: Schematic depicting the activation of PERK, ATF6 and IRE1 pathways within the unfolded protein response. The UPR is sensed via three transmembrane sensor proteins. Each of the sensors are activated when Bip, usually bound to these sensors on the ER lumen side, dissociates to bind to mis or unfolded proteins in the ER. The kinase PERK is activated upon ER stress perception and phosphorylates the translation initiation factor eIF2α to attenuate translation. Upon ATF6 activation, the protein is cleaved to liberate a transcription factor that migrates to the nucleus and upregulates the transcription of genes for the expression of chaperones. The activated cytosolic domain of IRE1 splices a 26 bp intron from the *XBP1* mRNA to generate the active *XBP1* mRNA that again acts as a transcription factor to upregulate expression of key foldases and chaperones that can help alleviate the ER stress. Red and green dashed lines indicate negative and positive feedback loops respectively.

1.4.1.1.3.2 Endoplasmic Reticulum Associated Degradation

The ERAD pathway is initiated when the build-up of mis- or un-folded proteins exceeds the ERs capacity to fold (or refold) polypeptides entering the ER, and functions to degrade these proteins. ERAD is a complex process, involving several pathways which are specific to a given class of unfolded protein. There is however a general process which is applied to the ERAD response. Firstly, mis- or un-folded proteins are recognised within the ER, then the proteins retro-translocated to the cytosol. As the protein enters the cytosol, it is then ubiquitinated on

the cytosolic surface of the ER by ubiquitin ligases to target it for degradation. The unfolded protein is extracted from the ER surface in an ATP dependent manner and released into the cytosol, where it is trafficked for degradation by the proteasome (Ruggiano *et al.*, 2014; Sano and Reed, 2013b; Stevenson *et al.*, 2016). In the event that ER stress cannot be resolved through either the UPR or ERAD pathways, apoptosis is triggered.

1.4.2 Downstream Purification of Recombinant mAbs from Cell Culture Harvests

Once cell culture has run to completion, the supernatant of the culture, containing the mAb that is secreted from the cell, is typically harvested by depth filtration or centrifugation methods to remove cells and debris. This results in a clarified liquid which is suitable for subsequent chromatography steps (Liu *et al.*, 2010). The specific methods used to harvest cultures is dependent on the cell line, culture viability at time of harvest and culture volume (Somasundaram *et al.*, 2018).

Protein A chromatography is generally the method of choice for the first capture chromatography step in a standard IgG purification and functions to purify an expressed IgG from other culture impurities (Bolton and Mehta, 2016; Miesegaes *et al.*, 2012). Protein A is a cell wall protein of *S.aureus* which binds only the Fc portion of IgGs. (Sheng and Kong, 2012), meaning that when harvested material is flowed through the column, the expressed IgG is immobilised, enabling impurities to flow through the column whilst the mAb is retained. Following loading and washing, the bound IgG is eluted using a low pH (3-4) buffer. This low pH can also be used as a viral inactivation step by holding the material at this pH for a set amount of time. Protein A purification is highly specific and results in a large reduction in host cell protein content (HCPs), with a clearance often in excess of 95-99%, however some HCPs remain after this step and must be reduced by additional polishing steps that also look to further reduce product impurities.

Anion exchange chromatography (AEX) is an effective method in removing negatively charged species, such as DNA, through using a positively charged resin to bind negatively species (Liu *et al.*, 2010; Strauss *et al.*, 2009). Cation exchange chromatography (CEX) is another polishing step which may be used to further separate the desired IgG from culture impurities such as HCPs. CEX uses a negatively charged resin which binds IgGs under specific salt and pH conditions; enabling impurities such as HCPs to flow through the column. The IgG can then be eluted by increasing the salt gradient (Connell-Crowley *et al.*, 2012). Once eluted the pH must be adjusted, then the material buffer exchanged into the desired formulation. Ultrafiltration and diafiltration methods are used to achieve this, during which material is concentrated then buffer exchanged

using centrifugal or pumping force to pass the material through a series of membranes (Liu *et al.*, 2010; Guo *et al.*, 2016; Yang *et al.*, 2017). Generally, material is exchanged into the buffering component of the formulation, then other excipients are spiked in after.

1.4.3 Formulation Development and Fill Finish Activities

Establishing an appropriate formulation for biotherapeutics, such as mAbs, is essential to ensure product safety, efficacy and shelf life through maintaining the stability of the product over time and providing a suitable delivery medium. Stability studies are used to evaluate the suitability of a formulation, during which samples of a drug are formulated and stored under a range of conditions for up to several months. Product stability is then routinely analysed at regular time points as described in section 1.5.

Product stability can be defined by a number of criteria, such as visual appearance and a drugs propensity to form aggregates, fragments and sub-visible particles over time. The formulation composition of a mAb can also influence the viscosity and concentration of a product, which in turn can impact on decisions regarding the mode of delivery and dosage (Awwad and Angkawinitwong, 2018; Matucci *et al.*, 2016; Roberts, 2014). Formulation development is therefore a key element when deciding on the drug format and may ultimately dictate if a drug can be self-administered, if a patient must see a doctor or nurse to receive an injection, or be admitted into hospital for treatment with higher drug volumes intravenously. Whether a drug should be formulated as a liquid or a lyophilised product also needs to be considered.

Other aspects to be considered when designing a formulation are the actual formulation and fill finish processes, transport and storage conditions of a product. For example, if a drug is being produced to treat a disease outbreak in remote parts of a country with a hot climate (where storage at 4^{o}C is likely to be unavailable) the formulation will have to withstand such conditions. Manufacturing and transport stresses can also impact the stability of a product, for example pump pressure during syringe filling (Krayukhina *et al.*, 2015; Gikanga *et al.*, 2017), and shear stress experienced during transport (Laptoš and Omersel, 2018; Wang *et al.*, 2007) have both been shown to induce mAb aggregation.

Formulation development must consider all of these potential issues to achieve a product which is safe for the patient, microbe free, has a stable pH, low viscosity, a good aesthetic (i.e. limited colour change and opalescence over time), maintains activity as a drug and has acceptable levels of aggregate and particle formation. Establishing a formulation which fulfils all of these criteria is essential to progress a product to market and in achieving approval from regulatory

authorities such as the US Food and Drug Administration (FDA) and European Medicines Agency (EMA).

1.4.4 Degradation of mAbs

mAbs, like most proteins, can degrade through a variety of mechanisms. These mechanisms can be broadly divided into two categories; chemical and physical degradation. Chemical degradation can take place in the form of reactions such as oxidation, deamidation, disulphide shuffling, hydrolysis, isomerisation and cross-linking (Wang *et al.*, 2007; Ionescu and Vlasak, 2010). Physical degradation is defined as denaturation or aggregation of a protein, and therefore refers to aggregation, fragmentation and particle formation (Wang *et al.*, 2007; Zhang *et al.*, 2018), although it is noted that fragmentation may also be chemically induced.

1.4.4.1 Mechanisms of Aggregation

Aggregation of a protein relates to its ability to maintain the correct low energy secondary, tertiary and quaternary structures whereby hydrophobic surfaces are not surface exposed. Mechanisms of protein aggregation have been extensively studied, yet much remains to be determined in terms of how aggregation of specific proteins occurs. There are several factors known to influence protein aggregation rates, including the specific amino acid sequence, temperature, pH, buffer composition, ionic strength and protein concentration. The term aggregate refers to a wide variety of species such as oligomers, soluble aggregates, insoluble aggregates, sub-micron aggregates, visible particles and sub-visible particles.

There are generally five mechanisms by which aggregation is considered to occur (Philo and Arakawa, 2009; Wang, 2010; Krishnamurthy and Manning, 2002; Siddiqi *et al.*, 2017) :

- Self-association
- Aggregation of conformationally altered monomer
- Aggregation of chemically modified monomer
- Nucleation controlled aggregation
- Surface induced aggregation

Self-association occurs when the native form of a monomer is able to associate with itself. This can be due to ‘sticky’ complementary patches on the monomer surface. Over time, the monomer is therefore able to associate to form oligomers, which may then be able to dissociate to form the native monomeric species again through reversible self-association. Over time, however, the formation of these oligomers can be greater than their dissociation, resulting in

these increasing in size until a point where several native units have associated, and oligomers begin to bind/associate with other oligomers. This interaction may become irreversible as covalent bonds and disulphide linkages form over time. An example of this mechanism of aggregation is seen in insulin (Brems *et al.*, 1992).

Aggregation of a conformationally altered monomer occurs in a similar manner, however in this instance the native monomer must undergo a conformational change first to cause it to self-associate. In the case of conformationally altered aggregation, it is not the native monomer which self-associates, but the altered species. Environmental stresses such as temperature and shear stresses can induce the conformational changes required for this mechanism of aggregation (Krishnamurthy and Manning, 2002; Wang, 2005). Despite the requirement of conformational changes, the resulting oligomers of aggregated species may incorporate the native monomer over time as oligomers grow in terms of their size and complexity.

Aggregation of a chemically modified product occurs via a very similar mechanism as for conformationally altered proteins, however in this instance a chemical modification triggers aggregation. Reactions such as oxidation or deamidation can alter a proteins charge or surface properties to promote self-association of the resulting species to form oligomers through creating 'sticky patches' or by reducing electrostatic forces which repel monomeric species from one another (Philo and Arakawa, 2009). As with conformationally altered aggregation, native monomers may also be incorporated into aggregates of chemically altered species.

Nucleation controlled aggregation is commonly responsible for the formation of visible particles and precipitants (Chi *et al.*, 2003). There are two types of nucleation aggregation; homogenous and heterogenous. During homogenous nucleation, the native monomer has a low propensity to form oligomers, however once an oligomer reaches a certain size, it can become energetically favourable for the native species to associate (Philo and Arakawa, 2009). Once this event has occurred after the initial lag phase, the subsequentially aggregation that follows to form larger oligomers is a rapid process. Heterogenous nucleation is propagated in a similar way, however in this instance the nucleation event stems from an impurity or contaminant.

Surface induced aggregation occurs at liquid-air or liquid-surface (i.e. container surface) interfaces. Hydrophobic driven interactions of the monomer at the liquid-air or liquid-surface interface can result in conformational changes within the protein. These altered species can then be released back into the main bulk of the material and self-associate to form oligomers which may also aggregate with the native species. This mechanism is similar to conformationally induced aggregation (Philo and Arakawa, 2009).

1.4.4.1.1 Sub-Visible Particle Formation

Sub-visible particles (SVPs) are defined as aggregates which are 1-100 µm in size, and are not visible to the naked eye (Singh *et al.*, 2010). SVPs may also pose a safety risk due to their potential to induce an immunogenic response (Carpenter *et al.*, 2009; Doessegger *et al.*, 2012), and are closely monitored throughout biotherapeutic protein formulation development and stability studies. Specifically, SVPs greater than 10 µm in size are required to be monitored by regulatory authorities, as outlined in section 1.5.1, however, particles <10 µm are not required to be reported; a decision which has sparked debate within both academia and industry.

Carpenter *et al.* (2009) raised concerns over the lack of regulation of particles less than 10 µm in size, arguing that a lack of understanding of the impact of particles <10 µm on autoimmune responses is justification in itself for erring on the side of caution, and to therefore impose mandatory monitoring of particles below 10 µm. They suggest that the development of instruments such as dynamic light scattering (DLS), micro flow imaging (MFI) and High Accuracy Liquid Particle counter (HIAC) now enable sufficient detection of particles <10 µm, and that limits should therefore be placed upon these. A report by Singh *et al.* (2010) directly addressed these concerns from an industrial perspective. The authors argue that whilst they agree that more research needs to be undertaken to understand the implications of particles <10 µm, current safety standards and routinely used methods to assess stability, are adequate to ensure patient safety. They also highlight issues with the accuracy of measuring particles <10 µm in size; comparing a variety of methods such as DLS, HIAC and MFI, and demonstrating significant variation between them.

Whilst these reports are almost 10 years old, there has been no change in regulatory guidance for SVPs <10 µm in size. There has also been little change in available technologies to monitor these, with variations between MFI and HIAC techniques reported as recently as February 2019 (Kiyoshi *et al.*, 2019). Throughout the stability studies presented in this thesis, SVPs from 1-100 µm were monitored and reported to cover the full range of SVPs and aggregate species present within formulated samples.

1.4.4.2 Visual Appearance

The aesthetics of a drug is another important formulation and subsequent stability parameter (Das, 2012). The visual appearance of a mAb can deteriorate in the form of yellowing/browning (Vijayasankaran *et al.*, 2013), visible particle formation (Doessegger *et al.*, 2012) and/or opalescence (Raut and Kalonia, 2016). Such visual phenomenon can be indicative of aggregate

formation, chemical reactions (such as oxidation), or phase separation (Raut and Kalonia, 2016) and can result from the degradation of the therapeutic itself, or of excipients within the formulation. Visible particles are typically > 100 µm in size, and usually consist of aggregated material. Visible particle content is limited by regulatory authorities based on the volume of the drug, and it is therefore important to monitor and minimise the formation of these species (USP, 2012).

1.4.4.2.1 Opalescence and Phase Separation

Opalescence relates to the physical stability of a biotherapeutic, and can be a pre-cursor to phase separation, and is frequently reported in formulated IgGs (Mason *et al.*, 2011; Raut and Kalonia, 2015; Sukumar *et al.*, 2004; Salinas *et al.*, 2010). Liquid-liquid phase separation is seen when a liquid formulation 'splits' into a highly concentrated protein phase (termed protein rich) and a diluted protein phase (termed protein lean) as depicted in Figure 1.5. This is generally observed at lower temperatures of around 4°C. Liquid-liquid phase separations are ultimately governed by the thermodynamics and kinetics of a system due to localised protein/particle concentrations (Raut and Kalonia, 2016).

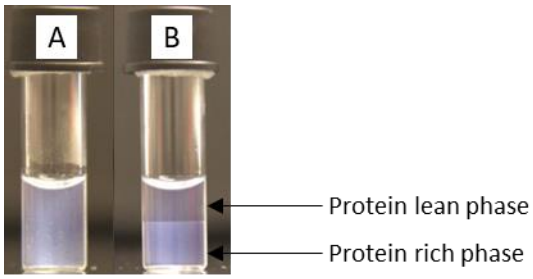

Figure 1.5: Example of (A) opalescence and (B) liquid-liquid phase separation of a mAb. Figure adapted from Raut and Kalonia (2016).

Opalescence is defined as the reflection of iridescent, and is typically observed as a cloudy 'blue' sheen which is visible against a dark background, as shown in Figure 1.5. Opalescence and turbidity are often used interchangeably in the literature, and are the result of light scattering due to the presence of aggregates/particles, or can be due to fluctuations in protein concentration within the solution. Opalescence is often associated with aggregate and SVP formation (Raut and Kalonia, 2016), however this is not always the case. For some proteins, opalescence can occur as a result of Rayleigh scattering (light scattering without a change in wavelength) without the presence of aggregates or particles (Salinas *et al.*, 2010; Sukumar *et al.*, 2004).

The aesthetics of a therapeutic does not necessarily reflect the stability of a product, but may impact on patient compliance. For example, a patient may assume a self-administered product is no longer fit for use if it looks turbid. The aesthetics of biotherapeutics is therefore required to be monitored by authorities, with developers generally seeking to minimise opalescence of a product wherever possible.

1.5 Assessing mAb Stability

To establish the shelf-life of a therapeutic product, stability studies must be carried out, during which the stability and quality of a drug is assessed. A variety of quality attributes must be evaluated and these data then submitted to regulatory authorities to seek approval for clinical trials and product release.

1.5.1 Official Guidelines on Product Stability

Several regulatory authorities exist worldwide to regulate drug manufacturing and development in different countries and continents. The International Council for Harmonisation of Technical Requirements for Pharmaceuticals for Human Use (ICH) was established in 1990 to harmonise regulations between these regulatory authorities, and to streamline drug approval procedures across different regions. Key regulatory documents therefore refer to ICH guidelines when discussing drug stability requirements and guidelines for product testing and manufacturing. The document Q1A (R2) (ICH, 2003) outlines recommended conditions for testing the stability of a protein based drug product, describing what would be necessary for a 'core stability data package'.

Table 1.1: ICH general recommendations for stability study parameters to assess the stability of a drug product.

Study type	Temperature	Length of study	Notes
Accelerated	40°C	6 months with 3 or 4 time points	
Intermediate	30°C	12 months with 4 time points	Can submit data from 6 months
Real		12 months	Can submit data from 6 months

The ICH recommends that stability studies are carried out on at least 3 batches of material which have been manufactured in the same way as intended for large scale production and that are packaged in the same materials as those intended to be used for distribution. They also state that a drug product must be tested under an accelerated temperature of 40°C, an intermediate temperature (25°C – 30°C), and the temperature intended for product storage. Table 1.1 summarises temperature requirements during stability studies.

Throughout the stability study, a product should be routinely inspected for any changes in quality. A significant change is defined as 'the failure of a drug to meet its specification'. Quantitative attributes (such as percentage aggregate content) are defined as significantly changing if:

- There is a >5% change in an assay from its T=0 value
- Any degradation product exceeds acceptance criteria
- Failure to meet criteria for appearance, physical attributes and functionality
- Failure to meet criteria for pH

Building on these recommendation, there are also guidelines specific to stability testing of biotechnological/biological products (ICH, 1995). This document states that guidelines in Q1A (R2) should be followed, but that for biologics, shelf life dating must be done on real time stability data at the proposed storage temperature. Despite frequent mention of acceptance criteria throughout ICH documents, the ICH itself does not set limits on qualitative and quantitative attributes, other than the bullet points outlined above. For this, the reader is referred to specifications outlined by individual regulatory authorities, and in many instances these are set on a case-by-case basis.

Particle counts are the only attribute for which a specific limit is set by the FDA. United States Pharmacopoeia (<788> Particulate Matter in Injections) states that for products with a volume of less than 100 mL, counts for particles ≥10 µm should not exceed 6000 and for particles ≥25 µm counts should not exceed 600.

1.5.2 Methods to Assess mAb Stability

The stability of a biotherapeutic must be assessed over time to establish a shelf-life as well as to ensure product safety and efficacy. To achieve this, material is formulated and incubated at a variety of storage conditions (for example temperature or humidity) for a number of weeks or months, and routinely assessed for various quality attributes such as aggregate/fragment formation and visual appearance, as discussed previously.

A variety of techniques can be used to assess product quality and aggregate formation within biotherapeutics over time. Each methodology or technique is only able to quantify/characterise aggregates within a set size limit (Figure 1.6), with no single approach able to assess particles across a continuum of size ranges. It can therefore be challenging to thoroughly quantify aggregates across a wide range of sizes due to the need to use multiple approaches to measure

these, each with their own limitations (Singh *et al.*, 2010; Zolls *et al.*, 2012; Carpenter *et al.*, 2009).

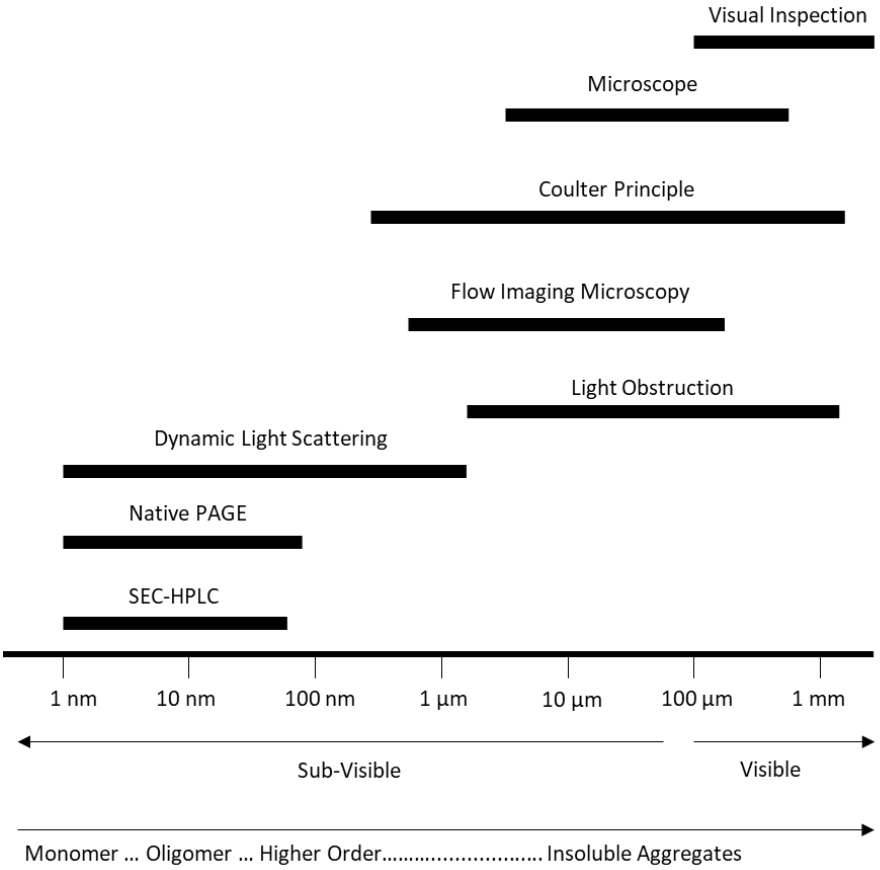

Figure 1.6: Schematic showing the size range detection of analytical techniques routinely used for the quantification of aggregates in biotherapeutics. Figure adapted from Mahler *et al.* (2009) and Singh *et al.* (2010).

1.5.2.1 Visual Inspection

Visual inspection involves assessing samples by eye to approximate quantities of particles >100 µm in size. Samples are compared against prepared standards to score visible particle formation, yellowing, browning, and opalescence (Zolls *et al.*, 2012). Regulatory authorities state that protein formulations must be essentially free of visible particles, and require visual inspection of samples during product development and manufacturing, however guidelines issued are not specific. For example, the European Pharmacopoeia monograph 2031 (Monoclonal Antibodies for Human Use) states that samples should be 'practically free of particles'. There is, however, much debate over the wording of these guidelines, with many questioning how to derive a clear meaning from such ambiguous criteria (Mathonet *et al.*, 2016; Zolls *et al.*, 2012; Melchore and Berdovich, 2012). Nevertheless, visual inspection can be a quick and effective way to track

degradation of a product over time, and to crudely compare the impact of varying formulation compositions and storage conditions on biotherapeutic stability.

1.5.2.2 Assessing Aggregation

1.5.2.2.1 Light Obscuration Methods

Light obscuration methods are commonly used to assess aggregates/particles, and are recommended as an approved technique by the FDA (USP, 2012) for the detection of aggregate species 1 µm to several millimetres in size (Zolls *et al.*, 2012; Narhi *et al.*, 2009). Light obscuration methods determine aggregate size, shape and quantities through detecting when aggregates within a sample obscure a light source (such as a laser). A sensor detects the light intensity, and equates the proportion of light blocked to the size of aggregates/particles within the sample. One example of this method is a HIAC instrument, which is routinely used to quantify particles 1 – 100 µm in size within pharmaceutical protein formulations (Narhi *et al.*, 2015; Zolls *et al.*, 2012). Light obscuration methods, however, do not enable differentiation between bubbles or silicone oil droplets in a sample and particles. As a result, there is high error associated with the quantification of particles < 10 µm in size (Sharma *et al.*, 2010b).

1.5.2.2.2 Flow Microscopy

Flow microscopy techniques quantify and characterise sub-visible particles by passing samples through a flow cell and photographing any particles that are present. The number of pixels for a particle is then mapped onto its size, enabling the user to gain information on particle quantities, size, morphology, aspect ratio and transparency (Huang *et al.*, 2009; Sharma *et al.*, 2010a; Zolls *et al.*, 2012). Such techniques provide particle counts and sizes based on equivalent circular diameter (ECD) and are considered more accurate than traditional light obscuration methods (Sharma *et al.*, 2010a; Sharma *et al.*, 2010b; Narhi *et al.*, 2009).

1.5.2.2.3 Size Exclusion High Performance Liquid Chromatography

Size exclusion high performance liquid chromatography (SEC-HPLC) is a common method for analysing therapeutic proteins for aggregation and fragmentation (Philo, 2009). This method typically measures soluble aggregates <100 nm in size. During SEC-HPLC protein samples are passed through a size exclusion column packed with fine porous beads made of dextran, agarose or polyacrylamide polymers with specific pore sizes, referred to as the stationary phase. Aggregates/fragments within the sample pass through the stationary phase at varying rates

based on their size, with smaller species taking longer to elute from the column due to being able to pass through the pores of the beads within the stationary phase (Philo, 2009; Khodabandehloo and Chen, 2017). The time which aggregates/fragments/monomers elute from the column therefore relates to the size of the species and are typically detected by absorbance at A_{280} nm, as depicted in Figure 1.7. The resulting chromatogram can then be integrated to establish the percentage content of aggregates, fragments and monomer within a sample.

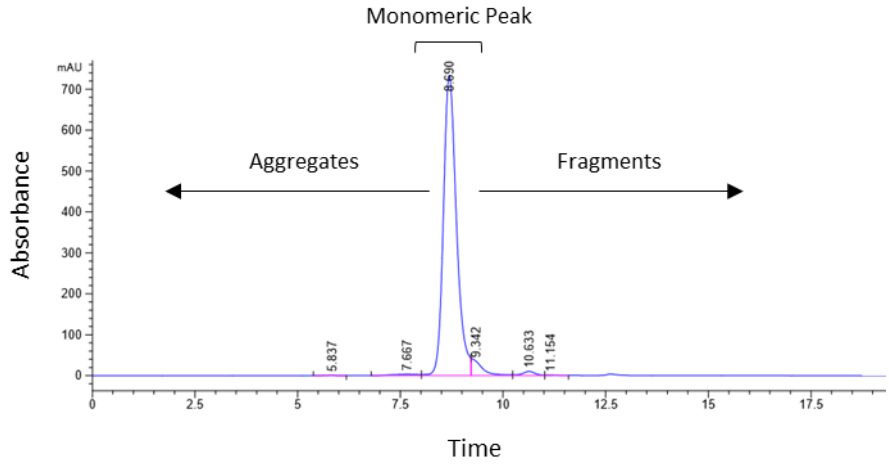

Figure 1.7: Example SEC-HPLC Chromatogram. When using this technique larger aggregates elute from the column faster than fragmented material, due to smaller species being retained in the column for longer as they are able to pass through holes within the porous stationary phase.

To flow a sample through the column a mobile phase is used, meaning that samples must be diluted in the corresponding mobile phase or compatible buffer prior to analysis. Samples therefore may not always be analysed in their original formulation nor at their original concentration, which can impact on the aggregates present. For example, the process of dilution alone may cause reversible aggregates to disassociate and to therefore not be detected using SEC-HPLC (Arakawa *et al.*, 2010; Philo, 2009; Khodabandehloo and Chen, 2017).

1.6 Excipients for Biotherapeutic Protein Formulation

Excipient is the term given to an inactive substance which is added to a drug product to maintain its stability and/or quality, and must be non-toxic and selected from a list of approved substances as outlined by regulatory bodies. Excipients can be broadly divided by function, as reported in Table 1.2, based on their effect (Davis, 1993; Jorgensen *et al.*, 2009). The effect of an excipient is, however, specific to the drug being formulated, the product concentration and drug format; and there is often overlap in terms of what impact a type of excipient may have.

For example, histidine can function as a buffering agent and as a stabiliser (Gervasi *et al.*, 2018; Baek *et al.*, 2017). Here the description is focussed around excipients for development of liquid formulations.

Table 1.2: Summary of excipient types and effects on biotherapeutic protein formulations with a selection of example compounds. Table adapted from (Jorgensen *et al.*, 2009).

Effect	Excipient Type	Example
Anti-adsorption	Surfactants	Polysorbate 20 and 80
	Polymers	Dextran, PEG
Oxidation Protection	Antioxidants	Ascorbic acid, Glutathione, Vitamin E
	Chelating Agents	Citric acid, EDTA
pH	Buffer Salts	Phosphate, sulphate
	Antacids	$Mg(OH)_2$, $ZNCO_3$
Stabilisers	Amino Acids	Alanine, Arginine, Histidine, Glycine, Lysine
	Sugars	Glucose, Sucrose, Trehalose
	Polyols	Glycerol, Mannitol, Sorbitol
	Salts	Sodium sulphate, potassium phosphate
	Chelating Agents	EDTA, Hexaphosphate
	Ligands	Phenol, Zinc
	Polymers	Cyclodextrin, Dextran
Tonicity	Salts	NaCl
Preservatives	Alcohol	Benzyl alcohol

1.6.1.1 Buffering Agents; Histidine

Buffering agents function to maintain the pH of a product throughout manufacturing and during a products shelf-life. Examples of buffering agents include TRIS (tris(hydroxymethyl)aminomethane) , sodium citrate, phosphate, acetate and amino acids such as histidine (Gervasi *et al.*, 2018; Jorgensen *et al.*, 2009; Abe *et al.*, 2013; Baek *et al.*, 2017). Histidine is reported as the most commonly used buffering agent, being used in 16% of all liquid products approved by the EMA between 1995 and 2018 (Gervasi *et al.*, 2018).

The side chain of histidine has a pK_a of pH 6, meaning that it is suitable for maintaining a product's pH under weakly acidic conditions. Histidine has also been shown to reduce the viscosity of humanised mAb solutions and has been shown to reduce protein-protein interactions (Chen *et al.*, 2003; Wang *et al.*, 2015). Studies have investigated potential mechanisms for the stabilising effect of histidine on proteins, however the impact and mechanisms of histidine-drug interactions are very much specific to the drug and formulation composition (Platts *et al.*, 2016).

1.6.1.2 Stabilisers; Arginine and Sucrose

Stabilising excipients function to (i) strengthen stabilising forces, (ii) to destabilise the unfolded form of a protein, or (iii) to preferentially bind the drug itself (Jorgensen *et al.*, 2009; Wang, 2015; Baek *et al.*, 2017). In this way, a protein can be stabilised through reducing self-association and therefore protein aggregation. Sugars, for example sucrose, and certain amino acids, for example arginine, can act as stabilisers.

Arginine is commonly used in the form of Arg-HCl. Arginine can function in formulations to prevent aggregation, promote protein folding, to reduce viscosity and to increase solubility; although, the specific mechanism(s) of action remain poorly understood (Arakawa *et al.*, 2004; Kheddo *et al.*, 2014; Gervasi *et al.*, 2018). Trout et al have developed and proposed the hypothesis, through a series of studies (Baynes *et al.*, 2005; Shukla *et al.*, 2011; Vagenende *et al.*, 2013), that arginine is able to self-associate into clusters, which in turn creates weakly hydrophobic interactions with aromatic side chains at the surface of a formulated drug. It is proposed that this interaction prevents aggregation by crowding out protein-protein interactions between drug molecules.

Sucrose is the second most commonly used stabiliser in liquid formulations approved in the EU between 1995 and 2015 (Gervasi *et al.*, 2018) and also functions to prevent protein aggregation. The pH of the formulation is particularly important and must be considered when using sucrose, as at a low pH sucrose can cause non-enzymatic glycosylation (glycation) of monoclonal antibodies (Hauptmann *et al.*, 2018) which can be detrimental to drug efficacy.

1.7 The Impact of Bioprocessing on Formulated mAb Stability

Product quality and stability is not only an issue during formulation development. Aggregation of mAbs has been reported throughout production (Paul *et al.*, 2018; Roberts, 2014; Shah, 2018; Velugula-Yellela *et al.*, 2018; Joshi *et al.*, 2014), highlighting how the bioprocess as a whole can influence the physical stability of mAbs. For example, host cell protein (HCP) content is established to influence downstream purification (Hogwood *et al.*, 2013; Hogwood *et al.*, 2014), with the HCP cathepsin D being linked to sub-visible particle formation within formulated IgG1s (Bee *et al.*, 2015). Intracellular HC and LC protein/mRNA ratios during biosynthesis of mAbs in the cell are also documented to impact on aggregate formation during upstream culture (Ho *et al.*, 2013; Ho *et al.*, 2015b). *HC* to *LC* mRNA ratios have been frequently studied in the context of productivity, with low *HC:LC* ratios reported to increase productivity (Jiang *et al.*, 2006; Schlatter *et al.*, 2005), however studies reported by Ho et al (2013; 2015b) have shown a link between high *HC* mRNA copy numbers and increased mAb aggregation during CHO cell culture.

Work by Gomez *et al.* (2012) has also shown a link between high *HC:LC* ratios and increased aggregation during temperature shifts from 37°C to 33°C.

Aggregation of mAbs during protein A purification has also been reported. A study by Joshi *et al.* (2014) compared the aggregation of two IgGs in buffer compositions routinely used in purification steps. The study found mAb aggregation was promoted upon exposure to elution buffers with a pH of 3, and that aggregation levels were higher in elution buffers consisting of citrate compared to acetate and glycine buffers. A further study by Mazzer *et al.* (2015) also found that elution buffers caused aggregation of an IgG4, and report further aggregation during low pH viral inactivation steps.

1.8 Aims of this Project

The impact of bioprocessing, consisting of upstream culture and downstream purification, during mAb manufacturing on product yield and quality has been reported; however, the link between intracellular stress during culture and formulated mAb stability has yet to be explored. As outlined above, stress during culture can impact the quality of the protein produced, which may have implications for the stability and formulation of such proteins.

This project set out to investigate the relationship between cellular stress, harvest day and formulated mAb stability through profiling ER stress during culture and comparing the stability of mAb material harvested and formulated at different times of culture. Specifically, this project set out to investigate;

1. How biomarkers of ER stress, at the transcript and protein level, change throughout culture between fed-batch and batch conditions; and if such biomarkers may be used to predict mAb stability.
2. If the stability profile of formulated mAb material changes between an 'early' and 'late' harvest; and if the duration of culture (and therefore duration/extent of cellular stress) can impact on formulated mAb stability.
3. If the format of cell culturing (i.e. 400 mL roller bottle cultures vs 10 L disposable bioreactors) impacts on biomarker profiles of ER stress, and the relationship between harvest day and formulated mAb stability.
4. If stress reporter constructs can be applied to measure ER and oxidative stresses in real time during fed-batch culture of mAb producing cell lines.

The work presented in this thesis was carried out in roller bottle cultures (400 mL – Chapter 3) and disposable bioreactors (10 L - Chapter 4) to work under industrially relevant conditions, and

assesses stability using approaches applied during industrial mAb production and formulation development, including SEC-HPLC and MFI, to compare product stability between harvest days. Additional analysis using atomic force microscopy (AFM) and circular dichroism (CD) spectroscopy was also undertaken to help further understand differences in particle content and conformation between material harvested at different culture times. Western blotting and qRT-PCR methods were routinely used to generate biomarker profiles of targets relating to ER stress at the protein and transcript level throughout culture. For work carried out with material from 10 L disposable bioreactors, RNA sequencing was also utilised on selected samples to further investigate transcriptional differences between cells at different points of culture (Chapter 5).

Finally, the use of stress reporter constructs containing stress response elements to assess ER and oxidative stress was explored, termed the ERSE (ER stress response element) and ARE (oxidative response element) respectively; where each stress response element would drive GFP expression in response to cellular stress (Chapter 6). After initial validation experiments, the ARE stress response element was transfected into small scale over-grow cultures to assess oxidative stress at different stages of culture across a panel of 4 cell lines, and compared to data obtained using a commercially available cell staining kit. The results from these studies are reported in the following chapters.

Chapter 2

Materials and Methods

2.1 Generation of Monoclonal Antibody Material

To investigate the relationship between ER stress, harvest day and mAb stability, three cell lines from the industrial collaborator (AstraZeneca) were used: 'NUT-B', 'PSS2' and 'NIP109 gDNA 132' which produce mAbs denoted as 184 (IgG2 λ light chain), 4212 (IgG1 λ light chain) and 109 (IgG1 κ light chain) respectively. Each cell line is referred to based on the mAb it produced, therefore cell lines are denoted throughout this thesis as cell lines 184, 4212 and 109. mAb 109 is established to be a stable molecule and is used as a control cell line/mAb in 10 L bioreactor, disposable bioreactor work only. All cell culture work was carried out in microbiology class II safety hoods (ThermoFisher Scientific, London, UK). All media and feed used throughout cell culturing is AstraZeneca proprietary, in-house media.

2.1.1 Roller Bottle Culture

2.1.1.1 Cell Lines and Maintenance

Cell lines 184 and 4212 were cultured in roller bottles under fed and batch conditions. Cells were taken from liquid nitrogen storage and thawed in a water bath at 37°C. 1 mL of thawed cells was then added to pre-warmed media in a 125 mL Erlenmeyer flask with vented caps, then the cell concentration determined using a ViCell XR (Beckman Coulter, High Wycombe UK) and more media added to the 'revival culture' to achieve a cell concentration of 3.0 $x10^5$ cells. All cultures were incubated at 37°C, 70% humidity and 4% CO_2 shaking at a speed of 140 rpm. Cells were then routinely sub-cultured for 3 passages before being bulked up to seed over-grow cultures. The cell lines used in this project utilise the glutamine-synthase (GS) selection system (Lonza 2007), therefore 25 µM MSX was used for selection throughout the revival and bulking up of cells, then removed for over-grow cultures.

2.1.1.2 Over-Grow Cultures

Over-grow cultures were seeded at a cell concentration of 0.5 $x10^6$ viable cells/mL for both cell lines, using in-house media without the addition of MSX. 6 fed cultures were seeded at a total volume of 320 mL, and 2 batch cultures at 400 mL in 2 L roller bottles with vented caps (Corning, New York, USA). Feed was added as per in-house protocols.

2.1.1.3 Harvesting of Material

Half of the roller bottles were taken for harvesting for each cell line on day 9 of culture (3 fed, 1 batch), then the remainder harvested on day 13 (3 fed, 1 batch). Cultures were harvested by centrifugation at 13000 xg for 20 minutes, then the supernatant sterile (0.22 µm) filtered using

vacuum 'stericups' (Merck, New Jersey, USA). Supernatants were then stored at 4°C for purification within a week of harvesting. Sampling was carried out on all cultures prior to harvesting (section 2.1.3).

2.1.2 10L Disposable Bioreactor Culture

2.1.2.1 Cell Lines and Maintenance

Cell lines 184, 4212 and 109 were used for 10L disposable bioreactor work. Cells were revived, passaged and bulked up as per section 2.1.1.1. The following biological replicates were run:

184 A and B

4212 A, B and C

109 A, B and C

2.1.2.2 Over-Grow Culturing

All over grow cultures were run under fed conditions with continuous glucose supplementation. Pump speeds to deliver glucose were calculated daily based on viable cell densities, existing glucose concentration and volumes of feed added using in-house methods to give a steady release of glucose over a 24 hour period.

10 L 'cell bag' disposable bioreactors (GE Life Sciences, Massachusetts, USA) were inoculated to achieve a cell concentration of 0.5 x10^6 cells/mL. Disposable bioreactors were incubated at 37°C on WAVE25 rockers, and continuously monitored for CO_2, O_2 and pH levels through DOOPT II and pHOPT sensors (GE Life Sciences, Massachusetts, USA) connected to UNICORN 6.4 software. Culture rocking speeds were set to 22 rpm and adjusted throughout culture based on online DO readings and cell concentration. All 'live' data gathered using UNICORN 6.4 software is referred to as online data. Data collected from other equipment is referred to as 'offline' data.

2.1.2.3 Harvesting of Cell Culture Material

Disposable bioreactor cultures were also harvested at two points during culture; day 8 and day 13. Filtration methods were used to harvest approximately 3.5 – 4 L of each culture on day 8, then the rest taken on day 13. Whilst cultures were still rocking, material was pumped through a custom made, closed filtration system (GE Life Sciences, Massachusetts, USA) consisting of a 0.45 µm filter followed by a 0.22 µm filter and a sterile collection bag. This process ensured all cells were removed and that supernatant material only was left. Filtered harvest material was

sampled for titre determination (section 2.1.3.3). Harvest material was then stored at 4°C for no more than 10 days before purification.

It is noted that in the case of wave bag material, cultures were not harvested in their entirety on day 8 and that this harvest may therefore be considered a sampling point instead. As material was obtained using the same methods as a complete harvest, however, this first point is termed as a harvest day throughout this thesis.

2.1.3 Sampling

2.1.3.1 Cell Concentration and Culture Viability

Where possible, cell counts were carried out daily for roller bottle and 10 L bioreactor cultures using a ViCell XR (Beckman Coulter, High Wycombe UK).

2.1.3.2 Cell Pellet and Supernatant Collection

Cell pellets were collected daily, where possible, for mRNA extraction (2 $x10^4$ cells) and intracellular protein analysis (1 $x10^7$ cells) based on viable cell counts. For roller bottle cultures, a single 'mRNA' and 'protein' cell pellet was taken for each culture. For 10 L bioreactor cultures triplicate 'mRNA' and 'protein' cell pellets were collected to give a technical repeat.

Supernatant samples were collected daily for 10 L bioreactor cultures only. 10 mL of culture was syringed out of each wave bag, then centrifuged at 13000 g for 5 minutes, then the supernatant retained. 1 mL of this was put aside for titre determination (section 2.1.3.3) and the remainder stored at -80°C.

2.1.3.3 Titre Determination

Samples were submitted for titre determination in-house, using methods as outlined by Daramola *et al.* (2014).

2.1.3.4 Metabolite Analysis (10 L Bioreactor Only)

As well as using online systems to monitor CO_2, O_2 and pH levels throughout culture, 10 mL samples were syringed from each wave bag system for offline metabolite analysis using a BioProfile Flex (Nova Biomedical, Massachusetts, USA). This enabled analysis of glucose concentration, lactate concentration, CO_2, O_2, ammonia and pH.

2.2 Purification of mAb Material from Harvested Supernatant

2.2.1 Protein A Purification

Protein A chromatography was used to purify mAb material from harvested supernatants. A standard in-house protocol was followed, using a low pH elution step. Different sized mAbSelect SuRe (GE Life Sciences, Massachusetts, USA) columns were selected based on titre data and were used with an AKTA Purifier or Pure system (GE Life Sciences, Massachusetts, USA).

2.2.2 pH Adjustment of Eluates

Eluate concentrations were determined by measuring absorbance at A_{280} with a DropSense16 instrument (Unchained Labs, Pleasanton, CA) before and after adjustment to pH 5-6 using a 1 M Tris solution. The following extinction coefficients were used to establish concentration; 184=1.75 $M^{-1}cm^{-1}$, 4212=1.65 $M^{-1}cm^{-1}$, 109=1.42 $M^{-1}cm^{-1}$. Eluates were then sterile filtered (0.22 µm) using vacuum filters (Merck, Massachusetts, USA) and stored at -80^{o}C.

2.3 Buffer Exchange

2.3.1 Roller bottle Material

pH adjusted eluates were thawed, then triplicate harvest day material pooled together. Material was then split in half to be buffer exchanged into two formulations using centrifugal concentrators with a molecular weight cut off of 30000 Da (Millipore, Massachusetts, USA), as per the manufacturer's instructions. Once material was buffer exchanged it was concentrated to 20 mg/mL. Formulations used are outlined in section 2.5.

2.3.2 10 L Disposable Bioreactor Material

Eluates were thawed, then buffer exchanged using Labscale TFF systems with 30 KDa cut off filters (Millipore, Massachusetts, USA). Samples were buffer exchanged into 20 mM histidine, pH 6.0, then their concentration measured and adjusted based on A_{280} readings to allow for spiking in of excipients. Excipients to achieve the final formulation were spiked in from sterile filtered stock solutions. All formulation compositions used in this work are outlined in section 2.5.

2.4 Vial Filling

Samples were sterile filtered using 0.22 µm syringe filters in a microbiology class II safety hood (ThermoFisher Scientific, London, UK). Autoclaved 3 cc glass vials (Schott, Strafford, UK) were then manually filled with 1.5 mL of sample and stoppered with steam sterilised, 13 mm liquid stoppers (West Pharmaceuticals, Pennsylvania USA).

2.5 Stability Study Outline: Buffers and Time-Points

The following two sections outline formulations used for material produced from roller bottle and 10 L bioreactor cultures. Formulations were selected based on in-house data of each mAb.

2.5.1 Roller Bottle Material

mAbs 184 and 4212 purified from roller bottle cultures on days 9 and 13 of culture were buffer exchanged (section 2.3.1) into the following formulations:

- 80 mM arginine-HCl, 120 mM sucrose, 20 mM histidine pH 6.0
- 160 mM arginine-HCl, 240 mM sucrose, 20 mM histidine pH 6.0

Vials containing 1.5 mL of material at a concentration of 20 mg/mL were incubated at 40^{o}C for 3 months. A single vial for each mAb taken for time point analysis at T=1 month and T=3 months. Methods used to evaluate stability at each time-point are outlined in section 2.6.

2.5.2 10 L Disposable Bioreactor Material

mAbs 184, 4212 and 109 purified from 10 L wave bag cultures harvested on days 8 and 13 of culture were buffer exchanged (section 2.3.2) into 20 mM histidine, then excipients added from stock solutions to achieve the following formulations:

- 80 mM arginine-HCl, 120 mM sucrose, 20 mM histidine pH 6.0
- 190 mM arginine-HCl, 20 mM histidine pH 6.0

Vials containing 1.5 mL of material at a concentration of 50 mg/mL were incubated at 40^{o}C and analysed at T=1 month and T=3 months.

2.6 mAb Stability Analysis

The techniques described below were used at each time-point to evaluate stability for each sample, using the same instrument settings and methods for both roller bottle and 10 L bioreactor material.

2.6.1 Visual Inspection

Samples were removed from incubation and left to reach room temperature. Each sample was visually inspected in a light chamber under controlled levels of lux, against a black and white background to enable colour change, particles and opalescence to be seen. Each sample was inspected for precipitation/sedimentation and phase separation before gentle agitation for particle, opalescence and yellowing assessment. Samples were scored against pre-made particle standards consisting of polystyrene beads (ranked 0 to 7 where 7 represents the most particles), and Nephelometry Turbidity standard solutions (ranked 0 to XI where XI is the most opalescent). Yellowing of samples was compared to yellow standards (ranked Y7 to Y1 where Y7 is colourless and Y1 is described is intensely yellow).

2.6.2 Analysis of Soluble Aggregates and Monomeric Species

2.6.2.1 Size Exclusion HPLC

Samples were analysed for percentage monomeric, aggregate and fragment species using an Agilent HP110 HPLC system (Agilent, California, USA) with a TSKgel SWx1 guard column (Tosoh Bioscience, Tokyo, Japan). A TSKgel G3000 SWx1 30 cm x 7.8 mm column (Tosoh Bioscience, Tokyo, Japan) was used to separate monomeric, aggregate and fragment species. UV detection was set at A_{280}.

2.6.2.2 Sample Preparation and Standards

Samples were diluted with their respective buffers to achieve a concentration of 10 mg/mL and filtered using 0.45 µm centrifugal filters (Millipore, Massachusetts, USA). Diluted samples were then transferred into glass vials (VWR, Pennsylvania, United States). Where possible, two 25 µL injections of each sample was analysed. Gel filtration standards (Bio-Rad, California, USA) was used at the beginning, middle and end of each sequence to monitor column performance. An in-house standard mAb was also used at the beginning and end of each sequence, for which retention times must fall in the range of 8.6 and 8.8 minutes.

2.6.2.2.1 Data Analysis

Acquired chromatograms were integrated using Agilent ChemStation software to give a percentage area for each peak. This data was then used to calculate rates of monomeric loss and aggregate/fragment gain over time.

2.6.3 Analysis of Sub-Visible Particle Formation

2.6.3.1 Micro-Flow Imaging

A 5200 Micro Flow Imager (Protein Simple, California, USA) with the accompanying analysis software, MVSS, was used to analyse sub-visible particle formation for all samples within 1 µm to 100 µm in size. Prior to analysis, the flow cell was cleaned with a 5% DEACON solution, followed by extensive washing with sterile filtered, ultrapure water. This wash routine was carried out between each sample. To analyse a sample, the flow cell was primed with 150 µL of sample, then 500 µL analysed for particle formation. Samples were not diluted prior to analysis.

2.6.3.2 Data Analysis

Sub-visible particle counts are grouped into the following size bins; ≥1 <2 µm ≥2 <10 µm, ≥10 <25 µm, ≥25<50 µm, ≥50<100 µm. To omit particles with a uniform morphology, such as silicone oil or bubbles, an aspect ratio of 0.85 or lower was applied.

2.7 Atomic Force Microscopy

2.7.1 Preparation of Samples

All sample preparation was carried out in a class II safety hood (ThermoFisher Scientific, London, UK). 10 L bioreactor material formulated in 80 mM arginine-HCl, 120 mM sucrose, 20 mM histidine from T=0 and after 3 months incubation at 40^{o}C only was analysed using AFM. All samples were diluted to 2 µg/mL in sterile filtered water. mAb 184 material harvested on day 13 was then further diluted 1:100 to enable imaging due to high amounts of aggregates and particles. 50 µL of each sample was then pipetted onto a cleaved, 10 mm mica disc, mounted on a 15 mm specimen disc (Agar Scientific, Essex, UK) and allowed to settle for 5 minutes whilst covered in a petri dish. Filter paper (Millipore, Massachusetts, USA) was used to wick away excess sample from the edge of the mica, then samples protected in petri dishes and left to dry overnight.

2.7.2 Image Acquisition Parameters and Processing

Samples were imaged using a MultiMode 8 Atomic Force Microscope with a NanoScope V controller and ScanAssist-Air silicon nitride tip probes (Bruker, Massachusetts, USA). Images were acquired using 'tapping mode', ensuring that laser alignment signal was set between 6 -7, and the vertical and horizontal differences to 0. Acquisition parameters are outlined in Table 2.1.

3 images were taken for each sample, ensuring to image different areas of the mica for each run. These images were then 'flattened' using NanoScope Analysis v1.5 software (Bruker, Massachusetts, USA) to remove any distortions. Each image was flattened by first, second then third order, using thresholding for each order. Thresholding values varied for each image as this number is adjusted based on visible background noise.

Table 2.1: **Parameters for AFM image acquisition using 'tapping mode'**.

Parameter	Setting
Sample Area	10 x 10 µM
Height Images	1024 x 1024 pixels
Aspect Ratio	1.00
X-offset	0 mm
Y-offset	0 mm
Scan Angle	90 °C
Scan Rotate	0.977 Hz
Amplitude Set Point	250 Mv
Drive Amplitude	122.38 Mv

2.8 Intracellular Protein Analysis

2.8.1 Cell Lysis

Cell pellets containing 1 x10^7 viable cells (sample collection outlined in section 2.1.3.2) were thawed into 1 mL of lysis buffer, resuspended and incubated on ice for 30 minutes. Samples were then centrifuged in a pre-cooled centrifuge at 4000 rpm for 10 minutes. Following this, the supernatant was retained for intracellular analysis. Cell lysates were prepared for SDS-PAGE analysis as outlined in section 2.9.2.

Cell lysis buffer consisted of 20 mM HEPES (Melford, Suffolk, UK), 100 mM sodium chloride, 10 mM sodium β-glycerophosphate (Sigma Aldrich, Missouri, USA) and 0.5% Tx100 (Sigma Aldrich, Missouri, USA). From this stock solution, 50 µL of 1 M sodium fluoride and 5 µL of 200 mM activated sodium orthovanadate were added per mL of lysis buffer to inhibit protein phosphatases. In addition, protease inhibitor tablets were also added (Roche, Basel, Switzerland) as per the manufacturers' instruction.

2.8.2 Lysate Preparation for SDS-PAGE Analysis

Lysates were prepared in reducing (50 mM Tris-HCl pH 6.8, 2% SDS, 10% glycerol, 1% β-mercaptoethanol, 12.5 mM EDTA and 0.02% bromophenol blue) and non-reducing (50 mM Tris-HCl pH 6.8, 2% SDS, 10% glycerol, 12.5 mM EDTA and 0.02% bromophenol blue) conditions. Samples were prepared to achieve a 1 x concentration of sample buffer, and an equal volume of each sample used in SDS-PAGE analysis.

2.8.3 SDS-PAGE Gel Composition and Running Conditions

Gels were prepared in 1.0 mm cassettes (Invitrogen, California, USA). Resolving gels were made to achieve a final composition of 12 % or 8 % acrylamide; and the stacking gel to 5% as in Table 2.2.

Table 2.2: **Component volumes to make four 12% and 8% acrylamide resolving gels, and 5% stacking gels.**

Component	Resolving		Stacking
	12 %	8 %	5%
Water	8.2 mL	9.3 mL	13.6 mL
30% Acrylamide	10 mL	5.3 mL	3.4 mL
1 M Tris pH 6.8	None	None	2.5 mL
1.5 M Tris pH 8.8	6.3 mL	5 mL	None
10 % SDS	250 µL	200 µL	200 µL
10 % Ammonium Persulfate	250 µL	200 µL	200 µL
TEMED	10 µL	12 µL	20 µL

Gels were placed into XCell SureLock Mini-Cell Electrophoresis (Life Technologies, California, USA) tanks and the chambers filled with a 1 x running buffer made from a 10 x stock solution (1 M glycine, 0.1 M Tris-base and 0.035 M SDS). Equal volumes of each sample were then loaded into the wells (volumes used depend on the target being blotted and are stated where blots or

gel images are shown) and gels run at 100 V through the stacking gel, and 150 V through the resolving. Gels were either Coomassie stained (section 2.9.1.4) or used for blotting (2.9.1.5).

2.8.4 Coomassie Staining of SDS-PAGE Gels

Gels were incubated in a Coomassie staining solution (1 g Coomassie brilliant blue G250, 500 mL methanol, 100 mL glacial acetic acid, 400 mL water) at room temperature on a shaker for half an hour, then rinsed in water and destained (240 mL methanol, 140 mL glacial acetic acid, 620 mL water) for an hour and left in ultrapure water overnight.

2.8.5 Western Blotting

All primary antibodies used in this project were diluted as required (Table 2.3) into a solution consisting of 5 % BSA (w/v) in TBST buffer (1.4 M sodium chloride, 0.1 M Tris-base pH 7.5 0.2 % Tween). All secondary antibodies are diluted into a solution consisting of 5 % (w/v) powdered milk in TBST buffer.

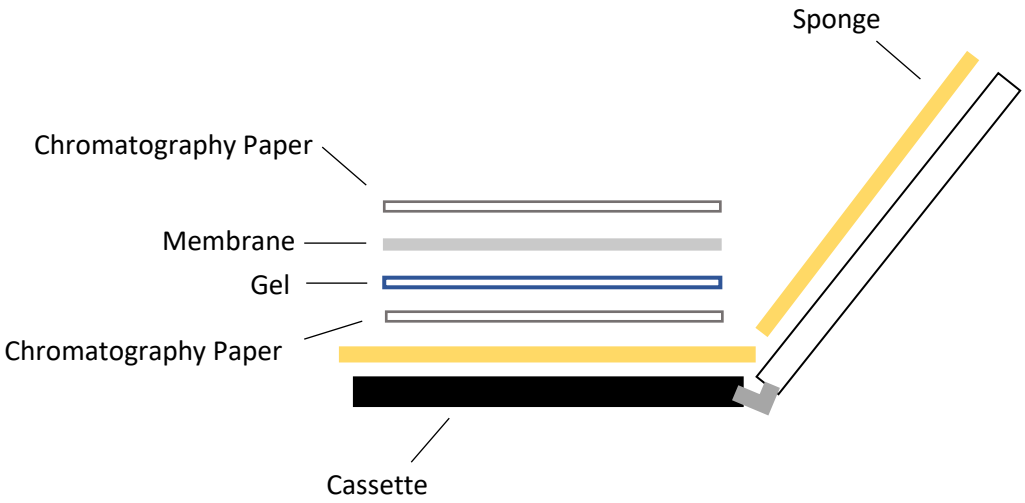

Figure 2.1: **'Sandwich' assembly for wet transfer of proteins from a SDS gel to nitrocellulose membrane.**

After SDS-PAGE (section 2.8.3) gels were removed from cassettes and assembled with sponges, chromatography paper and a piece of 0.45 µm nitrocellulose membrane (GE Life Sciences, Massachusetts, USA) to form a 'sandwich' for wet transfer, as in Figure 2.1. This 'sandwich' was then placed into a gel tank filled with a 1 x transfer buffer made from a 10 x stock (1 M glycine, 0.1 M Tris-base, 0.035 M SDS), using 10 % of the 10 X solution, 10 % methanol and 80% water. Transfer then took place at 4 ^{o}C for an hour at 0.75 Amps.

Table 2.3: Details of primary and secondary antibodies used in western blotting. Primary antibodies were diluted accordingly in 5% (w/v) BSA in TBST buffer, and secondary antibodies diluted in 5% (w/v) powdered milk in TBST buffer.

Primary Antibody					
Target	**Supplier**	**Product No**	**Dilution**	**Size (KDa)**	**Raised in**
Beta Actin	Sigma	A5441	1:5000	42	Mouse
eEF2	Cell Signaling	2332S	1:1000	95	Rabbit
eEF2-P	Cell Signaling	2331S	1:1000	95	Rabbit
eIF2α	Abcam	ab4837	1:1000	36	Rabbit
eIF2α-P	Abcam	ab4837-50	1:1000	40	Rabbit
Anti Whole IgG	The Binding Site	AP004	1:20000	150/50	N/A
Anti Kappa LC	The Binding Site	AP015	1:20000	25	N/A
Anti Lambda LC	The Binding Site	AP017	1:20000	25	N/A
Secondary Antibody					
Mouse	Daeko	P0447	1:1000		
Rabbit	Cell Signaling	7074	1:1000		

After transfer, the sandwich was disassembled and the nitrocellulose membrane placed in a methanol cleaned box. 10 mL of blocking solution (5 % (w/v) powdered milk in ultrapure water) was added and the membrane was left to incubate at room temperature for 30 minutes on a shaker. The blocking solution was then discarded and the membrane washed with a TBST buffer (1.4 M sodium chloride, 0.1 M Tris-base pH 7.5 0.2 % Tween). 4 mL of primary antibody was then added and the membrane incubated at 4^{o}C overnight on a rocker. The primary antibody was then removed, and the membrane washed in TBST for three 10 minute washes. If a secondary antibody was required, 4 mL of secondary was then added and the membrane left to incubate on a rocker for an hour at room temperature. The secondary was then discarded, and the blot washed for three 10 minute washes in TBST.

Membranes were incubated in Amersham ECL reagent (GE Life Sciences, Massachusetts, USA) as per the manufacturer's instructions for signal detection, then excess solution wicked away from the corners of the membrane. Blots were developed in a dark room by exposing ECL chemiluminescence film (GE Life Sciences, Massachusetts, USA) to the membranes. Exposure times depend on the target being blotted and are stated with each blotting image reported in this thesis.

2.8.5.1 Densitometry Analysis

Blots were scanned and saved, then the density of each band established using ImageJ 1.50i software (Schneider *et al.*, 2012). Each gel/blot contained a control sample which was used to

scale between gels, to compensate for differences in transfer efficiency, by dividing all band densities from the same gel by the density of the control band. To give a fold change in expression, densities were then made relative to day 3 samples.

2.9 Gene Expression Analysis

The following cell pellet samples collected from roller bottle cultures were used for mRNA extraction and subsequence qRT-PCR assays:

- Fed: Days 3, 6, 7, 8, 9, 10, 13 (from the 3 cultures that were harvested on day 13 only to give biological triplicate)
- Batch: Days 3, 4, 5, 6 ,7 (using cell pellets from both cultures to give biological duplicate)

For 10 L bioreactor wave bag cultures, cell pellets from each biological replicate were used to give triplicate samples for cell lines 109 and 4212, and duplicate for 184. Two pellets were analysed for each sample day to give a technical repeat. Samples were analysed for the following culture days:

- Days 3, 6, 8, 13

2.9.1 RNA Extraction and DNAse Treatment

Throughout all RNA work, RNAse free water and Eppendorfs were used. Work surfaces, pipettes and racks were cleaned using a 70% IMS solution and RNAsezap (Sigma Aldrich, Missouri, USA). Cell pellets consisting of 2 $x10^6$ viable cells (sampling outlined in section 2.1.3.2) were thawed into RLT buffer (Qiagen, Hilden, Germany) then the total mRNA extracted using an RNeasy kit (Qiagen, Hilden, Germany) as per the manufacturer's instructions. The concentration of mRNA in each sample was then quantified using a NanoDrop. All samples were then DNAse treated to prevent contamination from genomic DNA using an RQ1 RNase-Free DNase kit (Promega, Wisconsin, USA) as per the manufacturer's instructions, scaling up the reaction volumes to treat 2 µg of RNA in a total reaction volume of 22 µL. Samples were then diluted with RNAse free water to 25 ng/µL, and aliquoted into single use volumes to minimise freeze-thaw cycles for future qRT-PCR assays, and stored at -80^{o}C.

2.9.2 qRT-PCR Analysis

qRT-PCR assays were carried out in a 96 well format using non-skirted, white plates (BRAND, Berlin, Germany) in a DNAEngine Peltier thermocycler (BioRad, California, USA) with a Chromo4

real-time PCR detector (BioRad, California, USA) following the protocol outlined in Table 2.4. SYBR Green was used to detect amplified cDNA, using a one-step QuantiTect kit (Qiagen,Hilden, Germany) as per the manufacturer's instructions, scaling the reaction down from 25 µL to 20 µL. All primers (Tables 2.5 and 2.6) to detect genes of interest were designed over an intron and ordered from Eurofins (Luxembourg), or purchased (Qiagen, Hilden, Germany). Expression of GAPDH mRNA was used to normalise gene of interest expression throughout all plates.

To ensure DNAse treatment was successful, all samples were screened for genomic DNA contamination by running control qRT-PCR plates using the previously mentioned QuantiTect kit, this time replacing reverse transcriptase with water. Any signal detected in control plates would therefore be due to existing DNA present in the samples rather than from cDNA which had been reverse transcribed from RNA, as no reverse transcriptase would be present. Samples were then ran on a 2 % agarose gel to enable visualisation of any amplified DNA to ensure that any signal detected from the plate was due to SYBR Green background signal rather than cDNA.

Table 2.4: **Thermocycler programme used to run all qRT-PCR plates.**

Step	Parameter
1	50 °C for 10 minutes
2	95 °C for 5 minutes
3	95°C for 10 seconds
4	58 °C for 30 seconds
5	Plate read
6	Got to step 3 39 times
7	Melting curve from 58 °C to 95 °C. Plate read every 0.5 °C.

Table 2.5: **Primer sequences for amplification of genes of interest analysed by qRT-PCR to assess ER stress in Chapters 3 and 4**. Primers were designed over an intron to minimise the impact of any potential genomic DNA present in the samples.

Gene of Interest	Forward	Reverse
Chac1	Qiagen #PPJ11250A-200	
Pfdn2	CTTGGAAGGCAACAAAGAGC	CATCTTCCCCCATAAGACGA
ATF4	TCAAACCTCATGGGTTCTCC	GGCATGGTATCCAGGTCATC
Derl3	Qiagen #PPJ14396A-200	
Herpud1	CCTGGCTTCTCTGGCTACAC	TGTGAATAGGGGCTGGAGTC
Rpn1	GTTGAGCAGCACATTCAGGA	TTGGTGATGGAAAAGTCCAG
Hspa9	GTCAGGGAGAGCGAGAGATC	CCGCCAGAAGACTGGATTAC
BiP	AAACATTTGCCCCAGAAGAA	TGATCCGCATGACATTCAGT
Calreticulin	AGGCTCCTTGGAGGATGATT	TCCCACTCTCCATCCATCTC
RagC	GGAGGCTTTAACCCGACTTC	TCATTGGCCCTTTGATGAAT
GAPDH	GCCAAGAGGGTCATCATCTC	CCTTCCACAATGCCAAAGTT
Hsp90b	CTCACAGAGCCTGTGGATGA	CGTGAGACGCTGAGATACCA
109 HC	GCAAGGACTCCACCTACAGC	TGTTGAAGCTCTTGGTCACG
109 LC	CAAGTGCAAGGTCTCCAACA	ACCAGACAGGTCAGGGACAC
4212HC	GGAAAAGGGCTTGAGTGGAT	GATCCACTTCCCCATCACTG
4212 LC	TAATTTCAATCGGCCCTCAG	GAGGGTGGGGCTGTCATAG
184 HC	GGTAGCACAAGCTACGCACA	CTCAGATCTCAGGCTGCTCA
184 LC	ATAAGCGACCCTCAGGGATT	ATCCCATGTTCCGCAGTAAT

Table 2.6: Primers sequences used for validation of RNA sequencing data by qRT-PCR in Chapter 5. Primers were designed over an intron to minimise the impact of any potential genomic DNA present in the samples.

Gene of Interest	Forward	Reverse
Ptprn2_1	GACCTCCTGAAAGACCACGG	CCGAGGCTTGAGGACCAATT
Gbp7_2	CAGGAGGAAGGTTGAGCAGG	GAGGTGGCAGAACAGGAACA
Aurkb_2	ACGACTTTGAGATTGGGCGT	TGTTGGGATGTTGCAGGTGT
Atxn_1	ATCAGACGATGATCCCGCAC	AGGATGAGGCACTGACTTGC
Ler_1	AGGGTCCTCTTTCTCCTGCT	ATGAGCGCAGAGAGGGTTTC
Aebp_1	AGGACTACACCAACGGCATG	TGTTGTTCTCCCACTCACGG
Saa_1	TTTCCATGCCCGAGGAAACT	TGCTCCATGTCCTGTGAACC
Lum_1	TGACAGAGTCAGTGGGTCCA	GGCCAGAAGGAAGCTTAGCA
Rab38_1	TGTCTTCGATGTCACCAGGC	CACATCCTTCCCCTGGTCAC

2.9.3 Generation of Standard Curves for Relative HC and LC Copy Number Analysis

Separate plasmids encoding the heavy chain and light chain of each mAb were provided by AstraZeneca , plasmid sizes are listed in Table 2.7. The concentration of each stock in ng/µL, Avogadro's constant (6.022 $x10^{23}$) and the size of the plasmid was used to establish a copy number/µL as in Figure 2.2. Plasmids were then diluted appropriately in RNAse free water to achieve standard curve samples with plasmid copy numbers ranging from 1 $x10^8$ to 1 $x10^3$ copies/ µL. These standards for both HC and LC plasmids were then run with RNA samples collected during culture and used to extrapolate HC and LC copy numbers for each sample analysed using Opticon3 Software (BioRad, California, USA).

Table 2.7: Sizes of each plasmid encoding either the HC or LC for mAbs 109, 4212 and 184. Vector sizes were used to establish plasmid copy numbers to generate a standard curve for qRT-PCR analysis of HC and LC mRNA expression**.**

Plasmid	Size (bp)
109 HC	9543
109 LC	4736
4212 HC	9563
4212 LC	4736
184 HC	9548
184 LC	4636

Plasmids were then diluted appropriately in RNAse free water to achieve standard curve samples with plasmid copy numbers ranging from 1 $x10^8$ to 1 $x10^3$ copies/ µL. These standards for both HC and LC plasmids were then run with RNA samples collected during culture and used to extrapolate HC and LC copy numbers for each sample analysed using Opticon3 Software (BioRad, California, USA).

2.9.4 Data Analysis

2.9.4.1 $\Delta\Delta C_t$ and Fold Change Calculation

Opticon Monitor 3 software (BioRad, California, USA) automatically calculates $\Delta\Delta C_t$ values based on the set threshold and the signal obtained from wells defined as 'calibrators'. Thresholds were manually set for each plate. For all plates run, the housekeeping gene GAPDH was used to normalise gene of interest expression to. In order to do this using the Opticon Monitor 3 Software, each sample well containing primers for GAPDH amplification were set as calibrators. Each gene of interest sample was then selected with its corresponding calibrator, enabling the

software to carry out $\Delta\Delta C_t$ calculations to produce a relative difference value. This relative difference value was then exported and used to calculate the fold change in expression for each gene of interest across culture.

$$\text{Copy Number } /\mu L = \frac{\text{Plasmid Concentration (ng/}\mu L) \times (6.022 \times 10^{22})}{\text{Size of Plasmid (bp)} \times 10^{9} \times 325}$$

Figure 2.2: **Equation used to establish plasmid copy number.** Copy numbers were subsequently used to create standard curve samples with known copy numbers of HC and LC plasmid in to determine HC and LC mRNA expression using qRT-PCR.

For each gene of interest, 3 biological repeats were assayed for each sample day, excluding 10 L bioreactor mAb 184 cultures for which 2 biological repeats were available. For small scale work, samples collected from the three cultures which were harvested on day 13 were analysed only.

Prior to calculating fold changes, the relative difference per cell was established based on sampling and dilution throughout sample preparation (see equation in Figure 2.3). 2 $x10^6$ viable cells were sampled (section 2.1.3.2) for RNA extraction after which 60 µL of RNA was eluted for each sample, meaning that every 1 µL of RNA represents 3.33 $x10^4$ cells. 2 µg of RNA was DNAse treated in a total reaction volume of 22 µL (section 2.9.2.1), making a concentration of 90.90 ng/uL of RNA at this stage. Following DNAse treatment, samples were then diluted to 25 ng/µL giving a dilution factor of 3.636. This dilution factor is used in the equation outlined in Figure 2.3 to establish relative difference per cell.

From the relative difference per cell, fold change in expression was then established by normalising samples to data from day 3 samples. Data was normalised by dividing each relative difference per cell by the average relative difference across samples taken on day 3. Normalised relative differences were then averaged between biological repeats to give an average fold change in expression.

$$\text{Relative Difference per Cell} = \frac{\text{Relative Difference or Copy Number}}{\left(\frac{3.33 \times 10^{4} \text{ Cells} \times \text{Volume of Sample for 2 } \mu g}{3.363} \right) \times 1.6}$$

Figure 2.3: Equation used to establish relative difference in transcript expression per cell. 3.33 $x10^4$ is the number of cells per µL of extracted RNA, 3.636 is the dilution factor when DNAse treating 2 µg of DNA then diluting samples to 25 ng/µL, then 1.6 is the volume of RNA added into each sample well for qRT-PCR analysis.

2.9.4.2 Linear Regression Analysis

Linear regression analysis was used to assess the significance ($P < 0.05$) of the relationship between sample day and fold change in gene expression for data from roller bottle culture samples. MiniTab 18.1 software was used to carry out the analysis. R^2 values and P values were recorded for each gene of interest, where the R^2 value represents the percentage of variance which is caused by sample day and P values were established from one way ANOVA analysis.

2.9.4.3 Establishing Relative HC and LC Copy Number per Cell

The use of standard curve samples enabled HC and LC copy numbers to be established for each sample. From this, the copy number per cell was then calculated by using the equation outlined in Figure 2.3, using copy number in the equation instead of relative difference.

2.9.5 RNA Sequencing

Cell pellets from days 6,8 and 13 of 10L bioreactor cultures 184A and 184B were extracted as per methods outlined in section 2.9.1. Samples were shipped to Edinburgh Genomics for 100 bp paired end, total RNA sequencing using Nova-Seq Illumina sequencing.

2.9.5.1 RNA Sequencing Quality Check and Gene Assignment

FastQC software (Babraham Institute bioinformatics.babraham.ac.uk/projects/fastqc/) was used to check the quality of RNA sequencing data by analysing Phred scores and the percentage GC content within each sample. Gene counts were obtained using Salmon v0.11.3 based on the ENSEMBL CriGri_1.0 transcriptome (Patro *et al.*, 2017).

2.9.5.2 Differential Expression Analysis and Pathway Enrichment

Differential expression analysis was undertaken using R Studio, utilising the R/Bioconductor package DSEQ2 (Love *et al.*, 2014). Genes were considered differentially expressed if a fold change >2 was observed, and if the Benjamin-Hochberg adjusted p value was <0.1. KEGG and GO pathway enrichment was carried out in RStudio using the Bioconductor package gProfileR.

2.10 Molecular Biology Techniques to Create Stress Reporter Constructs

The following techniques were used to create and test reporter constructs to quantify ER and oxidative stresses throughout culture, where constructs are referred to as the ERSE (ER stress response element) and ARE (antioxidative response element) respectively. Plasmid maps and construction diagrams can be found in Appendix B and Chapter 6.

In short, each construct contains a stress response element which is bound by transcription factors produced within the cell in response to ER or oxidative stress. Upon being bound by these transcription factors, the stress response element drives expression of GFP which is placed downstream of the response element. GFP expression is therefore proportional to the stress response of the cell, and was measured using flow cytometry.

2.10.1 Preparation of Calcium Competent DH5α Cells

5 mL of LB media was inoculated with a colony of DH5α cells, and incubated overnight at 37°C, 200 rpm. 1 mL of this overnight culture was then used to inoculate 50 mL of LB in a 500 mL conical flask and grown to OD_{600} of 0.4-0.6, then transferred to a pre-chilled 50 mL falcon tube and centrifuged at 3500 rpm, 4°C for 15 minutes. Supernatants were then discarded and the cell pellets resuspended and in 10 mL of pre-chilled 100 mM $CaCl_2$ then incubated on ice for 30 minutes. Cells were then centrifuged as described above and resuspended in 100 mM $CaCl_2$, 15% glycerol. Cells were then dispensed in 100 µl into pre-chilled, sterile 1.5 mL sample tubes and stored at -80°C.

2.10.2 Transformation of DNA into Competent DH5α Cells

100 µL of competent cells were thawed on ice, then the total ligation mixture or 1 µL of plasmid DNA, added and gently mixed. Cells were incubated on ice for 30 minutes, then heat shocked at 42°C for 75 seconds and placed back on ice for 2 minutes. 990 µL of LB media was then added, and cells incubated at 37°C, 150 rpm for 1 hour. 200 µL of the culture was then plated onto a LB agar (1.5%) plate containing the appropriate antibiotic. LB plates were then incubated at 37°C overnight.

2.10.3 Purification of Plasmid DNA

Following transformation (section 2.11.2), a single colony was used to inoculate 5 mL of LB media with the appropriate antibiotic in. The culture was then left to grow overnight at 37°C, 200 rpm then centrifuged at 4000 rpm for 15 minutes at 4°C. The supernatant was then poured away and the cell pellet used for DNA purification using a Qiagen Mini Prep Kit (Qiagen, Hilden, Germany) following the manufacturer's protocol. The concentration of the eluted DNA was then checked using a NanoDrop.

2.10.4 Amplification of Target Sequences using Polymerase Chain Reaction

Phusion High-Fidelity DNA Polymerase (ThermoFisher, Massachusetts, USA) was used for all polymerase chain reactions (PCR), following a three-step protocol (Figure 2.4), as per the manufacturer's instructions, using 100 ng of template DNA, 0.5 µM forward and reverse primers and 10 mM dNTP mix (dATP, dTTP, dGTP, dCTP). The resultant PCR product was then analysed by agarose gel electrophoresis to confirm the presence of the desired DNA, and gel extracted for purification (2.11.5.1).

98 °C	30 sec	Initial Denaturation	
98 °C	10 sec	Denaturation	X 30 Cycles
60 °C	30 sec	Annealing	
72 °C	30 sec	Extension	
72°C	7 min	Final Extension	
4 °C	∞	Hold	

Figure 2.4: **Thermocycler Parameters for Three-step PCR Amplification of Target DNA.**

2.10.5 Agarose Gel Electrophoresis

1% or 2% agarose gels were prepared by heating 0.5 g or 1 g, respectively, in 50 mL of TAE buffer (400 mM Tris-acetate and 1 mM EDTA) until dissolved. Once cooled, 3 µL of ethidium bromide was added and the gel then cast with an appropriate comb inserted.

2.10.5.1 Purification of DNA from Agarose Gels

DNA bands were extracted from the agarose gel then weighed. DNA was then extracted using a Wizard SV Gel and PCR Clean-Up Kit (Promega, Wisconsin, United States) as per the manufacturer's instruction.

2.10.6 Restriction Digest of DNA

DNA restriction digests were carried out using FastDigest enzymes (ThermoFisher, Massachusetts, USA) or High-Fidelity enzymes (NEB, Massachusetts, USA) according to the manufacturer's instructions. Digested DNA was either separated from its DNA backbone by agarose gel electrophoresis, gel extracted and purified (as per section 2.11.5 and 2.11.5.1); or

purified in solution using a Wizard SV Gel and PCR Clean-Up Kit (Promega, Wisconsin, United States).

2.10.7 Dephosphorylation of DNA

Where required, digested DNA backbones were dephosphorylated using Thermosensitive Alkaline Phosphatase (TSAP) (Promega, Wisconsin, United States), as per the manufacturer's instructions, prior to setting up ligations.

2.10.8 DNA Ligation

All ligations were carried out using T4 DNA Ligase (Promega, Wisconsin, United States), using 3 µL of digested DNA backbone and 5 µL of insert with a total reaction volume of 10 µL as per the manufacturer's instructions. Ligations were either incubated at room temperature for 3-5 hours or at 4^{o}C over night before being used for transformations (section 2.11.2).

2.10.9 Primer and Oligonucleotide Design

Primers and oligonucleotides were designed to incorporate the required restriction sites as in Table 2.8, and were ordered from Eurofins (Luxembourg). Primers/oligonucleotides were diluted in nuclease free water to a concentration of 100 pmol/µL.

Table 2.8: **Primer and oligonucleotide sequences with incorporated restriction sites**

Primer/ Oligonucleotide name	Sequence	Restriction Sites
GFP/Mcherry F	TAT AAG CTT ATG GTG AGC AAG GGC GAG	HindIII
GFP R	ATA TCT AGA CTA CTT GTA CAG CTC GTC CAT GC	XbaI
mCherry R	ATA TCT AGA TTA CTT GTA CAG CTC GTC CAT GCC	XbaI
ARE F	TATGGTACCGTGACAAAGCACCCGTGACAAAGCACCCG TGACAAAGCACCCGTGACAAAGCACCCGTGACAAAGC ACCCGTGACAAAGCACCCGTGACAAAGCACCCGTGACA AAGCAGCTAGCTAT	MluI and XmaI
ARE R	ATAGCTAGCTGCTTTGTCACGGGTGCTTTGTCACGGGT GCTTTGTCACGGGTGCTTTGTCACGGGTGCTTTGTCAC GGGTGCTTTGTCACGGGTGCTTTGTCACGGGTGCTTTG TCACGGTACCATA	MluI and XmaI

2.10.10 Oligonucleotide Phosphorylation and Annealing

Forward and reverse oligonucleotides were phosphorylated using T4 Polynucleotide Kinase (PNK) (Promega, Wisconsin, United States) as per the manufacturer's instructions, then annealed in a thermocycler using the following programme:

- 98^{o}C incubation for 5 minutes
- temperature decrease by 2^{o}C every minute until 30^{o}C is reached
- hold at 4^{o}C

The resultant DNA fragment was then ran on a 1% DNA gel and extracted.

2.11 Utilising Stress Reporter Constructs

The stress reporter constructs created using the above techniques were tested in host CHO-S cell lines prior to being utilised in fed-batch over-grow culture for cell lines:

- 109 (producing mAb 109 – the same cell line used in 10L disposable bioreactor work)
- AB001 (producing mAb AB001 – an IgG1)
- 2223 (producing mAb 4212)
- 2491 (producing mAb 4212)

Note that neither cell line 2223 or 2491 is the same as that used in previously outlined roller bottle or bioreactor culturing.

During initial testing in the CHO-S cell line cells were transfected with ERSE or ARE stress reporter constructs, using an electroporation technique, then cultured in a 24 well plate format. Cells were then left to recover for 18 hours, and supplemented with tunicamycin or t-BHQ to chemically induce ER or oxidative stress respectively. Flow cytometry was then used to quantify GFP expression at T=0, 6 hours and 24 hours after tunicamycin or t-BHQ was added. Control cultures containing no drug were also analysed at each time point.

2.11.1 Initial Stress Reporter Construct Testing

Cells transfected for initial construct testing were cultured in a 24 well plate format, where culture volumes were 1 mL. This work was carried out at the University of Kent, and so CD-CHO Medium (ThermoFisher Scientific, London, UK) was used for the work described below, rather than AstraZeneca 's proprietary media which has been used in all other cell culture work. To test the ERSE and ARE reporter constructs, cells were treated with two concentrations of

tunicamycin or t-BHQ to chemically induce ER and oxidative stress respectively, as described below.

2.11.1.1 Transient Transfection of CHO-S Cells using Electroporation

$1x10^7$ viable cells were transfected for each well with 20 µg of plasmid DNA per well, where the DNA was diluted to a concentration of 200 ng/µL in 100 µL of TE buffer. Cells were centrifuged at 400 xg for 5 minutes, then the resultant supernatant poured off. The remaining cell pellet was resuspended in 700 µL of media and 20 µg of plasmid DNA added, then transferred to a 0.4 cm Gene Pulser Electroporation Cuvette (BioRad) to be electroporated using the BioRad Gene Pulser Xcell Electroporator using the following parameters: 300 V voltage, 960 µF capacitance and ∞resistance. 500 µL of transfected cells were added per well in a 24 well plate and placed in a static incubator at 37°C for 18 hours.

2.11.1.2 Initial Reporter Construct Testing using Tunicamycin and t-BHQ

Following transfection, cells were treated with tunicamycin or t-BHQ to chemically induce ER or oxidative stress respectively. For each drug, two concentrations were added to compare the stress response between samples. Each drug was dissolved in media with a final DMSO quantity of 0.2%, to give a final culture volume of 1 mL and DMSO content of 0.1% once supplemented. Media with DMSO only was added to control samples to give a final volume of 1 mL. For cells treated with tunicamycin, a concentration of 6 µM or 12 µM was added, and 50 µM or 100 µM for t-BHQ treated samples.

2.11.1.3 Flow Cytometry Analysis of Transfected Samples

Cells were taken from the relevant well and pelleted for flow cytometry analysis by centrifugation at 400 xg for 5 minutes. The resultant cell pellet was then resuspended in 1 mL PBS, then pelleted again. This final pellet was then resuspended in 500 µL of PBS and used for analysis. Samples were analysed for GFP and mCherry expression using a FACS Jazz instrument (BD, New Jersey, USA), acquiring 10,000 events per sample. Untreated and non-transfected samples were used to 'gate' scatter plots and histograms to ensure that only viable cells were analysed. The resultant data was then analysed using BD FACS Software 1.2.0.142.

2.11.2 Utilising Stress Reporter Constructs During Fed-Batch Overgrow Culture

All cell culture work utilising the ARE reporter construct in fed-batch overgrow culture was carried out at AstraZeneca , using proprietary feeds and media. Cell lines 109, AB001, 2223 and 2491 were transfected in triplicate on days 3, 6 and 11 of culture with the ARE reporter construct

to assess cellular oxidative stress responses on days 4, 7 and 12 of culture using FACS analysis. Nine 30 mL cultures were seeded at 0.5 x10^6 cells/mL for each cell line, and were labelled A-I. For each cell line the following cultures were therefore analysed at each time point: A,B and C were transfected on day 3 to be analysed on day 4, cultures D, E and F transfected on day 6 to be analysed on day 7 and cultures G, H and I transfected on day 11 and analysed on day 12. At transfection time points, each 30 mL culture was split in half, where one half was transfected with the ARE construct, and the other to be analysed for oxidative stress using a commercial stain. At each time point a positive control sample was prepared for both the transfected samples and stained samples, through treating 0.5 x10^6 cells with 200 µM TBHP as per the instructions for the commercial staining kit.

2.11.2.1 Transient Transfection of mAb Producing CHO Cell Lines Using PEI

Polyethylenimine (PEI) was used to chemically transform the 15 µg of ARE reporter plasmid into 15 mL of culture as per a standard AstraZeneca in-house protocol.

2.11.2.2 Flow Cytometry Analysis of Transfected Samples

0.5 x10^6 viable transfected cells were pelleted by centrifugation at 400 xg for 5 minutes. The resultant cell pellet was then resuspended in 500 µL of media. For positive control samples, 0.5 x10^6 cells were taken and incubated with 200 µM TBHP for 1 hour at 37°C. These samples were then pelleted and prepared in the same way as above.

Flow cytometry was carried out using a BDCanto flow cytometer, with the BD FACSDiva software, acquiring 10,000 events per sample. Untreated and non-transfected samples were used to 'gate' scatter plots and histograms. FlowJo software was used to plot and analyse histograms and scatter plots, and for statistical analysis.

2.12 Assessing Oxidative Stress During Fed-Batch Overgrow Culture Using a Commercial Cell Staining Kit

At each analysis time point (days 4, 7 and 12), 0.5 x10^6 cells were taken from un-transfected cultures to be stained using a CellROX Green kit (Invitrogen, California, USA) and were prepared as per the manufacturer's instruction.

2.13 Sample and Buffer Labelling Throughout this Thesis

Cell lines and mAbs used in Chapters 3, 4 and 5 are referred to as follows:

- Cell line 109, producing mAb 109
- Cell line 4212, producing mAb 4212
- Cell line 184, producing mAb 184

Harvest days in Figures are referred to as 'DX' where X is the day of culture, for example roller bottle fed-batch material was harvested on D9 and D13 of culture; and 10 L bioreactors on D8 and D13.

Biological replicates of 10 L bioreactor material are referred to as A, B and C; for example, 3 cultures were ran for cell line 109, denoted as 109A, 109B and 109C.

Buffers are referred to as the following (where 'arg' always refers to arginine-HCl):

- 80 mM arginine-HCl, 120 mM sucrose, 20 mM histidine pH 6.0 = 80 mM arg
- 190 mM arginine-HCl, 20 mM histidine pH 6.0 = 190 mM arg
- 160 mM arginine-HCl, 20 mM histidine pH 6.0 = 160 mM arg

Time points analysed during stability studies are referred to as T = X where X is the time point; for example, at 40^{o}C material was analysed at T = 1 month and T = 3 months. In Figures months is abbreviated to 'mth'.

In Chapter 6, the following cell lines were used and are referred to as follows, where mAb 4212 producing cell lines are not the same as 'cell line 4212' used in chapters 3 and 4:

- Cell line 109, producing mAb 109 (the same cell line as in Chapter 4)
- Cell line AB001, producing mAb AB001 (an IgG1)
- Cell line 2223, producing mAB 4212
- Cell line 2491, producing mAb 4212

Nine cultures were run for each cell line, denoted as A – I.

Chapter 3

Application of ER Stress Biomarkers to Predict Formulated Monoclonal Antibody Stability

Natalie E. Talbot[1], Emma J. Mead[1], Stephanie A. Davies[2], Shahid Uddin[2], C. Mark Smales[1]*

[1] Industrial Biotechnology Centre and School of Biosciences, University of Kent, Canterbury, Kent CT2 7NJ

[2]AstraZeneca , Milstein Building, Granta Park, Cambridge, CB21 6GH

DOI: 10.1002/biot.201900024

Key Words: Biomarkers; Bioprocess linking; Monoclonal Antibody; Stability; Sub-visible particles

3.1 Declaration of Contribution

The work described in this chapter has been published (doi: 10.1002/biot.201900024). All experimental work was planned, conducted and analysed by myself, with the exception of titre quantification which was completed by Andrew Smith at AstraZeneca . The listed co-authors helped with the design and analysis of experiments and were involved in editing the transcript.

The aim of this work was to investigate the impact of harvest day on formulated mAb stability, and to generate mRNA biomarker profiles for each cell line to understand how ER stress changes across culture, between fed-batch and batch conditions, and to compare profiles between cell lines.

For the purpose of this thesis, section and Figure numbers have been modified from the published version to allow accurate cross referencing throughout.

Please note that for the purpose of publication the two cell lines/mAbs used throughout this work were anonymised. Cell line/mAb A = 4212 and Cell line/mAb B = 184.

3.2 Abstract

For a therapeutic mAb to reach the clinic, the molecule must be produced at an appropriate yield and quality, then formulated to maintain efficacy and stability. The formation of sub-visible particles (SVPs) can impact on product stability and is monitored during formulation development however, the potential of a mAb to form such species can be influenced throughout the whole bioprocess. We investigate levels of intracellular ER stress perceived by cells, day of mAb harvest and the relationship to subsequent product stability of two mAbs (denoted A and B), produced in CHO cell lines, as determined by SVP content after accelerated stability studies. We show the propensity of mAb A to form SVPs can be predicted by transcript expression of biomarkers of cellular ER stress, heavy/light chain transcript and polypeptide amounts, and harvest day. Further, mAb A material harvested on day 9 of culture was more stable, in terms of SVP formation, than material harvested on day 13. These data suggest that ER stress perceived by CHO cells during culture can reflect the stability of a mAb, and that biomarkers of such stress could help define culture harvest time as a tool to control or reduce SVP formation in formulated mAbs.

3.3 Introduction

Chinese hamster ovary (CHO) cells are the expression system of choice for producing therapeutic monoclonal antibodies (mAbs) (Lai *et al.*, 2013; Wurm, 2004) largely due to their ability to undertake human-like post-translational modifications and their ability to achieve titres

exceeding 10 g/L (Gronemeyer *et al.*, 2014). However, in order for a therapeutic mAb to reach the clinic, it is not only necessary to produce the molecule at an appropriate yield and quality, but also to develop a product with a suitable mode of delivery, dosage and shelf life. Establishing an appropriate formulation is therefore key in maintaining the stability and quality of a drug product during storage, whilst also ensuring that the dosage is safe and efficacious when administered to patients.

Soluble aggregation, sub-visible particle (SVP) formation and fragmentation are among a range of product quality attributes which are monitored during bioprocessing and formulation development. These characteristics are also reported in data packages submitted to regulatory authorities as part of drug approval procedures. It has been reported that the presence of aggregates and particles in mAb formulations have the potential to cause autoimmune responses in patients and can impact on drug safety and activity (Ratanji *et al.*, 2014; Manning *et al.*, 1989; Manning *et al.*, 2010; Roberts, 2014; Singh *et al.*, 2010). As a result, the monitoring and control of aggregates during fermentation, downstream processing and formulation development is important for ensuring the safety and efficacy of mAbs destined for use in the clinic. Whilst the formation of subvisible particles may be monitored at different stages of the whole bioprocess, the greatest emphasis on monitoring is during formulation development. Thus, although mAb stability and propensity to form SVPs can be potentially influenced throughout bioprocessing, it is somewhat surprising that there have been few studies that look to establish a link between upstream bioprocessing, formulation development and SVPs as a measure of product stability.

The production of a mAb is typically divided into three stages; upstream culturing, downstream purification and formulation/fill finish. Traditionally these processes have been considered independent, however there is a growing appreciation that the entire bioprocess should be considered as a whole (Gronemeyer *et al.*, 2014; Rathore *et al.*, 2015; Torkashvand and Vaziri, 2017), including how upstream and downstream processes may impact product quality before the material is provided to the formulation scientist. During upstream culturing, endoplasmic reticulum (ER) stress can be induced via amino acid or glucose deprivation, high recombinant protein load and the accumulation of unfolded/misfolded proteins (Rutkowski and Kaufman, 2004; Roy *et al.*, 2017; Harding *et al.*, 2003; Hetz, 2012). Such stress is responded to via the activation of the unfolded protein response (UPR) and ER associated degradation (ERAD). These pathways serve as quality control mechanisms to maintain homeostasis through relaying information from the ER lumen to the nucleus, enabling cells to adapt to, remove and prevent the build-up of misfolded/unfolded proteins. Alternatively, the UPR will trigger cell death in the

event of unresolvable stress (Zolls *et al.*, 2012; Szegezdi *et al.*, 2006; Schroder, 2006; Schroder, 2008; Chakrabarti *et al.*, 2011; Bravo *et al.*, 2013; Sano and Reed, 2013a). These quality control mechanisms are often activated in CHO cell lines producing high quantities of recombinant material (Cudna and Dickson, 2003; Schroder, 2008; Schröder and Kaufman, 2005), and as a result ER stress can impact cell growth and productivity. In turn, such stress may affect protein folding, assembly and post translational modifications (such as glycosylation patterns) leading to aggregate and/or fragment formation which can compromise product quality and ultimately impact the stability of final product (Torkashvand *et al.*, 2015; Torkashvand and Vaziri, 2017; Ho *et al.*, 2015a; Ishii *et al.*, 2014). Thus, the impact of the bioprocess on product quality should be considered when material is provided to the formulation scientist.

Previous studies have reported ER stress experienced by cells during culture through the use of mRNA biomarker profiling. Such studies have demonstrated that CHO cells grown under both batch (Prashad and Mehra, 2015; Maldonado-Agurto and Dickson, 2018) and fed-batch (Roy *et al.*, 2017) conditions are under increased stress as cultures progress. Surprisingly however, the relationship between increased culture stress and the stability of formulated mAbs has, to date, not been examined. Here, we use two industrial CHO cell lines expressing different mAbs to determine the ER stress response profile under fed-batch and batch conditions. Subsequently, we investigate the stability of the formulated mAbs harvested during different stages of culture, and therefore produced when cells are experiencing different levels of stress, by monitoring soluble aggregate, fragment and SVP formation. Our studies show that the two mAb producing cell lines elicit differing ER stress response profiles, and that these profiles change as cultures progress. Importantly, we show that for one of the two mAbs studied, harvest day has a pronounced impact on formulated mAb stability, as determined by SVP formation. More specifically, we show that mAb A material from an early (day 9) harvest, when ER stress is lower, forms significantly fewer SVPs than that from a late (day 13) harvest, when biomarkers of ER stress are elevated.

3.4 Materials and Methods

3.4.1 Cell Culture

Two AstraZeneca suspension CHO cell lines, each expressing a model monoclonal antibody (mAb) were used in this study. For the purposes of this study these are denoted as cell line A which produced mAb A, an IgG1, and cell line B which produced mAb B, an IgG2. To generate material for mRNA profiling and stability studies, un-fed batch and fed-batch cultures were run

for each cell line using AstraZeneca proprietary media and feed. Cultures were seeded at a concentration of 0.5 x10^6 viable cells/mL and maintained in roller bottles (Coring, USA) under the following conditions; shaking at 140 rpm, 70% relative humidity and 4% CO_2. Half of the fed-batch cultures were harvested on day 9 of culture (denoted early harvest) and the remaining harvested on day 13 (denoted late harvest). Supernatant material was harvested by centrifugation at 10,000 x g for 20 minutes at 4oC. Cell concentrations and culture viability were determined daily using the trypan blue exclusion method on a ViCell Beckman Coulter instrument (CA).

3.4.2 Determination of Monoclonal Antibody Concentrations

Concentrations were determined using protein A HPLC as previously reported (Daramola *et al.*, 2014).

3.4.3 Sampling of Cells for mRNA and Protein Analysis

Viable cell pellets of 2x10^6 or 1x10^7 cells were collected for mRNA and protein analysis respectively on each day of culture from day 3 onwards. Cells were sampled by centrifugation at 8000 x g for 5 minutes at 4^{o}C. Pellets were snap frozen on dry ice and stored at -80^{o}C.

3.4.4 Purification of Monoclonal Antibody from Cell Culture Supernatant

mAb material was purified using protein A chromatography following AstraZeneca 's in-house protocol which utilizes a low pH elution step. The pH of the eluted material was adjusted to pH 5.5 and 0.22 µm sterile filtered under vacuum (Millipore). All material was then stored at -80^{o}C.

3.4.5 Formulation of Protein A Purified mAb Material

The purified mAb material was thawed and buffer exchanged using centrifugal concentrators (Millipore) into two buffers. mAb A material was buffer exchanged into either 20 mM histidine, 160 mM arginine-HCl, pH 6.0 or 20 mM histidine, 80 mM arginine-HCl, 120 mM sucrose, pH 6.0. MAb B material was buffer exchanged into either 20 mM histidine, 80 mM arginine-HCl, pH 6.0 or 20 mM histidine, 240 mM sucrose, pH 6.0. The material was then concentrated to 20 mg/mL and 0.22 µm sterile filtered (Millipore) before aliquoting 1.5 mL into 3 mL glass vials.

Formulations used in this study were selected based upon previous work and knowledge of the selected IgGs at AstraZeneca .

3.4.6 Sub-Visible Particle Counting

Micro Flow Imaging (MFI) was carried out using a MFI 5200 (Protein Simple) to count SVPs in formulated mAb samples ranging in size from 1 to 100 µm. Prior to analysis, the MFI system was primed with 150 µL of sample, then 500 µL of sample analysed. An aspect ratio of >0.85 was applied to omit any spherical species (such as bubbles) from the data set.

3.4.7 Analysis of Aggregate, Fragment and Monomeric Species

mAb samples were analysed for monomer, aggregate and fragment content using isocratic Size Exclusion High Performance Liquid Chromatography (SEC-HPLC) using a TSKgel G3000SWXL column (Tosoh Bioscience) attached to an Agilent HPLC 2100 system. 25 µL of each sample was injected, and the absorbance monitored at 280 nm. The resultant chromatograms were integrated to establish the percentage of soluble aggregate, monomer and fragment species present.

3.4.8 Total RNA Extraction and DNAse Treatment

Cell pellet samples were thawed into RLT buffer (Qiagen) and RNA extracted using an RNeasy kit with shredder columns and on column DNAse treatment (Qiagen). The eluted RNA was diluted to a concentration of 25 ng/µL.

3.4.9 mRNA Expression Analysis by qRT-PCR

Qiagen QuantiFast SYBR Green RT-PCR kits were used for qRT-PCR as previously described [30]. The expression for each gene of interest (GOI) was then compared to that of glyceraldehyde 3-phosphate dehydrogenase (GAPDH), an endogenous control, and the change in expression of each sample calculated using the ΔΔCt method [31]. An average ΔΔCt across biological repeats was established and normalised to day 3 samples to calculate a fold change in expression for each GOI. Linear regression analysis was then carried out using Minitab17 software (version 17.3.1) to assess the relationship between sample day and fold change in GOI expression. The R2 value and statistical significance ($P < 0.05$) of this relationship was determined for each

transcript. To assess HC and LC transcript copy numbers a standard curve was generated, using plasmid DNA as the template, to extrapolate transcript copy numbers from. Primer sequences used for qRT-PCR experiments are listed in Supplementary Table 3.1. GOI for qRT-PCR experiments were selected based upon previous studies [12, 27-28] that also used qRT-PCR to analyse the fold change of genes related to ER stress.

3.4.10 Western Blotting to Determine Intracellular HC and LC Protein Expression

Cell pellets were re-suspended in 2 mL of lysis buffer as described by Mead et al (Mead *et al.*, 2015). Equal volumes of cell lysate from each sample were then analysed by SDS-PAGE using a standard protocol (Laemmli, 1970). A 'wet blotting' technique was used to transfer proteins onto a nitrocellulose membrane. Membranes were blocked using 5% w/v milk powder in Tris-buffered saline before washing the membrane and addition of an appropriate horseradish peroxidase (HRP) conjugated primary antibody (anti-human IgG or anti-human lambda light chain, The Binding Site, both diluted 1:20,000) for chemiluminescence detection. Membranes were incubated in primary antibody solution for 18 hours at 4^{o}C. Densitometry analysis of bands was performed using ImageJ 1.50i software (Schneider *et al.*, 2012). Sample loading was normalised to total protein expression using corresponding Coomassie stained gels (Supplementary Figure 3.3).

3.5 Results

A number of studies have assessed changes in gene expression profiles throughout culture of IgG producing CHO cell lines (Tamosaitis and Smales, 2018). Of particular relevance to the work reported here are those that report changes in gene expression related to UPR and ERAD pathways. For example, Prashad and Mehra (2015) compared the mRNA expression of 17 genes within these pathways between high and low recombinant protein producing cell lines grown under batch conditions. A more comprehensive study by Maldonado-Agurto and Dickson (2018) assessed a panel of 27 genes throughout batch culture and investigated the impact of prolonged cell culture on the UPR and ERAD pathways, as well as evaluating the impact of chemically induced ER stress. Both studies showed that during prolonged batch culture, cells experience increased ER stress as culture duration progressed. Surprisingly, there has been little work relating cellular UPR stress, day of culture and final formulated antibody stability despite the fact that it is known that cellular stress can impact on the quality of recombinant protein produced. We have therefore compared the profile of key UPR and ERAD transcripts between batch and fed-batch conditions of mAb producing CHO cell lines to determine the degree of such

stress perceived by the cell during culture. Importantly, we have then related these biomarker profiles to the subsequent stability of Protein A purified mAb harvested at different stages of culture, when the cells were under different UPR and ERAD stress as determined from the transcript profiles.

3.5.1 Analysis of mAb Producing CHO Cell Line Growth and Productivity Characteristics

To compare the UPR and ERAD response of the model cell lines between fed and batch conditions, and to generate mAb material harvested at different points of culture, 6 fed-batch and 2 batch cultures were run for each cell line. Under batch culture conditions, the two cell lines had similar growth profiles, product yields and cell specific productivities (Qp) (Figure 3.1 and Supplementary Table 3.2). Both cell lines reach a maximum average viable cell concentration on day 6 of culture, being 9.6 $x10^6$ cells/mL for cell line A and 10.0 $x10^6$ cells/mL for B. After this point, both cell lines entered a decline phase with culture viabilities dropping from 92% on day 6 to 81% on day 7 for A, and 92% to 72% for B. By day 10 of culture, when the cultures were terminated, viabilities were 25% and 41% for A and B respectively (Figure 3.1). The majority of the material was produced over the first 7 days with only a small increase in product yield after an additional 3 days of culture for both cell lines. Qp was similar between cell line A (0.7 pg/cell/day) and B (0.5 pg/cell/day) (Supplementary Table 3.2).

The viable cell concentrations under fed-batch conditions for both cell lines were considerably higher than those under batch conditions. There was also a notable difference between growth profiles and mAb production for the two cell lines (Figure 3.1). Cell line A fed-batch cultures reached the end of growth phase on day 6, when cultures were 98% viable and had a maximum viable cell concentration of 21.0 $x10^6$ cells/mL, on day 9 of culture. After this the number of viable cells declined, although the culture viability declined from day 6 and was 50% when cultures were terminated on day 13. Although this is lower than might be used in a commercial industrial setting, this culture viability was considered appropriate for establishing whether there was a correlation between culture day/viability and the stability of the subsequent mAb material as assessed from the propensity to form SVPs.

Cell line B reached the end of growth phase one day later on day 7, but attained a much lower maximum viable cell concentration of 14.5 $x10^6$ cells/mL. This cell concentration was maintained in cell line B until the end of culture (Figure 3.1). On day 13, the culture viability had decreased to 61%. This difference in viable cell concentrations meant that the IVCD of cell line A over the 13 day fed-batch culture was approximately 1.35 times that of cell line B (Supplementary Table

3.2). With regard to mAb production, cell line A produced a titre of 2308 mg/L on day 9 and 2907 mg/L on day 13, whilst cell line B had a titre of 1665 mg/L on day 9 and 2445 mg/L on day 13 (Supplementary Table 3.2). Thus 79% of total mAb material was produced in the first 9 days of culture for cell line A, whilst 68% of the material in cell line B was produced in the first 9 days. Further, although the overall yield of mAb from cell line A was higher than cell line B, under fed-batch conditions, the Qp of cell line B was 1.7x that of cell line A (14.2 pg/cell/day compared to 8.3 pg/cell/day).

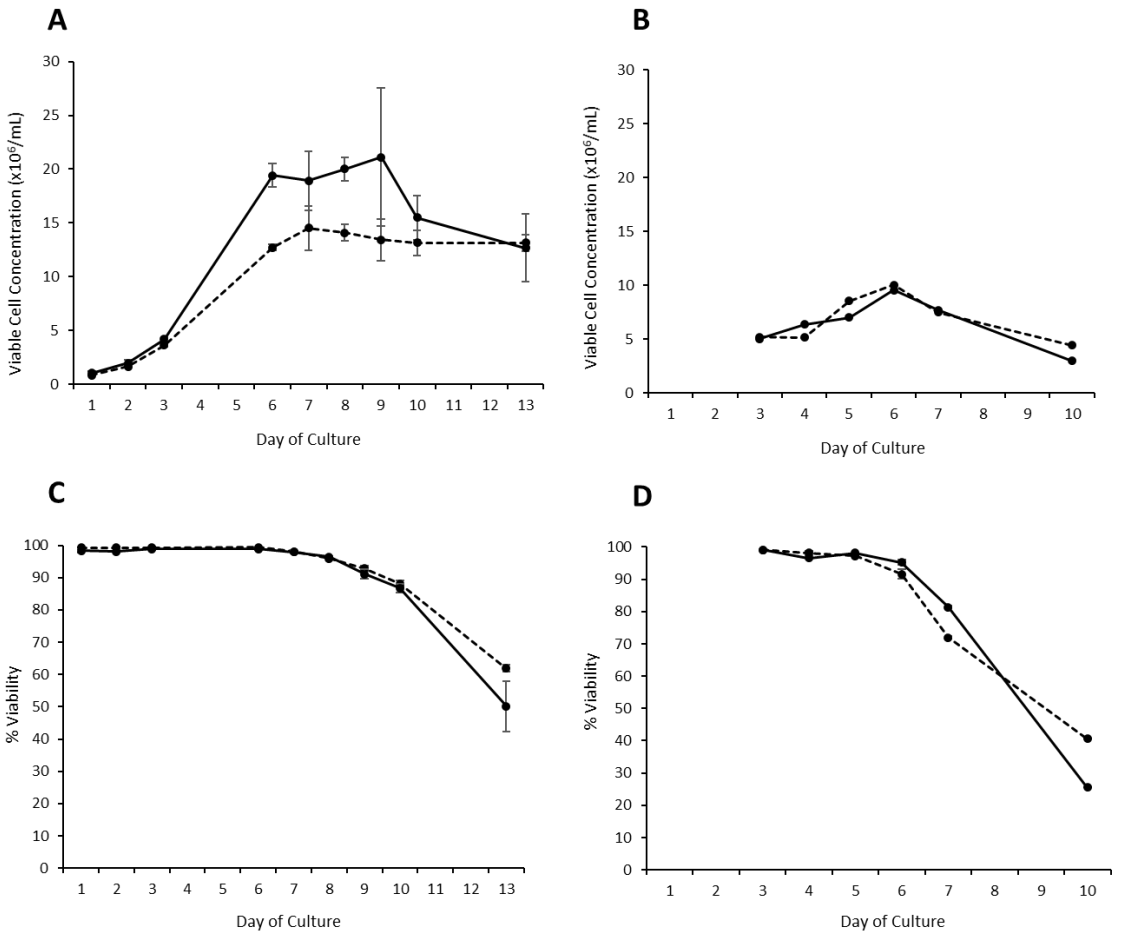

Figure 3.1. Growth Characteristics of Cell Lines Under Fed-Batch and Batch Conditions. Where solid lines represent cell line A and dashed lines cell line B. (**A**) fed-batch viable cell concentration, (**B**) batch viable cell concentration, (**C**) fed-batch percentage viability and (**D**) batch percentage viability. Fed-batch cultures were harvested in triplicate on day 9 (early harvest) and day 13 (late harvest) of culture, then the material purified for subsequent stability studies to compare mAb stability between an early and late harvest. Cultures were sampled daily from day 3 onwards for mRNA and protein expression analysis. Error bars represent the mean +/- one standard deviation.

3.5.2 Profiling of ER Stress mRNA Transcript Biomarkers

In order to link upstream stress during synthesis of mAb in the cell with stability when formulated and harvest day, it was necessary to first establish that the model cell systems here did indeed perceive different levels of stress throughout culture. It is well established that increased recombinant protein production can contribute to ER stress (Hetz, 2012; Maldonado-Agurto and Dickson, 2018; Prashad and Mehra, 2015; Rutkowski *et al.*, 2006; Rutkowski and Kaufman, 2004), we therefore assessed ER stress in our model cell lines throughout culture using qRT-PCR to monitor the expression of 11 genes (summarised in Table 3.1) as 'biomarkers' of ER stress relative to the expression of glyceraldehyde 3-phosphate dehydrogenase. We then analysed this data by linear regression analysis, where a greater R^2 value indicates a stronger relationship between two variables (Supplementary Figure 3.1). A change in the amount of a target transcript was considered statistically significant when p <0.05, with the results being compared between culture conditions (fed-batch and batch) and cell lines. All significantly changing genes were found to be upregulated as cultures progressed, indicating increased ER stress.

More ER biomarker transcripts were found to be significantly upregulated in expression over culture under batch conditions than fed-batch (5 for batch and 4 for fed in cell line A, 7 and 3 respectively for cell line B, Table 3.1). In both cell lines, the expression of *atf4, ragc* and *rpn1* transcripts was significantly increased during batch cultures compared to fed-batch cultures. *Chac1* and *hspa9* expression was also significantly increased as culture progressed under batch conditions compared to fed-batch in cell line B cultures but not cell line A. Therefore, the number of ER stress related genes significantly upregulated in batch samples compared to fed-batch was increased, indicating that cells grown under batch conditions were under greater ER stress than those cultured under fed conditions.

Under fed conditions, *calreticulin* and *herpud1* were the only two ER biomarker transcripts that significantly increased in expression throughout culture for both cell lines A and B. A significant increase in *bip* and *hsp90b* expression was observed in cell line A only under fed-batch conditions, while *derl3* expression increased in cell line B only. The magnitude of the change of each of these transcripts is depicted in Supplementary Figure 3.2.

Table 3.1: Summary of Linear Regression Analysis for each gene of interest (GOI) and function of the corresponding proteins. Fold change in expression for each GOI was analysed using qRT-PCR, then used in linear regression analysis to build a model predicting how the GOI expression changed with culture conditions and day as a marker of ER stress. One-way ANOVA was then used to evaluate those genes of interest significantly change over culture, where * denotes a significance level of P <0.05, and ** denotes P <0.01. The fold change in expression increased throughout culture for all genes of interest. Data from days 3, 6, 7, 8, 9 10 and 13 were analysed for fed samples, and days 3, 4, 5, 6 and 7 for batch.

Gene of Interest	Encoded Protein Function	Cell Line A		Cell Line B	
		Fed	Batch	Fed	Batch
ATF4	Transcription factor reported to enhance the expression of UPR related targets such as CHOP and GADD34		*		**
BIP	Hsp70 molecular chaperone, functioning to retain proteins in the ER until appropriately folded	*	*		**
Calreticulin	Functions as a chaperone to aid folding of glycoproteins, as well as being involved in calcium storage in the ER	*	**	**	
Chac1	Pro-apoptotic protein which functions as part of the UPR; expression of chac1 is activated by ATF4				*
Derl3	Member of the Derlin family, functions as part of the ERAD response to translocate misfolded proteins for degradation			**	*
HerPud1	Functions as part of the ERAD pathway to maintain ER homeostasis	*		*	
Hsp90b	Member of the heat shock family of proteins, functions sequentially with BiP as a chaperone to aid the folding of proteins	*			
Hspa9	Hsp70 family member, found in the mitochondria and ER				*
Pfdn2	One of four beta subunits which comprise Prefoldin; a chaperone which assists the folding of newly synthesised polypeptides				
RagC	Regulates mTOR signalling.		*		*
Rpn1	Forms part of the regulatory 26S Proteasome subunit and is therefore involved in the ERAD response		**		*

3.5.3 Analysis of mAb Heavy and Light Chain Expression at the Transcript and Protein Level

The abundance of HC and LC transcripts and polypeptides within CHO cell lines producing IgGs has previously been investigated (Maldonado-Agurto and Dickson, 2018; Prashad and Mehra, 2015), with some groups establishing a relationship between increased HC:LC ratios and productivity (Lee *et al.*, 2009b; Li *et al.*, 2007; Wijesuriya *et al.*, 2018; Schlatter *et al.*, 2005; Ho *et al.*, 2013) and other studies linking HC:LC ratios to aggregate formation (Ho *et al.*, 2013; Ho *et al.*, 2015b). Increased HC polypeptide expression can result in ER stress, as excess HC polypeptides are retained in the ER for re-folding or degradation by molecular chaperones such as BiP and Hsp90b if they are unable to assemble with the LC (Feige *et al.*, 2010b). As we wished to link industrially relevant upstream cellular stress with formulated mAb stability, we therefore investigated fed-batch culture samples for HC and LC intracellular expression at the transcript and polypeptide level.

HC:LC transcript copy number ratios were analysed between cell lines A and B under fed and batch conditions (Figure 3.2 and Supplementary Table 3.3). For cell line A, *HC* transcript numbers were significantly higher than those for the *LC* on every sample day under batch and fed-batch conditions, with the exception of day 13 for fed-batch cultures (Figure 3.2). Fed-batch *HC* transcript numbers peaked on day 9 at 2.9 $x10^4$ transcripts per cell compared to the *LC* which also peaked on day 9 at 6.1 $x10^3$ transcripts per cell. Batch culture *HC* transcript numbers reach a maximum of 1.5 $x10^4$ transcripts per cell on day 6, when *LC* transcript numbers were low. Cell line B on the other hand, had greater *LC* transcript numbers than *HC* under both fed and batch conditions. Thus, cell line A had a much higher amount of *HC* mRNA than *LC*, whilst cell line B had a higher amount of *LC* transcript than HC (Figure 3.2).

Intracellular polypeptide amounts were analysed by western blotting which allows relative changes in HC or LC to be assessed throughout culture and between the two cell lines using densitometry (Figure 3.3). The profile of intracellular HC expression at the polypeptide level during fed-batch culture (Figure 3.3) was consistent between the two cell lines throughout culture. HC expression increased for both cell lines approximately 7-fold by day 13 of culture relative to day 3. There was no significant change in HC polypeptide expression between days 6, 7 and 8 however, a significant fold change was observed between days 8 and 9 for both cell lines. There were obvious differences in LC polypeptide expression during fed-batch culture between the two cell lines. Cell line B showed a greater change in the amount of LC present relative to day 3 throughout culture, whilst there was a dramatic 3-fold increase in LC

polypeptide expression between days 8 and 9 of culture in cell line B which was not observed in cell line A samples (Figure 3.3).

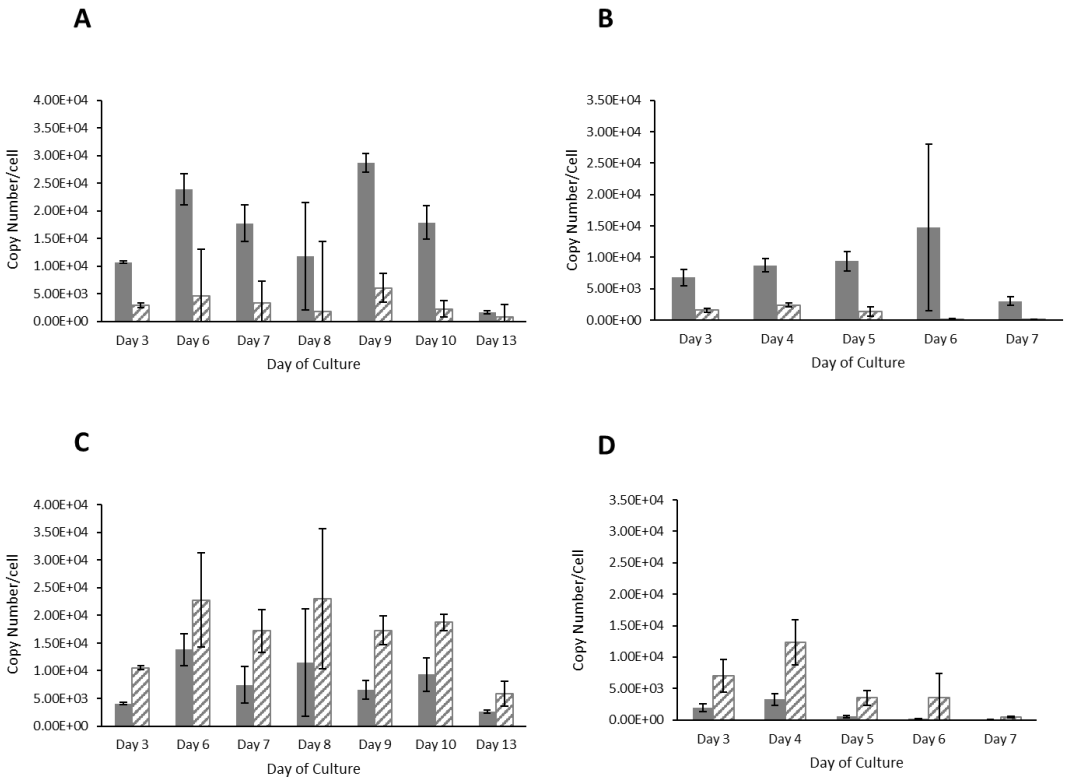

Figure 3.2. HC and LC Transcript Copy Numbers Produced in Cells Under Fed-batch and Batch Conditions. Cell line A fed-batch (**A**) and batch (**B**) cultures; and cell line B fed-batch (**C**) and batch (**D**). Copy numbers were established using qRT-PCR with a DNA standard curve. Solid bars show heavy chain transcript copy numbers, and striped bars show the light chain. Error bars are the mean +/- one standard deviation.

Differences between *HC* and *LC* transcript expression in the two cell lines was partially reflected at the polypeptide level, with *LC* transcript amounts, and the increase in LC polypeptide throughout culture compared to day 3, higher in cell line B than cell line A. This was less pronounced for the relationship between *HC* transcript copy numbers and HC intracellular polypeptide. Although there was more *HC* transcript in cell line B than A, the change in HC polypeptide compared to day 3 in both cell lines showed a similar increase between day 8-9, even though *HC* transcript numbers were similar across days 6-10 of culture (Figure 3.3). Comparing the polypeptide and transcript data for cell line A, *HC* transcript numbers were consistently higher than *LC*, however at the polypeptide level it was only from day 9 that HC expression was higher than earlier days. Further, for early harvest material (day 9), intracellular HC amounts at the polypeptide level increased similar to that of the LC up to this point, compared to the late harvest (day 13), for which HC amounts were elevated from day 9 compared to earlier days (Figure 3.3). For mAb B, generated from cell line B, that did not show

an increase in particle numbers with harvest day (see below), there was less variation in *HC* or *LC* transcript (or polypeptide) amounts between the two harvest days.

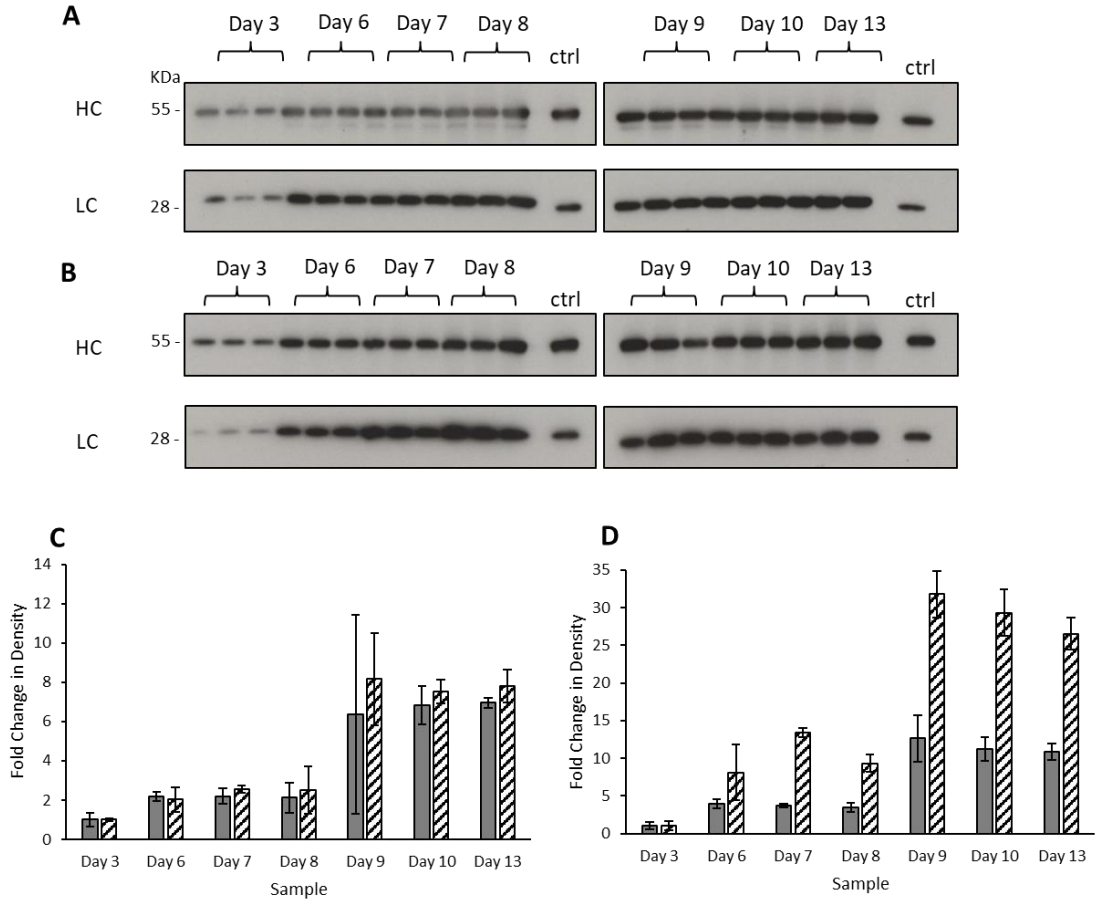

Figure 3.3. Intracellular HC and LC Polypeptide Expression. Western blotting of fed-batch cell lysates for (**A**) cell line A and (**B**) cell line B, and (**C**) densitometry analysis comparing HC polypeptide expression and (**D**) LC polypeptide expression. Solid bars show cell line A, and striped bars show cell line B. Error bars represent the mean +/- one standard deviation.

3.5.4 Effect of Harvest Day during Fed-Batch Culture on Monoclonal Antibody Stability

The main focus of this study was to investigate whether a relationship exists between increased intracellular ER stress experienced during CHO cell culture, day of harvest and formulated product stability. As the model cell lines used in this study did show differences in both ER stress responses and HC/LC expression throughout culture, we set out to determine if these observations related to the stability of formulated mAbs as determined by the propensity of the material harvested at different times throughout culture to form SVPs. We thus investigated mAb stability by evaluating soluble aggregate, fragment and SVP formation over time under

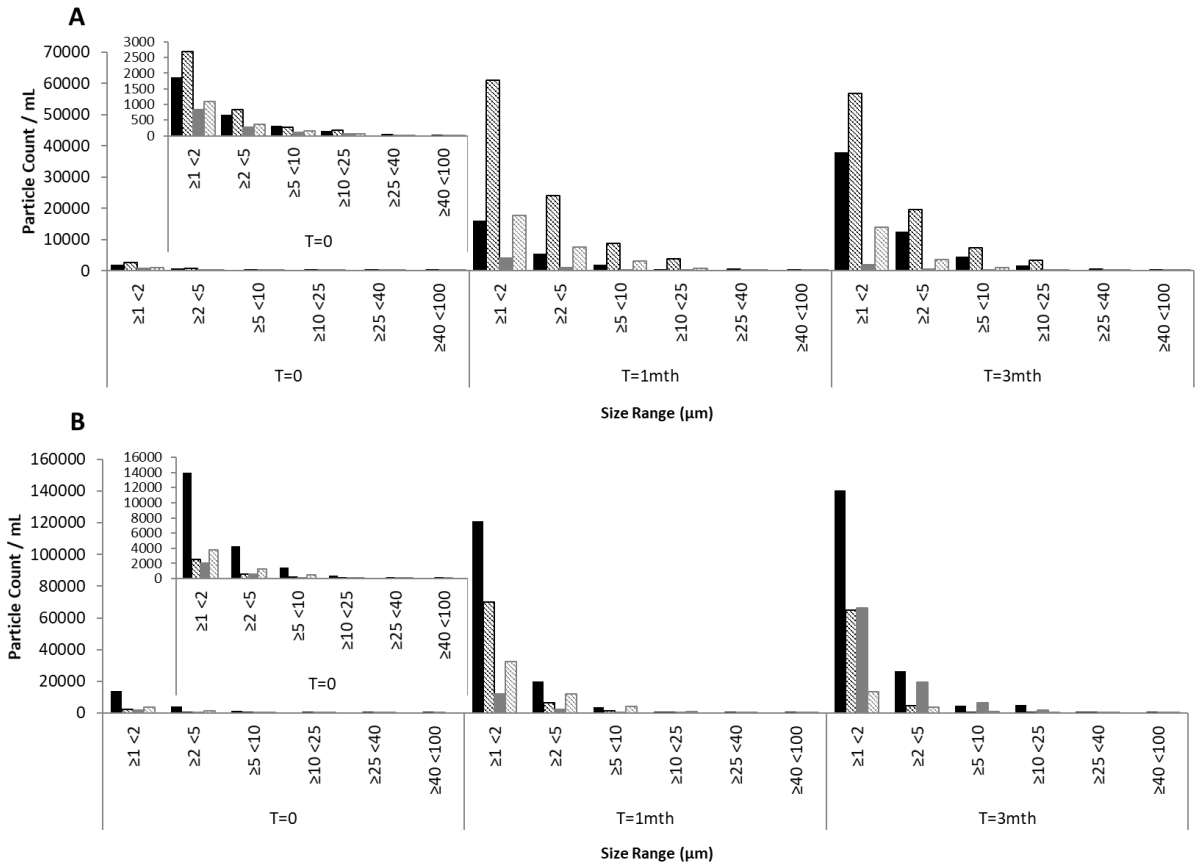

Figure 3.4. Sub-Visible Particle Formation of Formulated mAb Determined by MFI Analysis. Sub-visible particle counts per mL of (**A**) mAb A, where darker bars represent material formulated in 20 mM histidine, 80 mM arginine-HCl, 120 mM sucrose, pH 6.0 and lighter bars represent 20mM histidine, 160 mM arginine-HCl, pH 6.0. Striped bars represent material from the day 13 harvest and solid bars from the day 9 harvest. Figure (**B**) are sub-visible particle counts for mAb B samples, where darker bars represent material formulated in 20 mM histidine, 240 mM sucrose, pH 6.0 and lighter bars represent material formulated in 20 mM histidine, 80 mM arginine-HCl, 120 mM sucrose. Striped bars show material from a day 13 harvest and solid bars represent the day 9 harvest. Samples were analysed at T=0 and after 1 month and 3 months incubation at 40°C.

accelerated temperature (40°C) conditions. As discussed previously, particle and aggregate formation may cause autoimmune responses in patients, and the formation of such species can also impact on product efficacy (Matucci *et al.*, 2016; Wang, 2005; Manning *et al.*, 2010; Heal and McGivan, 1998). Due to such concerns, regulatory authorities request that manufacturers of therapeutics such as mAbs report SVP levels in their drug products. The current specifications require that particles greater than 10 µm and 25 µm are reported (United States Pharmacopoeia <788>). Particles less than 10 µm are currently not required to be monitored, however their significance in autoimmune responses and product quality is an area of significant debate (Carpenter *et al.*, 2009; Corvari *et al.*, 2015; Das, 2012; Narhi *et al.*, 2015; Singh *et al.*, 2010). The

emergence of technologies such as MFI enable monitoring of particles as small as 1 µm, and we therefore report SVPs in the range of 1-100 µm in size.

To investigate whether harvest day (and therefore differing levels of ER culture stress) impacts on soluble aggregate, fragment and SVP formation, mAb material from an early (day 9) and late (day 13) harvest was purified and formulated in two different buffers. Particle analysis for mAb A (Figure 3.4) showed material from the late day 13 harvest consistently had higher numbers of particles relative to the samples harvested on day 9. This was observed across all time points, buffers and particle size ranges. Furthermore, the mAb A material which was formulated in 80 mM arginine-HCl, 120 mM sucrose had higher numbers of particles compared to when formulated in 160 mM arginine only. As both arginine and sucrose stabilise proteins through different mechanisms, it is unclear from this data whether this observation is down to a stabilising effect of increased arginine-HCl concentrations or due to the absence of sucrose. To complement SVP data, we also undertook SEC-HPLC analysis, however this revealed no change in monomer, soluble aggregate or fragment levels across the different harvest day or formulations (Supplementary Table 3.4).

Conversely, mAb B material showed no relationship between harvest day and particle amounts across size ranges, time points or formulations although generally there were higher numbers of particles for mAb B samples than mAb A material. As for the mAb A SEC-HPLC analysis, there was no discernible change in monomer, soluble aggregate or fragment levels over time across the different harvest day or formulations for mAb B material (Supplementary Table 3.4).

3.6 Discussion

Although previous studies have reported ER stress mRNA biomarker profiles within CHO cell cultures producing IgG molecules under batch culture conditions, and have reported on HC and LC mRNA/protein expression and the relationship between HC:LC ratios and Qp (Lee *et al.*, 2009b; Maldonado-Agurto and Dickson, 2018; Prashad and Mehra, 2015), surprisingly these observations have not been related to the product stability later in the bioprocess, particularly when formulated in a drug product format. A number of studies have begun bridging the gap between upstream cell culture performance and product quality, analysing the impact of increased HC expression on aggregate formation (Ho *et al.*, 2013; Ho *et al.*, 2015b). However, only one study to our knowledge reports biomarker profiles for cells cultured under fed-batch conditions (Roy *et al.*, 2017), and there are no studies that investigate the stability of the subsequent purified mAb material when formulated and subjected to accelerated stability studies such as those routinely used during formulation development. We therefore set out to

bridge this gap by relating ER perceived cell stress with harvest day and stability of the subsequent purified mAb as determined by determining the propensity of the material to form particles under accelerated stability study conditions.

The mAb stability data presented here shows a relationship between observations at the molecular level with regard to perception of ER stress and intracellular HC/LC transcript and polypeptide ratio during fed-batch culture and the propensity of formulated mAb to form SVPs under temperature stress conditions. Specifically, we show that for one of the cell lines investigated (cell line-A), fed-batch mAb material harvested on day 9 of culture is more stable, in terms of SVP formation, than for material harvested from day 13 of culture. The second cell line investigated, (cell line B) on the other hand, showed no trend regarding the day of harvest and SVP formation of the formulated mAb.

When analysing the growth and productivity, mRNA biomarker profiles and HC/LC polypeptide and transcript data between the two harvest days for cell line A, there are several observations which may account for the differences observed in stability at different harvest days. Firstly, there is an increase in the amount of intracellular HC in cell line A later in culture. Associated with this is a significant increase in *BiP* and *Hsp90b* expression over culture in cell line A only, suggesting that cells harvested on day 13 of culture were under elevated ER stress compared to day 9 and that mAb made between days 9-13 was done so under elevated intracellular stress conditions. BiP binds polypeptides as they enter the ER and will bind both the LC and HC of an IgG. Whilst LC can fold independently of the HC, the folding of the heavy chain CH_1 domain requires association with a folded LC that displaces bound BiP as folding occurs and the HC and LC associate (Feige *et al.*, 2010b). In the event of excess HC polypeptide expression, BiP and Hsp90b therefore function to retain the HC in the ER maintaining this in a state for association with the LC or directing excess polypeptide for degradation (Feige *et al.*, 2010b; Schroder, 2008).

When evaluating this data in combination with the observation of high HC:LC (>2) transcript ratios and low Qp, it is not surprising to see significantly elevated *Bip* and *Hsp90b* expression in cell line A as cultures progress, with such stress likely to be underpinned by the observed accumulation of excess HC polypeptide in the ER. Cells at the late harvest point (day 13) have therefore been under elevated ER stress for a longer period of time than cells from the early harvest on day 9. These observations at the molecular level during upstream culture suggest that ER stress, caused by high *HC:LC* mRNA ratios and an accumulation of HC polypeptide relate to an increase in SVP formation of mAb A material from the late (day 13) harvest. Thus, we propose that the upregulation of ER stress biomarkers is indicative of conditions under which

synthesised mAb has a greater propensity to form SVPs. The ER stress markers themselves (discussed below) do not directly contribute to the formation of increased SVPs. Further, although the Qp of cell line A expressing mAb A was lower than that of cell line B (expressing mAb B), yet had higher ER stress levels as determined by changes in the transcripts of the ER biomarkers, we propose that the lower Qp of cell line A reflects the difficult to express nature of the mAb A molecule that places an increased load on the ER and results in reduced mAb secretion.

Cell line B elicited a different ER stress response to cell line A, also providing a rationale for the mAb A showing a different propensity to form SVPs on different harvest days but not mAb B. The transcript for *Derl3* significantly changed across culture in cell line B only and there was not a change in *Bip* or *Hsp90b*. Derl3 is a member of the Derlin family of proteins which respond as part of the ERAD pathway to maintain ER homeostasis through retro-translocating misfolded or unfolded proteins from the ER into the cytosol for degradation (Kadowaki *et al.*, 2015; Oda *et al.*, 2006). *Derl3* expression increased from day 8 of culture onwards (Supplementary Figure 3.2), meaning that Derl3 expression was elevated at both the early and late harvests. This suggests that cell line B acts upon perceived ER stress sooner than cell line A, and that through activating the ERAD pathway, is better able to cope with a high recombinant protein load. As a result, the cell line maintains a higher culture viability (61% on day 13 for cell line B compared to 50% for cell line A, Figure 3.1), a higher Qp and generates mAb material less prone to SVP formation. Moreover, cell line B consistently has low *HC:LC* transcript ratios, meaning there was excess LC to drive HC folding and mAb assembly.

As expected, biomarker profiling also showed that batch cultures perceive greater ER stress than fed-batch, with more genes significantly changing in expression for batch cultures than for those that were fed (Table 3.1). When grown under batch culture conditions, the two cell lines elicit very similar growth profiles and give similar mAb productivities. Biomarker monitoring reflects these observations, with 4 common genes significantly changing over time between the two cell lines under batch conditions, compared to just 2 for fed-batch. Fed-batch conditions therefore enable molecular differences between cell lines to be determined which, under batch conditions, are not observed. Further, the different cell lines and mAb product propensity to form SVPs may be influenced by host cell proteins remaining after the purification process. Host cell protein content would be expected to increase at the later time point and can be cell line specific, providing a possible explanation as to why there is no ER stress biomarker correlation for cell line B.

Finally, we asked what impact these observations could have on upstream culture decisions with regard to harvest day, that subsequently influence the stability of the mAb in the final product. Generally, CHO cultures producing recombinant proteins, such as mAbs, will run either until a set number of days have passed or until culture viability drops below a predefined threshold. Our data, however, shows that in the case of cell line A, material harvested earlier in culture when perceived ER stress is lower is less prone to forming particles than that harvested later in culture when increased ER stress is perceived. We therefore propose that cellular stress biomarker profiles could be incorporated into cell line development and fed-batch culturing strategies to identify culturing strategies and a day of harvest that maximises product yield and formulated mAb stability, rather than rely on setting a harvest day based on culture longevity or viability alone. The work reported here has shown that the use of ER stress biomarker profiles is cell line and/or product specific; and thus whether day of harvest has an impact on stability, and use of stress biomarkers, should be assessed for each molecule and cell line.

3.7 Acknowledgements:

We are grateful to the Biotechnology and Biological Sciences Research Council of the UK for a studentship to N.E.T. (BB/M016013/1). We thank Andrew Smith (AstraZeneca , Cambridge) for assistance with titre determination.

3.8 Supplementary Tables and Figures

Supplementary Table 3.1: qRT-PCR Primer Sequences used to Determine Transcript Fold Change in Expression Relative to GAPDH.

Gene	Forward	Reverse
Chac1	Qiagen #330001 XM_003512603	
Pfdn2	CTTGGAAGGCAACAAAGAGC	CATCTTCCCCCATAAGACGA
ATF4	TCAAACCTCATGGGTTCTCC	GGCATGGTATCCAGGTCATC
Derl3	Qiagen #330001 XM_007649056.1	
Herpud1	CCTGGCTTCTCTGGCTACAC	TGTGAATAGGGGCTGGAGTC
Rpn1	GTTGAGCAGCACATTCAGGA	TTGGTGATGGAAAAGTCCAG
Hspa9	GTCAGGGAGAGCGAGAGATC	CCGCCAGAAGACTGGATTAC
BiP	AAACATTTGCCCCAGAAGAA	TGATCCGCATGACATTCAGT
Calreticulin	AGGCTCCTTGGAGGATGATT	TCCCACTCTCCATCCATCTC
RagC	GGAGGCTTTAACCCGACTTC	TCATTGGCCCTTTGATGAAT
GAPDH	GCCAAGAGGGTCATCATCTC	CCTTCCACAATGCCAAAGTT
Hsp90b	CTCACAGAGCCTGTGGATGA	CGTGAGACGCTGAGATACCA

Supplementary Table 3.2: Cell Productivity Under Fed-Batch and Batch Conditions. Averate titre, intergral viable cell density (IVCD) and specific productivity (Qp) for fed-batch (n=6 on day 9, n=3 on day 13) and batch (n=2 on day 7, n=1 on day 10) cultures for cell lines A and B.

Cell Line	Titre (mg/mL)			
	Batch		Fed	
	Day 7	Day 10	Day 9	Day 13
A	374	398	2308	2907
B	310	324	1665	2445
	Average IVCD/mL ($x10^6$)			
A	38	56	100	166
B	39	57	71	123
	Average Qp (pg/cell/day)			
A	0.7		8.3	
B	0.5		14.2	

Supplementary Table 3.3: HC to LC Transcript Ratios for Fed-Batch Samples. Average (n=3) HC:LC transcript copy number ratios for fed-batch samples from cell lines A and B were determined using qRT-PCR.

Sample	HC:LC Ratio	
	A	B
Day 3	3.52	0.38
Day 6	5.03	0.63
Day 7	5.29	0.42
Day 8	6.60	0.48
Day 9	4.55	0.38
Day 10	7.33	0.51
Day 13	2.07	0.45

Supplementary Table 3.4: Rate of Soluble Monomer Loss, Aggregate Gain and Fragment Gain per Month. Rates were calculated from SEC-HPLC analysis of formulated mAb samples at T=0 and after incubation at 40°C for 1 month and 3 months.

	Sample	% Change per Month		
		Monomer	Aggregate	Fragment
A	Day 9 80 mM arginine 120 mM sucrose	-3.22	0.72	2.50
	Day 13 80 mM arginine 120 mM sucrose	-2.86	0.42	2.44
	Day 9 160 mM arginine	-2.85	0.79	2.06
	Day 13 160 mM arginine	-2.87	0.52	2.36
B	Day 9 80 mM arginine 120 mM sucrose	-2.28	0.39	2.13
	Day 13 80 mM arginine 120 mM sucrose	-2.54	0.75	1.79
	Day 9 240 mM sucrose	-1.68	1.25	0.43
	Day 13 240 mM sucrose	-1.98	1.68	0.31

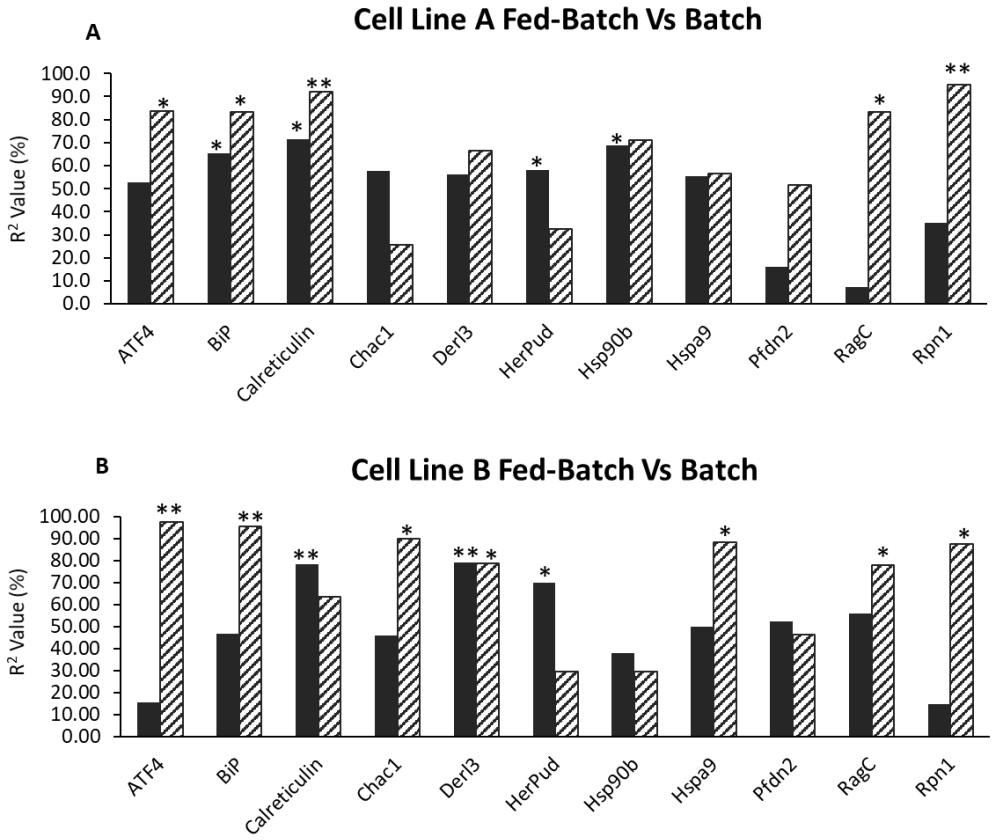

Supplementary Figure 3.1: Linear Regression Analysis of qRT-PCR Data to Assess the Statistical Significance (P<0.05) of the Relationship Between Day of Culture and Fold Change in Expression for Each Gene of Interest for (A) Cell line A and (B) Cell Line B. Fed-batch data is shown in solid bars, and batch in striped. R^2 values indicate the percentage of data with is accounted for by the model. * indicates a P<0.05 and ** P<0.001.

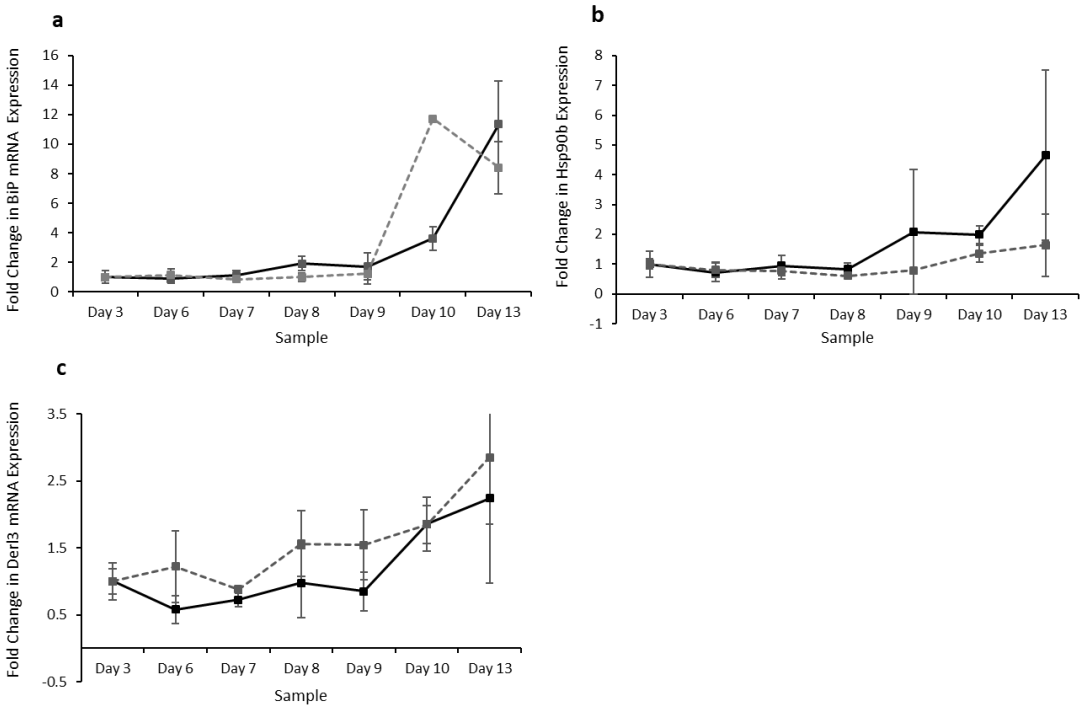

Supplementary Figure 3.2: Fold Change in Expression of (A) *bip,* (B), *hsp90b,* and (C) *derl3* Genes Under Fed-Batch Conditions Relative to Day 3 Expression, Determined Using qRT-PCR. Fold changes for cell line A are denoted with a solid line, and cell line B with a dashed line.

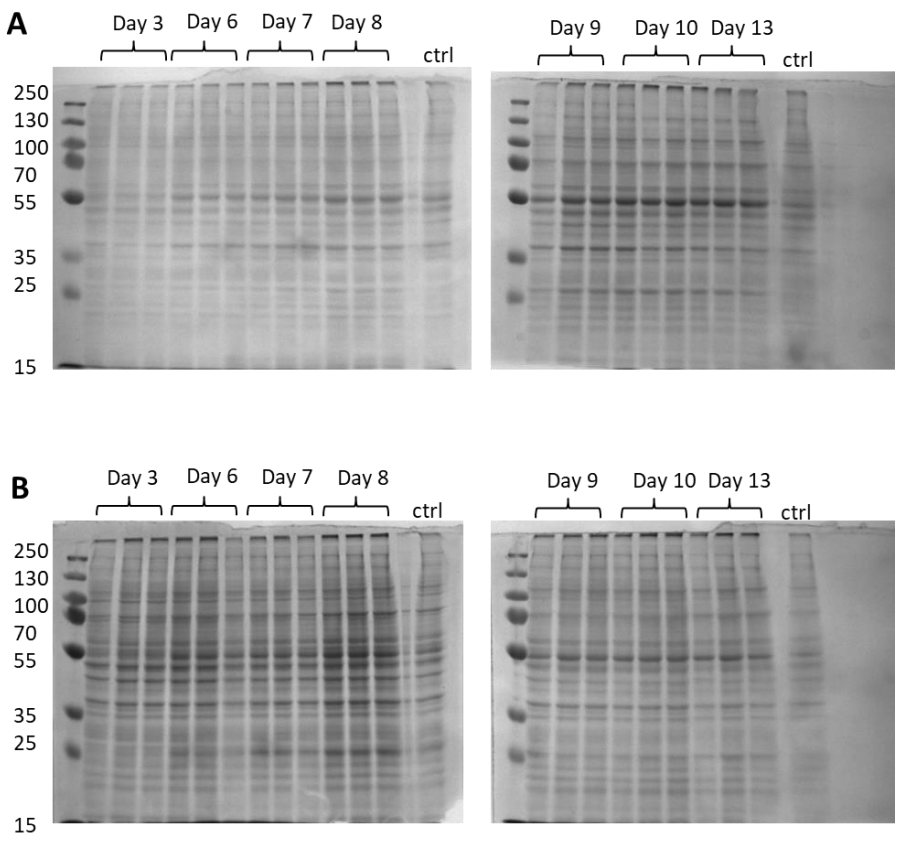

Supplementary Figure 3.3: Coomassie Stained SDS-PAGE Gels for Cell Lysate Samples Collected from (A) Cell Line A and (B) Cell Line B. Gels were loaded with equal sample volumes and the total lane density established and made relative to a control sample ran on each gel. These densities were then used to normalise the corresponding western blots of HC and LC polypeptides.

3.8.1 Limitations

All mAb material for use in stability studies was purified using protein A chromatography. Although this method is an industrial standard, it is noted that material was not further purified using further steps such as cation exchange chromatography. As a result, HCPs are likely to be present within samples and may impact on the differences in stability profiles observed between material from the early and late harvest. Ways to address this issue are further discussed in Chapter 4 (section 4.11.1).

Another aspect not assessed throughout this work is the chemical and structural differences between mAb material. Such information could have been obtained using Mass Spectrometry techniques to understand the cause of stability differences between harvest days and mAbs. Without such data, it is impossible to underpin the cause of the observed differences in SVP formation of mAb A (4212) samples between harvest days.

The qRT-PCR data presented a difference between ER stress responses of cell line A and B under fed conditions, and similarities under batch. It is, however, impossible to understand how these observations translate to the protein level. As discussed, obtaining antibodies to bind the corresponding targets for western blot analysis is challenging as there are very few primary antibodies which are affective in CHO samples. Without such data it is not possible to understand if a significant increase in gene expression may correspond to a significant increase in expression at the protein level, and therefore if a change in transcript expression is enough to impact on cellular functions.

Chapter 4

Investigating the Relationship Between Culture Harvest Day, ER Stress and Formulated mAb Stability in 10 L Disposable Bioreactors

4.1 Introduction

Overexpression of recombinant proteins is established to increase ER stress experienced by CHO cells during culture (Ruggiano *et al.*, 2014; Cudna and Dickson, 2003). Such stress can impact on protein folding and assembly, making ER stress a factor which can ultimately influence product quality. Previous studies have profiled genes relating to ER stress throughout CHO cultures expressing recombinant proteins (Du *et al.*, 2013; Maldonado-Agurto and Dickson, 2018; Prashad and Mehra, 2015),however the majority of studies sampled cells from batch culture, with only one study to our knowledge profiling such ER stress under industrially relevant, fed-batch conditions (Roy *et al.*, 2017). Moreover, no study to date has set out to relate cellular stress to formulated mAb stability.

4.2 Aims of this Chapter

The work presented in chapter 3 demonstrated a cell line/product specific link between harvest day and SVP formation, with mAb 4212 material harvested on day 9 of culture producing significantly less SVPs than that from a day 13 harvest when formulated and assessed under accelerated stability conditions. Furthermore, biomarker profiling revealed different ER stress responses between cell lines 4212 and 184 at the transcript level. This data, combined with HC:LC transcript and polypeptide analysis, suggested that cell line 4212 experienced increased ER stress due to high HC:LC transcript ratios (>2) compared to cell line 184 for which HC:LC ratios were < 0.7. The findings from this work are further investigated in this chapter, setting out to determine if these observations scale from roller bottle cultures to industrially relevant, 10 L disposable bioreactors. Here, fed-batch cultures only are evaluated, and the relationship between harvest day, ER stress and formulated mAb stability is further explored. To investigate mAb stability, formulated material was incubated at 40^{o}C for up to 3 months and routinely analysed for SVP formation, aggregate/fragment content and visual appearance. Furthermore, the work presented in this chapter builds on previous work to compare particle/aggregate formation at the nanometre level, using atomic force microscopy (AFM), and characterises structural differences between harvest days and biological repeats using near-UV CD spectroscopy.

4.3 Growth Profiles and Productivity of Cell Lines Cultured in 10 L Disposable Bioreactors Under Fed-Batch Conditions

Cell lines 109, 4212 and 184 (producing mAbs 109, 4212 and 184 respectively) were cultured under fed-batch conditions in 10 L disposable bioreactors, using a WAVE25 system (see section 2.1.2.2). mAb 109 has previously been established to be a stable molecule, during AstraZeneca

in-house studies, and was introduced as a control cell line/mAb for large scale work. To compare the stability of material from a day 8 and day 13 harvest, half of each bioreactor was harvested on each respective harvest day (section 2.1.2.3) for protein A purification and subsequent formulation.

4.3.1 Growth and Productivity of Cell Line 109

Three biological repeats were run for cell line 109; denoted as 109A, 109B and 109C. Until day 4, all three repeats showed similar viable cell concentrations and percentage viabilities (Figure 4.1). From day 5 onwards, however, culture 109A has a different growth profile to 109B and 109C, reaching higher viable cell concentrations. Culture 109A peaked at 15.55 x10^6 viable cells/mL on day 10 of culture, whereas cultures 109B and 109C peaked at 9.6 x10^6 and 8.52 x10^6 viable cells/mL, respectively, on days 11 and 10 (Figure 4.1).

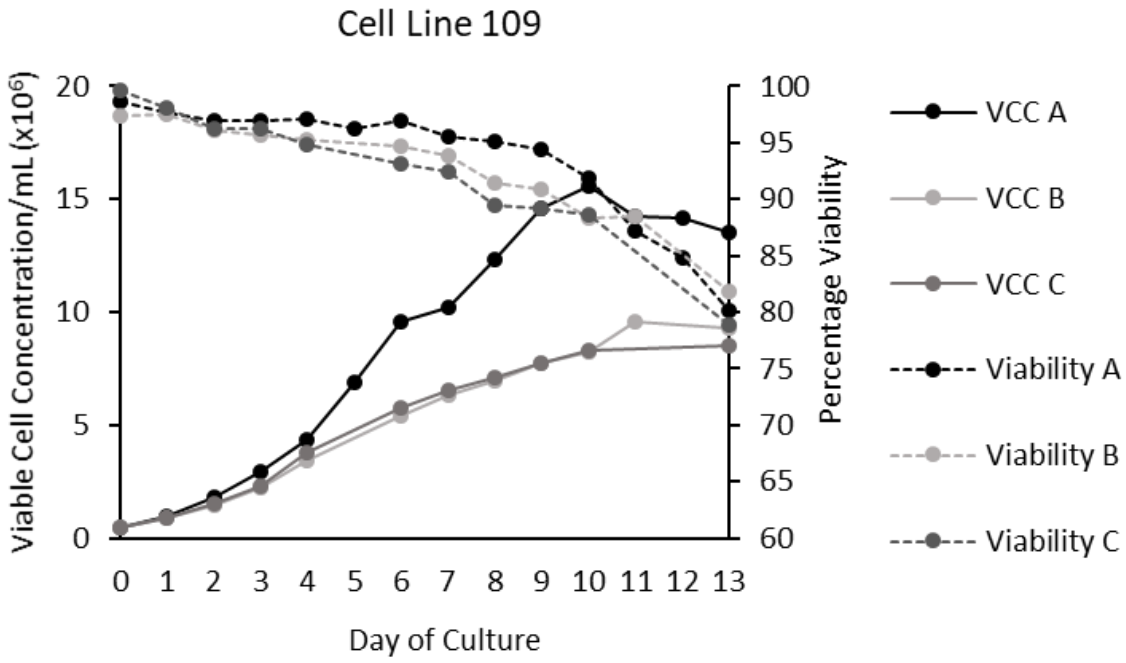

Figure 4.1: **Viable cell concentration (VCC) per mL of culture, and the percentage of cells that were viable (culture viability) on each day of culture for cultures 109A, 109B and 109C grown in 10 L disposable wave bag bioreactors.**

On the first harvest day (day 8) there was a viable cell density of 12.31 x10^6 cells/mL for culture 109A, and 7.11 x10^6 cells/mL for cultures 109B and 109C. At this time, culture viabilities were 95.1%, 91.5% and 89.5% respectively. At the second harvest day (day 13) cell densities plateaued to 13.5 x10^6, 8.63 x10^6 and 8.52 x10^6 cells/mL for cultures 109A, 109B and 109C; with culture viabilities decreasing to 80.2%, 81.9% and 78.8% respectively.

Interestingly, despite differences in growth profiles, cultures 109A, 109B and 109C achieved similar titres throughout culture (Table 4.1A), with mAb concentrations of 693, 527 and 628 mg/L respectively on day 8 and 2017, 1714 and 1962 mg/L on day 13. There were, however, differences in Qp between the three biological repeats (Table 4.1B). As culture 109A achieved and maintained higher viable cell concentrations and cell viability throughout culture, 109A achieved a Qp of just 18.05 pg/cell/day compared to 24.33 and 29.27 pg/cell/day for repeats 109B and 109C.

Table 4.1A, 4.1B and 4.1C: **Titre and Specific Productivity Data for mAb 109 Producing Cultures** (**4.1A**) Titre data, where PF refers to harvested samples post filtration, and were the concentrations of mAb used to calculate column capacity for protein A purification of harvest material. (**4.1B**) Specific productivity (Qp), calculated by plotting (**4.1C**) Integral viable cell densities (IVCD) (Appendix A.1) against titre and calculating the gradient of the line of best fit.

A

	Titre (mg/L)		
Day	109A	109 B	109 C
3	51	51	61
6	299	246	292
7	456	341	421
8	693	527	628
8 PF	**648**	**510**	**586**
9	910	683	823
10	1173	908	1108
13	2017	1714	1962
13 PF	**2014**	**1716**	**1915**

B

Culture	Qp (pg/cell/day)	Average
109 A	18.05	
109 B	24.33	23.9
109 C	29.27	

C

Day	IVCD (x10^6 cells/mL)		
	109A	109B	109C
3	4.42	3.725	3.79
6	21.925	21.185	16.375
7	31.81	27.805	22.545
8	43.06	35.14	29.38
9	56.515	43.135	36.815
10	71.59	52.065	44.855
13	114.525	70.965	70.115

4.3.2 Growth and Productivity of Cell Line 4212

All three biological repeats of cell line 4212 reach similar viable cell concentrations (Figure 4.2), with cell concentrations peaking on day 10 at 27.5, 27.8 and 30.3 x10^6 viable cells/mL for cultures 4212A, 4212B and 4212C respectively. At the first harvest, on day 8, culture viability is at 98.8%, 97.3% and 98.7%, for cultures A, B and C; with viable cell densities of 23.4, 26.7 and 28.1 x10^6 cells/mL. At the second harvest, on day 13 of culture, viabilities drop to 88.8%, 81.6% and 84.9% respectively, with viable cell concentrations at 28.3, 24.3 and 26.2 x10^6 cells/mL. Viable cell

densities therefore remained more-or-less constant between the day 8 and day 13 harvests, with an average drop in culture viability of 15.4%.

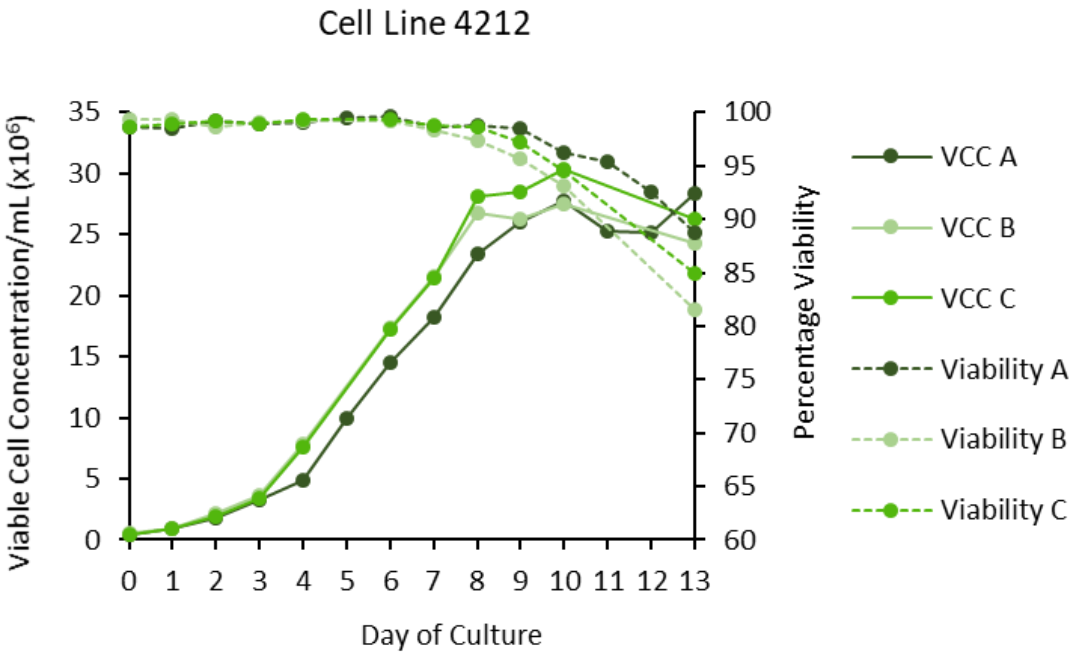

Figure 4.2: **Viable cell concentration (VCC) per mL of culture, and the percentage of cells that were viable (culture viability) on each day of culture for cultures 4212A, 4212B and 4212C grown in 10 L disposable wave bag bioreactors.**

Despite the observed similarities in growth characteristics, substantial differences in productivity were observed between biological replicates, with culture 4212A consistently producing much more material than 4212B and 4212C (tables 4.2A and 4.2B). On day 8 of culture (the first harvest) culture 4212A produced 1764 mg/L of mAb compared to 1206 mg/L and 1156 mg/L for cultures 4212B and C respectively. This difference in productivity was further amplified by day 13 of culture (the second harvest) with culture 4212A reaching a titre of 5502 mg/L, which is 1.6-fold greater than that of cultures B (3277 mg/L) and C (3418 mg/L). Between the two harvest days, there was a 3-old difference in titre for 4212A, a 2.5-fold difference for 4212B and 2.8-fold for 4212C. The observed titres and differences between biological replicates were also reflected in the Qp data, with culture 4212A having a Qp of 28.06 pg/cell/day compared to 15.7 and 15.6 pg/cell/day for the 4212B and 4212C cultures.

Table 4.2A, 4.2B and 4.2C: **Titre and Specific Productivity Data for mAb 4212 Producing Cultures** (**4.2A**) Titre data, where PF refers to harvested samples post filtration, and were the concentrations of mAb used to calculate column capacity for protein A purification of harvest material (**4.2B**) Specific productivity (Qp), calculated by plotting (**4.2C**) Integral viable cell densities (IVCD) (Appendix A.1) against titre and calculating the gradient of the line of best fit.

A

	Titre (mg/L)		
Day	4212 A	4212 B	4212 C
3	101	65	57
6	691	450	437
7	1126	784	728
8	1604	1072	1043
8 PF	**1764**	**1206**	**1156**
9	2423	1469	1485
10	3243	1975	2009
13	5397	3277	3418
13 PF	**5502**	**3214**	**3352**

B

Culture	Qp (pg/cell/day)	Average
4212 A	28.06	
4212 B	15.7	19.8
4212 C	15.6	

C

Day	IVCD (x10^6 cells/day)		
	4212A	4212B	4212C
3	4.545	5.17	4.75
6	28.275	36.14	35.12
7	44.705	55.595	54.48
8	65.575	79.755	79.25
9	90.305	106.275	107.575
10	117.175	133.175	137.035
13	195.71	210.92	221.95

4.3.3 Growth and Productivity of Cell Line 184

Two biological replicates were run for cell line 184; denoted as 184A and 184B. Both repeats had almost identical growth profiles (Figure 4.3), peaking at a maximum viable cell concentration of 18.61 and 19.83 x10^6 viable cells/mL on day 10 of culture, for 184A and 184B respectively.

On the first harvest for 184 cultures (day 8), culture viabilities were 97% and 97.4% with viable cell concentrations of 14.43 and 15.7 x10^6 cells/mL respectively for cultures 184A and 184B. On the second harvest day (day 13) culture viabilities dropped to 73.9% and 75.1% with viable cell concentrations of 15.79 and 17.25 x10^6 cells/mL.

The two biological repeats also had very similar productivity profiles (tables 4.3A and 4.3B). At the first harvest, a titre of 1152 mg/L and 1168 mg/L was achieved for culture 184A and 184B respectively. On day 13 these titres increased to 3643 mg/L and 3812 mg/L; giving a threefold increase in titre between the two harvest days. The two biological repeats also had similar Qps of 26.71 and 27.45 pg/cell/day.

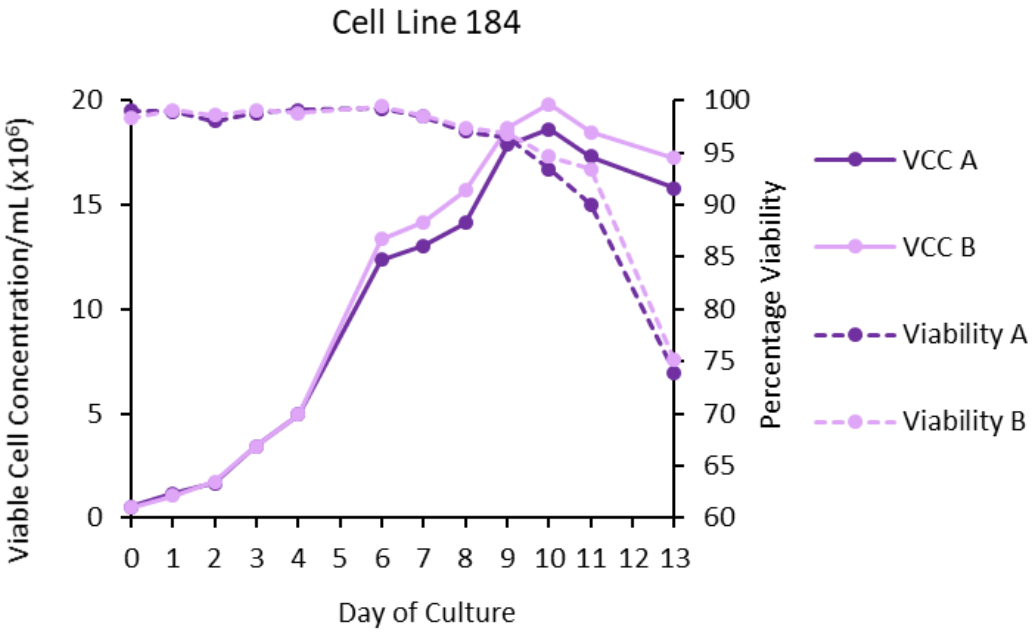

Figure 4.3: **Viable cell concentration (VCC) per mL of culture, and the percentage of cells that were viable (culture viability) on each day of culture for cultures 184A and 184B grown in 10 L disposable wave bag bioreactors.**

Table 4.3A, 4.3B and 4.3C: **Titre and Specific Productivity Data for mAb 184 Producing Cultures** (**4.3A**) Titre data, where PF refers to harvested samples post filtration, and were the concentrations of mAb used to calculate column capacity for protein A purification of harvest material (**4.3B**) Specific productivity (Qp), calculated by plotting (**4.3C**) Integral viable cell densities (IVCD) (Appendix A.1) against titre and calculating the gradient of the line of best fit.

A

	Titre (mg/L)	
Day	184 A	184 B
3	86	84
6	535	536
7	728	768
8	1152	1168
8 PF	**1172**	**1174**
9	1620	1650
10	2235	2277
13	3643	3812
13 PF	**3612**	**3824**

B

Culture	Qp (pg/cell/day)	Average
184 A	26.71	27.1
184 B	27.45	

C

Day	IVCD (x10⁶ cells/mL)	
	184A	184B
3	4.855	4.775
6	26.365	27.295
7	39.065	41.07
8	52.655	56.01
9	68.665	73.195
10	86.915	92.445
13	137.975	147.315

4.4 Extracellular Metabolite Analysis of 10 L Disposable Bioreactors Under Fed-Batch Conditions

Throughout fed-batch culturing, cell culture supernatant samples were taken for extracellular metabolite analysis on a daily basis, as outlined in section 2.1.3.4. Offline data refers to that collected using a BioProfile flex by syringing samples from each culture. Online data refers to that collected throughout culture using probes within the WAVE25 systems.

The resulting metabolite data was used to further compare the behaviour of different biological repeats of the same cell line, and to determine the quantities of glucose and proprietary feed for supplementation. It is noted that offline pH readings were used to calibrate online pH probes over the first 3 days of culture, and therefore any variation between online and offline readings at this point is not considered real.

4.4.1 Cell Line 109 Metabolite Profiles

Offline ammonia, pH and glucose (Figure 4.4) concentrations were similar between all three biological repeat cultures for cell line 109, with ammonia levels gradually increasing throughout culture and pH and glucose concentrations remaining constant. However, culture 109A deviated from 109B and C for offline CO_2, O_2 and lactate levels, mirroring observations in growth and productivity between the three cultures (described in section 4.2.1). Between days 4 and 8, the CO_2 concentration in culture 109A dropped from 119 mm Hg to 68.3 mm Hg, then increased on day 10 to 111 mm Hg. Cultures 109B and C showed a different profile, with CO_2 levels dropping on day 8 from 128 mm Hg to 74 mm Hg in culture 109B, and 104.7 mm Hg to 48.4 mm Hg for 109C. From day 8 onwards, CO_2 levels plateaued in cultures 109B and C and did not increase again as seen in culture 109A.

Cultures 109B and 109C also had similar offline O_2 concentrations throughout culture, with levels gradually declining as cultures progressed. However, culture 109A does not follow the same trend of a general decline, with increases on days 6 and 8. The offline O_2 profile contradicts levels recorded using online methods (Figure 4.5), for which dissolved oxygen (DO) concentrations in culture 109A spiked on day 8 only.

Finally, from day 0 to 5 of culture lactate levels (Figure 4.4) were very similar between the biological triplicate cultures. Until day 8 of culture, the three cultures show the same overall trend in terms of lactate concentrations; with the observed lactate concentrations increasing until day 8 of culture. After this point, however, lactate concentrations in culture 109A drop

significantly below that of cultures 109B and 109C; reducing to a concentration of 0.72 g/L compared to 1.73 and 2.01 g/L for cultures 109B and 109C respectively.

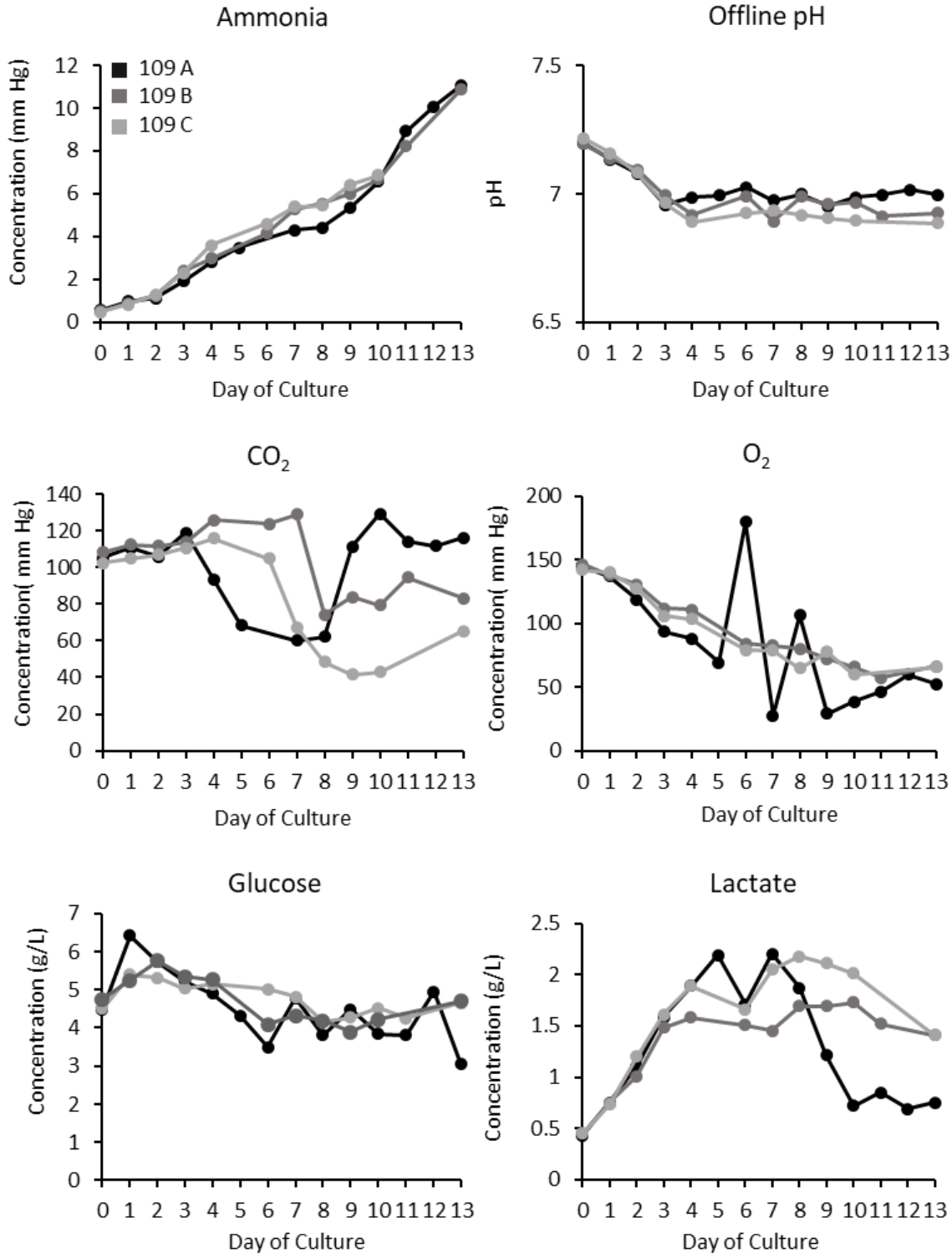

Figure 4.4: **Offline metabolite data for 10 L wave bag cultures 109A, 109B and 109C collected using a BioProfile Flex.** Data was collected daily for extracellular ammonia, CO_2, O_2, glucose and lactate concentrations in the cell supernatant.

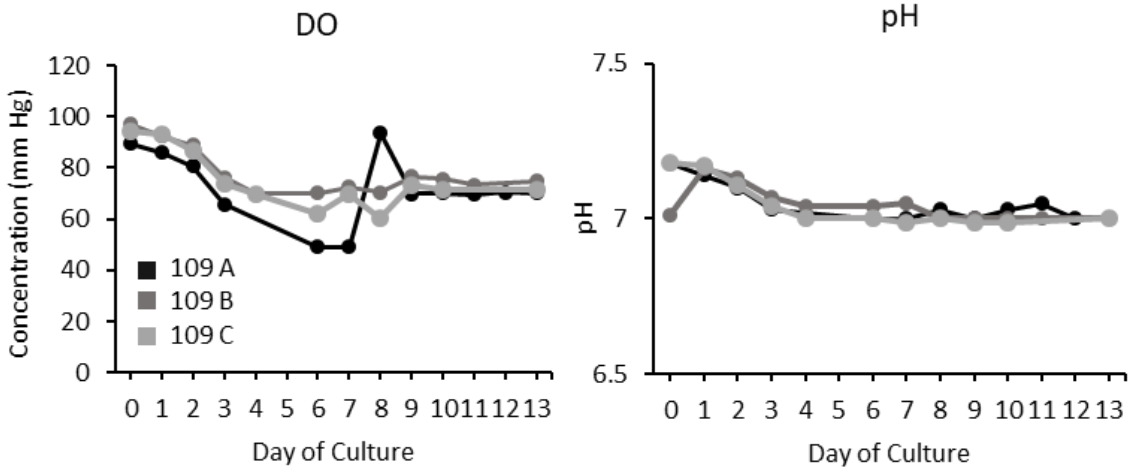

Figure 4.5: Online dissolved oxygen (DO) and pH readings for cultures 109A, 109B and 109C collected throughout culture using probes within the 10 L WAVE25 system. Black lines represent culture 109A, light grey 109B and mid-grey 109C.

4.4.2 Cell Line 4212 Metabolite Profiles

Offline ammonia, pH and glucose extracellular concentrations (Figure 4.6) followed the same trends for all three cultures of the mAb 4212 producing cell line, with ammonia levels increasing throughout culture, pH remaining constant and glucose levels decreasing from days 4 to 8, then increasing again.

Offline O_2 concentrations showed the same overall tend between replicates, however, O_2 concentrations spiked on day 5 for culture 4212A from 107 g/L to 183 g/L, before dropping to 17 g/L on day 6 with concentrations being more comparable to those recorded for cultures 4212B and 4212C (51 g/L and 7 g/L respectively) at this time. Online DO readings revealed a general plateau in oxygen concentrations from day 7, with all three cultures showing a similar profile in terms of dissolved oxygen concentrations (Figure 4.7.)

When comparing the offline O_2 data to the online DO readings, discrepancies were seen between the two. Online data for culture 4212A showed lower concentrations than those determined by offline readings, with online readings recording a high of 110 g/L compared to 183.6 g/L for offline readings. Online O_2 levels in culture 4212A were also much lower than 4212B and 4212C between days 0 to 7. Offline CO_2 concentrations were similar between the cultures from day 0 to 5. After day 5, lactate concentrations for 4212A decreased to approximately 1.89 g/L on day 9, whilst lactate concentrations for 4212B and 4212C were comparable at 2.11 g/L and 1.61 g/L respectively.

Ammonia, CO_2 and glucose levels were the only metabolites of those measured which showed a difference in concentration between the two harvest days (days 8 and 13).

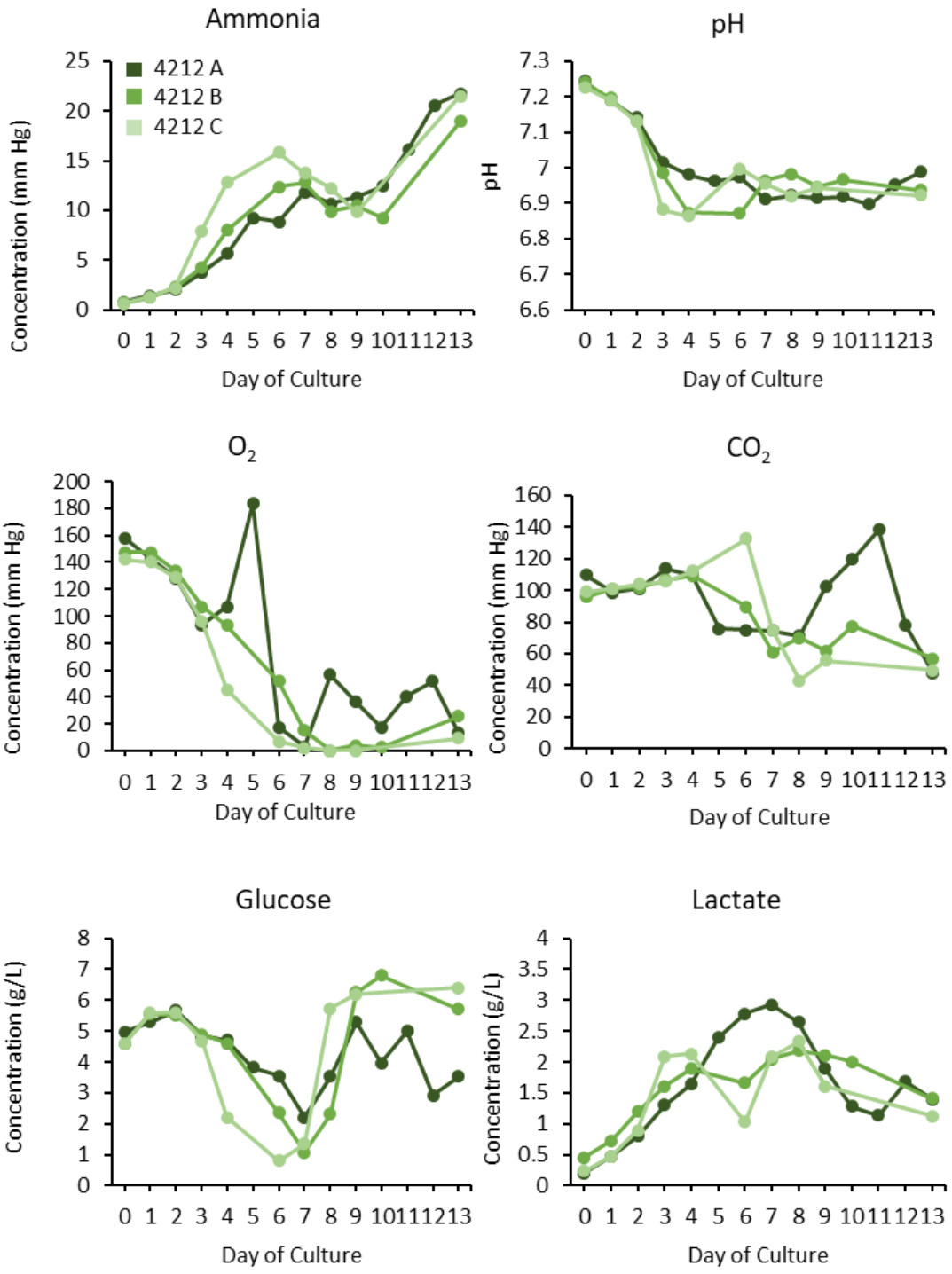

Figure 4.6: **Offline metabolite data for 10 L wave bag cultures 4212A, 4212B and 4212C collected using a BioProfile Flex**. Data was collected daily for extracellular ammonia, CO_2, O_2, glucose and lactate concentrations in the cell supernatant.

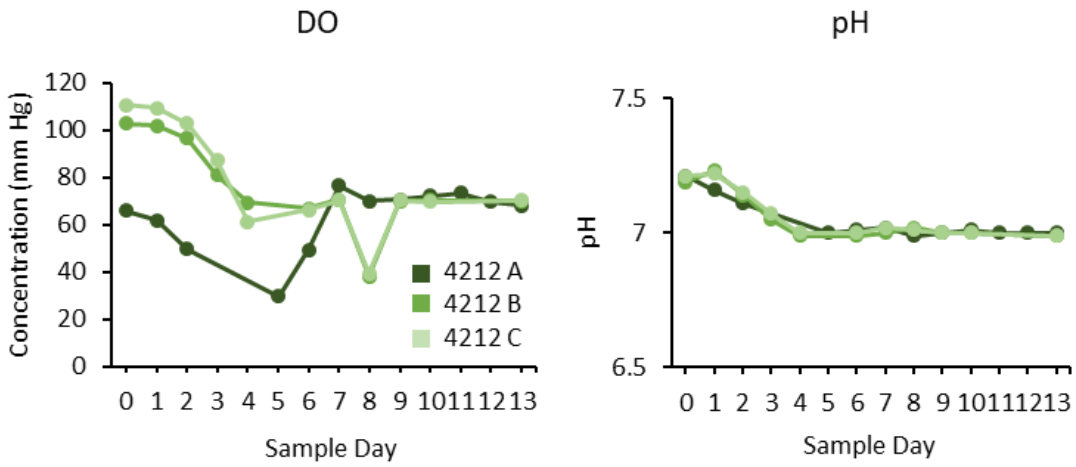

Figure 4.7: Online dissolved oxygen (DO) and pH readings for cultures 4212A, 4212B and 4212C collected throughout culture using probes within the 10 L WAVE25 system.

4.4.3 Cell Line 184 Metabolite Profiles

Both biological repeat cultures showed almost identical offline data for all metabolites analysed (Figure 4.8), in agreement with the similar growth and productivity profiles observed. Ammonia concentrations peaked at 10.8 mm Hg on day 7 of culture, then decrease to 6 mm Hg on day 10 before rising again to 12.7 mm Hg on day 13. There was therefore a difference in ammonia levels measured between the two harvest days.

Offline and online pH readings were more-or-less constant throughout culture. CO_2 concentrations showed a general decline over time, dropping from 112.1 mm Hg on day 7 to 49.2 mm Hg on day 8 in culture 184A, and from 80.9 mm Hg to 50.1 mm Hg in culture 184B.

Offline O_2 levels were also consistent between the two cultures, with the exception of day 5, when the O_2 concentration peaked at 169.3 mm Hg in culture 184A, compared to 91.5 mm Hg in 184B. When comparing between the two harvest days (day 8 and day 13), O_2 levels were similar with an average concentration of 18.9 mm Hg on day 8 and 54.15 mm Hg on day 13 (Figure 4.8).

Lactate concentrations also followed the same trend between the two cultures, with little variation between the day 8 (average 2.3 g/L) and day 13 (average 1.8 g/L) harvests.

Online metabolite measurements (Figure 4.9) were also similar between cultures, with the online pH data mirroring that recorded offline. Online DO readings were also similar between biological replicate cultures, with the exception of day 8, when concentrations in culture 184A dropped from 69.8 mm Hg to 47.6 mm Hg compared to the 184B culture which increased to 86.6 mm Hg.

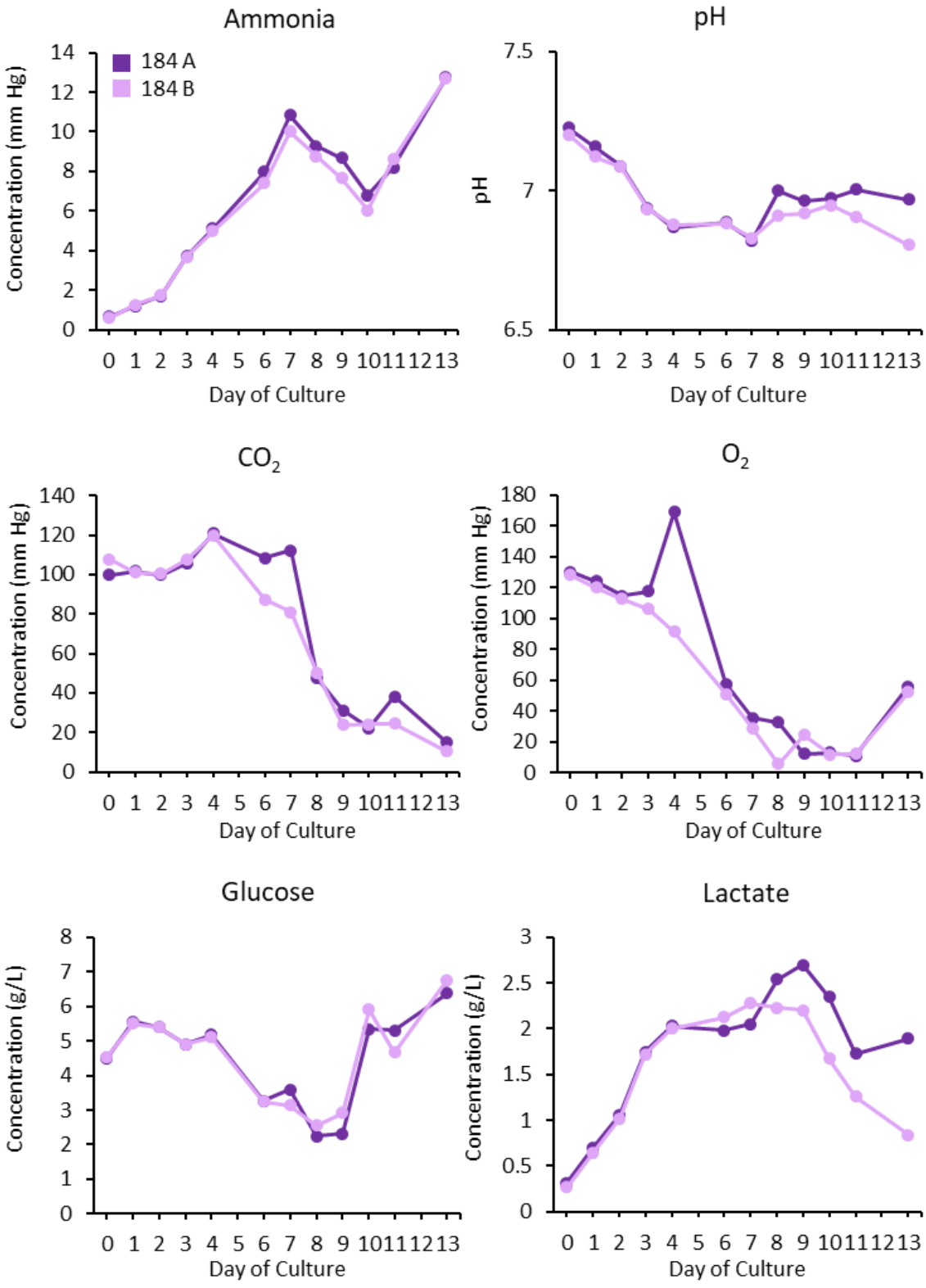

Figure 4.8: **Offline metabolite data for 10 L wave bag cultures 184A and 184B collected using a BioProfile Flex.** Data was collected daily for extracellular ammonia, CO_2, O_2, glucose and lactate concentrations in the cell supernatant.

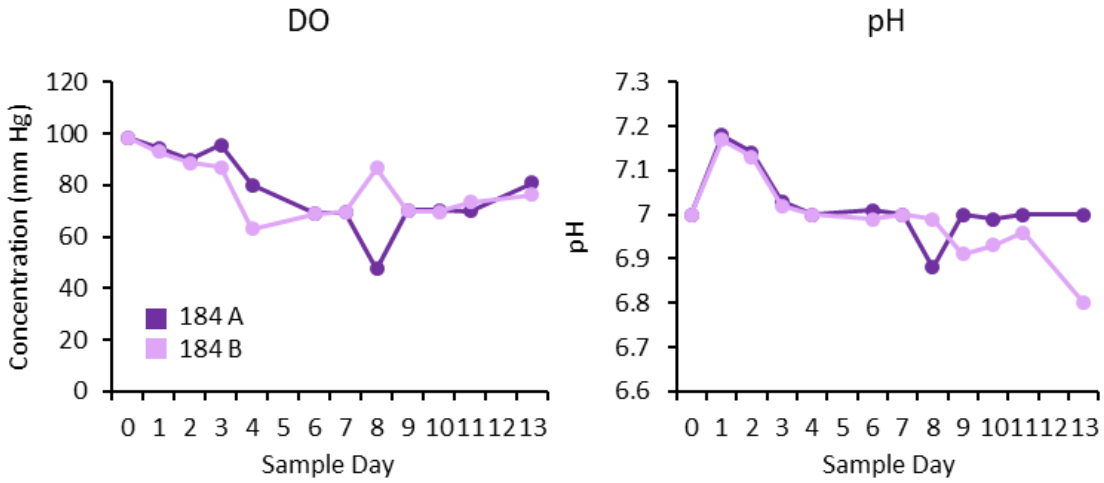

Figure 4.9: **Online dissolved oxygen (DO) and pH readings for cultures 4212A, 4212B and 4212C collected throughout culture using probes within the 10 L WAVE25 system.**

4.5 mRNA Biomarker Profling

In Chapter 3, qRT-PCR was used to assess ER stress throughout roller bottle culture by assessing the fold change in expression of a panel of genes known to encode proteins involved in the UPR and ERAD pathways (summary of the target genes and encoded protein functions is shown in Table 3.1, Chapter 3). This work established that the expression of all of these ER stress related transcripts increased over culture, and highlighted different combinations of significantly changing genes between cell lines 184 and 4212 (see Table 3.1). In this chapter, the same set of transcripts were therefore investigated to determine (i) if their expression changed throughout large scale, 10 L disposable bioreactors, (ii) if transcript biomarker profiles were different between cell lines expressing different mAbs and (iii) if these biomarker profiles relate to subsequent formulated mAb stability.

For this analysis all biological replicates were analysed in technical duplicates, however, when cultured in 10 L bioreactors under fed-batch conditions, no significant change was observed across all genes of interest for each cell line (Appendix A). Technical replicates showed good reproducibility throughout the qRT-PCR assays, providing good evidence that there is no significant change in expression of the transcripts that were analysed throughout culture.

In order to assess the wider transcriptome, and how this may change throughout culture, further mRNA samples were extracted from cell pellets collected from culture 184A and 184B for total RNA sequencing. The results from this work are later described in Chapter 5.

4.6 Western Blot Analysis for Markers of ER Stress

Following qRT-PCR analysis (section 4.5.), western blotting of eEF2 and eIF2α in their total and phosphorylated forms was carried out. These targets were selected as markers of overall ER stress at the protein level, where an increase in the amount of phosphorylated protein indicates an increase in ER stress.

4.6.1 Western Blot Analysis of eIf2α and eEF2 Expression Throughout Fed-Batch Culture of Cell Line 109

For cell line 109, western blot analysis revealed no change in eEF2, eEF2-P, eIF2α and eIF2α-P expression (Figure 4.10) across all days of culture analysed. There was also no difference between biological repeats, suggesting that mAb 109 does not impose an ER stress response on the cell under the culture conditions used for this experiment.

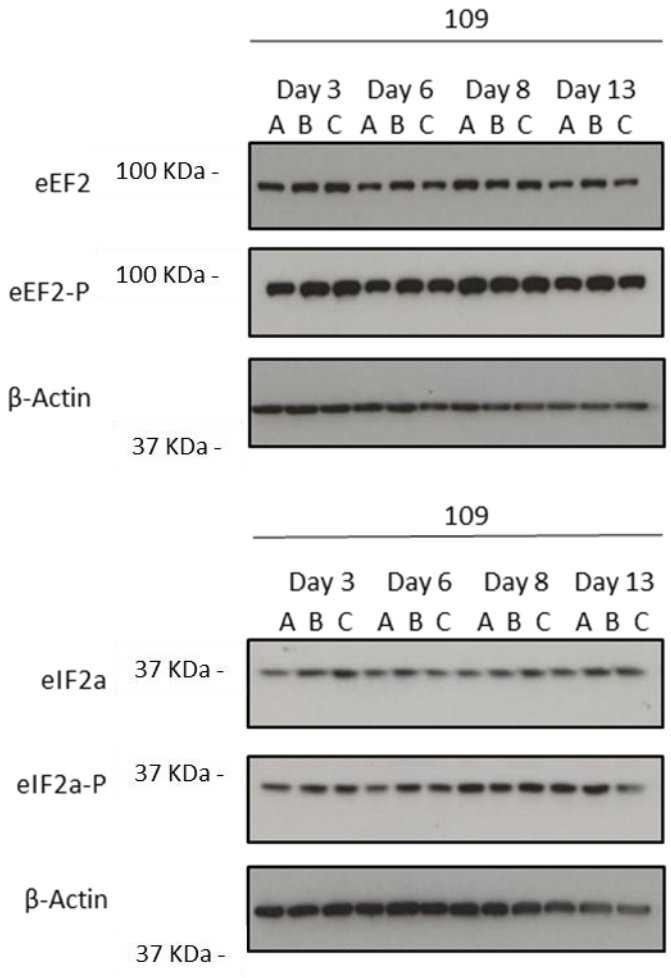

Figure 4.10: Western blot analysis of total eEF2, eEF2-P, total eIF2α and eIF2α-P intracellular expression in cell lysates from cultures 109A, 109B and 109C. 10 µL of prepared lysate was loaded for each sample. Phosphorylated forms of each respective protein are indicators of ER stress.

4.6.2 Western Blot Analysis of eIf2α and eEF2 Expression Throughout Fed-Batch Culture of Cell Line 4212

Western analysis of lysates from cell line 4212 cultures showed no change in expression of total eEF2 and eEF2-P across sample days or between biological replicates. There was therefore no change in total eEF2 and eEF2-P expression between the two harvest days studied.

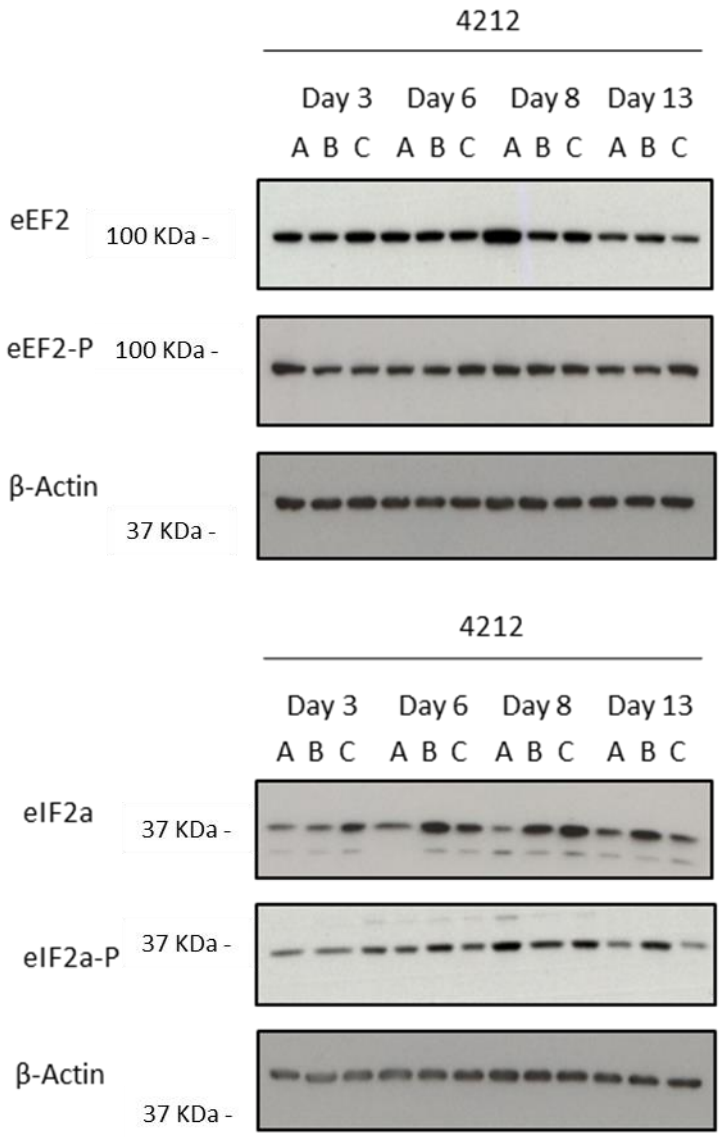

Figure 4.11: Western blot analysis of total eEF2, eEF2-P, total eIF2α and eIF2α-P intracellular expression in cell lysates from cultures 4212A, 4212B and 4212C. 10 µL of prepared lysate was loaded for each sample. Phosphorylated forms of each respective protein are indicators of ER stress.

There was, however, a change in eIF2α and eIF2α-P expression across culture (Figure 4.11). Unlike total eEF2 expression, total eIF2α expression was not constant throughout culture, with differences in expression observed between biological replicates. Overall, less total eIF2α

expression was seen in culture 4212A compared to cultures 4212B and 4212C, for which expression was consistent between the two biological replicates. This further mirrors the observations in cell growth and productivity described in section 4.3.2. eIF2α-P expression in culture 4212A was lower until day 8 of culture, when a marked increase in expression was observed, which then decreased by the second harvest on day 13. For culture 4212B, expression of eIF2α-P increases throughout culture by a small amount, however there was no difference in expression between days 8 and 13. For culture 4212C, eIF2α-P expression was greater on day 8 than day 13. As eIF2α-P is a potential indicator of ER stress perception, this suggests that 4212A was eliciting a greater ER stress response on day 13 of culture compared to day 8, that there was no difference in ER stress response within culture 4212B; and that 4212C was under more stress on day 13 of culture than day 8.

4.6.3 Western Blot Analysis of eIf2α and eEF2 Expression Throughout Fed-Batch Culture of Cell Line 184

As with the previous observations for growth and productivity, eEF2, eEF2-P, eIF2α and eIFα-P expression profiles were well conserved between 184A and 184B biological replicate cultures. Total eEF2 expression was more-or-less consistent across culture, except for notable drop in expression on day 13 (Figure 4.12). eEF2-P expression shows more variation, with constant expression between days 3 and 8, then a more exaggerated drop on day 13.

eIF2α expression increased across both cultures until day 8 of culture, then decreased on day 13. Expression of eIF2α-P increased as culture progressed, with a large increase in expression on day 8 and day 13 of culture relative to day 3, evident from western blotting (Figure 4.12).

Western blotting analysis therefore suggests an increased ER stress response on day 8 of culture (first harvest day) than on day 13 (second harvest day) for cultures 184A and 184B.

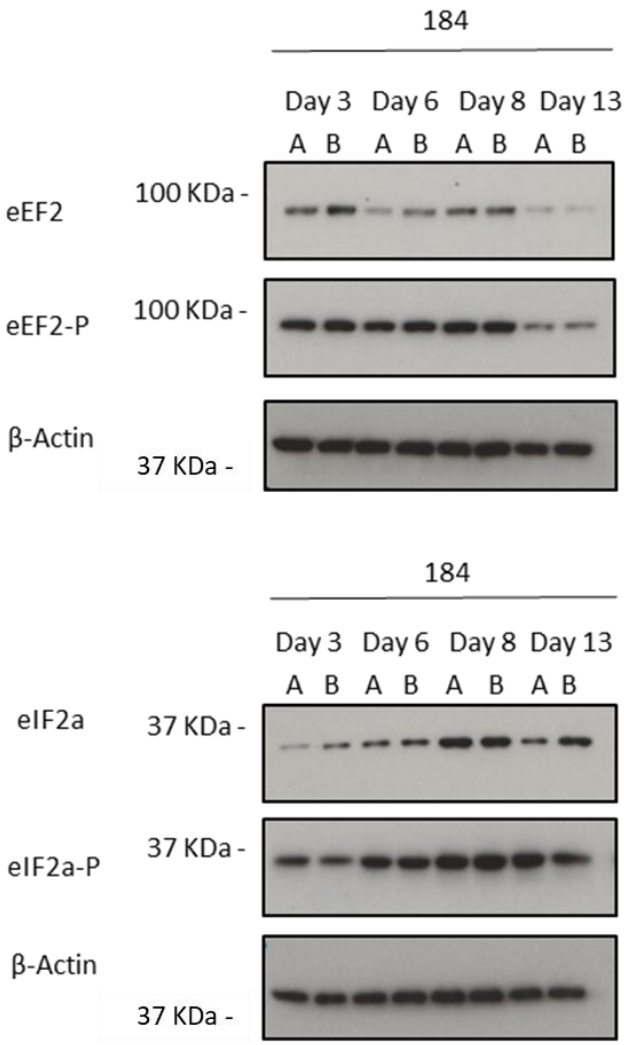

Figure 4.12: Western blot analysis of total eEF2, eEF2-P, total eIF2α and eIF2α-P intracellular expression in cell lysates from cultures 184A and 184B. 10 µL of prepared lysate was loaded for each sample. Phosphorylated forms of each respective protein are indicators of ER stress.

4.7 Intracellular Heavy Chain and Light Chain mRNA and Polypeptide Expression Throughout Culture

HC and LC intracellular expression was analysed at both the transcript and protein level using qRT-PCR and western blotting techniques. All biological replicates were analysed. The transcript copy number was established by extrapolating from a DNA standard curve (described in section 2.10.3 and 2.10.4.3). Samples from days 3, 6, 8 and 13 were analysed.

4.7.1 Heavy Chain and Light Chain mRNA and Polypeptide Analysis for Cell Line 109

Each biological replicate culture of cell line 109 produced higher relative copy numbers of *LC* transcript than the *HC* transcript across all sample days analysed (Figure 4.13). As a result of this, there were low *HC:LC* ratios of < 0.75 on each sample day (Table 4.4). The same profile in the

HC/LC transcript copy numbers was observed across all three biological replicates, with an increase in *HC* transcript numbers per cell after day 3 of culture, when *HC* transcript numbers were more-or-less the same for the remainder of culture. *LC* transcript copy numbers showed a large increase between days 3 and 6, after which time *LC* mRNA transcript numbers per cell remained similar for the rest of culture. Little variation is seen between the biological replicates, with an average standard deviation of 13.2 *HC* copies and 22.7 *LC* copies.

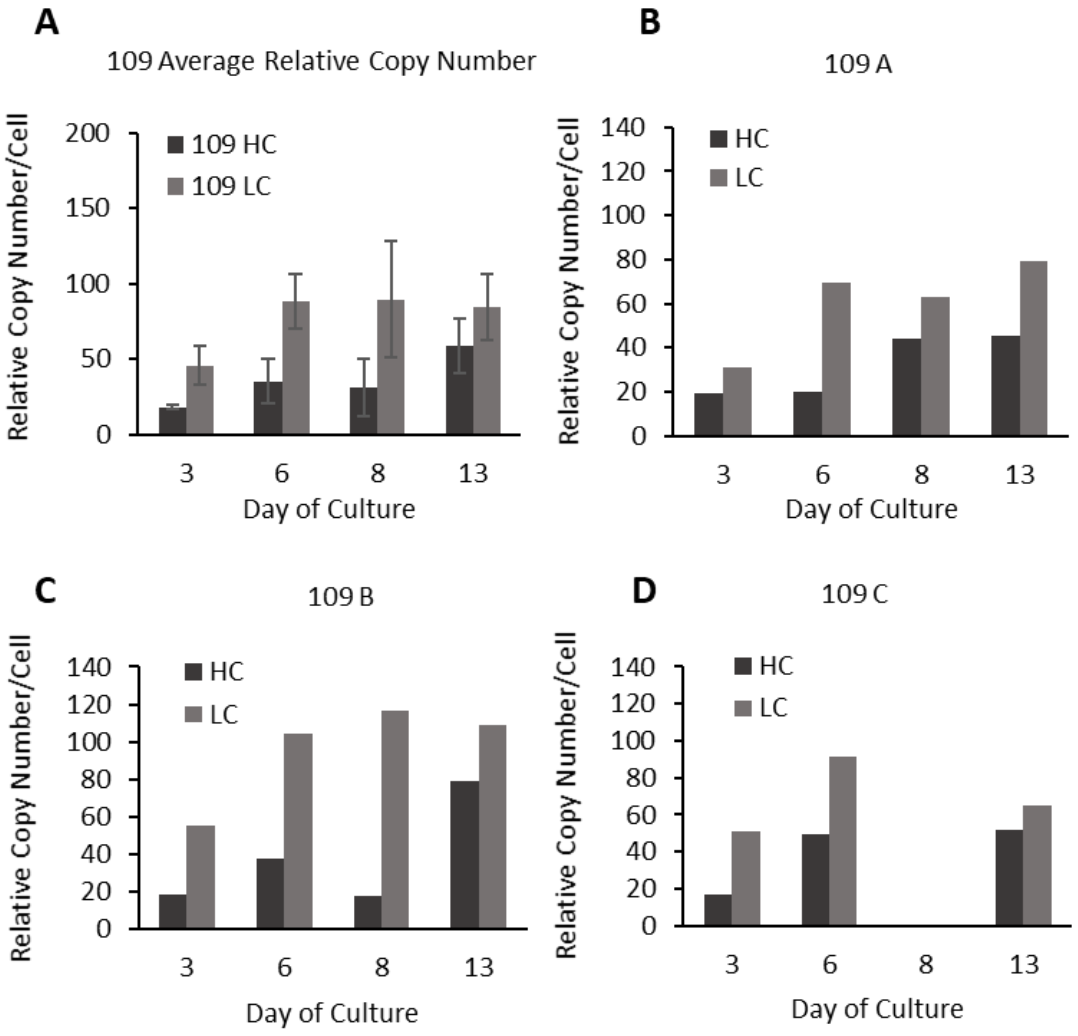

Figure 4.13: **Relative HC and LC mRNA transcript copy number per cell for cultures 109A, 109B and 109C**. (**A**) Average relative copy numbers across all biological replicates (n=3), where error bars show the mean +/- one standard deviation. Note that day 8 samples for 109C were eliminated from the analysis due to evaporation.

Table 4.4: **Average relative HC:LC mRNA transcript copy number ratios for the three cell line 109 cultures.**

Sample	HC:LC Ratio
Day 3	0.40
Day 6	0.40
Day 8	0.35
Day 13	0.70

This similarity in *HC/*LC transcript expression between biological replicates was also observed at the protein level (Figure 4.14). The band intensity for both the intracellular HC and LC expression was very similar between cultures 109A, 109B and 109C for each sample day. Interestingly, the LC was observed as two bands, a higher molecular weight band and a lower band that equates to the size of the final LC polypeptide incorporated into the assembled mAb (Figure 4.14). This suggests that the observed higher molecular weight band is a species that contains the ER leader sequence that has not been cleaved off at the time of sampling. An increase in both HC and LC intracellular protein expression was observed throughout culture, with day 13 expression greater than that on day 3 for all cultures.

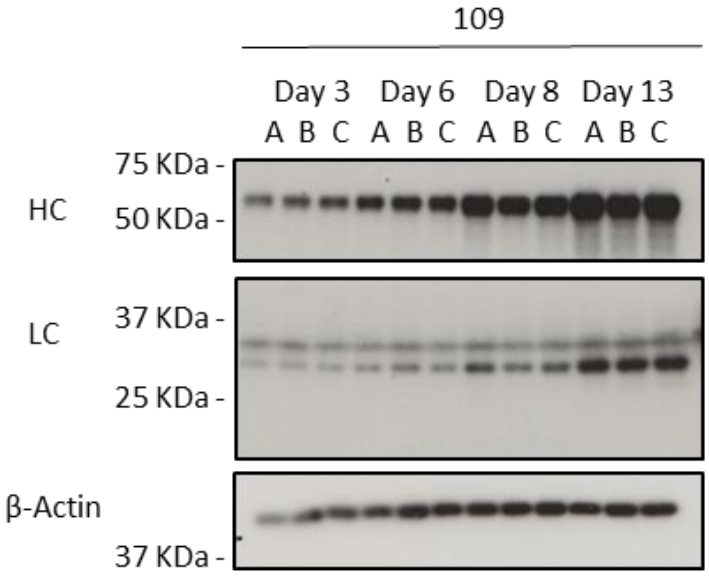

Figure 4.14: Intracellular HC (upper panel), LC (middle panel) and beta actin (lower panel) polypeptide expression in cultures 109A, 109B and 109C. Samples were analysed under reducing conditions on an SDS-PAGE gel with 3 µL of lysate being loaded for each sample.

4.7.2 Heavy Chain and Light Chain mRNA and Polypeptide Analysis for Cell Line 4212

The analysis of samples from cell line 4212 showed high *HC* to *LC* transcript ratios on each day of culture, for all biological replicate cultures (Figure 4.15). The analysis showed higher *HC* mRNA transcript copy numbers than *LC* mRNA transcript numbers, with an average ratio of *HC:LC* transcript exceeding 6.5 (Table 4.5). Although there was variation in the exact *HC* mRNA transcript numbers between biological replicate cultures, *HC* mRNA numbers were consistently greater than the *LC* on each sample day (Figure 4.15).

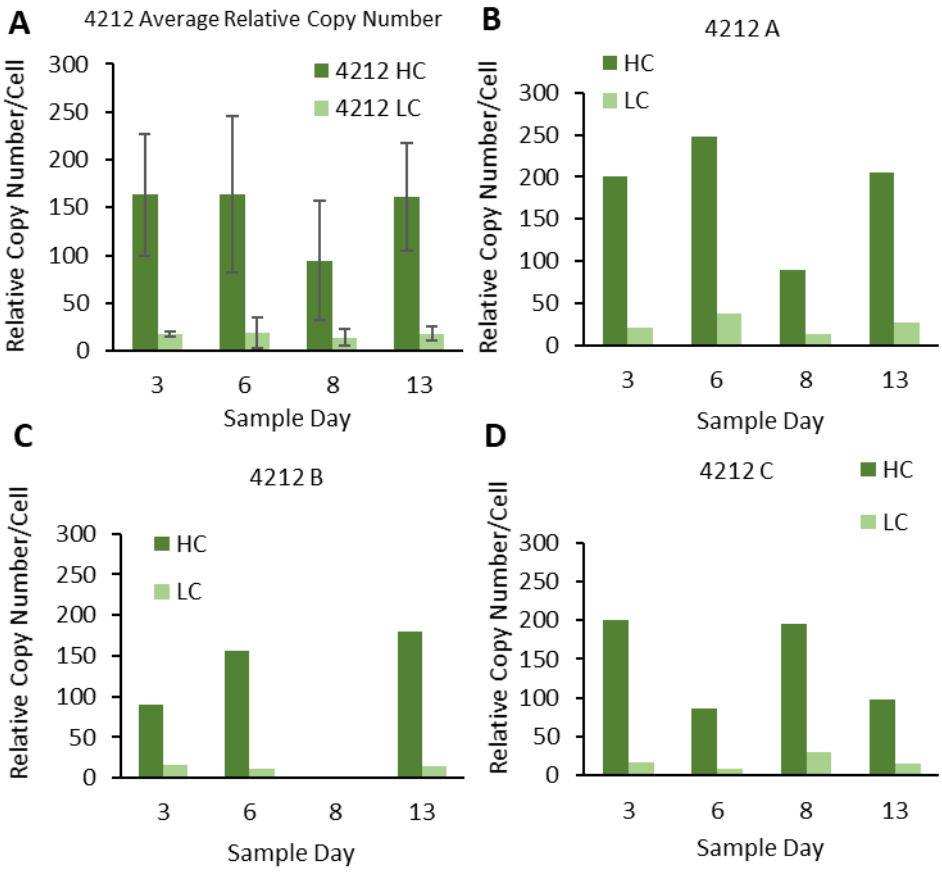

Figure 4.15: Relative HC and LC mRNA transcript copy number per cell for cultures 4212A, 4212B and 4212C. (**A**) Average relative copy numbers across all biological replicates (n=3), where error bars show the mean +/- one standard deviation. It is noted that day 8 samples from 4212B gave very low copy numbers. This result was verified by repeating the qRT-PCR assay 3 times.

Table 4.5: Average relative HC:LC mRNA transcript copy number ratios for cell line 4212 cultures.

Sample	HC:LC Ratio
Day 3	9.00
Day 6	8.75
Day 8	6.61
Day 13	8.74

For culture 4212B, *HC* and *LC* copy numbers were low (approximately 0.8 for each) on day 8. The assay was repeated a further two times for these samples and the same results were obtained. However, such low transcript numbers do not fit with the other analyses and are unlikely; this perhaps reflected an issue with the actual samples from this day and hence the data for this day and culture were ignored in subsequent interpretation of the data.

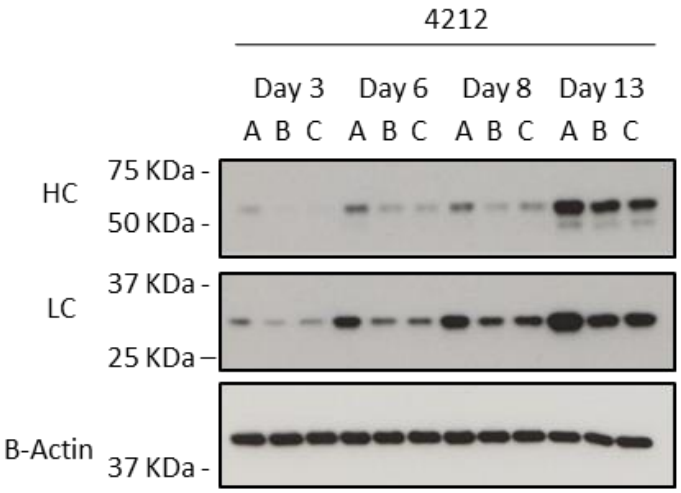

Figure 4.16: Intracellular HC (upper panel), LC (middle panel) and beta actin (lower panel) polypeptide expression in cultures 4212A, 4212B and 4212C. Samples were analysed under reducing conditions on an SDS-PAGE gel with 3 µL of lysate being loaded for each sample.

Western blot analysis of intracellular HC and LC protein expression (Figure 4.16) was consistent with secreted mAb productivity data (section 4.2.2), showing higher HC and LC expression in culture 4212A throughout each sample day relative to cultures 4212B and 4212C. For each biological replicate, HC and LC expression increased throughout culture, with a notable increase in LC and HC expression between the first (day 8) and second harvest (day 13). Potential degradation in HC protein can be seen on day 13 for all samples, as indicated by the presence of

a lower molecular weight band. Interestingly, the LC was observed as a single band, unlike in the case of the 109 samples (see Figure 4.14), suggesting that the ER signal sequence on the 4212 LC was rapidly cleaved unlike in the case of the 109 molecule. Further, despite very low *HC* and *LC* mRNA transcript copy numbers on day 8 of culture for 4212B, western blot analysis showed the presence of HC and LC expression at levels similar to that observed in culture 4212C for this sample day, providing more evidence that the transcript data for 4212B samples were not an accurate reflection of the actual quantities.

4.7.3 Heavy Chain and Light Chain mRNA and Polypeptide Analysis for Cell Line 184

The HC and LC mRNA transcript numbers in the samples from the 184 cultures were much more similar to each other than for the 109 and 4212 samples previously discussed (Figure 4.18) and there was less variation in the transcript numbers throughout culture. As a result of this, throughout culture the *HC:LC* mRNA transcript ratios were around 1 (Table 4.6). When comparing the individual biological replicates to each other, samples from the 184A culture had higher *LC* mRNA transcript copy numbers than *HC,* with the exception of day 3 when *HC* and *LC* transcript numbers were comparable. *HC* and *LC* copy numbers both increased between day 3 and day 6, then plateaued for the remainder of culture (Figure 4.18). Samples from culture 184B had higher *LC* copy numbers than the corresponding *HC* mRNA numbers throughout culture with the exception of day 8, when *HC* transcript expression was greater than the *LC* (Figure 4.17).

Western blot analysis (Figure 4.18) of samples from the 184 cultures showed that intracellular HC and LC protein expression increased throughout culture for both replicates, with a large apparent increase from day 6 of culture to day 8. A further increase in intracellular HC and LC expression was also observed between harvest days (day 8 and day 13). As with previous observations in growth and productivity for the two 184 fed-batch cultures, both biological replicates showed similar HC and LC protein expression.

Table 4.5: Average relative HC:LC mRNA transcript copy number ratios for cell line 184 cultures

Sample	HC:LC Ratio
Day 3	0.88
Day 6	0.95
Day 8	1.21
Day 13	0.86

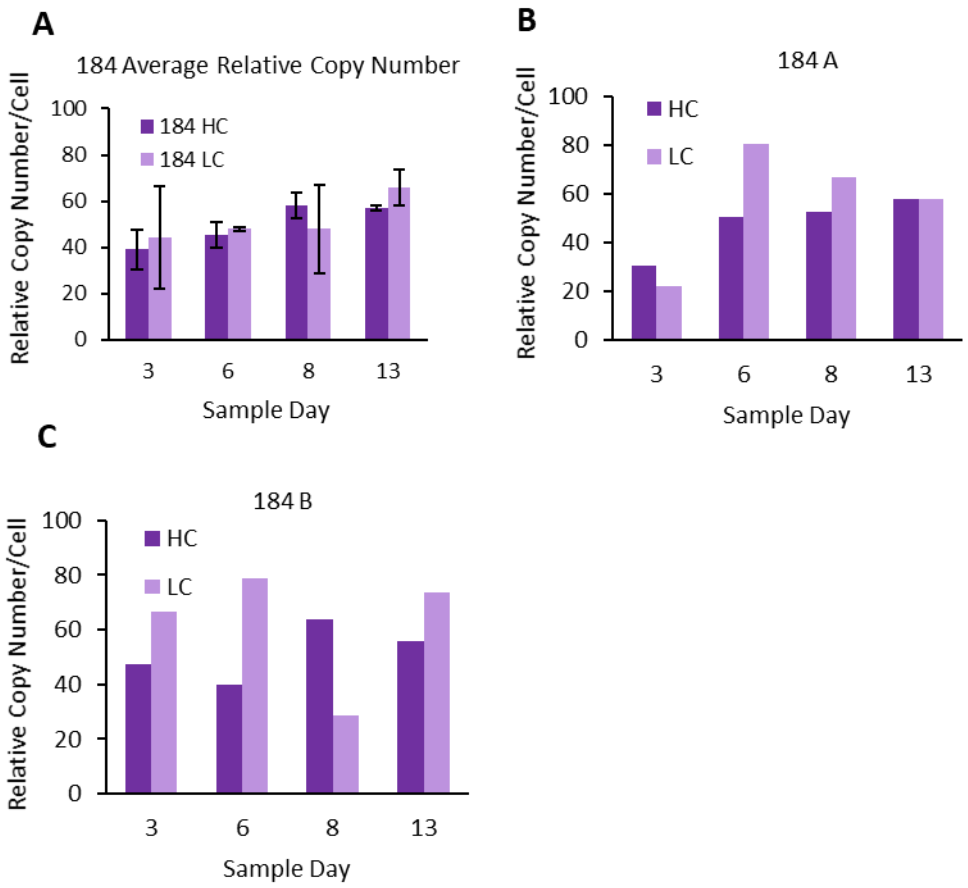

Figure 4.17: Relative HC and LC mRNA transcript copy number per cell for cultures 184A and 184B. (**A**) Average relative copy numbers across all biological replicates (n=2), where error bars show the mean +/- one standard error.

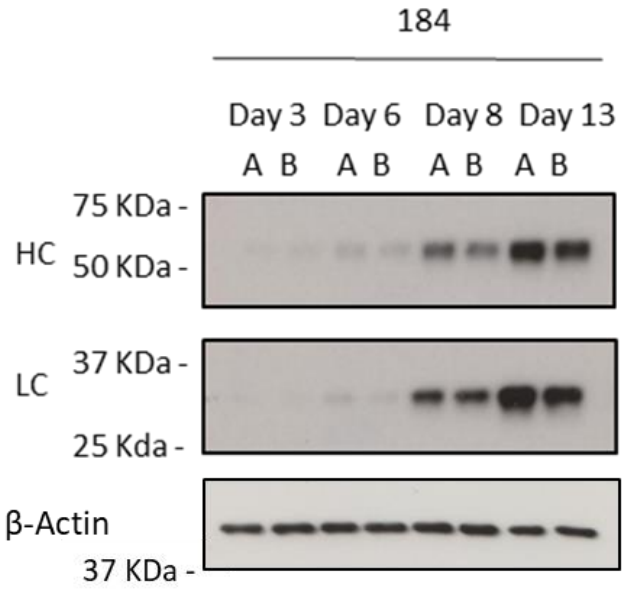

Figure 4.18: **Intracellular HC (upper panel), LC (middle panel) and beta actin (lower panel) expression in cultures 184A and 184B**. Samples were analysed under reducing conditions on an SDS-PAGE gel with 3 µL of lysate being loaded for each sample.

4.8 Stability of Purified mAbs from Different Harvest Days of 10L Disposable Bioreactor Cultures

Purified mAb material was used from each biological replicate of the different mAbs/cell lines investigated in this study to compare the stability profile of each molecule from day 8 and day 13 harvests. After protein A purification of the mAbs from culture harvests, the material was formulated in 80 mM Arg and 190 mM Arg (see Section 2.11 for details on buffer and sample abbreviations) at a concentration of 50 mg/mL and vialled in 1.5 mL aliquots. Vials were then incubated at 40^{o}C in the dark for up to 3 months to represent accelerated stability conditions used in industrial stability studies. Samples were routinely inspected for visible degradation, aggregate/fragment formation and SVP content as per methods section 2.6. Images of vials are included with the SVP data, however tables outlining visual standard scores are presented in Appendix Tables A.1, A.2 and A.3.

All samples were analysed for stability at T=0, T=1 month and T=3mths.

4.8.1 Stability of mAb 109 Material from Day 8 and Day 13 Harvests Under Accelerated Stability Conditions at 40^{o}C

Stability profiling of mAb 109 material, as determined by the formation of SVPs (Figure 4.19) revealed no relationship between harvest day and particle formation with no difference observed between day 8 and day 13 mAb material in either the 80 mM or 190 mM Arg buffers across all biological replicate cultures. In other words, at the T=0 time point, no difference in the SVP formation was observed between harvest days or biological replicates for both formulations. Furthermore, no difference in overall SVP formation was observed between the 80 mM and 190 mM Arg formulations, with the exception of culture 109B day 8 material at T=1 month for which particle counts were greater in the 80 mM Arg buffer compared to 190 mM Arg buffer (Figure 4.19.)

At T=1 mth an increase in SVP formation was observed for all samples in both the 80 mM and 190 mM Arg formulations, however at the T=3 mth time-point there was no change from the T=0 data in either formulation. For all samples analysed at all time points, the majority of particles were 1 – 10 µm in size (Table 4.6), with over 91% of the total SVP count falling in this size range. For each size range there was an increase in the formation of SVPs greater than 10 µm over time, however there was no rend between harvest days or buffers (Table 4.7). Visually, there was no difference between mAb 109 material across biological replicates, harvest days or

formulations throughout the study, as evidenced in Figure 4.20, which shows images of vials from the T=3 mth time point.

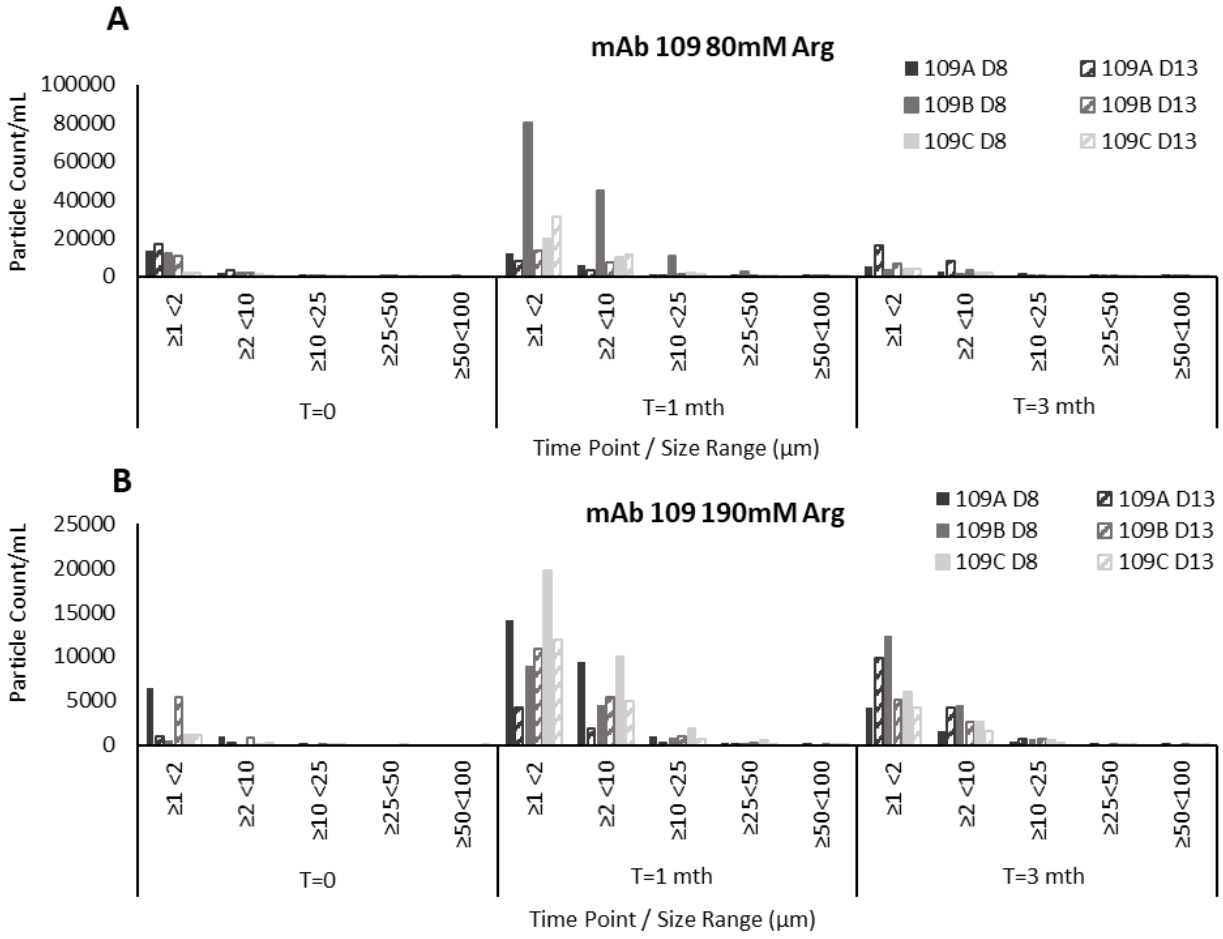

Figure 4.19: Analysis of SVP count per mL of mAb 109 material harvested at day 8 and day 13 from cultures 109A, 109B and 109C formulated in (A) 80 mM arginine-HCl, 120 mM sucrose and 20 mM histidine or (B) 190 mM arginine-HCl and 20 mM histidine. Samples were analysed at T=0 and after incubation at 40°C for T=1mth and T=3mths.

Table 4.6: Percentage of total SVP counts which fall within 1 – 10 µm and 10 – 100 µm size ranges mAb 109 samples incubated at 40°C for up to three months.

Sample	% of Total SVP Count											
	T=0				T=1mth				T=3mth			
	80 mM arg		190 mM arg		80 mM arg		190 mM arg		80 mM arg		190 mM arg	
	≥1 <10	≥10 <100	≥1 <10	≥10 <100	≥1 <10	≥10 <100	≥1 <10	≥10 <100	≥1 <10	≥10 <100	≥1 <10	≥10 <100
109A D8	99.6	0.4	99.6	0.4	91.9	8.1	94.7	5.3	93.7	6.3	92.2	7.8
109A D13	99.6	0.4	99.8	0.2	93.4	6.6	96.2	3.8	92.9	7.1	94.1	5.9
109B D8	99.2	0.8	99.6	0.4	90.4	9.6	92.2	7.8	92.9	7.1	95.0	5.0
109B D13	99.7	0.3	99.4	0.6	91.7	8.3	92.3	7.7	91.2	8.8	91.3	8.7
109C D8	98.0	2.0	98.4	1.6	92.1	7.9	92.1	7.9	91.3	8.7	92.8	7.2
109C D13	98.7	1.3	99.6	0.4	95.7	4.3	95.1	4.9	92.4	7.6	94.0	6.0

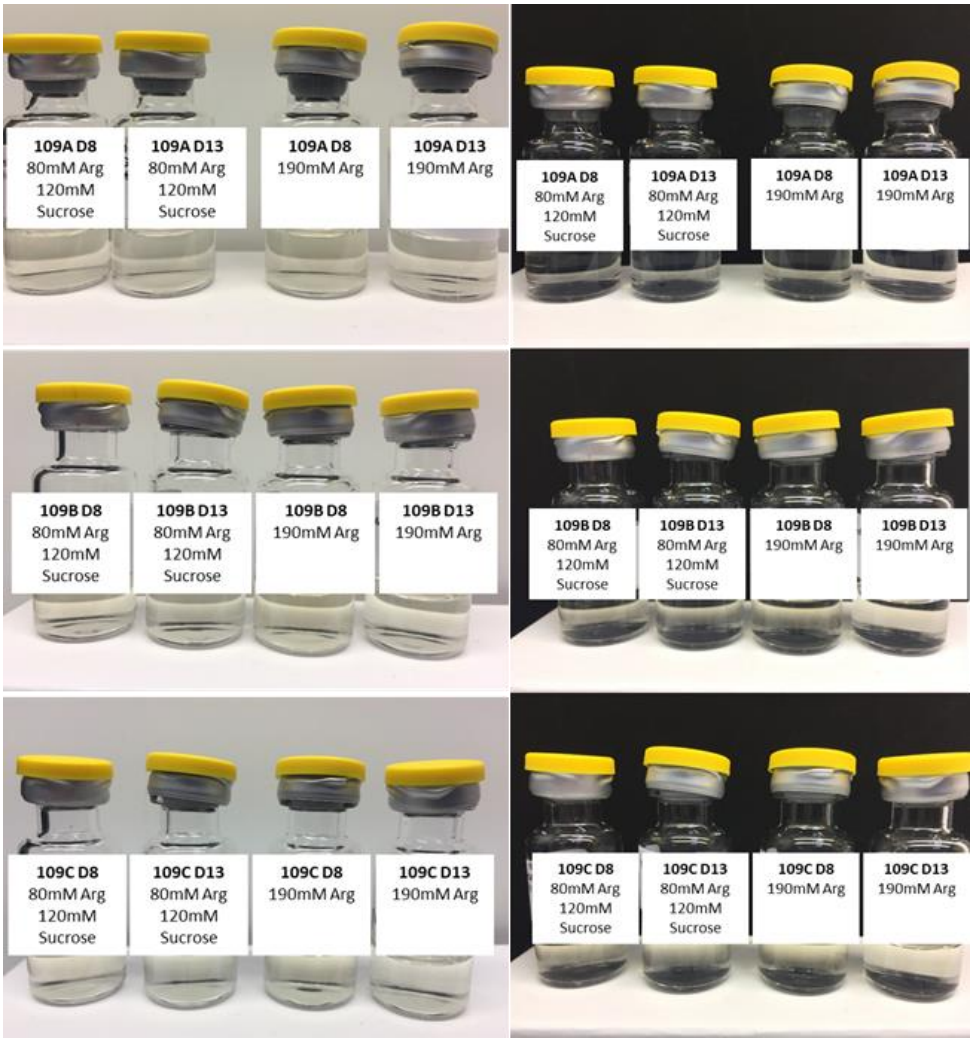

Figure 4.20: Images of mAb 109 material on white and black backgrounds after incubation at 40°C for 3 months. Material was formulated in 80 mM arginine-HCl, 120 mM sucrose and 20 mM histidine (80 mM Arg) or 190 mM arginine-HCl and 20 mM Histidine (190 mM Arg).

4.8.2 Stability of mAb 4212 Material from Day 8 and Day 13 Harvests Under Accelerated Stability Conditions at 40°C

Stability profiling of mAb 4212 material, as determined by the formation of SVPs, revealed no conserved harvest day trend between biological replicates or formulations (Figure 4.21 and 4.22).

At T=0 there was no difference in SVP formation between samples formulated in 80 mM Arg (Figure 4.21) with the exception of material from culture 4212B day 8, for which particle counts were much higher for particles ≥1<10 µm in size. For samples formulated in 190 mM Arg

however, some variation was seen between samples, with 4212A day 13 material having greater numbers of particles than that from the day 8 harvest. On the other hand, 4212B and 4212C day 8 material gave rise to more particles than that from day 13. When visually inspecting 80 mM Arg samples, 4212A day 8 material was more opalescent than that harvested at day 13. For 4212B and 4212C there was no visual difference between harvest days. When formulated in 190 mM Arg, 4212A day 13 material was slightly more opalescent than 4212A day 8 samples. No difference was observed between harvest days for material from 4212B and 4212C cultures.

Overall SVP numbers increased for all size ranges in all samples at T=1 month for 4212 material, with material from the 4212B and 4212C cultures having higher SVP counts than 4212A material in either formulation. There was no difference in particle formation between harvest days for 4212A and 4212B samples formulated in 80 mM Arg, however 4212C day 13 material gave rise to higher particle numbers than that from day 8. This observation in SVP formation of the 4212C material at T=1 month was also observed for samples formulated in 190 mM Arg (Figure 4.22). Despite an increase in SVPs in 4212C day 13 material, day 8 material was more opalescent during visual inspection than that from day 13 for both formulations. For samples formulated in 80 mM Arg at T=1 month, 4212A and 4212B day 8 material was much more opalescent than that from day 13. When formulated in 190 mM Arg, however, 4212A culture day 13 samples were more opalescent than day 8, while the trend for 4212B samples remained as day 8 material being more opalescent than day 13.

For 4212 samples stored at 40^{o}C for T=3 months, SVP formation of material formulated in 80 mM Arg was reduced, compared to the 1 month samples, and had decreased back to levels similar to those recorded at T=0. There was no difference observed between biological replicates or harvest days. In terms of the visual appearance of material formulated in 80 mM Arg, day 8 material was more opalescent than day 13 material for mAb from cultures 4212A and 4212B, as previously observed at T= 1 month.

For 4212C culture material, this trend was reversed with day 13 material being slightly more opalescent than that from day 8. For samples formulated in 190 mM Arg, particle counts also decreased at T=3 months to levels comparable to those at T=0, with 4212A and 4212B day 8 material producing slightly more SVPs than that from day 13 harvest material. Visually, all samples showed a profile in line with those at T=1 month, with 4212A day 13 material more opalescent than that from day 8; and 4212B and 4212C day 8 material appearing more opalescent than that from day 13 (Figure 4.22.)

Overall, the majority of total SVPs observed were less than 10 µm in size (Table 4.7.), with more than 91% of the total count falling into this category. Over time, there was a small increase of 1-5% in particles greater than 10 µm. There was however, no trend observed between harvest days or biological replicates.

Table 4.7: Percentage of total SVP counts which fall within 1 – 10 µm and 10 – 100 µm size ranges mAb 4212 samples incubated at 40°C for up to three months.

Sample name	% of Total SVP Count											
	T=0				T=1mth				T=3mth			
	80 mM arg		190 mM arg		80 mM arg		190 mM arg		80 mM arg		190 mM arg	
	≥1 <10	≥10 <100	≥1 <10	≥10 <100	≥1 <10	≥10 <100	≥1 <10	≥10 <100	≥1 <10	≥10 <100	≥1 <10	≥10 <100
4212A D8	94.0	6.0	98.9	1.1	97.7	2.3	95.8	4.2	96.8	3.2	97.9	2.1
4212A D13	96.6	3.4	95.7	4.3	89.0	11.0	89.0	11.0	97.5	2.5	92.8	7.2
4212B D8	96.0	4.0	98.2	1.8	98.5	1.5	96.1	3.9	98.2	1.8	93.9	6.1
4212B D13	97.1	2.9	98.7	1.3	93.5	6.5	92.5	7.5	91.3	8.7	96.3	3.7
4212C D8	92.5	7.5	94.2	5.8	95.3	4.7	94.9	5.1	95.8	4.2	93.8	6.2
4212C D13	98.3	1.7	97.0	3.0	91.9	8.1	91.6	8.4	91.9	8.1	92.0	8.0

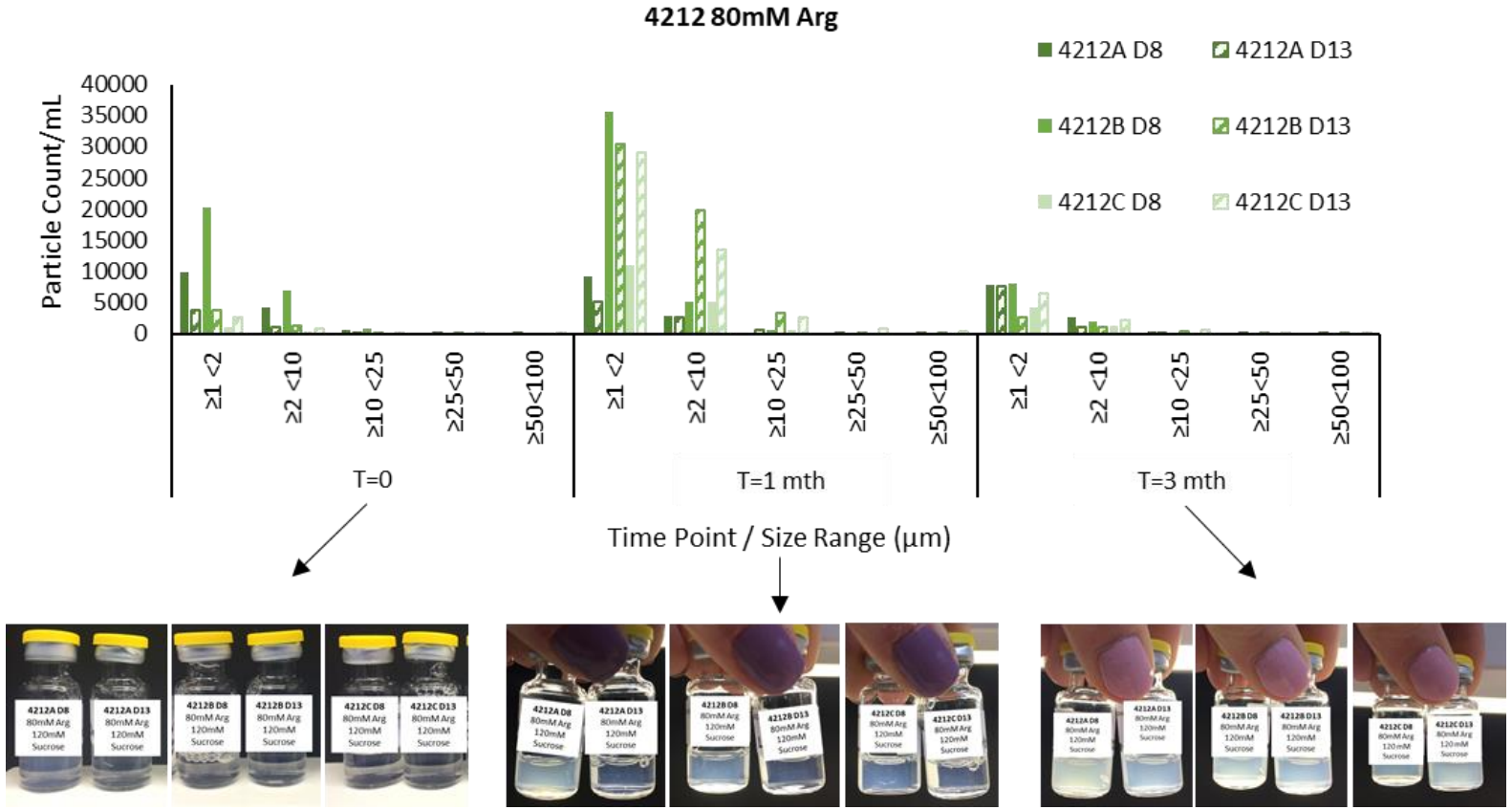

Figure 4.21: Analysis of SVP numbers per mL of mAb 4212 material and visual inspection of material harvested on day 8 and day 13 from cultures 4212A, 4212B and 4212C formulated in 80 mM arginine-HCl, 120 mM sucrose and 20 mM histidine. Samples were analysed/visually inspected at T=0 and after incubation at 40°C for T=1mth and T=3mths.

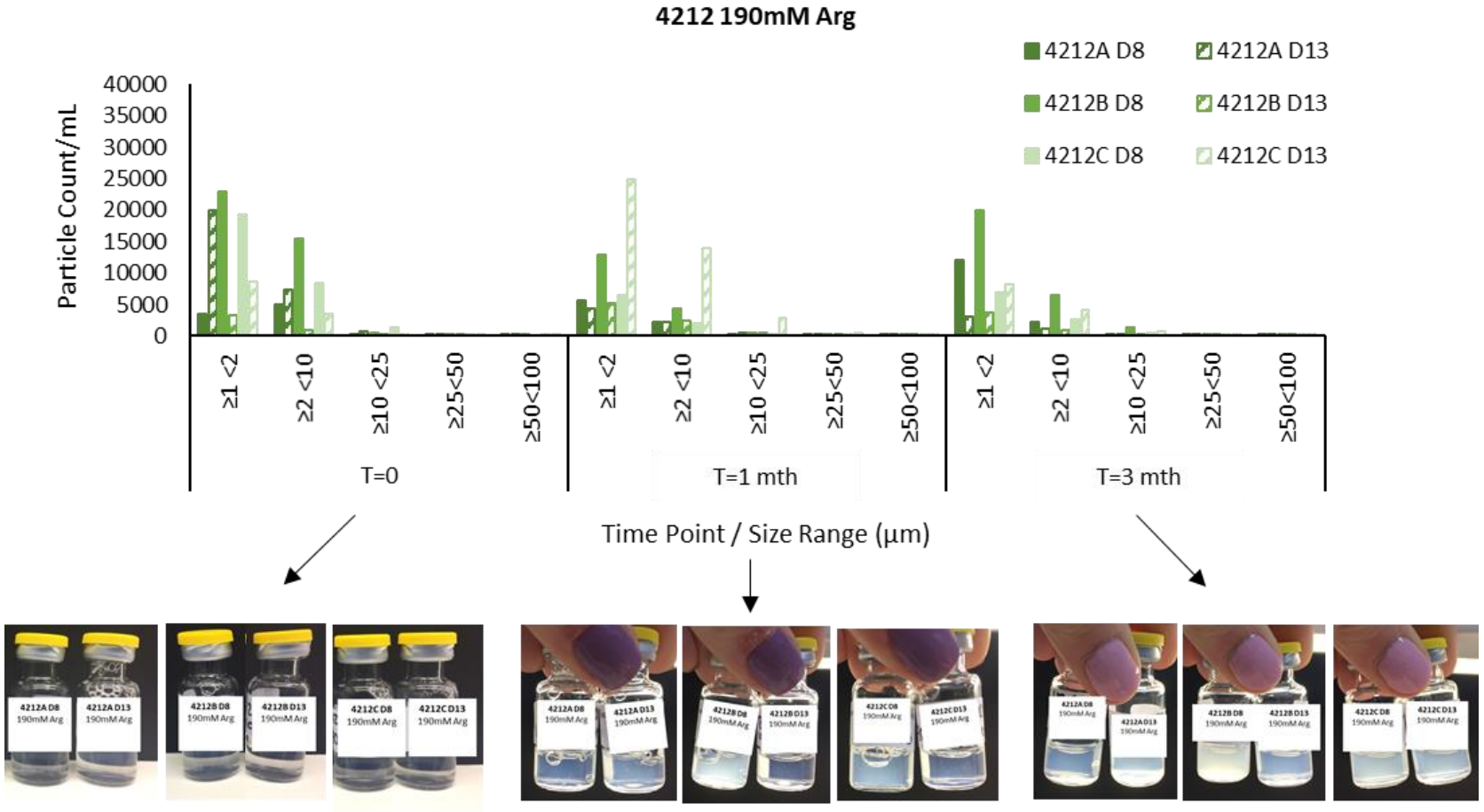

Figure 4.22: Analysis of SVP numbers per mL of mAb 4212 material and visual inspection of material harvested on day 8 and day 13 from cultures 4212A, 4212B and 4212C formulated in 190 mM arginine-HCl and 20 mM histidine. Samples were analysed/visually inspected at T=0 and after incubation at 40°C for T=1mth and T=3mths.

4.8.3 Stability of mAb 184 Material from Day 8 and Day 13 Harvests Under Accelerated Stability Conditions at 40°C

Analysis of the stability of mAb 184 samples by monitoring of SVPs revealed a consistent relationship between harvest day and SVP formation, with SVP formation increased for material harvested on day 13 of culture compared to that from day 8 (Figure 4.23A-B, and 4.24A-B). 184A culture day 13 material at T=0 had at least a 4-fold increased number of SVPs than that from day 8 harvest material across all size ranges and formulations. The measured SVP levels were marginally elevated for samples formulated in 80 mM Arg than those in 190 mM Arg. For 184B culture material however, day 8 material produced more SVPs in 80 mM Arg at T=0 than material harvested on day 13. For 184B material formulated in 190 mM Arg, day 13 material gave rise to more observed SVPs.

When 184 mAb material was analysed for SVPs at T=1 month, day 13 material from both biological culture replicates generally produced more SVPs than that from the day 8 harvest. At this time point (T=1 mth), the difference between the two harvest days was less pronounced in the 80 mM Arg formulation (Figure 4.23A-B) for material from both replicates compared to samples formulated in 190 mM Arg (Figure 4.24A-B). For 184B samples formulated in 80 mM Arg however, there was no difference between the two harvest days compared to 190 mM Arg formulated samples for which day 13 material produced greater numbers of SVPs.

At T=3 months the two biological replicates showed very similar profiles in terms of SVP formation (Figure 4.23A and 4.23B). Higher SVP counts were recorded in the 80 mM Arg formulation than 190 mM Arg, with day 13 SVP analysis of samples formulated in 80 mM Arg saturating the MFI instrument at a maximum count of 31168800 particles/mL, compared to day 8 material for which an average total SVP count of 46301 particles/mL was obtained. The same profile was observed for samples formulated in 190 mM Arg (Figure 4.23A and 4.23B).

Visual inspection of 184 formulated samples (Figures 4.23A-B, 4.24A-B) showed further similarities between the behaviour of the two biological culture replicates, with day 13 material being consistently more opalescent and yellow than that harvested at day 8 at all time points, and in both formulations. As with the 4212 and 109 mAb samples, the majority of SVP content recorded for mAb 184 samples were sized between 1- 10 µm (Table 4.9). At T=3 months day 8 material had a slightly higher percentage of total material >10 µm in size than that from day 13 harvest samples in both buffers. For example, in 80 mM Arg, 10.9% of SVPs were greater than 10 µm for 184A day 8 material compared to 4.9% for day 13 material; and 3.8% for 184B day 8 material compared to 0.6% for 184B day 13 harvest mAb.

Table 4.8: Percentage of total SVP counts which fall within 1 – 10 µm and 10 – 100 µm size ranges mAb 184 samples incubated at 40°C for up to three months.

Sample name	% of Total SVP Count											
	T=0				T=1mth				T=3mth			
	80 mM arg		190 mM arg		80 mM arg		190 mM arg		80 mM arg		190 mM arg	
	≥1 <10	≥10 <100	≥1 <10	≥10 <100	≥1 <10	≥10 <100	≥1 <10	≥10 <100	≥1 <10	≥10 <100	≥1 <10	≥10 <100
184A D8	96.4	3.6	98.0	2.0	95.9	4.1	92.0	8.0	89.1	10.9	91.2	8.8
184A D13	99.0	1.0	99.4	0.6	93.5	6.5	91.7	8.3	95.1	4.9	94.1	5.9
184B D8	99.0	1.0	98.8	1.2	91.2	8.8	93.4	6.6	96.2	3.8	91.6	8.4
184B D13	98.3	1.7	99.2	0.8	93.3	6.7	97.5	2.5	99.4	0.6	93.6	6.4

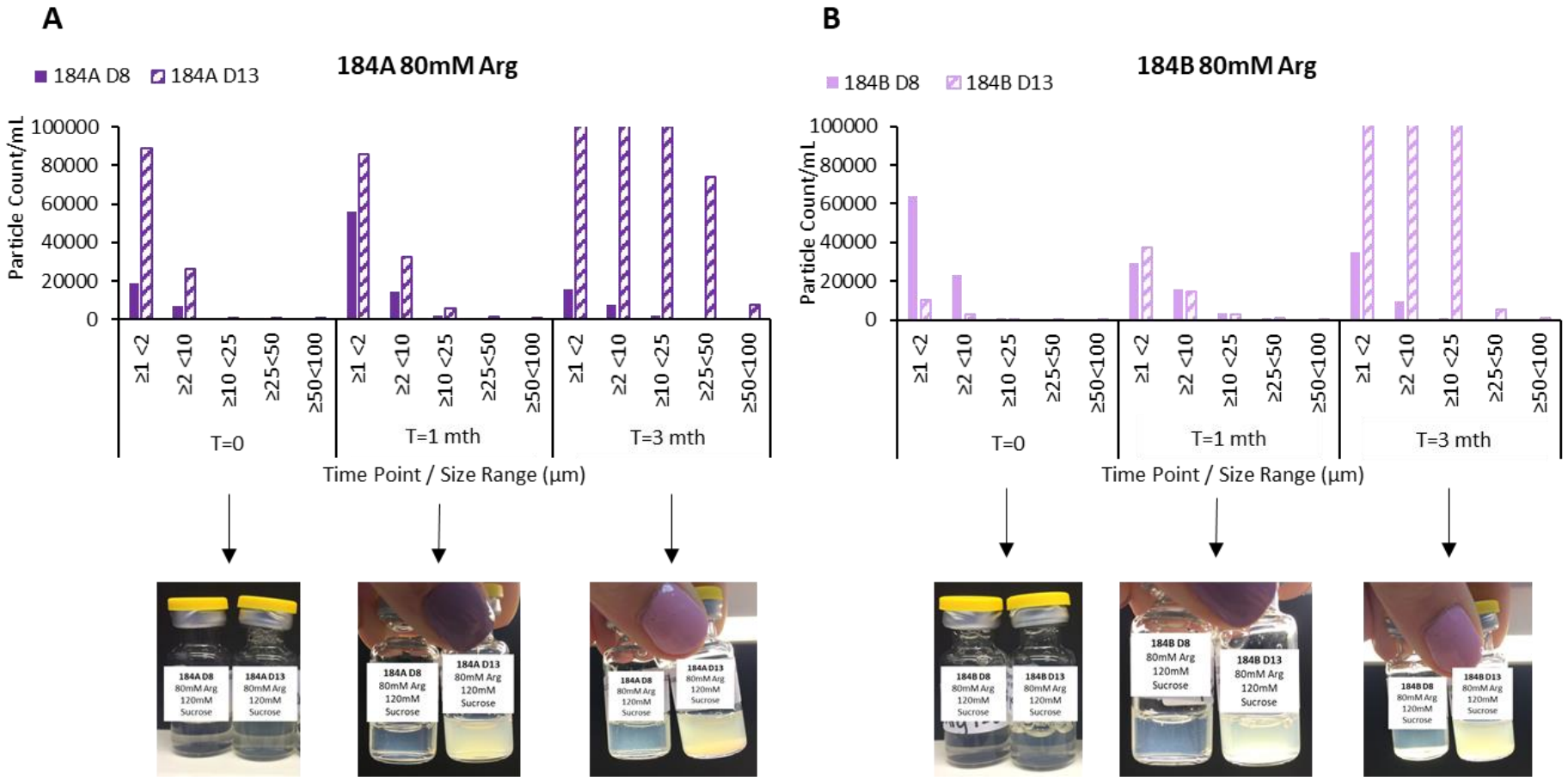

Figure 4.23A and 4.23B: Visual inspection and SVP count per mL of (A) mAB 184A and (B) mAb 184B material harvested at day 8 and day 13 of culture formulated in 80 mM arginine-HCl, 120 mM sucrose and 20 mM histidine. Samples were analysed/visually inspected at T=0 and after incubation at 40°C for T=1mth and T=3mths. Day13 material at T=3mths saturated the MFI instrument, exceeding 31168800 particles/mL.

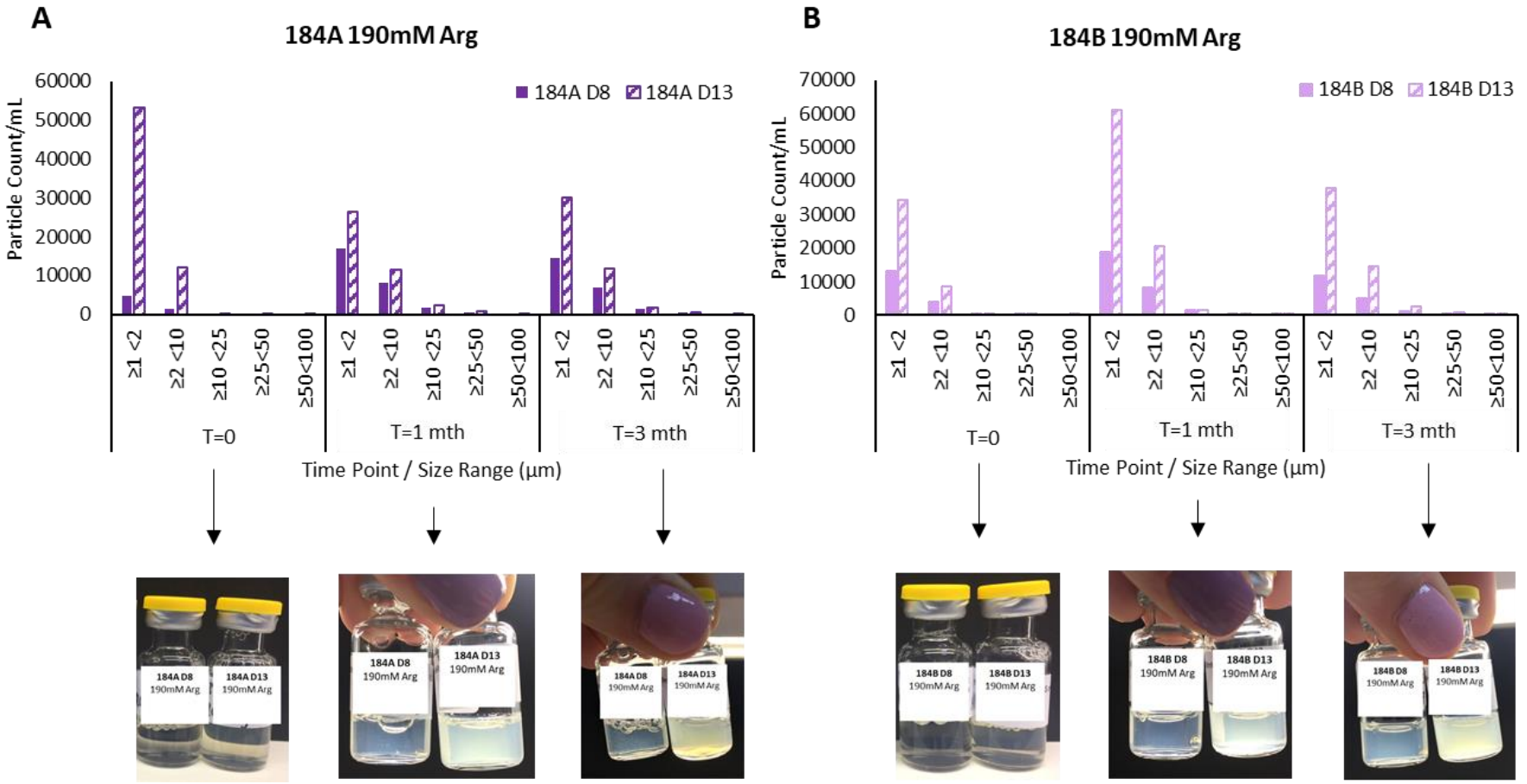

Figure 4.24A and 4.24B: Visual inspection and SVP count per mL of (A) mAB 184A and (B) mAb 184B material harvested at day 8 and day 13 of culture formulated in 190 mM arginine-HCl and 20 mM histidine. Samples were analysed/visually inspected at T=0 and after incubation at 40°C for T=1mth and T=3mths.

4.8.4 SEC-HPLC Analysis of all mAbs

SEC-HPLC was used to determine monomer, aggregate and fragment content within each formulated sample at each time point (i.e T=0, 1mth and 3mth). From this data, a rate of monomeric loss and aggregate/fragment generation per month was calculated (Table 4.9). For all three mAbs investigated in this study, no relationship between harvest day and monomeric loss or aggregate/fragment generation was observed, with similar levels of monomer loss observed between all samples.

One notable observation from the SEC data was that for 4212A material, for which a much higher monomer loss was observed compared to biological replicate material from 4212B and 4212C cultures. When formulated in 80 mM Arg, 4212A day 8 and day 13 material lost three times more monomeric material per month than material from 4212B and 4212C culture. Furthermore, 4212A material aggregate content increased more rapidly, and to a greater extent, than 4212B and 4212C culture material. When formulated in 190 mM arginine however, no difference was observed between material from 4212 biological replicates.

Table 4.9: Rate of monomer loss and aggregate/fragment generation per month, as determined by size exclusion HPLC analysis for all mAb samples incubated at 40°C for 3 months. Samples were formulated in 80 mM arginine-HCl 120 mM sucrose and 20 mM histidine or 190 mM arginine-HCl and 20 mM histidine.

80 mM Arg 120mM Sucrose

Sample	DAY 8 Rate per month (%)			DAY 13 Rate per month (%)		
	Monomer	Aggregate	Fragment	Monomer	Aggregate	Fragment
109A	-2.29	0.05	2.26	-2.53	0.10	2.42
109B	-2.52	0.11	2.41	-2.78	0.21	2.58
109C	-2.58	0.16	2.41	-2.74	0.22	2.52
4212A	-3.80	-0.80	4.60	-6.12	0.18	5.95
4212B	-0.37	-0.19	0.56	-2.50	-0.12	2.62
4212C	-1.59	-0.42	2.01	-2.94	0.05	2.94
184A	-2.49	1.69	0.80	-1.85	0.86	0.99
184B	-1.24	0.91	0.26	-2.20	1.22	0.97

190 mM Arg

Sample	DAY 8 Rate per month (%)			DAY 13 Rate per month (%)		
	Monomer	Aggregate	Fragment	Monomer	Aggregate	Fragment
109A	-2.35	0.03	2.32	-2.58	0.06	2.52
109B	-2.80	0.10	2.70	-2.97	0.20	2.76
109C	-2.89	0.17	2.72	-2.90	0.20	2.70
4212A	-2.67	1.39	1.28	-2.21	-0.43	2.79
4212B	-2.42	-0.29	2.71	-2.93	-0.35	3.28
4212C	-2.40	-0.12	2.52	-2.88	-0.01	2.89
184A	-2.30	1.28	0.86	-1.76	0.43	1.38
184B	-3.83	2.78	0.96	-2.79	1.55	1.24

40°C

4.9 Analysis of Aggregate and Particle Formation in mAb Samples using Atomic Force Microscopy

AFM was used to assess aggregate and particle formation at the nanometre level for mAb samples formulated in 80 mM Arg. Material from samples at T=0 and after incubation at 40^{o}C for 3 months were analysed using this technique.

For mAb 109 and mAb 184 samples, no trend in particle/aggregate formation between biological replicates or harvest days was observed at the nanometre level using AFM. Images collected for these samples are presented in Appendix Figure A.9.

However, AFM imaging of mAb 4212 material from T=0 and after incubation at 40^{o}C for 3 months, revealed differences in the morphology of aggregate/particles between biological replicates (Figures 4.25 and 4.26). At both time points, AFM revealed networks of amorphous material present in 4212A samples from both the day 8 and day 13 harvests. 4212B and 4212C samples, however, had smaller punctate areas of aggregates/particles at both time points.

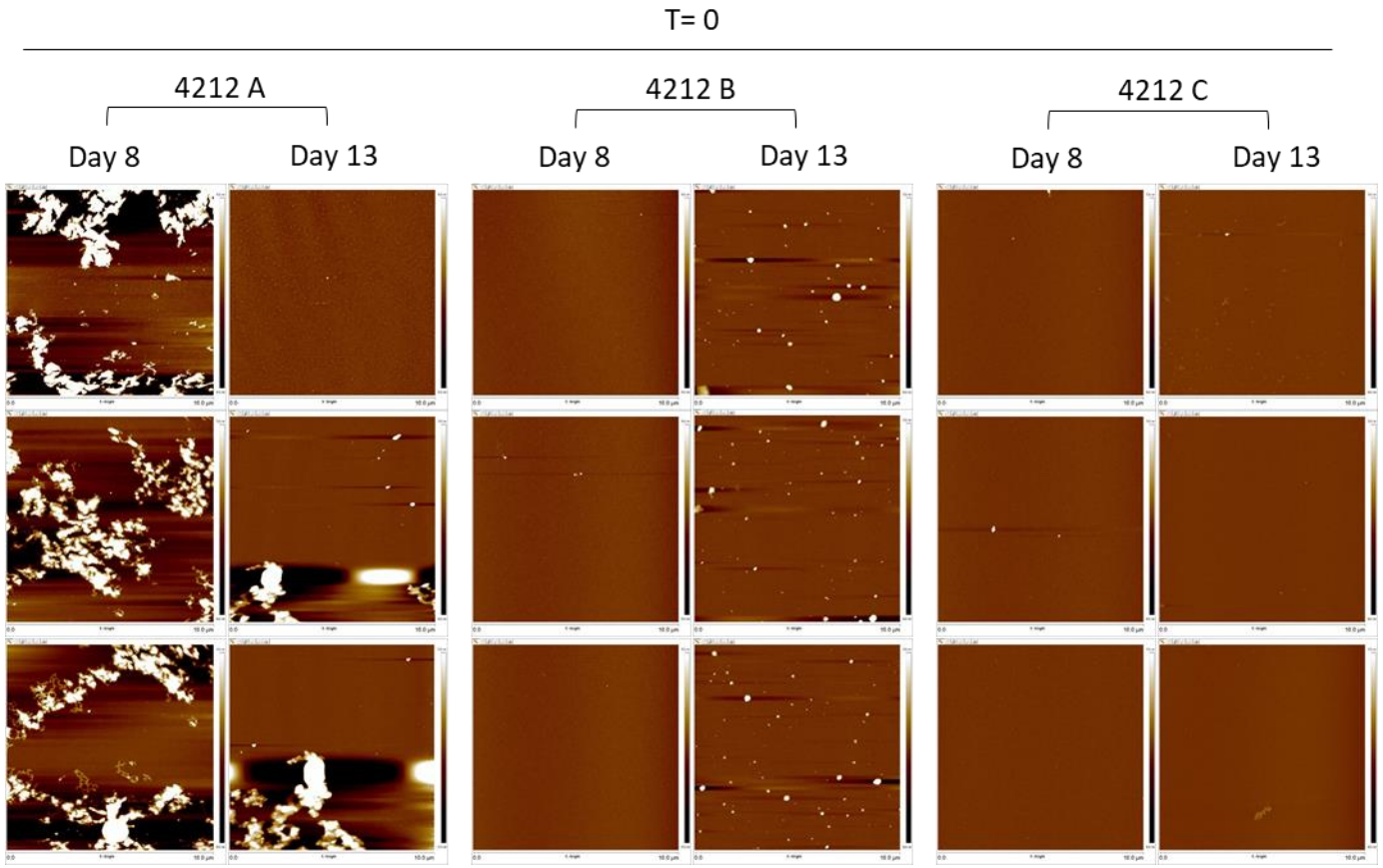

Figure 4.25: AFM analysis of mAb 4212 material from samples formulated in 80 mM arginine-HCl, 120 mM sucrose and 20 mM histidine at T=0. Samples from stability studies were diluted with sterile filtered ddH_2O to 0.002 mg/mL for imaging.

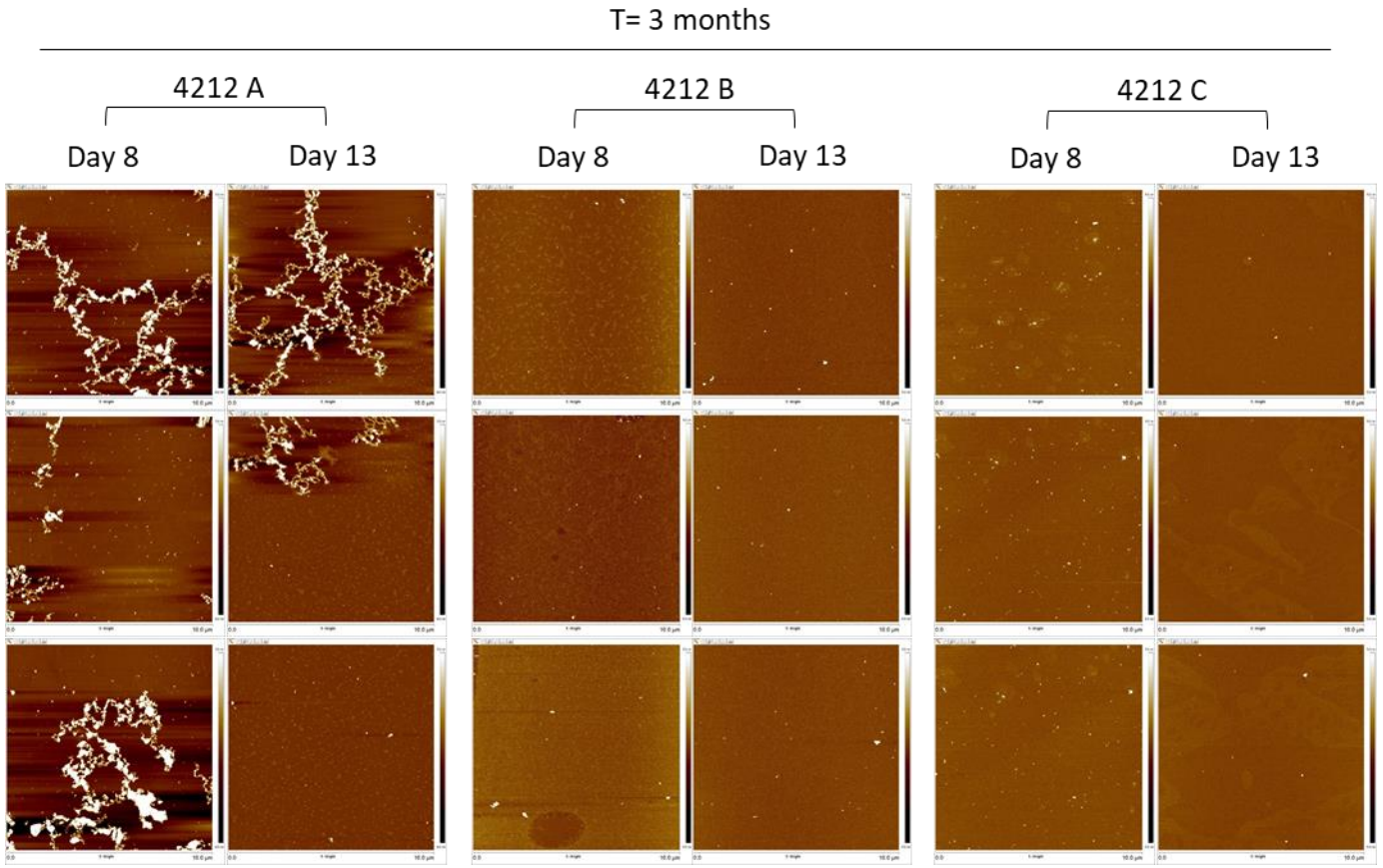

Figure 4.26: AFM analysis of mAb 4212 material from samples formulated in 80 mM arginine-HCl, 120 mM sucrose and 20 mM histidine and incubated at 40°C for 3 months. Samples from stability studies were diluted with sterile filtered ddH_2O to 0.002 mg/mL for imaging.

4.10 Conformation Characterisation of Formulated mAb Samples using Near-UV CD Spectroscopy

To further investigate the observed stability differences between day 13 and day 8 harvests of mAb 184 material, and differences between 4212 biological replicates, near-UV CD spectroscopy was used to determine if there were any conformational differences between samples. For this assay, samples were diluted in their respective buffer from 50 mg/mL to 10 mg/mL. Samples from T=0 and after 3 months incubation at 40°C were analysed in this way. Near-UV CD spectroscopy is often referred to as a proteins 'finger print region' due to its ability to show spectra unique to a protein (Kelly and Price, 2000). Such spectra provides information on the environment in which aromatic amino acids are present, however the exact aromatic residues in a sequence which contribute to a specific spectrum cannot be elucidated from this data alone. It is therefore noted that whilst CD spectroscopy can reveal conformational differences between samples, the specifics as to which amino acids contribute to a spectrum, and differences between samples, cannot be established using this technique. The following presented spectra were therefore used to evaluate if any conformational differences were observed in samples over time, between biological replicates or between harvest days, rather than to establish exact structural changes.

4.10.1 Near-UV CD Spectroscopy Analysis of mAb 109 Samples

mAb 109 samples showed little variation in their near-UV CD spectra, with maxima observed at 295 nm and minima between 265 and 280 nm (Figures 4.27 and 4.28). 109A and 109C culture material showed no variation in spectra between harvest days and time points in either formulation. For 109B material however, there was variation in the spectra between day 13 material at T=0 and T=3 months when formulated in 80 mM Arg. There was no difference in minima and maxima, nor oscillation patterns between the two, however a drift was observed between the two samples, with day 13 T=0 sitting 'lower' than day 13 material at T=3 months. Due to inadequate sample volume, it was not possible to assay 109B day 8 samples from T=0 and T=3 month time points meaning that it is not possible to determine if there is a difference in spectra between harvest days for mAb 109B. When formulated in 190 mM Arg however, no difference in spectra was observed (Figure 4.28B).

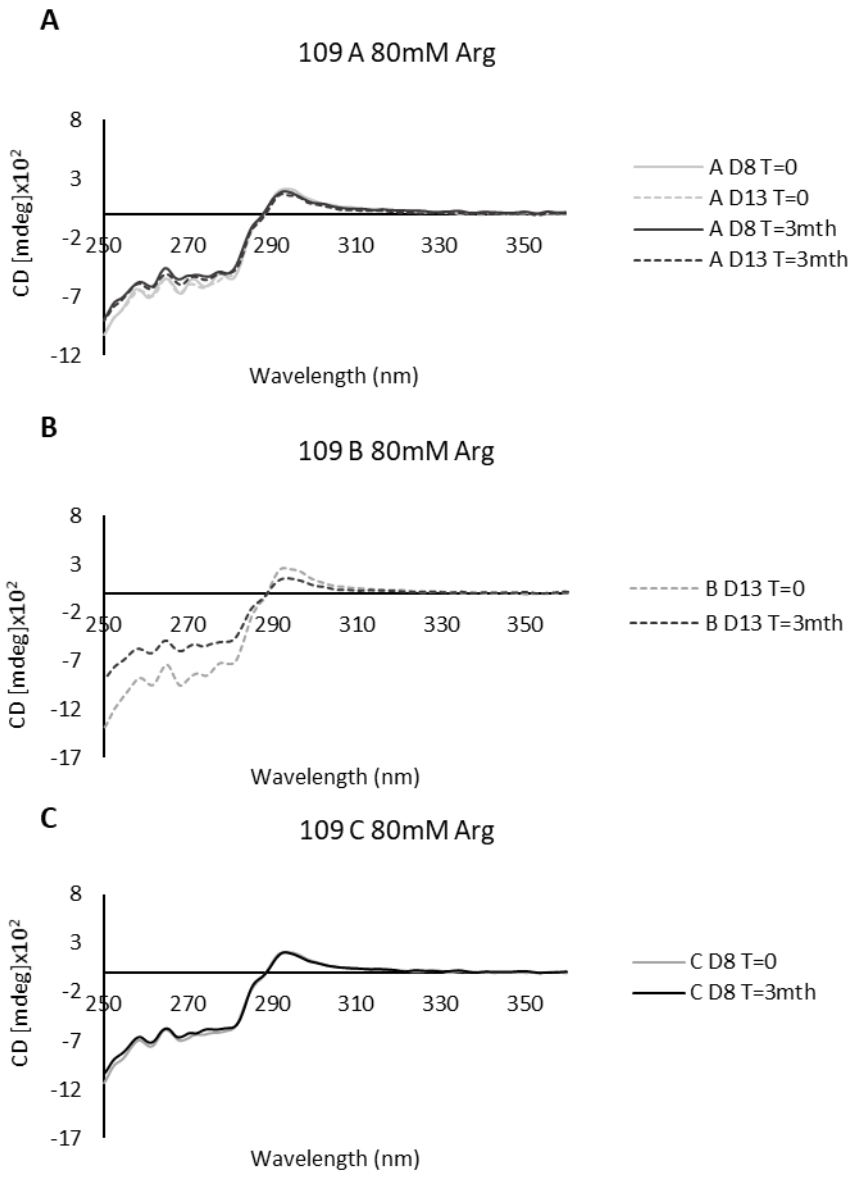

Figure 4.27 Near-UV CD spectra of mAb 109 samples harvested on day 8 and day 13 of 109A (A), 109B (B) and 109C (C) cultures, formulated in 80 mM arginine-HCl, 120 mM sucrose and 20 mM histidine at T=0 and after incubation at 40°C for 3 months. Note that insufficient sample was available to assay 109B D8 and D13 at T=0, and 109C D13 T=0 and D8 T=3 months.

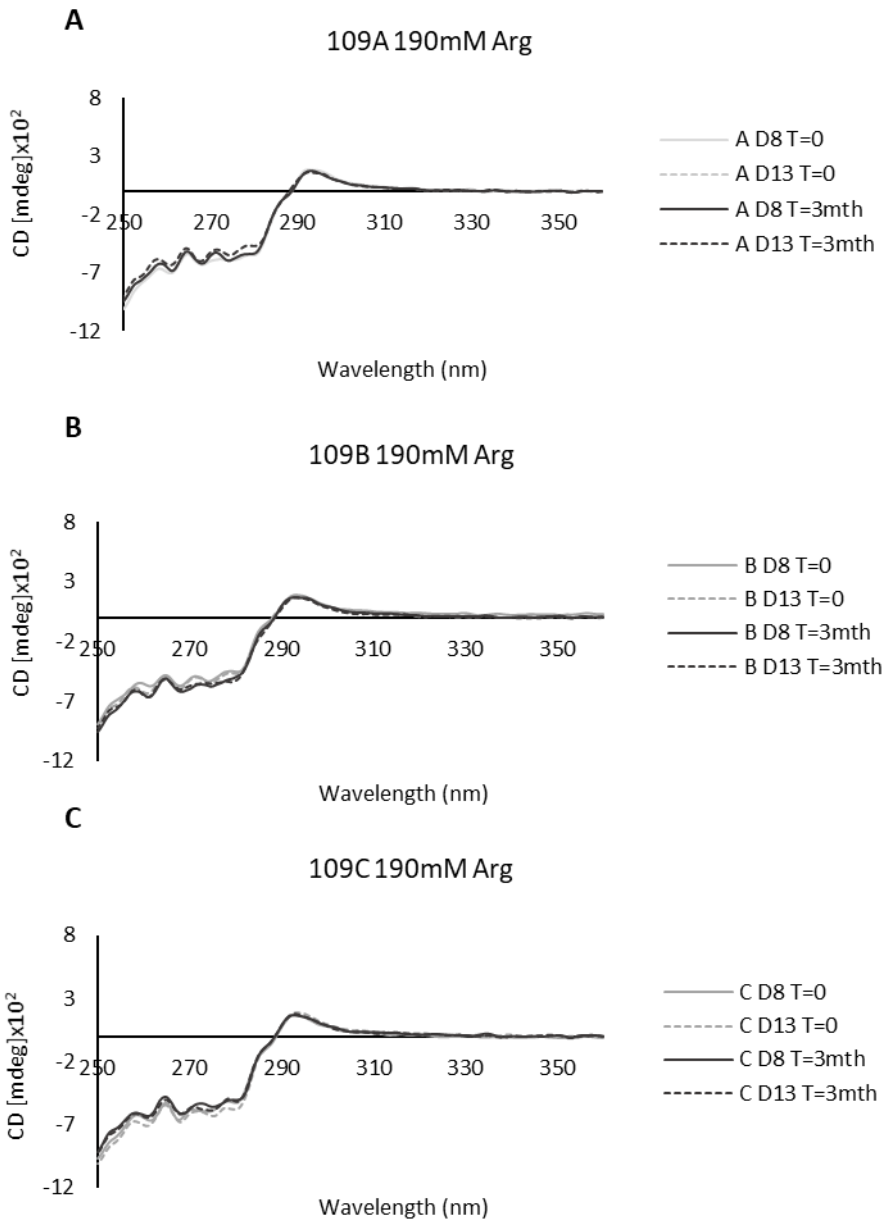

Figure 4.28A Near-UV CD spectra of mAb 109 samples harvested on day 8 and day 13 of 109A (A), 109B (B) and 109C (C) cultures formulated in 190 mM arginine-HCl and 20 mM histidine, at T=0 and after incubation at 40°C for 3 months.

4.10.2 Near-UV CD Spectroscopy Analysis of mAb 4212 Samples

When investigating mAb 4212 replicate culture samples individually, 4212A samples showed the greatest variation in their CD spectra compared to those for 4212B and 4212C samples for both the 80 mM Arg (Figures 4.29A, B and C) and 190 mM Arg formulations (Figures 4.30A,B and C). When formulated in 80 mM Arg, 4212A day 8 T=0 sample was different from the remaining 4212A samples, with increased signal at 288 and 295 nm. In the 190 mM Arg formulation, sample 4212A day 13 at T=0 showed this same increase in signal at 288 and 295 nm.

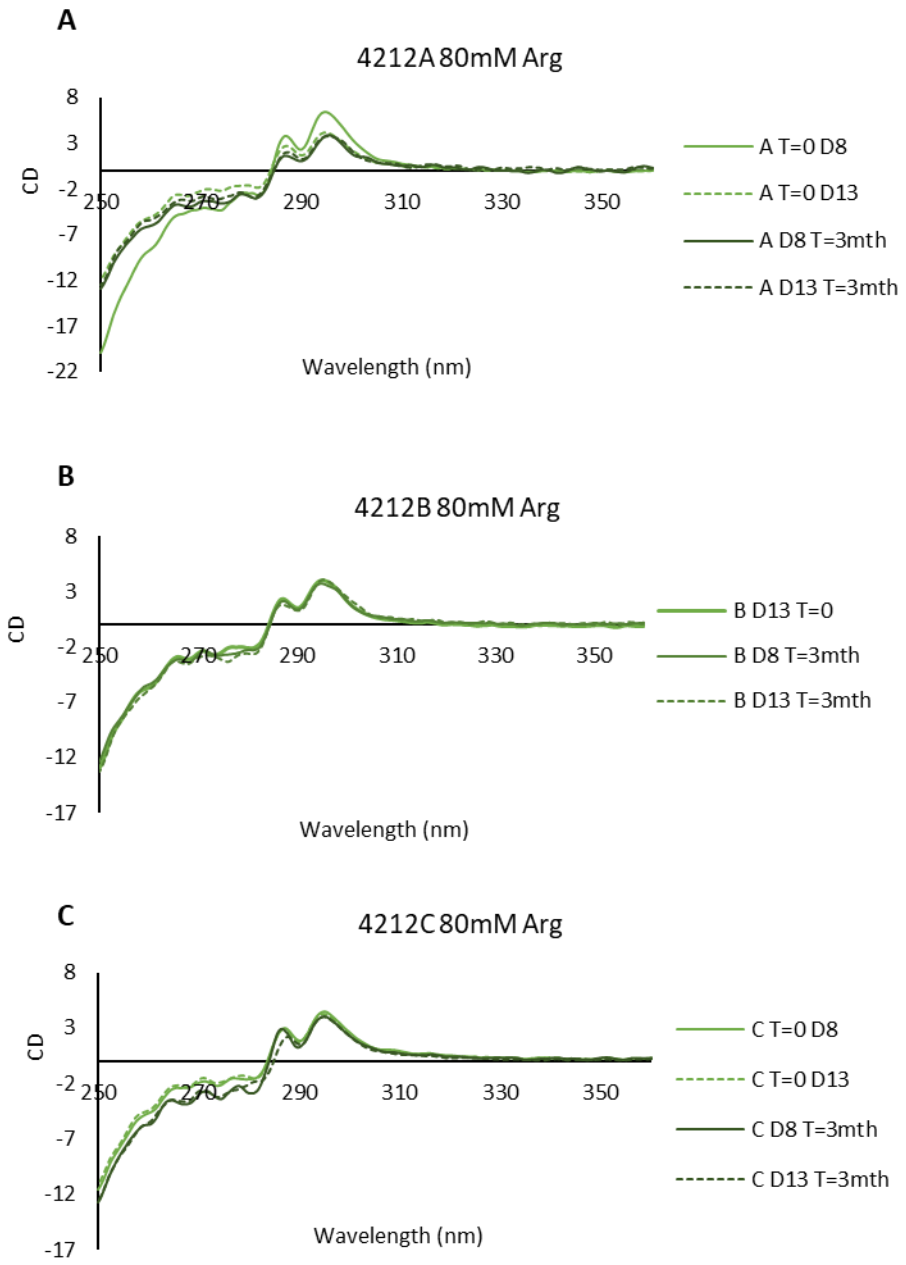

Figure 4.29A, 4.29B and 4.29C: Near-UV CD spectra of mAb 4212 samples harvested on day 8 and day 13 of 4212A (A), 4212B (B) and 4212C (C) cultures, formulated in 80 mM arginine-HCl, 120 mM sucrose and 20 mM histidine at T=0 and after incubation at 40°C for 3 months. Note that insufficient sample was available to assay 4212B day 8 T=0.

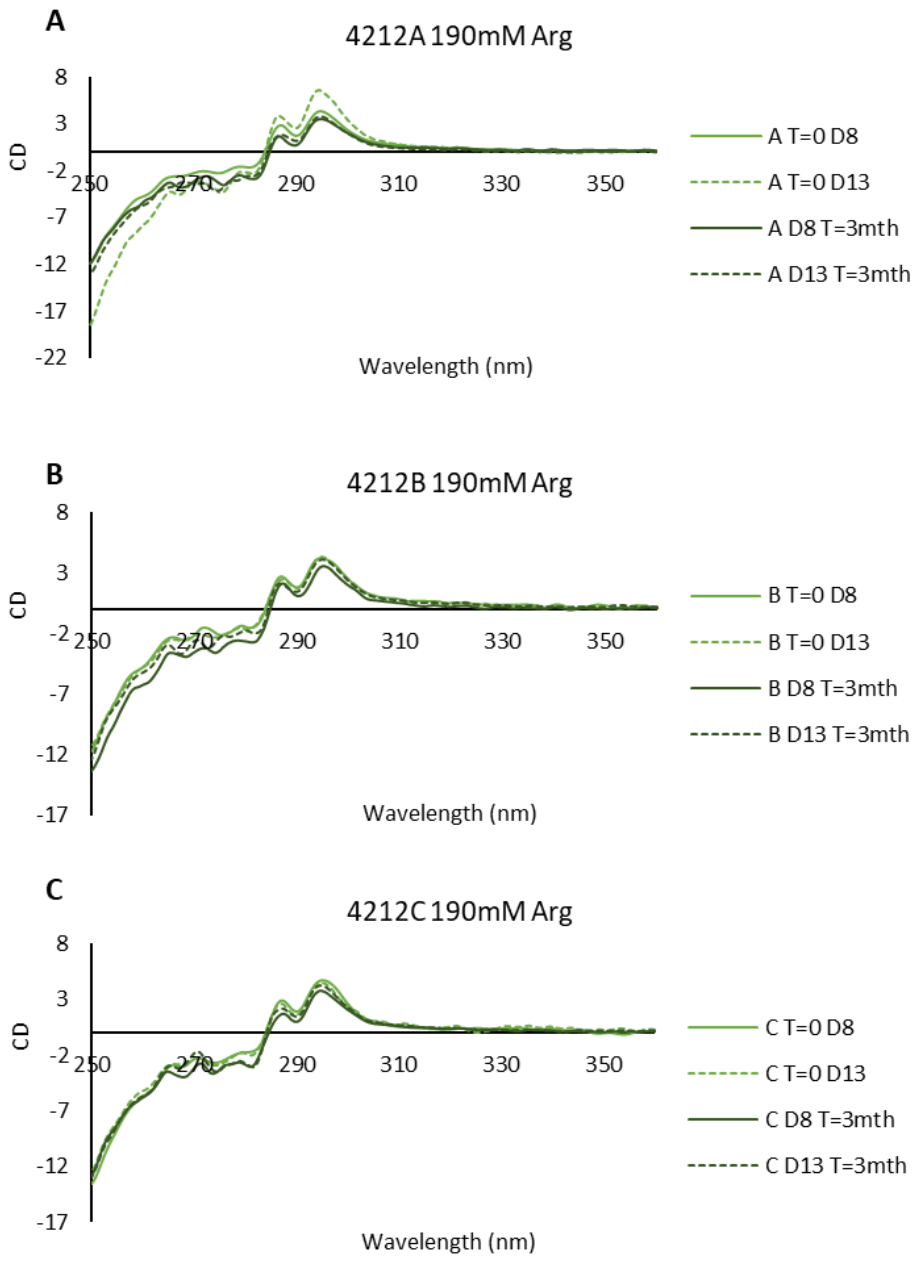

Figure 4.30A, 4.30B and 4.30C: Near-UV CD spectra of mAb 4212 samples harvested on day 8 and day 13 of 4212A (A), 4212B (B) and 4212C (C) cultures, formulated in 190 mM arginine-HCl, and 20 mM histidine at T=0 and after incubation at 40°C for 3 months.

Material from biological replicates 4212B and 4212C showed little variation in their CD spectra between formulations. In terms of the overall shape of the spectra, all samples from all three biological replicates in either formulation showed good homology; with minima at approximately 275 nm and maxima at 295 nm. There was no harvest day trend observed between biological replicates.

4.10.3 Near-UV CD Spectroscopy Analysis of mAb 184 Samples

Near-UV CD spectra of mAb 184 material showed conformational differences between time points and harvest days (Figures 4.31A, B, C and D). These conformational differences were observed within the spectra between 260 and 280 nm. Differences were observed between spectra for 184A day 13 samples at T=0 and T=3 months; as well as between 184B day 8 T=0 and T=3 months samples. For 184A day 13 samples, a maximum is observed at 290 nm for both T=0 and T=3 months, however a minimum was observed at 275 nm for the 184A day 13 at T=3 months sample only. For 184B day 8 samples, a maxima was observed for both time points at 290 nm, however at 280 nm the day 8 sample from T=0 produced a CD signal of -2, compared to -3 for T=3 months.

Insufficient sample was available to analyse 184A day 8 and 184B day 13 samples formulated in 80 mM Arg at T=0, meaning that it was only possible to compare conformational differences between harvest days at T=3 months. At 280 nm a minima was observed for sample 184A day 13 T=3 months with a CD signal of -5 compared to a signal of -3 for 184A day 8 at T= 3 months. A similar pattern was observed for 184B day 8 and day 13 samples at T=3 months with a minima at approximately 275 nm.

When 184 mAb samples were formulated in 190 mM Arg, clear differences in the CD spectra between time points were observed, with T=0 and T=3 months data grouping separately from each other between 260 and 280 nm for both biological culture replicates. When comparing between harvest days at T=0, 184A day 13 samples gave a peak at 280 nm, compared to day 13 for which no peak was observed around this wavelength. At T=3 months, 184A day 8 samples had a subtle peak at 270 nm, whereas day 13 samples did not. Furthermore, a dip in CD signal for 184A day 13 T= 3 months was observed at 275 nm but not for day 8 harvest samples. For 184B samples, differences between harvest days at T=0 were subtler than those observed for 184A samples. The CD signal of 184B day 13 T=0 dipped at 280, 275 and 268 nm, however the corresponding day 8 sample showed no dip in CD signal at these wavelengths. At T=3 months, 184B day 8 spectra showed greater oscillation in its CD signal between 260 and 290 nm than that for day 13 harvest samples.

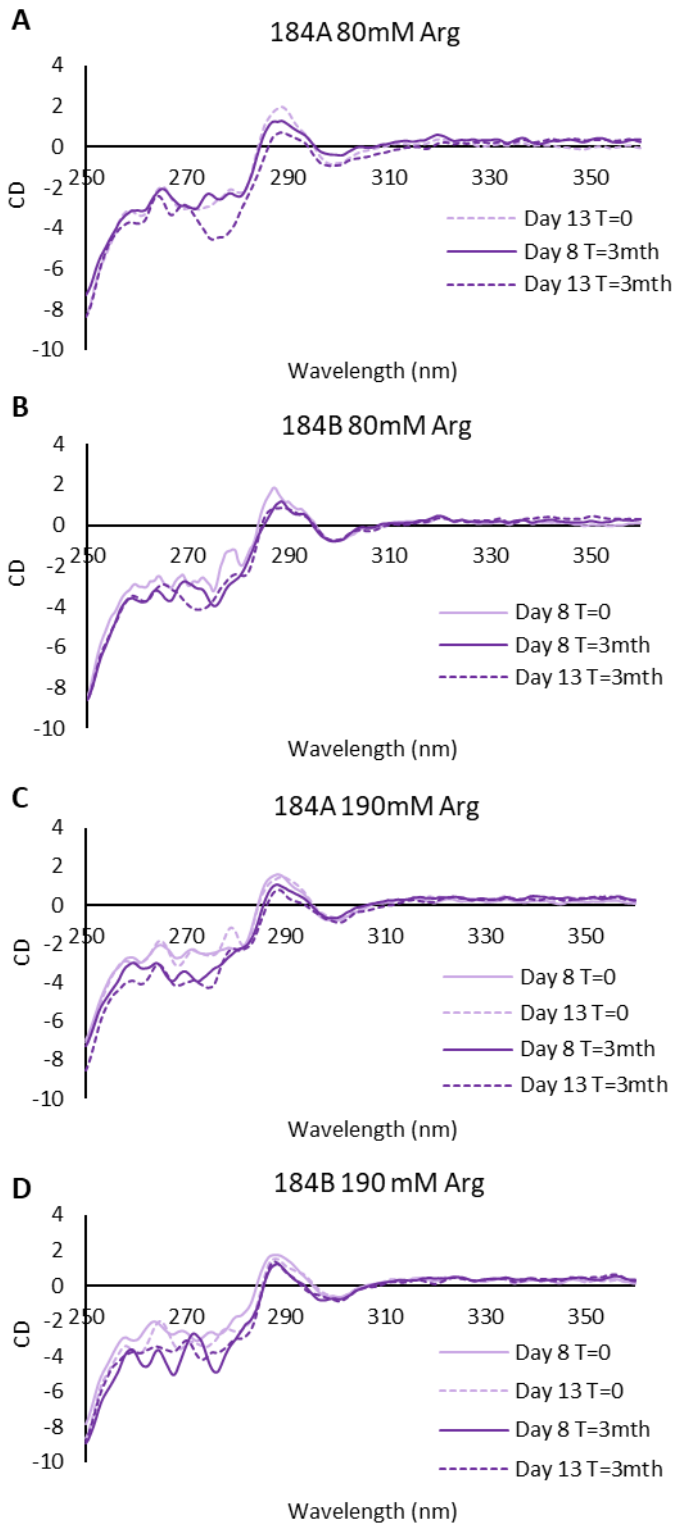

Figure 4.31A, 4.31B, 4.31C and 4.31D: Near-UV CD spectra of mAb 184 samples harvested on day 8 and day 13 of culture, formulated in (A and B) 80 mM arginine-HCl, 120 mM sucrose and 20 mM histidine and (C and D) 190 mM arginine-HCl and 20 mM histidine, at T=0 and after incubation at 40°C for 3 months. Note than insufficient sample was available to analyse 184A day 8 T=0 and 184B day 13 T=0 formulated in 80 mM arg.

4.11 Summary of Results and Discussion

The aim of the work in this chapter was to further investigate the relationship between ER stress, culture harvest day and formulated mAb stability, and to further expand on the data presented in Chapter 3. To do so, three cell lines (known as 109, 4212 and 184 that were each expressing a different monoclonal antibody) were cultured in 10 L disposable bioreactors under fed-batch conditions. Culture supernatant and cell samples were collected to ascertain if the relationships observed in the roller bottle study (Chapter 3) were also observed under controlled, bioreactor conditions with regard to the cellular perception of ER stress and the impact of harvest day on formulated mAb stability.

Cell lines 109 and 184 showed good homology between biological replicates in terms of growth and productivity, total and phosphorylated eEF2 and eIF2α expression, SVP formation, visual mAb degradation and mAb conformation. On-the-other-hand, biological replicates of 4212 material showed variation across all assays, with the 4212A culture having a much higher titre than the 4212B and 4212C cultures, and in turn appearing to be under greater ER stress as determined by western blotting. Furthermore, mAb material from the 4212A culture produced particles at the nanometre level which were different in morphology to those imaged for mAb material from 4212B and 4212C cultures. The CD spectra of 4212A mAb material was also different from the material from replicate cultures B and C. These data suggest that, in the case mAb 4212 producing cell line, there is a relationship between the productivity, the perceived ER stress of cells during that culture and subsequent particle morphology.

When evaluating ER stress at the transcript level, no significant change was observed for any of the 11 GOI analysed across all three cell lines. In contrast, previous work carried out using roller bottle cultures (400 mL) showed different combinations of these genes changing in expression over time for each cell line. These ER biomarker profiles do not therefore translate to ER stress perception by these cell lines in fed-batch 10 L disposable bioreactors. When comparing cell growth and culture viability between the two culture systems this is not surprising, as culturing in bioreactors enabled cells to be maintained in a more controlled environment. For example, DO and pH levels were monitored and maintained throughout in the 10 L cultures and glucose was supplemented as required to maintain a set level based upon metabolite data. Cultures grown in 10 L bioreactors therefore maintained higher culture viabilities than the cultures grown in roller bottles, with culture viabilities being maintained such that these were still >70% on day 13 of culture, compared to a range of 25-60% in the roller bottle cultures at this time. Disposable 10 L bioreactor cultures therefore maintained culture viability for a greater amount of time, with

protein and RNA work showing that the cells experienced less ER stress during bioreactor culturing than when the cells were cultured in roller bottles.

Whilst the transcript data of ER biomarkers showed little change across culture in terms of their expression when cells were cultured in 10 L bioreactors, at the protein level western blotting of total and phosphorylated eEF2 and eIF2α showed changes in ER stress during culture for cell lines 4212 and 184; suggesting that the 4212 and 184 cell lines are responding to ER stress via the phosphorylation of key target proteins. Phosphorylation is a rapid method of changing the activity of existing protein machinery and allows a rapid response to ER stress. Together, this data suggests the response to ER stress during bioreactor culturing is much less than in the roller bottle cultures, but that nevertheless, ER stress is experienced. For cell line 109 however, no change in ER stress in the context of eEF2 and eIF2α phosphorylation, was observed. Based on these results, total mRNA sequencing (RNAseq) analysis was carried out on cell line 184 samples, as these showed the greatest variation in ER stress and a relationship between harvest day and mAb stability. This data is presented and discussed in Chapter 5.

Stability profiling of the panel of mAbs harvested at different points of culture was undertaken through evaluating SVP formation, visual appearance and soluble aggregate/fragment formation of samples. These analyses revealed a consistent relationship between culture harvest day and product stability for mAb 184. Material harvested on day 13 from cultures 184A and 184B produced many more SVPs, and was much more opalescent and yellow than material from day 8, demonstrating that mAb 184 material harvested on day 13 of culture is less stable than that from day 8. For mAb 109 material there was no observed difference between harvest days. For mAb 4212 material, stability data was inconclusive when evaluating the impact of harvest day on product stability, with particle counts, visual inspection and SEC-HPLC analysis giving conflicting data with regard to mAb stability from the different harvest days. For example, the 4212A samples formulated in 190 mM Arg from day 8 of culture produced greater numbers of SVPs than samples from day 13 of culture. During visual inspection, however, the day 13 material was more opalescent than that from day 8. Furthermore, SEC-HPLC analysis showed no difference in aggregate/fragment generation or monomeric loss between the two harvest days of 4212 A.

Interestingly, the stability data presented in Chapter 3, of mAb material generated from roller bottle cultures, revealed a relationship between SVP formation and harvest day for mAb 4212 material, with no trend observed for mAb 184. When considering the data presented from roller bottle cultures and 10 L disposable bioreactor work in combination, a relationship is observed

between mAb stability (in the context of SVP formation and visual appearance), ER stress, harvest day and Qp and culture format. The mode of culture and regulation of DO, pH and glucose also impact on cell performance, and levels of/ responses to ER stress and the stability of formulated mAb material. Moreover, bioreactor data further confirms that this complex relationship is cell line and/or mAb specific.

Previous studies have assessed the expression of genes relating to ER stress throughout culture of mAb producing CHO cell lines. The majority of these studies have investigate the ER response across batch cultures (Hernandez Bort *et al.*, 2012; Maldonado-Agurto and Dickson, 2018; Prashad and Mehra, 2015), with just two studies to our knowledge investigating transcript biomarkers of ER stress during fed-batch culture (Du *et al.*, 2013; Roy *et al.*, 2017).

With relevance to the studies reported here, Prashad and Mehra (2015) evaluate ER stress throughout batch culture of two IgG producing CHO cell lines, denoted as a high producer and a low producer. The study used qRT-PCR to assess the expression of 17 genes at the transcript level relating to ER stress as well as profiling HC and LC mRNA amounts. Through such biomarker profiling, the study established that there was an earlier (day 3-4) UPR response in the high producing cell line, compared to the low producer (day 7), suggesting that productivity was linked to a cell lines ability to act on ER stress. Thus, the concept that enhanced productivity places additional ER stress on CHO cells, combined with the established phosphorylation of eiF2α in response to ER stress (Brostrom and Brostrom, 1998; Harding *et al.*, 2000; Guan *et al.*, 2014), may partially, explain the differences observed between biological replicate cultures of cell line 4212. The 4212A culture had higher titres than cultures 4212B and 4212C, with western blot analysis also revealing increased eIF2α-P expression in cells from the 4212A culture compared to the 4212B and 4212C cultures on day 8. From days 3-8 of culture, the mAb titre and levels of eIF2α-P were similar between all 3 cultures, however from this point onwards a large divergence in productivity was observed between cultures 4212A and cultures 4212B and 4212C. Thus, although there was increased production of mAb from the 4212A culture, this was also associated with an elevated ER stress response. It may therefore be that culture 4212A is better able to deal with ER stresses associated with recombinant protein loads and cell culturing, and therefore able to achieve a higher Qp than cultures 4212B and 4212C; or that producing higher quantities of material (relative to B and C) resulted in increased ER stress.

As discussed above, eEF2 can be phosphorylated in response to ER stress (Patel *et al.*, 2002), resulting in a slowing of translation elongation, and hence global protein synthesis. Western blot analysis of phosphorylated eEF2 showed that eEF2-P quantities were constant in cell lysates of

cultures 184A and 184B until day 8 of culture, after which point, on day 13, levels were greatly reduced (Figure 4.12). This suggests that (a) the cells were under more stress during days 3-8 of culture, compared to day 13, or (b) the cells respond more effectively to ER stress during days 3-8 of culture, after which the cells are no longer able to effectively cope or the stress was alleviated. In the event of unresolvable ER stress, the UPR induces cell death (Bravo *et al.*, 2013; Chakrabarti *et al.*, 2011; Hetz, 2012; Kincaid and Cooper, 2007; Rutkowski and Kaufman, 2004; Sano and Reed, 2013b), hence high levels of ER stress may impact on viable cell concentrations and culture viability. In the case of both 184 cultures however, this does not appear to be the case for days 3-8, as viable cell concentrations continued to increase until day 10 of culture, and culture viability decreased from day 8 onwards. When comparing the stability of mAb 184 material from the day 8 and day 13 harvests, it appears that material harvested on day 13 is less stable than that from day 8 as determined by the propensity to form SVPs and from visible degradation. Collectively these observations suggest it is more likely that eEF2-P expression is indicative of a more effective ER stress response during days 3-8 within cell line 184 cultures.

As outlined earlier, there are few studies that have investigated any link(s) between transcript or protein biomarker profiles of particular cellular stresses and the stability of the final mAb product. There are however, a number of studies that have investigated the relationship between HC and LC transcript and protein amounts and ratios, and how this compares to product quality and/or cell line productivity from CHO cell lines (Ho *et al.*, 2013; Ho *et al.*, 2015b; Jiang *et al.*, 2006; Schlatter *et al.*, 2005). For example, Schlatter *et al.* (2005) investigated optimal *HC:LC* mRNA ratios of mAb producing, stable and transiently transfected cell lines. The study concluded that the optimal *HC:LC* ratio depends on whether a cell line is stably or transiently transfected, but that excess *LC* transcript (relative to the corresponding *HC)* correlated to efficient mAb folding and therefore also to increased productivity. Prashad and Mehra (2015) also described similar findings and relationships. Furthermore, high *HC:LC* ratios have been associated with increased HC polypeptide aggregation (Lee *et al.*, 2009a; Vanhove *et al.*, 2001), as well as with diminished intact protein quality in terms of aggregation propensities and glycosylation patterns (Ho *et al.*, 2013; Ho *et al.*, 2015b). Indeed, Ho et al (2015) assessed aggregation of an IgG produced from cell lines with differing *HC:LC* ratios. Aggregation was then assessed for protein A purified mAb samples using SEC-HPLC. The study reported 10% aggregate levels for cell lines with what was considered a high *HC:LC* ratio (3.4), compared to just 1% aggregate for the same IgG expressed by a cell line with a low *HC:LC* ratio (0.3).

The results presented from the mAb material generated from roller bottle cultures (Chapter 3) also explored potential links between high *HC:LC* ratios and product quality. The data showed that for mAb 4212, whereby the cell line had what was considered a high *HC:LC* mRNA ratio, there was decreased productivity (relative to cell line 184), a unique ER stress biomarker profile and high SVP formation of formulated material from a late (day 13) harvest compared the mAb material from the early harvest day (day 9). When culturing cell line 4212 in 10 L disposable bioreactors, a high *HC:LC* ratio was once again observed, however qRT-PCR analysis showed no change in any of the ER stress biomarker GOI assessed. As such, the ER stress biomarker profiling does not match between the roller bottle and bioreactor cultures. With the exception of culture 4212A, cultures 4212B and 4212C show decreased productivity compared to cultures 184A and 184B. The reason for this is not clear, with the 4212A culture being very different to the other two replicates in terms of growth and productivity. Growth was reduced in the 4212A culture but productivity increased, suggesting that the cells in culture 4212A were able to produce more mAb and to mitigate stress that might arise from high *HC:LC* ratios in a more effective manner than 4212B and 4212C cultures (as discussed above). Furthermore, stability data evaluating the relationship between day of harvesting mAb material, SVP formation, visual degradation and aggregation/fragmentation did not reveal any conclusive relationship between these parameters for 4212 mAb bioreactor generated material.

To our knowledge, no study has investigated the impact of upstream culture stress and duration on subsequent formulated mAb stability, as determined by the analysis attributes including aggregation, fragmentation and presence of SVPs. Park *et al.* (2017) did evaluate host cell protein (HCP) content throughout culture of a mAb producing CHO cell line under fed-batch and batch conditions, and investigated monomer, aggregate and fragment content of protein A purified material on different days of culture (Park *et al.*, 2017). In this study the investigators sampled batch cultures on days 3, 5 and 8; and fed-batch cultures on days 3, 8 and 12, and reported no aggregates were present under either batch or fed-batch conditions. There were however differences in the total monomer content and fragment formation across culture, with batch day 3 samples having 0.7% fragment content compared to 3.7% on day 8; and fed-batch samples on day 3 1.9% compared to 6.8% on day 12 and an associated loss of monomer content. Interestingly, formulated mAb 184 samples showed no difference in their SEC-HPLC profile between harvest days or biological replicates after protein A purification (Appendix Table A.4) However, there was a difference in SVP amounts and visual quality observed between day 8 and day 13 samples at T=0, with material harvested later in culture being of poorer quality based on these attributes. The study by Park et al (2017) also highlighted different HCP content between

sample days and culture conditions, with HCP concentrations 2.2-fold greater in fed-batch cultures than batch, and shown to increase throughout culture. HCPs have been shown to impact protein stability; for example, Bee *et al.* (2015) identify the HCP cathepsin D as the cause of particle formation in a formulated IgG1. It is therefore possible that HCP content influences the stability of mAb material over time, and the amount of HCP present could be different between cultures. It therefore stands to reason that HCP content may underpin the differences observed in the stability of the 184 material from the different harvest days, and could also influence 4212 culture material. Future work could further investigate the number of HCPs present between cultures and identify those present to determine if this did indeed relate the observed harvest day stability trends and to the subsequent 4212 mAb stability observed.

Finally, whilst a difference was observed in the mAb stability of 184 mAb harvested on different days of culture, the stability data for mAb 4212 was inconclusive with regard to whether harvest day impacted subsequent stability. When comparing SVP formation to visual inspection of samples, particle concentrations frequently contradicted opalescence scores of the mAb formulated material. The opalescence of a sample is generally associated with particle/aggregate formation, as these species scatter light and cause sample turbidity. This however, is not always the case, with examples of opalescence being reported due to Rayleigh scattering (Salinas *et al.*, 2010), and it is therefore possible that Rayleigh scattering may account for differences in opalescence in mAb 4212 samples. A further point of note is that samples were filtered (through a 0.45 µm filter) prior to SEC-HPLC analysis, and thus particles which are 0.45 µm – 1 µm in size are not quantified by this analysis. Samples also had to be diluted from 50 mg/mL to 10 mg/mL for SEC-HPLC analysis which may have disrupted some of the aggregated species present within the sample. It is therefore possible that the aggregate species responsible for the observed opalescence trends within mAb 4212 samples were not detected using MFI and SEC-HPLC techniques.

4.11.1 Limitations

When evaluating the data and conclusions presented in Chapter 4, limitations regarding SEC-HPLC, AFM, CD Spectroscopy, purification techniques and the format of stability studies should be considered.

For SEC-HPLC, AFM and CD spectroscopy, samples require significant dilution from 50 mg/mL to 10 mg/mL, 0.002 mg/mL and 10 mg/mL respectively. Through such dilution, aggregated species may be forced apart or induced, meaning samples are no longer representative of the species present in stability study analysis. It should also be noted that for AFM, samples had to be diluted

in water only to enable use of the technique, hence stabilising excipients within the original formulation were also significantly diluted.

All material used throughout the work presented in this thesis was purified from culture using protein A chromatography. Whilst this technique is an industry standard for purifying mAbs, the use of protein A chromatography alone is not representative of industrial or manufacturing conditions, where further polishing steps are typically used. In the case of the data presented in chapters 3 and chapter 4 it is possible that HCP content is influencing the stability data observed. As previously discussed, (section 1.7) it is established that HCP content can induce mAb aggregation, hence the impact of HCPs between biological replicates, harvest days and culture conditions cannot be ruled out based on the work presented. To work towards conclusions which are fully representative of industrial best practice, further polishing steps (such as anion exchange chromatography) should also be used when purifying mAb material prior to formulation. Furthermore, HCP content should be extensively explored between samples through the use of commercially available ELISA and western blotting kits to profile and compare HCP content within samples before and after purification. This lack of HCP data, and limitations of the above-mentioned techniques, means it is not possible to understand the cause of any stability differences between harvest days and biological replicate material discussed in section 4.11.

Stability studies are a proven method to determine the stability of therapeutics. In the case of the work presented here, however, an alternative approach of comparing samples at T=0 may have been more appropriate through enabling a more robust comparison between harvest days, replicates and culture conditions by making more material available for a wider variety of assays. Techniques such as thermal melt CD Spectroscopy could be used to gain an understanding of the thermal stability of each mAb and to explore the structural integrity of material from different harvests. Such data could be used to inform decisions regarding incubation temperatures for any subsequent stability studies, to design a study specific to each mAb/formulation. Having more material available would also enable experiments to be carried out to understand structural and chemical differences (such as glycosylation profiles) between material from different biological replicates, culture conditions and harvest days through the use of techniques such as mass spectrometry. Exploring both physical and chemical degradation in this way would enable a more rounded understanding of the complex relationship between cellular stress, harvest day and mAb stability.

Chapter 5

Mapping the Cellular Response of Cell Line 184 Throughout Culture and Between Harvest days using RNA Sequencing

5.1 Introduction

Previous studies have evaluated the expression of genes relating to ER stress throughout fed and batch cultures producing recombinant proteins using qRT-PCR methods, and related the change in expression of such genes to the recombinant load on the ER (Roy *et al.*, 2017; Maldonado-Agurto and Dickson, 2018; Prashad and Mehra, 2015). However, to our knowledge no literature has explored how such ER stress biomarker profiles may link or relate to the stability of the final recombinant protein once purified and formulated. Whilst qRT-PCR is a powerful tool for investigating changes in the expression of specific genes, this method only enables the detection of pre-selected genes of a manageable size (a small panel of genes, usually in the tens but usually not more than a few hundred at most), meaning that the selection of those genes to investigate is biased by the investigator and the breadth of any such biomarker profiles generated are limited. To build upon the work presented in Chapters 3 and 4, we therefore used RNA sequencing (RNAseq) to investigate the entire transcriptomic profile of cell line 184 samples from days 6, 8 and 13 of fed-batch culture. In order to achieve this, Illumina 100 bp, paired end sequencing was carried out using a commercial supplier, Edinburgh Genomics.

As discussed in previous chapters, several studies have been reported where genes relating to ER stress in mAb producing CHO cell lines were profiled using qRT-PCR (Roy *et al.*, 2017; Maldonado-Agurto and Dickson, 2018; Prashad and Mehra, 2015). Studies utilising RNAseq to profile such stresses are, however, limited with just one study to our knowledge utilising RNASeq to investigate ER stress responses in CHO cell lines (Schroder, 2015). This study investigated differences in ER stress responses between 14 CHO clones producing factor VIII (FVIII), and reported that the three most significantly enriched pathways in the highest producing clones were those relating to the UPR, ER stress responses and oxidative stress. Furthermore, the study identified 21 genes relating to ER stress responses which were significantly differentially expressed between clones, and showed that cellular ER stress responses correlated to FVIII productivity. The study did not, however, compare transcriptomic profiles between culture time points or relate this data to the quality or stability of the FVIII product produced.

There have been many more studies that have used RNASeq to investigate transcriptional differences in CHO cell lines that may contribute to variations in mAb titres and growth rates. Such studies generally use RNAseq to identify targets for cell line engineering to improve product titres and to achieve robust culture growth (Chen *et al.*, 2017; Reinhart *et al.*, 2018; Orellana *et al.*, 2018; Sha *et al.*, 2018; Tamosaitis and Smales, 2018). Across these studies, the

most commonly enriched pathways relating to improved cell growth and productivity are cell cycle, phagosome, lysosome and steroid biosynthesis. Pathways relating to ER stress responses do not generally feature as significantly enriched. Despite such studies, RNAseq has not been applied to investigate how stress induced by mAb production, and across culture during fermentation, might relate to the stability of a purified and formulated mAb product.

5.1.1 Aims of this Chapter

The work presented in Chapter 4 showed that mAb 184 material harvested on day 13 of culture was less stable than that harvested on day 8, in terms of the propensity of this mAb to form SVPs and the opalescence of the material once formulated and subjected to accelerated stability studies. Western blot analysis of protein targets phosphorylated in response to ER stress suggested a difference in stress response at the protein level between harvest day 8 and day 13, however qRT-PCR analysis of genes relating to ER stress showed no change at the transcript level, based on the pre-selected panel of genes analysed. Further investigations into such stress responses at the protein level is limited by the low throughput nature of western analysis, and due to the limited availability of primary antibodies which cross react with CHO cell protein samples. Thus, to further investigate cellular stress throughout culture, and to relate this to the formulated mAb stability, RNA sequencing of cell line 184 samples from days 6, 8 and 13 was undertaken to determine transcriptional differences throughout culture and between harvest days which may impact on secreted mAb stability. RNA seq data was evaluated to compare differentially expressed genes between biological replicates (184A and 184B) and sample days in a pairwise manner, then analysed for pathway enrichment using KEGG and GO databases to assess which pathways were up or down regulated between replicates and sample days.

5.2 Quality Assessment of RNA Sequencing Data

Prior to analysing the RNAseq data for differentially expressed genes between samples, the quality of the data was first assessed by analysing Phred scores using FastQC software. A Phred score is a measure of the quality of base identification during nucleotide sequencing. In FastQC analysis Phred scores are assigned to each nucleotide and converted to ASCII (American Standard Code for Information Interchange) characters to give a quality score. Phred and the FastQ format is widely used in assessing Illumina sequencing data (Cock *et al.*, 2010).

Figure 5.1 shows a plot of mean Phred scores at each nucleotide position of each 100 bp sequence strand for all of the samples subjected to RNAseq. Each sample had a calculated Phred score >20 (Macmanes, 2014), and therefore the sequence data generated for each sample was deemed of adequate quality for subsequent differential gene expression analysis. As well as plotting the Phred score at each nucleotide position, the number of 100 bp sequences with a given Phred score can also be determined, as reported in Figure 5.2. This enables any sequence subsets of 100 bp reads with poor quality to be identified and removed from the analysis. Figure 5.2 depicts the number of 100 bp sequences with a particular Phred score for all samples, showing a single population of sequences which all had an appropriate quality Phred score (>20) as depicted by the peak in counts at a Phred score of 38.

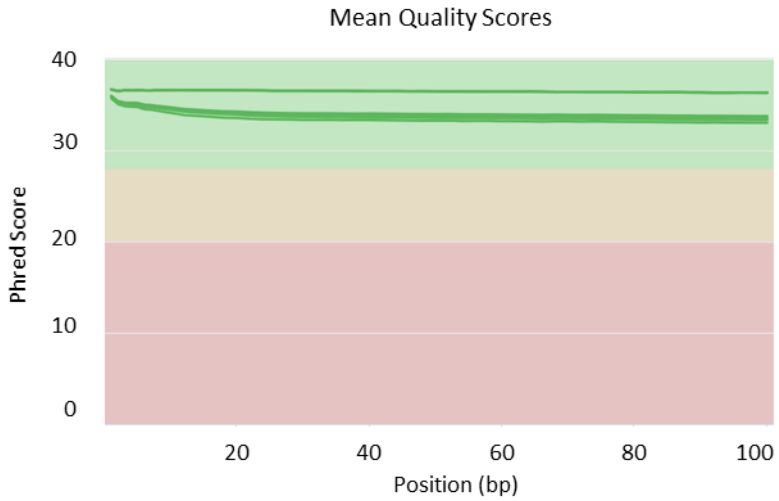

Figure 5.1: Mean quality scores for Illumina RNA sequencing output at each nucleotide position along the 100 bp sequences for all cell line 184 samples (from days 6, 8 and 13 of culture). Phred scores generated using FastQC software were used as the measure of quality, where a Phred score >20 is considered good quality for further analysis. Red proportions of the graph represent Phred score ranges of poor data quality, orange indicates moderate quality and green highlights scores which equate to good data quality.

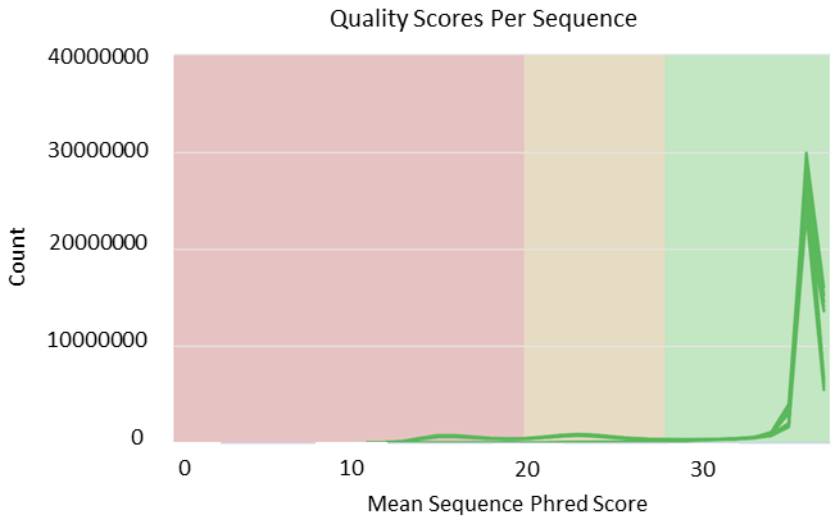

Figure 5.2: Mean Phred quality scores per 100 bp sequence for all cell line 184 samples from days 6, 8 and 13 of culture. The number of 100 bp sequences with a given Phred score were quantified to establish if any sequence subsets were of poor quality with a Phret score <20. Red proportions of the graph represent Phred score ranges of poor data quality, orange indicates moderate quality and green highlights scores which equate to good data quality.

5.3 Comparison of RNASeq Gene Expression Between Sample Days and Biological Replicates of Cell Line 184 Samples

To compare the gene expression profiles between cell line 184 harvest days and biological replicates, scatter plots of each gene against the corresponding fold change in expression were generated and are reported in Figure 5.3. Each sample day showed good homology between biological replicates, with the plotted points fitting closely to the diagonal line for samples from both cultures 184A and 184B on each day (e.g. Culture A day 6 vs culture B day 6 in top right hand corner, Figure 5.3). There was variation in gene expression as expected between biological replicates but differential gene expression was much more marked between sample days, as indicated by plotted points deviating further from the diagonal line. For example, a comparison of culture A day 6 v culture A day 13 (AD6 v AD13, Figure 5.3) revealed many points deviating from a diagonal line whilst the AD13 v BD13 comparison showed a similar pattern as depicted by points assembling along the diagonal. Those genes that lie the furthest from the diagonal are those with the greatest change in expression between the two samples being compared.

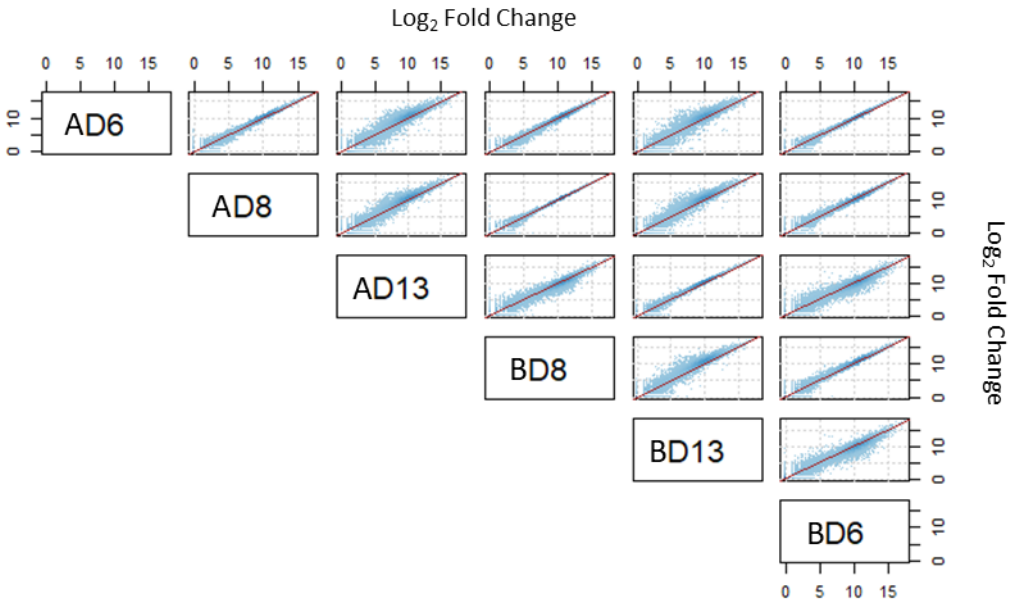

Figure 5.3: Scatter Plots of the log-fold Change in Expression of all Genes Present in RNA Seq data of Cell Line 184 Samples, Where Sample day and Biological Replicates are Compared. Samples were analysed from day 6 (D6), day 8 (D8) and day 13 (D13) from cultures 184A (A) and 184B (B).

Gene expression profiles determined by RNASeq can also be visualized using a heat map to compare between samples days and biological replicates, as shown in Figure 5.4. The heat map showed good consistency between biological replicates, as denoted by darker shading between replicate samples of the same day, indicating that the data from each replicate was close to each other. Clustering depicted within the resulting dendrogram also showed high similarities between biological replicates from the same day of culture, and further differences between sample days as culture progressed (i.e. days 6 and 8 were more similar than days 6 and 13) as indicated by biological replicates of the same sample day sharing the same branch, and sample days further apart clustering in higher branches (Figure 5.4).

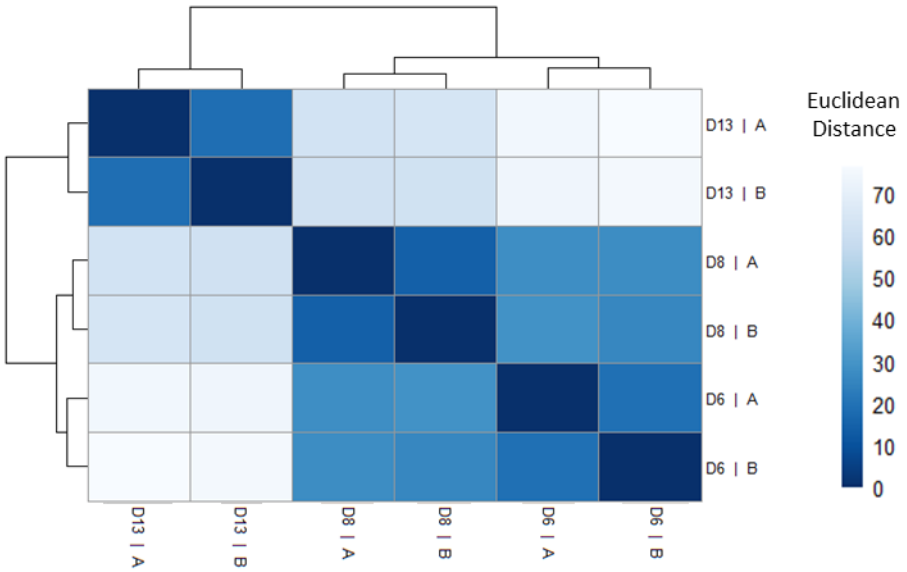

Figure 5.4: Heat Map with Dendrogram Depicting the Relationship of Culture Sample day and Biological Replicate RNAseq datasets. Euclidean distances were used to depict sample-to-sample distances, where darker shading indicates samples which show more similarity in their transcriptomic profile.

5.4 Differential Gene Expression Analysis

Differential expression analysis of transcripts from the RNAseq dataset was used to determine and compare significantly changing genes between samples days and biological replicates. Genes were considered to have a significant change in expression, and therefore to be differentially expressed between two sample days, if there was a $\log_2$ fold change >2 where P<0.1.

Table 5.1: Number of Differentially Expressed Genes (DE) Between Sample Days in Cell Line 184 RNAseq Data Sets. Genes were defined as differentially expressed if the $\log_2$ fold change was >2 and where P<0.1.

Sample Days	Number of DE Genes
Day 6 vs Day 8	12
Day 6 vs Day 13	986
Day 8 vs Day 13	510

When comparing the RNAseq data of samples from days 6 and 8, only 12 genes were found to be differentially expressed between these culture time points (Table 5.1). However, when the

gene expression profiles were compared between days 6 and 13, 986 transcripts were found to be differentially expressed using the criteria outlined above. When the day 8 data were compared with that from day 13, 510 transcripts were found to be differentially expressed (Table 5.1). Thus, the number of differentially expressed genes increased as the time between sample days increased.

Volcano plots were also generated to visualize the number of differentially expressed genes that were up- or down-regulated between sample day comparisons (Figure 5.5). All differentially expressed genes in the comparison between samples taken on days 6 and 8 of culture were upregulated on day 8 compared to day 6, whereas a combination of upregulated and downregulated genes were observed in comparisons between days 6 and 13, and days 8 and 13; with the majority of differentially expressed genes being down regulated on day 13 compared to the earlier culture day in both cases (Figure 5.5).

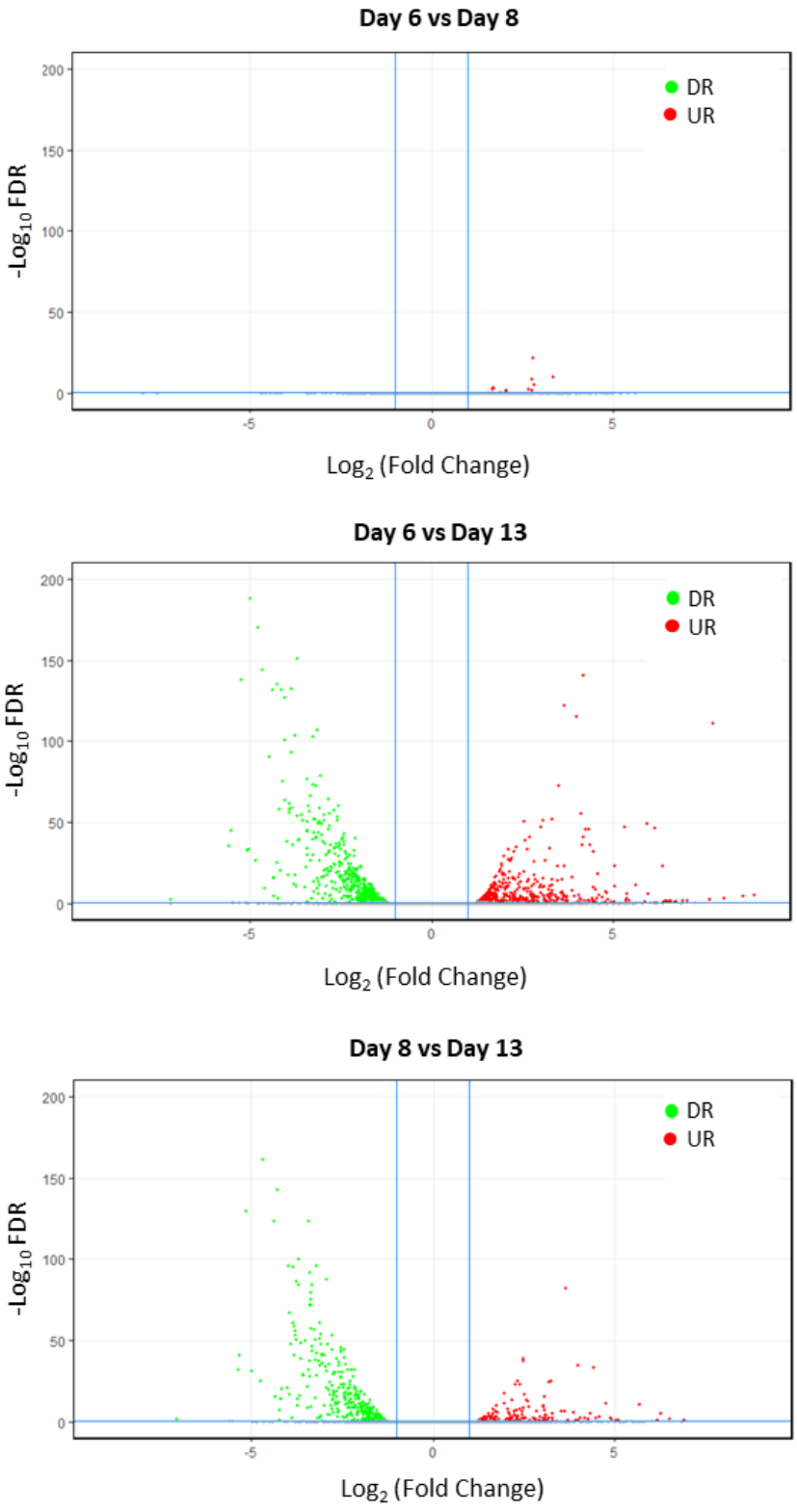

Figure 5.5: Volcano plots of differentially expressed genes between days 6 and 8, days 6 and 13 and days 8 and 13 of fed-batch culture of cell line 184 as determined by RNAseq analysis. Downregulated genes (DR) are shown in green, upregulated (UR) genes are shown in red, where blue lines indicate the cut off $\log_2$ fold change of 2 that was set as the minimum requirement for a gene to be considered differentially expressed.

Principle component analysis (PCA) of differentially expressed genes was also undertaken to establish how global differential expression profiles grouped between biological replicates and culture sample days. The resulting PCA is reported in Figure 5.6, and shows that the culture sample days group separately from each other, with biological replicates grouping together on each sample day. This analysis showed that 84% of variance between samples was captured by the first two principle components and confirms that the differentially expressed genes at each day of culture are statistically significantly different from each other.

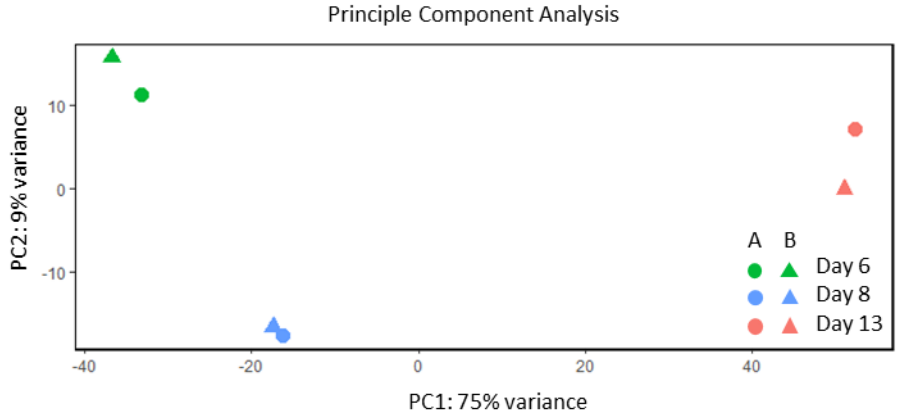

Figure 5.6: Principle Component Analysis (PCA) of differentially expressed genes on Days 6,8 and 13 of culture for samples from cultures 184A and 184B. Principle components 1 and 2 present 84% of the total variance within the data set.

5.5 Pathway Enrichment Analysis

To begin to unravel the potential impact of differentially expressed genes on cellular processes, pathway enrichment was carried out using Gene Ontology (GO) and Kyto Encyclopedia of Genes and Genomes (KEGG) databases. Both databases establish pathway groupings based on *in silico* data and published findings amongst healthy and disease states.

5.5.1 KEGG Pathway Enrichment

Due to the limited number of differentially expressed genes between days 6 and 8 of culture, it was not possible to generate KEGG enrichment pathway maps between these two sample days. However, it was possible to generate such pathway maps for the other comparisons. Figure 5.8 reports the results of KEGG pathway enrichment analysis for differentially expressed genes between days 6 and 13, and 8 and 13 of culture. This analysis showed enrichment of 17 pathways

with differentially expressed genes for the day 6 v 13 comparison, and 12 pathways for the day 8 v 13 comparison (Figure 5.9).

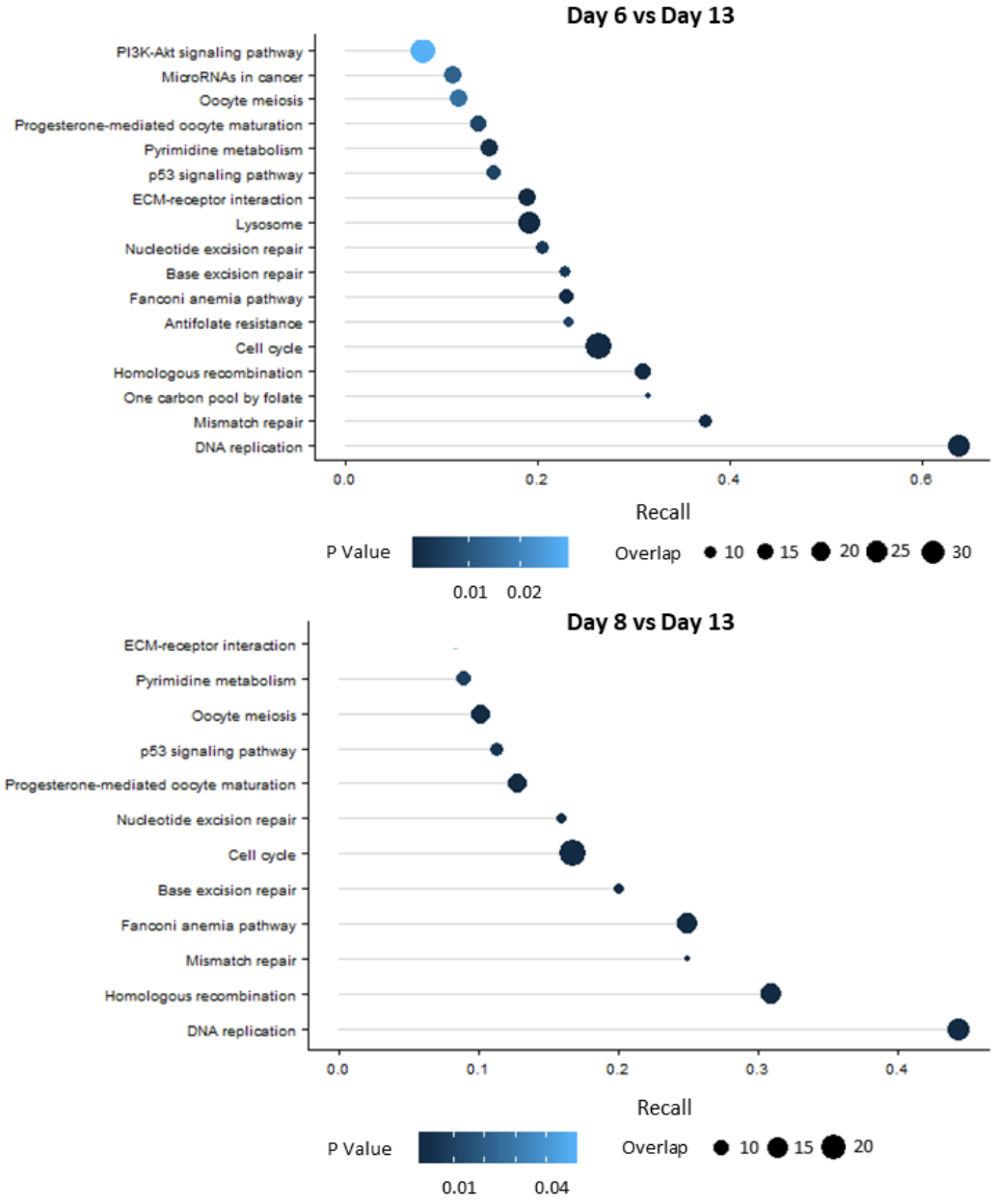

Figure 5.7 KEGG Pathway Enrichment Analysis of Differentially Expressed Genes Between Samples of Cell Line 184 Cultures on Days 6 and 13, and Days 8 and 13. Note that KEGG enrichment could not be carried out between days 6 and 8 due to there being only 12 genes differentially expressed between these two culture time points. Larger circles indicate a higher proportion of differentially expressed genes present within an assigned pathway and therefore a greater overlap. The P value associated with assignment of a pathway is indicated by a colour gradient, where lighter colours indicate a smaller P value and therefore greater statistical significance.

All but 5 pathways were common between the two comparisons, with PI3K-AKt signalling, micro RNAse in cancer, Lysosome, one carbon pool by folate and homologous recombination significantly changing between days 6 and 13, but not between days 8 and 13. The pathways identified all relate to DNA synthesis, repair and maintenance and the cell cycle. In both comparisons, the cell cycle pathway showed the largest overlap with other pathways (30) and lowest P value, as indicated by the size and colour of the plotted point. DNA replication possessed the highest recall in both comparisons and therefore had greatest number of genes assigned to this pathway. When comparing pathway enrichment between days 6 and 13, the pathway one carbon pool by folate showed the least overlap. No pathways associated with protein synthesis, or that reflect an increased recombinant protein load, were identified via KEGG pathway analysis.

5.5.2 GO Pathway Enrichment

For GO enrichment analysis, the number of significantly changing pathways reported is required to be specified. Here, the top 20 significantly changing pathways are presented in Figure 5.9. As with KEGG pathway analysis, pathway enrichment is only reported for comparisons between days 6 and 13, and days 8 and 13 of culture due to the low number of differentially expressed genes between days 6 and 8 of culture.

17 out of the 20 pathways presented were common between the two differential expression comparisons, with the majority of pathways relating to DNA replication/repair and the cell cycle. Intracellular non-membrane bound organelle, non-membrane bound organelle and chromosome organisation were significantly impacted between days 8 and 13, but not days 6 and 13. Kinetochore, DNA dependent DNA replication and DNA replication were significantly impacted between days 6 and 13 only, and had high statistical significance as indicated by small circle plots. In both comparisons, the spindle pathway had the greatest P value, followed by chromosome organisation and DNA metabolic processes in the Day 8 vs Day 13 comparison. All other pathways show very similar P values for both comparisons.

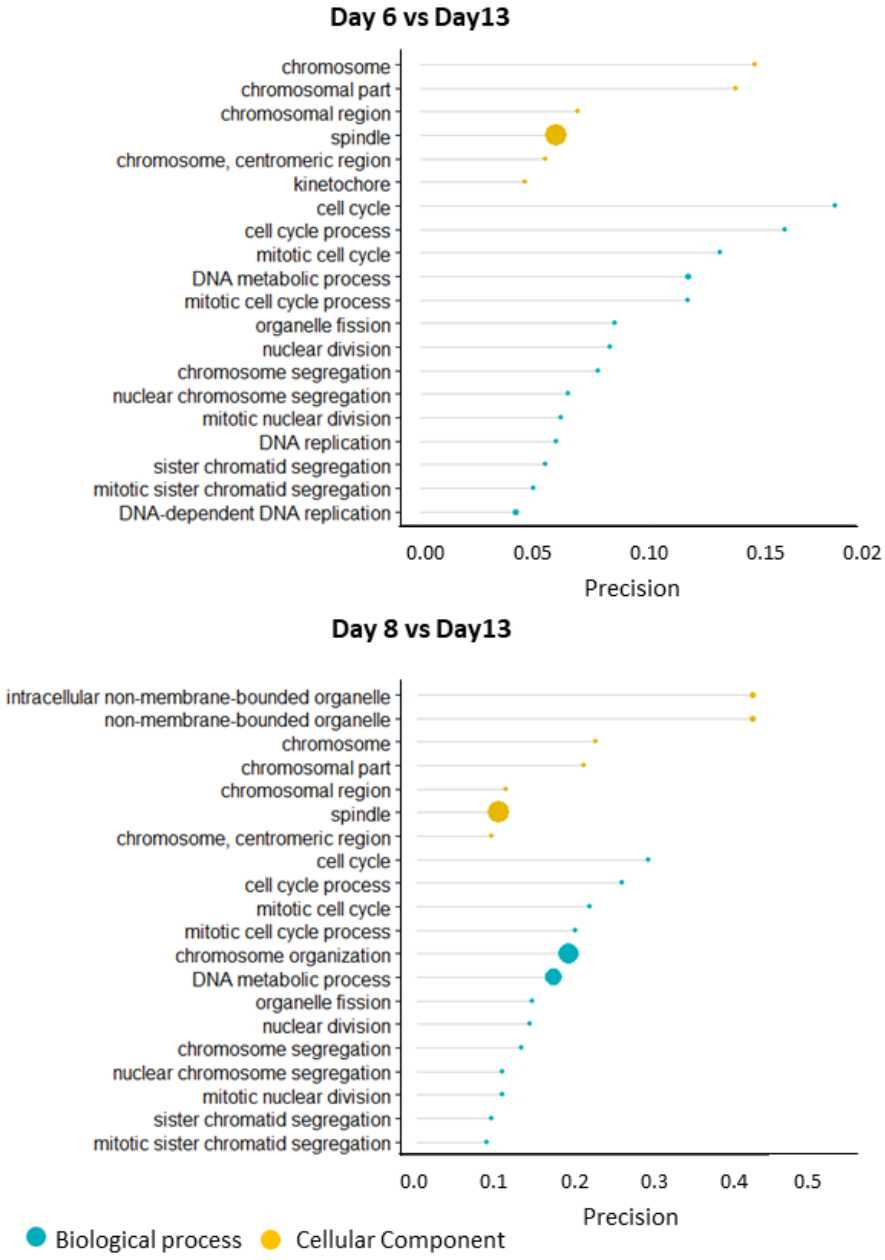

Figure 5.9: GO Pathway Enrichment Analysis of Differentially Expressed Genes Between Samples of Cell Line 184 Cultures on Days 6 and 13, and Days 8 and 13. Note that KEGG enrichment could not be carried out between days 6 and 8 due to the small number (12) of differentially expressed genes observed between these two time points. Smaller circles indicate smaller p values associated with the pathway assignment.

5.6 Validation of RNA Sequencing Data by qRT-PCR

To validate the RNA sequencing data, qRT-PCR was used to determine and confirm the fold change in expression of 8 genes. These genes were selected at random to validate the RNAseq data set, and the trend in relative expression of these genes between the sample days across

culture, as determined by qRT-PCR, were compared to the changes in gene expression (as determine by transcript numbers) established from the RNA sequencing data. The genes selected for analysis, the size of the mRNAs (in bp) and function of these are listed in Table 5.2 below. The subsequent comparison between the relative change in the selected genes expression determine by qRT-PCR (relative to the house keeping gene β-actin) with that determined by RNAseq is reported in Figure 5.10.

Table 5.2: List of Genes Randomly Selected for Validation of RNASeq Data using qRT-PCR. For each gene the corresponding protein function, forward and reverse primer sequences and fragment size (bp) is listed.

Gene/Protein Name	Function	Forward Primer	Reverse Primer	Size (bp)
Aebp	Member of carboxypeptidase A family. Functions as a transcriptional repressor and plays a role in cell differentiation	AGGACTACACCAACGGCATG	TGTTGTTCTCCCACTCACGG	171
Atxn	Chromatin binding factor	ATCAGACGATGATCCCGCAC	AGGATGAGGCACTGACTTGC	248
Aurkb	Part of the aurora kinase subfamily of serine/threonine kinases. Involved in regulation of chromosomal alignment during mitosis and meiosis	ACGACTTTGAGATTGGGCGT	TGTTGGGATGTTGCAGGTGT	186
Gbp7	Involved in cytokine signaling in the immune system.	CAGGAGGAAGGTTGAGCAGG	GAGGTGGCAGAACAGGAACA	192
Ler	Involved in DNA binding and transcriptional regulation	AGGGTCCTCTTTCTCCTGCT	ATGAGCGCAGAGAGGGTTTC	128
Lum	Regulates collagen fibril organization	TGACAGAGTCAGTGGGTCCA	GGCCAGAAGGAAGCTTAGCA	225
Ptprn2	Involved in vesical mediated secretory processes	GACCTCCTGAAAGACCACGG	CCGAGGCTTGAGGACCAATT	221
Saa3	Secreted in response to inflammation	TTTCCATGCCCGAGGAAACT	TGCTCCATGTCCTGTGAACC	115

The patterns in gene expression profiles (relative difference to the house keeping gene β-actin) of all the selected genes analysed using qRT-PCR showed good agreement with those trends observed in the RNA seq data, with the exception of *Atxn1* (Figure 5.4). With the *Atxn1* qRT-PCR data, the day 13 sample of culture 184B had a higher relative expression than the corresponding 184A sample, compared to the RNA sequencing data for which expression between the two cultures on day 13 was similar. Nevertheless, the qRT-PCR data was considered to be sufficiently consistent with the RNAseq derived data to be confident that the RNAseq data was an appropriate representation of the gene expression of target transcripts, and therefore for all other transcripts.

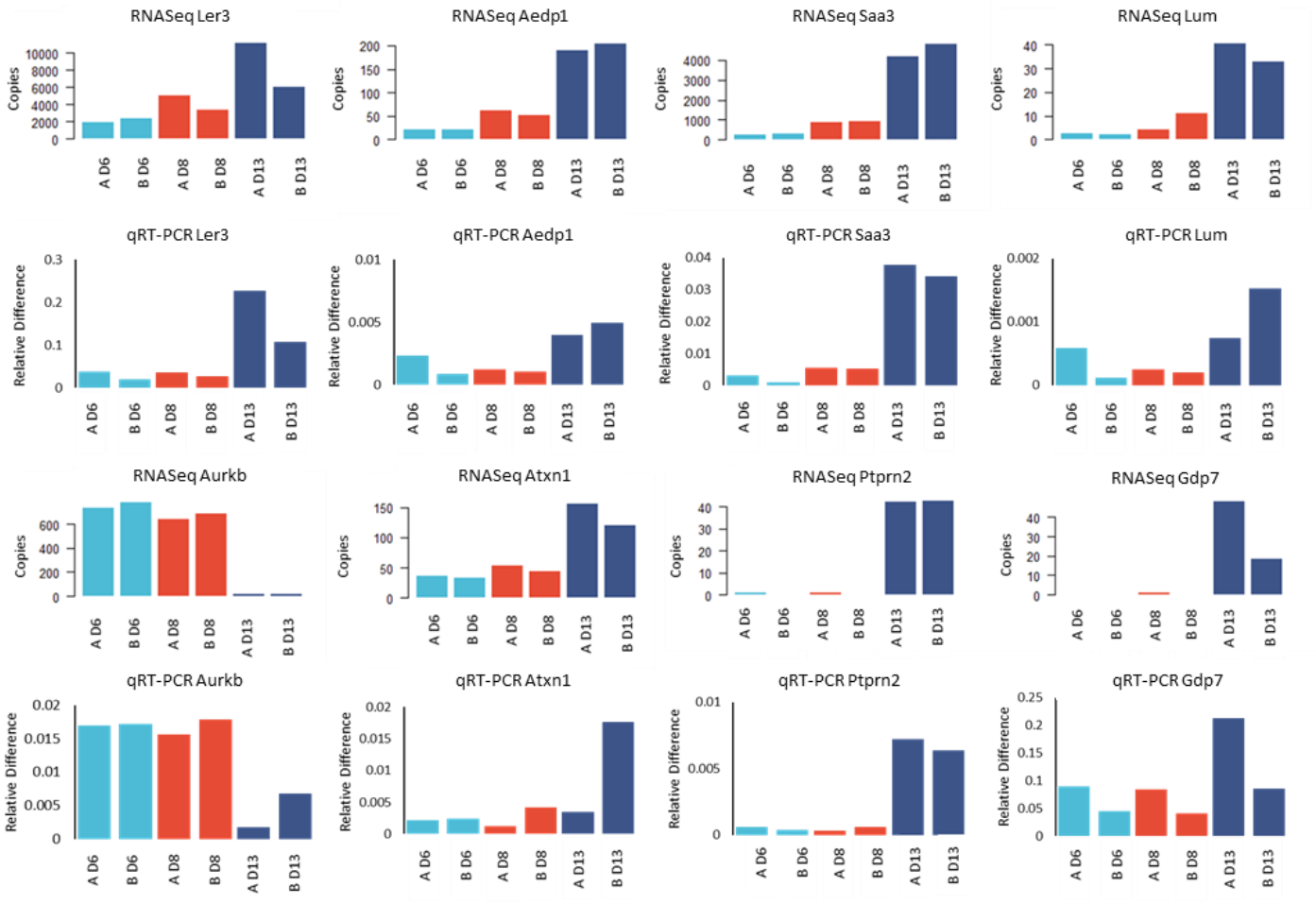

Figure 5.10: Validation of RNASeq Data Using qRT-PCR. The pattern in transcript copy number (established using RNASeq) and fold change in expression (established using qRT-PCR with β-Actin as the house keeping gene) was compared for 8 randomly selected genes for biological replicate samples of cell line 184 from days 6,8 and of culture. Light blue bars show data from day 6, red bars show day 8 and dark blue bars show day 13.

5.7 Comparison of RNASeq Analysis to the Original Panel of Genes Relating to ER Stress Response Pathways Analysed by qRT-PCR

In Chapters 3 and 4, the fold change in expression of a panel of 11 genes relating to ER stress responses were analysed using qRT-PCR (primer sequences Table 2.5 Chapter 2 and functions outlined in Table 1, Chapter 3). Here, the transcript copy numbers determined from RNASeq analysis of cell line 184 samples have also been analysed as reported in Figure 5.11. The qRT-PCR analysis of cell line 184 samples in Chapter 4 (Appendix A3-A.8) showed no significant differences in the expression of the selected target transcripts across culture, however some differences were observed in transcript copy numbers from the RNASeq data. No change in transcript copy numbers was observed by RNAseq for *atf4, hspa9, chac1, derl3, Pfdn2 or calreticulin* transcript expression between sample days, however a difference was observed for *hsp90b, herpud* and *bip* transcripts. As with previous assays, transcript copy numbers were similar between biological replicates.

Herpud transcript copy numbers on day 13 of culture were double those observed on days 6 and 8, with approximately 3000 and 5000-6000 copies being measured respectively. The same trend was also observed for the transcript of *hsp90b*, with approximately 100,000 copies measured on days 6 and 8 compared to 200,000 copies on days 13. The *bip* transcript also showed a similar profile, with 250,000-300,000 transcript copies on day 13 compared to 100,000-150,000 copies on days 6 and 8. Collectively these increases in transcript numbers, at later culture time points compared to earlier in the culture, suggest increased ER stress is perceived by the cells later in culture, in agreement with the qRT-PCR studies on roller bottle cultures reported in Chapter 3.

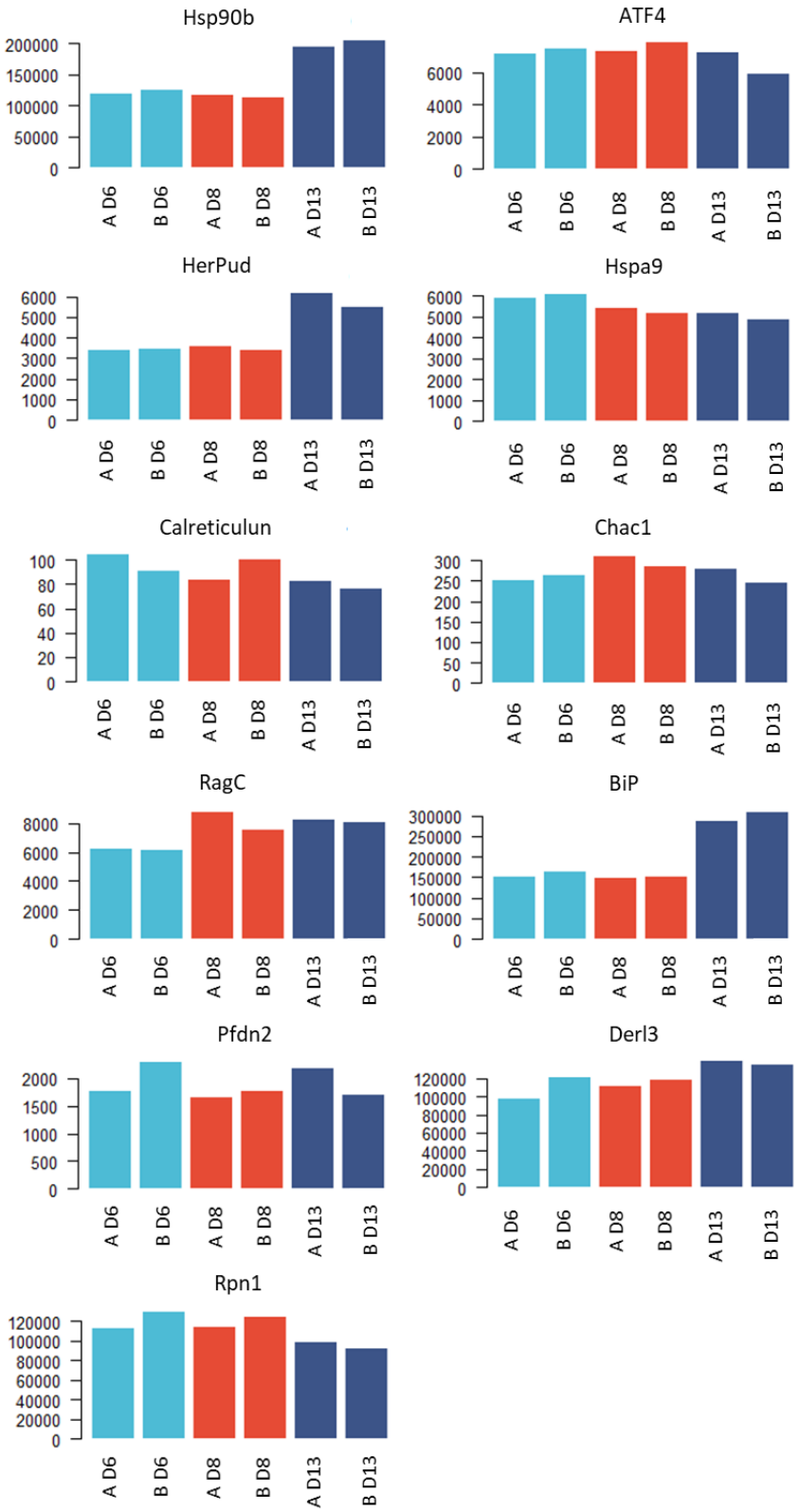

Figure 5.11: Transcript Copy Numbers for the Original Panel of 11 Genes Relating to ER Stress Response Pathways Determined by RNASeq for Cell Line 184 Samples. Total mRNA from days 6 (light blue), 8 (red) and 13 (dark blue) were analysed from biological replicate cultures 184A and 184B.

5.8 Discussion

The aim of this chapter was to evaluate the cellular response at the global transcript level across fed-batch culture of the 184 cell line, using samples taken at various stages across culture, as described in Chapter 4. Differences in gene expression could then be identified and used to determine if transcript biomarkers profiles could be used to predict the impact of cellular stress on the stability of the secreted, purified and formulated mAb (where mAb stability is assessed by quantifying sub-visible particle formation). To investigate this, total RNA was extracted from cell pellets collected on days 6, 8 and 13 of fed-batch culture from 184A and 184B disposable bioreactor cultures, and subjected to RNA sequencing using a commercial provider.

A number of studies have now reported the use of RNAseq to compare gene expression profiles between CHO cell lines, with varying productivities and rates of growth, to identify differentially expressed genes which may be linked to increased cellular productivities or robust growth (Orellana *et al.*, 2018; Sha *et al.*, 2018; Tamosaitis and Smales, 2018). Other studies have also used RNAseq to investigate the impact of nutrient deprivation on CHO cell transcriptomic profiles (Gowtham *et al.*, 2017) and to investigate changes in the expression of genes associated with mAb glycosylation (Konitzer *et al.*, 2015). We therefore sought to apply RNA seq to begin to identify genes and pathways that may be associated with the differences in mAb 184 stability reported in Chapter 4.

Quality assessment of RNAseq data sets using FastQC software showed that all data were of good quality, as indicated by high Phred scores >20 (Figures 5.1 and 5.2). Furthermore, validation of the expression profiles of a selected set of transcripts using qRT-PCR reproduced the same trend(s) in gene expression across a panel of 8 genes, as those observed in the RNASeq data. When comparing transcript copy numbers from the RNAseq data with the relative expression of the original panel of 11 genes determined by qRT-PCR, RNASeq analysis showed almost identical data between biological replicates, with no change in copy numbers across culture for 8 of the 11 genes analysed. However, *Hsp90b, herpud* and *bip* all showed an increase in transcript copy numbers on day 13 of culture relative to days 6 and 8, whilst the qRT-PCR data showed no change in the relative expression of any of these genes. This suggests that the cells do experience an increased ER stress load later in culture. The discrepancy between the RNAseq and qRT-PCR results may be explained by qRT-PCR data being analysed relative to a house keeping gene to plot the fold change in expression of a gene, rather than establishing an exact copy number which is achieved with RNASeq. RNASeq will therefore always offer more accurate data than qRT-PCR. When comparing qRT-PCR data in Chapter 4 to the RNASeq data plotted in Figure 5.11,

and taking into account data for the 8 'validation genes' in Figure 5.10, qRT-PCR and RNASeq analysis matched for 15 out of the 19 genes compared. qRT-PCR data therefore validated the quality of the RNAseq data, and the qRT-PCR analysis carried out and reported in Chapters 3 and 4.

Results previously reported in Chapter 4 (growth and productivity Figure 4.3 and tables 4.3A and 4.3B; western blot analysis Figure 4.13, and stability data tracking SVP formation over time Figures 4.23A, 4.23B, 4.24A and 4.24B), showed that biological replicates from cell line 184 fed-batch culture gave consistent results in terms of the analysis of RNASeq data. The RNASeq transcript profile of both the 184 A and B samples from each day of culture grouped together in transcript analysis scatter plots and heat maps (Figures 5.3 and 5.4.). Biological replicates also grouped together when comparing differentially expressed genes using PCA (Figure 5.6), demonstrating that cells within cell line 184 biological replicate cultures were progressing through culture with similar behaviour. When the gene expression profiles of different sample days were compared, these grouped separately in scatter plots, heat maps and PCA plots, reflecting the fact that there were significant differences in transcriptomic profiles between 184 cells at different stages of culture on different days in both biological replicates. This reflects the different environment and stresses that cells are subjected to as cultures progress over time, and is also a reflection of the cellular responses associated with such changes. For example, stresses linked to mAb production may increase over time. As cells produce higher quantities of mAb at later stages of culture nutrient availability changes, shear stresses accumulate (due to the number of cells in the bioreactor), and toxic metabolic by-products build up (e.g. lactate) (Brunner *et al.*, 2017; Ritacco *et al.*, 2018).

Previous work presented in Chapters 3 and 4 focused on investigating the change in expression of genes relating to ER stress throughout culture as biomarkers that might reflect the stability of subsequent formulated mAb material. Here, GO and KEGG pathway enrichment of RNASeq data did not highlight changes in any pathways relating to the ER or ER stress responses, with the majority of pathways identified relating to DNA replication, DNA repair and the cell cycle. No studies to our knowledge have used RNASeq to investigate ER stress at the transcript level of mAb producing CHO cell lines, however a study by Schroder (2015) investigated the impact of Factor VIII (which is known to aggregate in the ER) production on the CHO transcriptome using RNASeq. In the Schroder study, RNASeq analysis of 14 FVIII producing CHO clones grown under batch conditions was carried out, with samples taken from a single time point. The study revealed a correlation between increased productivity and upregulation of 21 genes involved in ER function and stress responses including *biP*, *hsp90b*, *herpud1* and *calreticulin;* which have

been analysed as part of the work presented in Chapters 3 and 4 of this thesis. Furthermore, pathway analysis showed the top 3 pathways significantly impacted by differential gene expression between clones were the UPR, the ER stress response pathway and an oxidative stress pathway. Following on from these observations, a selection of PDIs and calreticulin (note that BiP was not selected due to other studies showing upregulation of this chaperone did not impact FVIII production) were upregulated in one of the 14 clones, although this did not increase the amount of FVIII produced.

The majority of published RNASeq studies of mAb producing CHO cells focus on comparing cell productivities and growth. When comparing these findings to those presented in this chapter, the pathways highlighted appear to be routinely associated with over-grow culture conditions, and match pathway enrichment data reported in other mAb producing CHO cell lines (Tamosaitis and Smales, 2018). For example, a study by Reinhart *et al.* (2018) identified DNA replication, cell cycle and lysosome pathways (amongst several others) as being enriched in high producing CHO cell lines, which are also identified in KEGG pathway enrichment of mAb 184 samples reported here. Cell cycle and lysosome KEGG pathway enrichment has been linked to increased productivity and cell growth in 19 transcript sequencing studies, as described by Tamosaitis and Smales (2018). These pathways were significantly enriched between days 6 and 13 of culture in the study presented here. It could therefore be hypothesised that the differential regulation of these pathways is related to the high specific productivity of cell line 184. These pathways are involved in regulating cell growth, responding to DNA damage and in plasma membrane repair, cell signalling and energy metabolism. All of these processes may therefore help sustain growth and productivity. The most logical way to test this hypothesis would be to manipulate these pathways by knocking down/out or by up regulating specific key genes in these identified pathways to determine the impact on cell growth and productivity, and to then assess the stability of the formulated mAb. To better understand the impact of growth and productivity on the transcript profile of cell line 184 throughout culture, further mAb 184 producing cell lines could also be cultured, sampled and RNA sequenced.

It is not possible to determine the relationship between mAb 184 stability and the transcriptomic profiles generated from this RNASeq data, however, there is a change in gene expression between harvest days with 510 differentially expressed genes observed between harvest days (8 and 13). To begin linking transcript data to mAb stability, a panel of cell lines producing mAb 184 with varying Qps; and further cell lines producing mAbs with a variety of stability issues (such as phase separation and fragmentation), would ideally be subjected to RNAseq analysis. Moreover, cell lines 4212 (for which the relationship between harvest day and stability could

not be determined) and 109 (which produced a mAb that was consistently stable in terms of SVP formation) samples could also be sequenced to give further insight into cell lines/mAbs with a variety of stability profiles and differing harvest day impacts. Such data would build the foundations to help determine specific genes and pathways which (i) relate to the synthesis of specific mAb products, (ii) relate to specific stability issues and (iii) which may be used as effective biomarkers to indicate suitable harvest times for improved formulated product stability.

5.8.1 Limitations

To work towards understanding which pathways at the transcript level significantly change in response to cellular stress, duration of culture, culture conditions and between biological replicates; a wide panel of cell lines need to be explored, with control samples also introduced to understand what pathways are enriched in response to recombinant protein expression, and which are enriched due to cell culture conditions.

The RNAseq data presented in this chapter is from just two biological replicates of a single cell line which severely limits any conclusions which can be made. Although sample days from each biological replicate group together, with PCA data highlighting significant differences between each sample day, it is impossible to understand how such differences relate to the mAb produced, or the corresponding stability data presented in Chapter 4. To pick out pathways specific to cellular stresses which may be induced through synthesis of a specific mAb, a variety of cell lines producing mAbs with differing stability issues (e.g phase separation vs fragmentation) need to be sequenced and analysed.

A variety of cell lines producing the same molecule with a range of titres should also be studied to understand how recombinant protein load may impact on cellular processes at the transcript level. RNAseq analysis of a panel of host cell lines, which do not produce any recombinant material, would be an essential next step in successfully utilising RNASeq to understand the impact of mAb production on a cell line. Host cell lines would act as control samples to generate a baseline of RNASeq data which would represent typical cellular stresses that arise as a result of cell culture conditions only, rather than mAb production. Through comparing mAb producing cell lines to this control data, pathways with relevance to mAb production can then be unpicked to reveal transcript targets which relate to stresses associated with recombinant protein production, such as ER stress and oxidative stress response pathways. From this data, a panel of targets should then be selected to up- or down-regulate within specific cell lines to test what genes do and don’t impact on the cells ability to product high or low titres. This same principle

can be applied when comparing data from cell lines producing mAbs with different stability issues, where transcripts can be picked out and engineered to understand if the stability profile of a mAb is impacted by the expression of specific genes or up/down-regulation of specific pathways.

Chapter 6

Investigating the Use of Stress Reporter Constructs to Assess ER and Oxidative Stresses During Fed-Batch Culture of CHO Cells

6.1 Introduction

It has been widely reported that during the expression of recombinant proteins, mammalian cells can experience increased ER and oxidative stresses (Halliwell, 2014; Gille and Joenje, 1992; Schroder, 2008; Sano and Reed, 2013b; Cudna and Dickson, 2003). Such stresses can impact on culture viabilities, culture duration and product quality. During the previous work presented in this thesis, transcriptional analysis was undertaken to assess cellular stress responses throughout culture using qRT-PCR and RNA sequencing, with an emphasis on biomarkers of ER stress. Such techniques, however, can be low through-put (RNAseq) and expensive (both qPCR and RNAseq if large numbers of samples are required to be analysed); and require laborious and careful sample processing to ensure high quality data. Whilst these methods are useful for monitoring and detecting transcriptional responses within cells, it would be advantageous to also monitor cellular stress responses in real time. One such way to achieve this is through the use of fluorescent stress reporter constructs, whereby the expression of such constructs is under the control of transcriptional elements involved in cellular stress responses.

A number of previous studies have successfully applied transcriptionally responsive reporter constructs to monitor ER stress, and hence the UPR, within CHO cell lines during culture (Boyce *et al.*, 2005; Wang *et al.*, 1998; Roy *et al.*, 2017; Du *et al.*, 2013). In particular, the study by Du *et al* and Roy *et* al successfully applied reporter constructs to assess the activation of the UPR across a panel of mAb producing cell lines. Each of these studies used the same basic principle, whereby a transcriptional stress response element, upstream of a promoter driving the reporter (GFP), is activated by transcription factors that are upregulated when the cell perceives ER stress, thus leading to enhanced reporter, in this case GFP, expression. GFP expression was then quantified using microscopy and/or flow cytometry to enable the cellular stress response to be monitored throughout culture in real time. Sample preparation using such reporter systems is straight forward, as expression may be used transiently or stably. Once transfected, cells can then be monitored to evaluate the impact of specific chemicals and/or conditions, then easily sampled for flow cytometry analysis.

6.1.1 Aims of this Chapter

The previous work presented in Chapters 3, 4 and 5 investigated ER transcript biomarker profiles, using qRT-PCR and RNASeq, to assess ER stress responses throughout culture; and to analyse differentially expressed genes and enriched pathways. These responses were then related to the day of culture, day of mAb harvest and the subsequently stability of the

formulated mAb under different conditions. In this Chapter, we investigate the use of stress reporters to measure ER and oxidative stress throughout fed-batch culture for a panel of mAb producing CHO cell lines. Constructs designed to report ER stress responses include an ER Stress Response Element (ERSE) upstream of the promoter driving the reporter gene expression (and have been termed ERSE reporters), whilst oxidative stress reporters contain an antioxidative response element (ARE) and are referred to as such. Constructs were designed with a DFP reporter of the appropriate stress, enabling differences in cellular stress responses to be analysed and compared between cell lines and time points using flow cytometry to assess GFP expression

For this work, the following cell lines/mAbs were used:

- Cell line 109 producing mAb 109 (the same cell line used in Chapter 4)
- Cell line AB001 producing mAb AB001
- Cell line 2223 producing mAb 4212
- Cell line 2491 producing mAb 4212

It is noted that the mAb 4212 producing cell lines are not the same as those used previously in Chapters 3 and 4.

6.1.2 Basic Design and Principle of Stress Reporter Constructs

The basic design of each stress response construct consists of a stress response element, followed by an appropriate promoter, in this case either an SV40 promoter or TATA box, then GFP as the reporter protein (Figure 6.3).The constructs generated for this study also included, downstream of this, an SV40 promoter driving mCherry expression to serve as a normaliser. Sequences for ER and oxidative stress response elements were taken from (Du *et al.*, 2013) and Wang *et al.* (2006) respectively. These ER and oxidative stress response motifs are recognised, and bound by, key transcription factors involved in response pathways relating to each type of stress, which in turn increase promoter activity and promote the transcription of GFP. GFP expression is therefore relative to the level of ER or oxidative stress response within the cell, and is used to compare relative stress responses at different stages of culture, and to evaluate chemically induced stress.

6.1.2.1 The ER Stress Response Element (ERSE)

Du *et al.* (2013) describe the construction and use of an ER stress response vector to monitor the UPR in stable mAb producing cell lines. The motif (Figure 6.1) used in the reporter vector is

recognised by transcription factors ATF6 and XBP1, which are key transcription factors upregulated as part of the UPR, and was placed upstream of a TATA promoter. The ERSE therefore refers to monitoring of the UPR only, rather than total ER stress. The group validated the reporter system through transient transfection of HEK293 cells, using tunicamycin and thapsigargin to chemically induce the UPR, and also co-transfected cells with vectors for the over-expression of the ATF6 and XBP1 transcription factors to further confirm the sensitivity of the vector. The group then created mAb producing and parental CHO cell lines which stably expressed the reporter construct, and used the resulting cells to show an increase in GFP expression (and therefore an increase in UPR) in mAb producing CHO cell lines compared to the parental controls during 10 day fed-batch over grow culture. More specifically, the group established an increase in UPR responses across all mAb producing cell lines from day 7 of culture onwards, which correlated to an increase in titre. We therefore sought to utilise this ERSE in reporter constructs to assess ER stress during culture of a panel of mAb producing CHO cell lines to further understand how ER stress changes throughout culture, and how such stress may be profiled to understand the impact of harvest day on mAb stability.

6.1.2.2 The Antioxidant Response Element (ARE)

Wang *et al.* (2006) cloned an ARE to investigate the impact of anti-cancer drugs on oxidative stress responses. The stress response element is recognised and bound by *nrf2*, which functions in the cell to trigger transcription of further genes involved in drug resistance and oxidative stress responses. In this particular case, the ARE was used upstream of an SV40 promoter to drive reporter gene expression. The resulting ARE construct was tested transiently in human liver carcinoma (HepG2), mouse liver carcinoma (Hepa), human mammary carcinoma (MCF7) and CHO carcinoma cell lines, using a luciferase reporter system to assess oxidative stress responses resulting from *nrf2* binding to the ARE. All cell lines were treated with the redox cycling agent tert-butylhydroquinone (t-BHQ) to establish the most sensitive cell line to take forward for stable transfections. MCF7 cell lines proved to be the most sensitive to oxidative stresses, with a 50-fold increase in luciferase activity compared to a 2-3-fold change in HepG2, CHO and Hepa cell lines. ARE sensitivity to *nrf2* expression was also verified through generating cell lines overexpressing *nrf2* and with the gene knocked out.

Despite CHO cells not being further studied in the work by Wang *et al* (2006), we sought to utilise the reported ARE sequence to generate an oxidative stress reporter construct to investigate oxidative stress perception in CHO cells at various stages of cell culture in mAb producing cell lines. We hypothesised that mAb production may cause sufficient oxidative stress for the ARE

to be effective in driving reporter gene expression in this instance. On the basis that the ERSE utilised a TATA promoter and the ARE utilised a SV40 promoter, the decision was taken to construct vectors for each stress response element containing either promoter.

6.2 Construction of Stress Reporter Constructs

The methods detailing the restriction digests, ligations, transformations, PCR reactions and oligo annealing to construct the reporter constructs are described in Chapter 2. All plasmid maps and primer sequences can be found in Appendix B and Chapter 2 respectively.

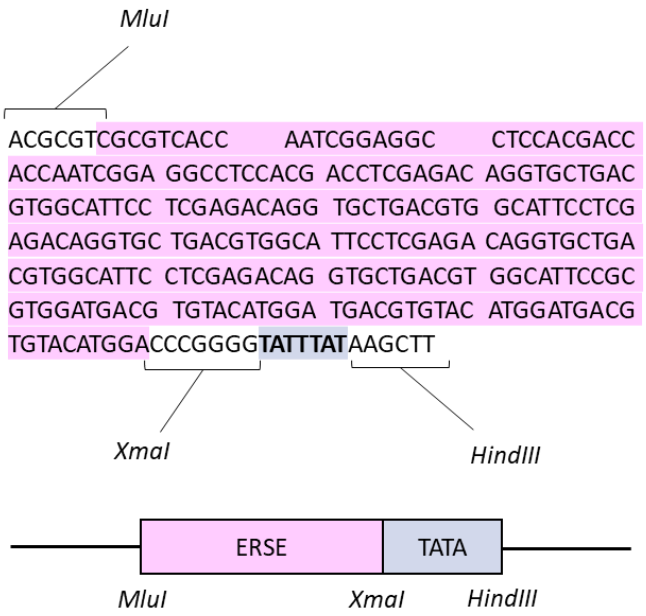

Figure 6.1: Schematic showing the sequence and design of the ERSE with a TATA box downstream to drive GFP expression. The ERSE was taken from Du *et al* 2013, and a TATA Box placed downstream with restriction sites in place to enable the ERSE to be used without the TATA box. A vector containing this sequence was synthesised commercially by GeneArt.

The vector PGL3P-ERSE-GFP-mCh was constructed first, as outlined in Figure 6.3, followed by PGL3-ERSE-TATA-GFP-mCh, then PGL3-ARE-TATA-GFP-mCh and PGL3P-ARE-GFP-mCh as described in Figures 6.4 and 6.5. The ERSE sequence was designed with a TATA box downstream (Figure 6.1), and commercially synthesised, with an XmaI restriction site between the stress response element and TATA box to allow the ERSE to be digested from the synthesized plasmid with or without the TATA sequence. The ARE construct was produced by annealing appropriately designed oligos to produce a fragment of doubled stranded DNA containing the ARE sequence as outlined in Figure 6.2. Test restriction enzyme digests, using *HindIII,* for the stress reporter

constructs are shown in Figures 6.6 and 6.7, confirming successful ligation of the appropriate sequence into the vectors, which was subsequently verified by DNA sequencing. Table 6.1 outlines details of all the vectors created for this Chapter.

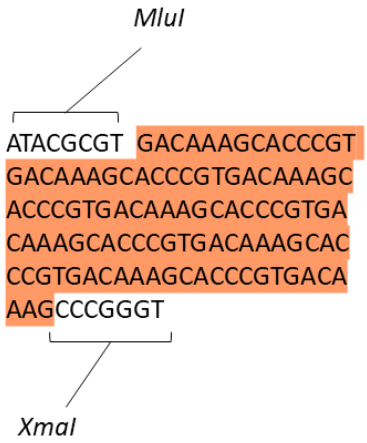

Figure 6.2: ARE Sequence with *MuI* and *XmaI* restriction sites for subsequent cloning. The ARE sequence was taken from Wang *et al* (2006). Oligos were designed containing this sequence, annealed and digested with the corresponding restriction enzymes to insert the ARE sequence into the digested vector backbones.

Table 6.1: List of vectors used to construct ERSE and ARE stress reporter constructs. Details of digests and ligations carried out are detailed in figures 6.3, 6.4 and 6.5.

Vector Name	Size (bp)	Notes
PGL3P	5010	
PGL3	4818	
PGL3P-GFP	4047	
PGL3-GFP	3855	
PGL3P-mCh	4038	
PGL3P-ERSE-GFP	4281	
PGL3-ERSE-TATA-GFP	4076	
PGL3P-ERSE-GFP-mCh	**5479**	**Denoted ERSE-SV40**
PGL3-ERSE-TATA-GFP-mCh	**5274**	**Denoted ERSE-TATA**
PGL3-ARE-TATA-GFP	3942	
PGL3-ARE-TATA-GFP-mCh	**5140**	**Denoted ARE-TATA**
PGL3P-ARE-GFP	4147	
PGL3P-ARE-GFP-mCh	**5345**	**Denoted ARE-SV40**

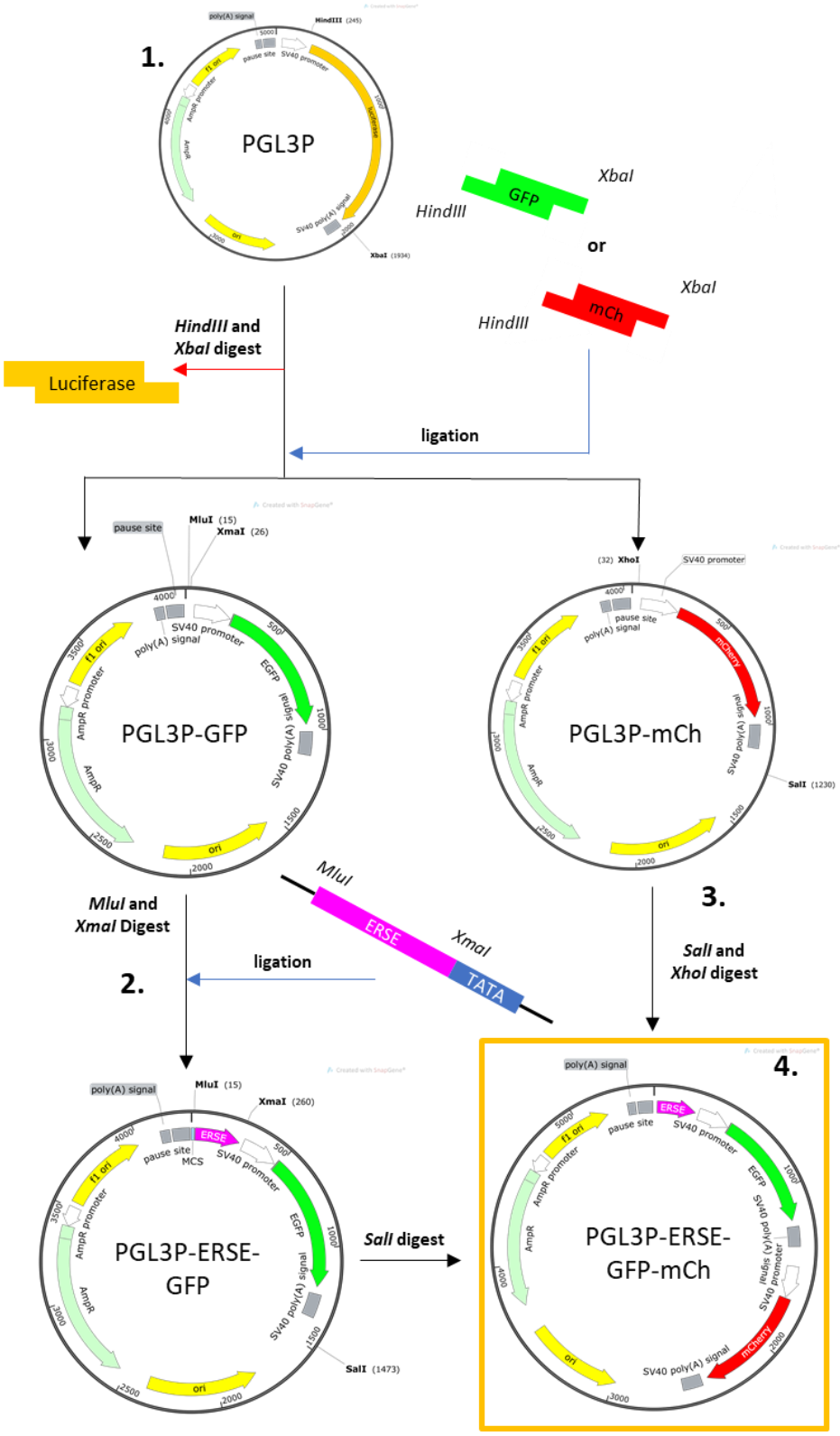

Figure 6.3: Schematic showing construction of the PGL3P-ERSE-GFP-mCh stress reporter vector. (1) Luciferase was excised from the PGL3P vector by *HindIII* and *XbaI* digestion, then GFP or mCherry PCR fragments digested, with the corresponding restriction enzymes, and ligated into the PGL3P backbone to produce PGL3P-GFP or PGL3P-mCh. **(2)** PGL3P-GFP was digested with *MluI* and *XmaI* alongside the synthesized ERSE-TATA plasmid to yield a PGL3P-GFP backbone and ERSE fragment which were ligated together. **(3)** PGL3P-mCh was digested with *SalI* and *XhoI* to give a SV40-mCh fragment; the PGL3P-ERSE-GFP vector was then digested with *SalI* only and dephosphorylated. **(4)** The PGL3P-ERSE-GFP backbone and SV40-mCh fragment were ligated together to produce the PGL3P-ERSE-GFP-mCh (**ERSE-SV40**) construct.

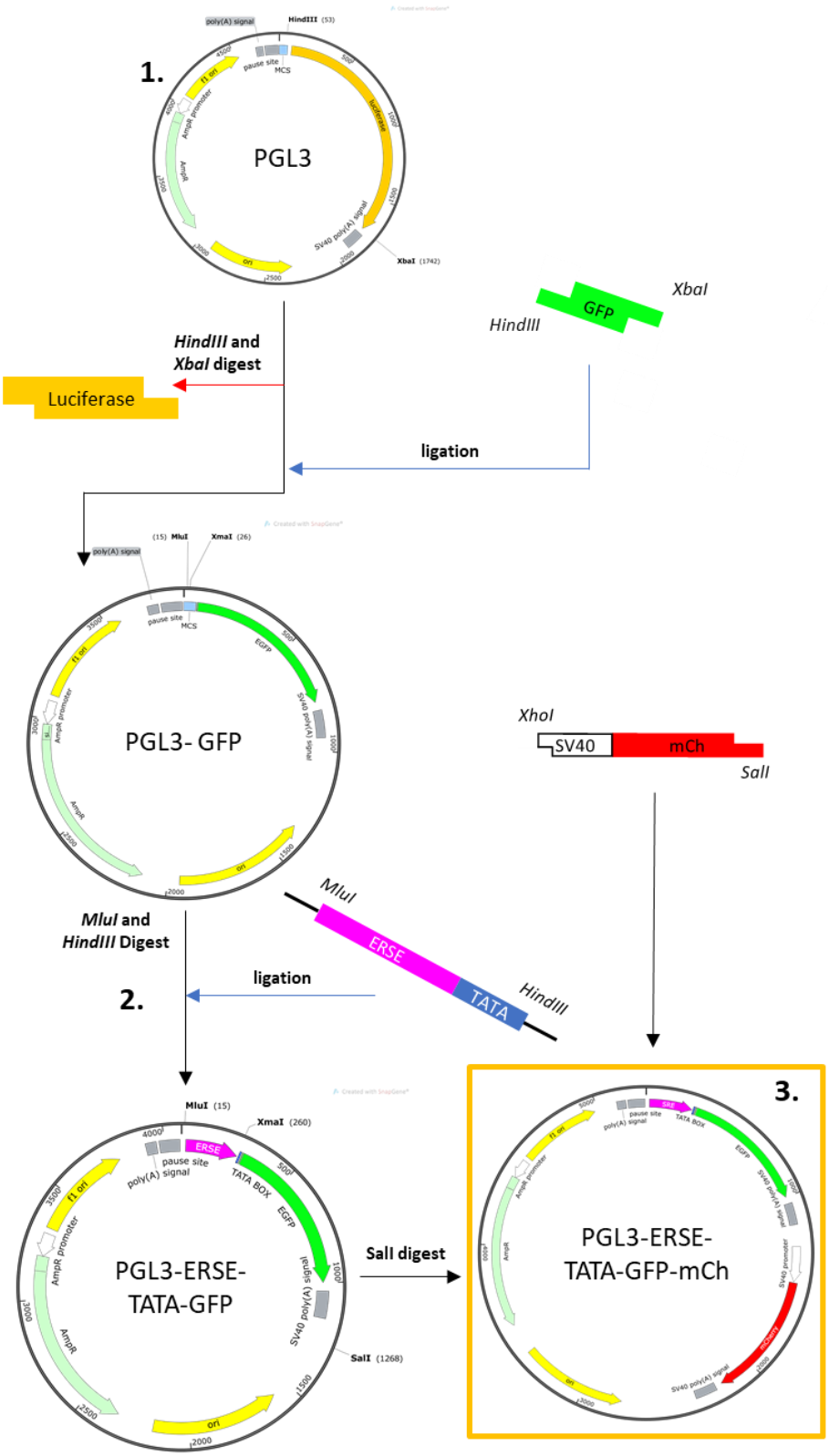

Figure 6.4: Schematic showing construction of the PGL3-ERSE-TATA-GFP-mCh stress reporter vector. (1) Luciferase was excised from the PGL3 vector by *HindIII* and *XbaI* digestion, then GFP or mCherry PCR fragments, digested with the corresponding restriction enzymes, were ligated into the PGL3 backbone. **(2)** PGL3-GFP was digested with *MluI* and *HindIII*, alongside the synthesized ERSE-TATA plasmid to yield a PGL3-GFP backbone and ERSE-TATA fragment which were ligated together. **(3)** PGL3-ERSE-TATA-GFP was digested with *SalI* only and dephosphorylated, then ligated with an SV40-mCh fragment generated in step 3 of Figure 6.3 to produce the PGL3-ERSE-TATA-GFP-mCh (**ERSE-TATA**) construct.

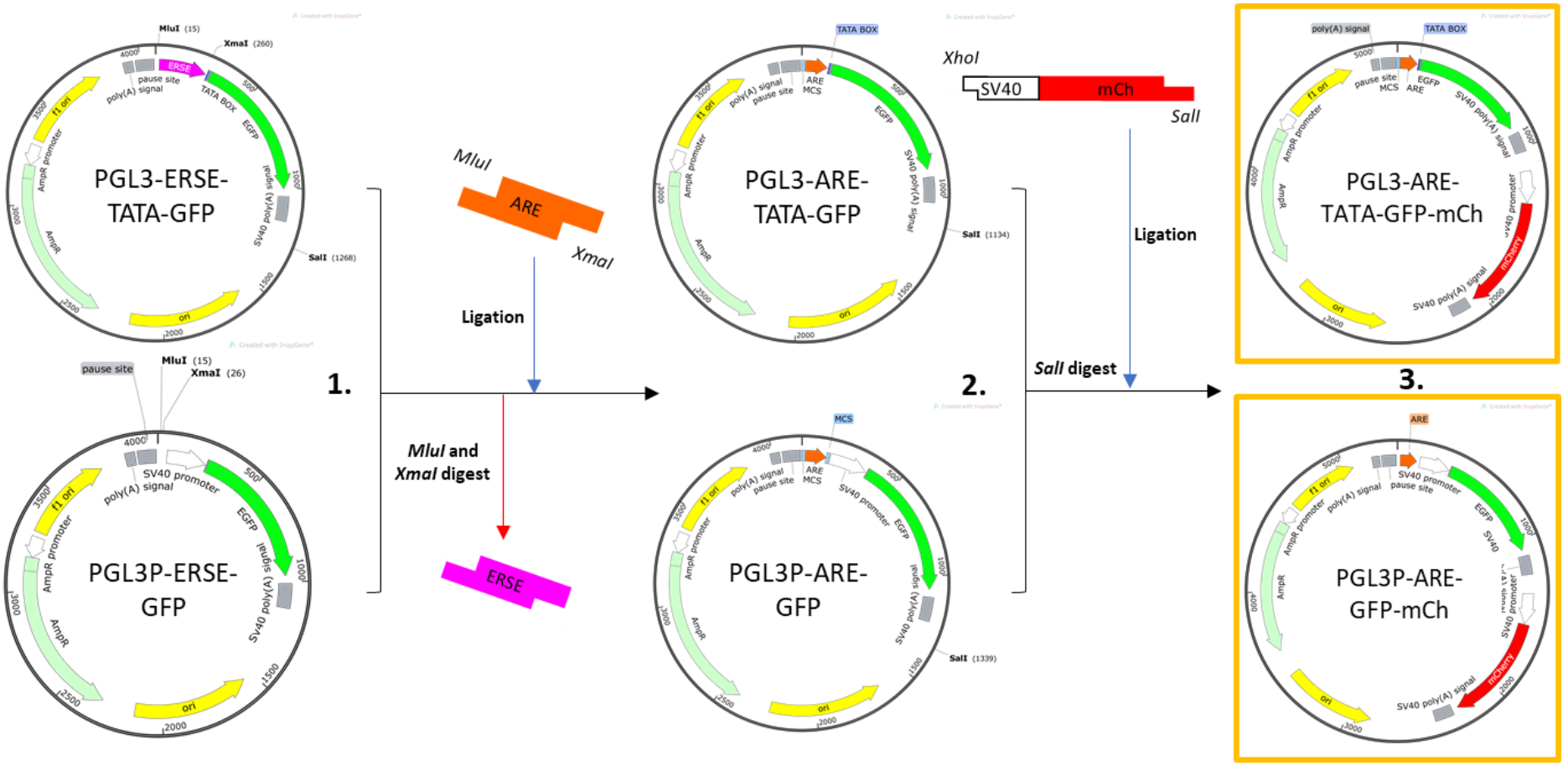

Figure 6.5: Schematic showing construction of PGL3P-ARE-GFP-mCh and PGL3-ARE-TATA-GFP-mCh stress reporter vectors. (1) PGL3-ERSE-TATA-GFP and PGL3P-ERSE-GFP were digested with *MluI* and *XmaI* restriction enzymes to remove the ERSE sequence. The ARE fragment (produced by oligo annealing) was digested with the corresponding enzymes and ligated to produce PGL3-ARE-TATA-GFP or PGL3P-ARE-GFP. **(2)** PGL3-ARE-TATA-GFP and PGL3-ARE-GFP were digested with *SalI* only and dephosphorylated. **(3)** Each backbone was then ligated with the SV40-mCh fragment generated in step 3 of Figure 6.3 to produce PGL3-ARE-TATA-GFP (**ARE-TATA**) or PGL3P-ARE-GFP-mCh (**ARE-SV40**) constructs.

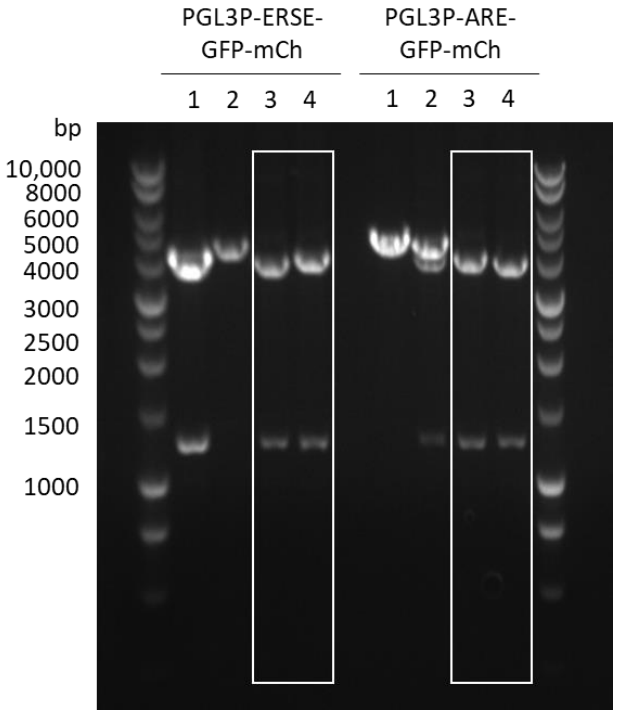

Figure 6.6: **DNA agarose gel showing test digest of PGL3P-ERSE-GFP-mCh and PGL3P-ARE-GFP-mCh constructs with *HindIII*.** Four mini-prepped samples were digested for each vector, then two DNA sequenced. Boxes indicate the two preparations sent for sequencing, which were subsequently shown to be correct and used in future work. Total vector sizes and expected test digest fragments are as follows; PGL3P-ERSE-GFP-mCh 5479 bp (expected fragments 1207 bp + 4272 bp); PGL3P-ARE-GFP-mCh 5345 bp (expected fragments 1207 bp + 4138 bp).

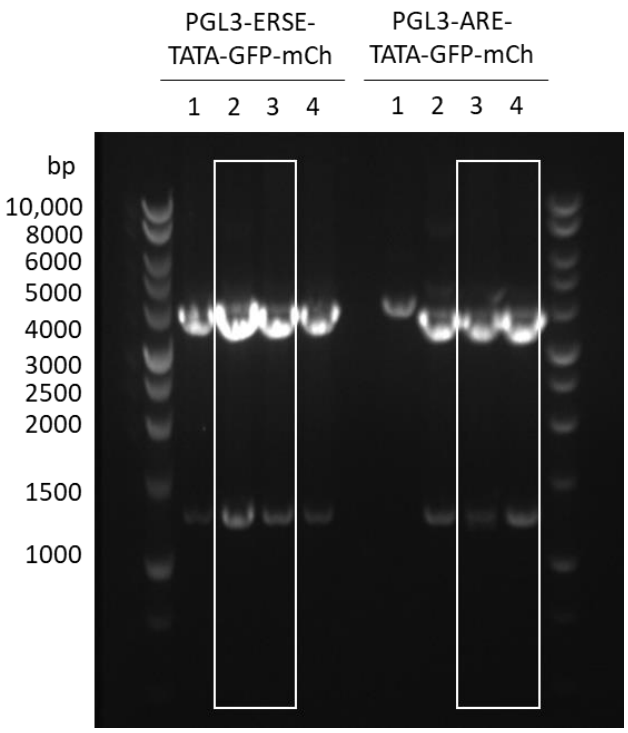

Figure 6.7: DNA agarose gel showing test digest of PGL3-ERSE-TATA-GFP-mCh and PGL3-ARE-TATA-GFP-mCh constructs with *HindIII*. Four mini-prepped samples were digested for each vector, then two DNA sequenced. Boxes indicate the two preparations sent for sequencing, which were subsequently shown to be correct, and used in future work. Total vector sizes and expected test digest fragments are as follows; PGL3-ERSE-TATA-GFP-mCh 5274 bp (expected fragments 1207 bp + 4067 bp); and PGL3-ARE-TATA-GFP-mCh 5140 bp (expected fragments 1207 bp + 3933 bp).

6.3 Initial Validation of Reporter Gene Constructs

Prior to using the stress reporter constructs to assess stress responses in CHO cells during over-grow culture, all four constructs were validated by transient transfection into a non-producing, CHO-S host cell line using tunicamycin or t-BHQ to induce ER or oxidative stress respectively. Initial investigations were carried out in a 24-well plate format, with 1 $x10^7$ viable cells transfected and plated into 500 µL of media per well. Cells were then left in a static incubator overnight before the appropriate drug (dissolved in media and DMSO) was added at two concentrations (based on previously described work by Du *et al* (2013) and Wang *et al* (2006)) to achieve a total volume of 1 mL, and final DMSO content of 0.1% (v/v). 1 mL cultures were also set up with no drug added, to provide control samples at each time point. Triplicate wells were used for each condition and time point. The drug concentrations were as follows:

- Tunicamycin (ERSE) added at 6 µM (1 x drug) or 12 µM (2 x drug)
- t-BHQ (ARE) added at 50 µM (1 x drug) or 100 µM (2 x drug)

Cells were then analysed for GFP and mCherry expression by flow cytometry at T=0 (when no drug was added), then at 6 hours and 24 hours post drug. Further method details are outlined in Chapter 2.

Note, that from this point onwards, stress response vectors are referred to as **ERSE-SV40** (PGL3P-ERSE-GFP-mCh), **ERSE-TATA** (PGL3-ERSE-TATA-GFP-mCh), **ARE-SV40** (PGL3P-ARE-GFP-mCh) and **ARE-TATA** (PGL3-ARE-TATA-GFP-mCh), as in Table 6.1.

6.3.1 Validation of the ERSE-SV40 and ERSE-TATA Reporter Constructs

Validation of the ERSE constructs in response to perceived ER stress would be shown by observing an increase in GFP expression denoted by an increased in the intensity of peaks in flow cytometry histograms and these peaks shifting to the right, relative to control samples. This, however, was not observed during validation of the ERSE-SV40 and ERSE-TATA constructs.

The ERSE-TATA reporter construct showed no shift in GFP or mCherry expression upon the addition of tunicamycin at both 6 µM and 12 µM, relative to control samples at T=0, 6 hour and 24-hour time points, as seen in histograms presented in Figures 6.8 and 6.9. Furthermore, there was also no difference in GFP and mCherry expression between time points. This data can also be visualised using scatter plots, which can be found in Appendix B. This was also generally the case for the SV40 promoter construct, although there was one replicate sample where an increase in GFP expression was observed at 24 h post drug addition at the 2x drug concentration.

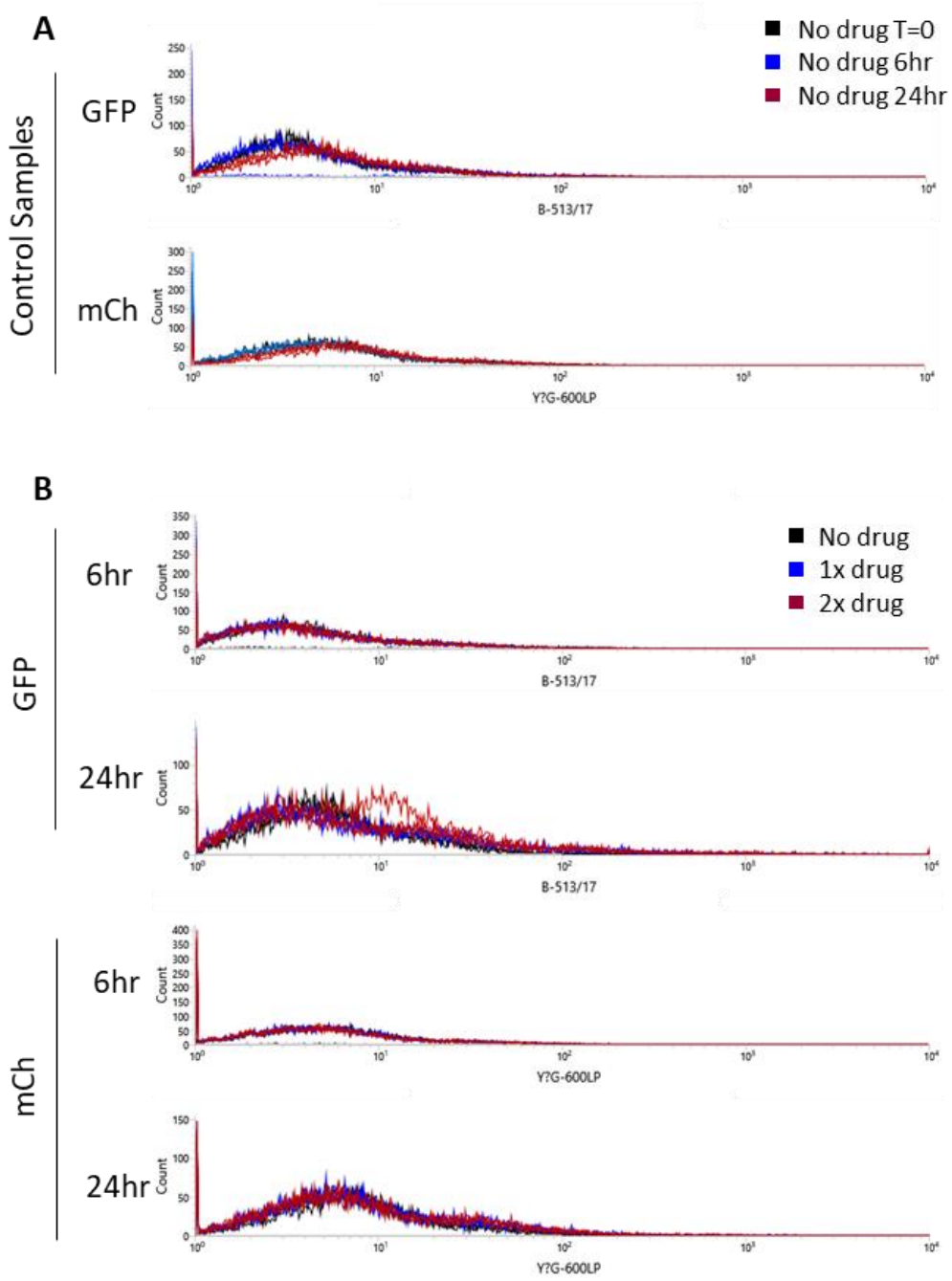

Figure 6.8: Histograms generated from flow cytometry data showing GFP and mCherry fluorescence in CHO-S cells transiently transfected with the ERSE-SV40 stress reporter construct and treated with different concentrations of tunicamycin. Triplicate samples are plotted for each condition and time point. **(A)** Control samples with no drug added at T=0, 6 hour and 24-hour time points **(B)** Samples treated with 6 µM (1 x drug - blue) or 12 µM (2 x drug - red) of tunicamycin. The no drug addition samples for each time point are also overlaid (black) for comparison. Corresponding scatter plots can be found in Appendix B.

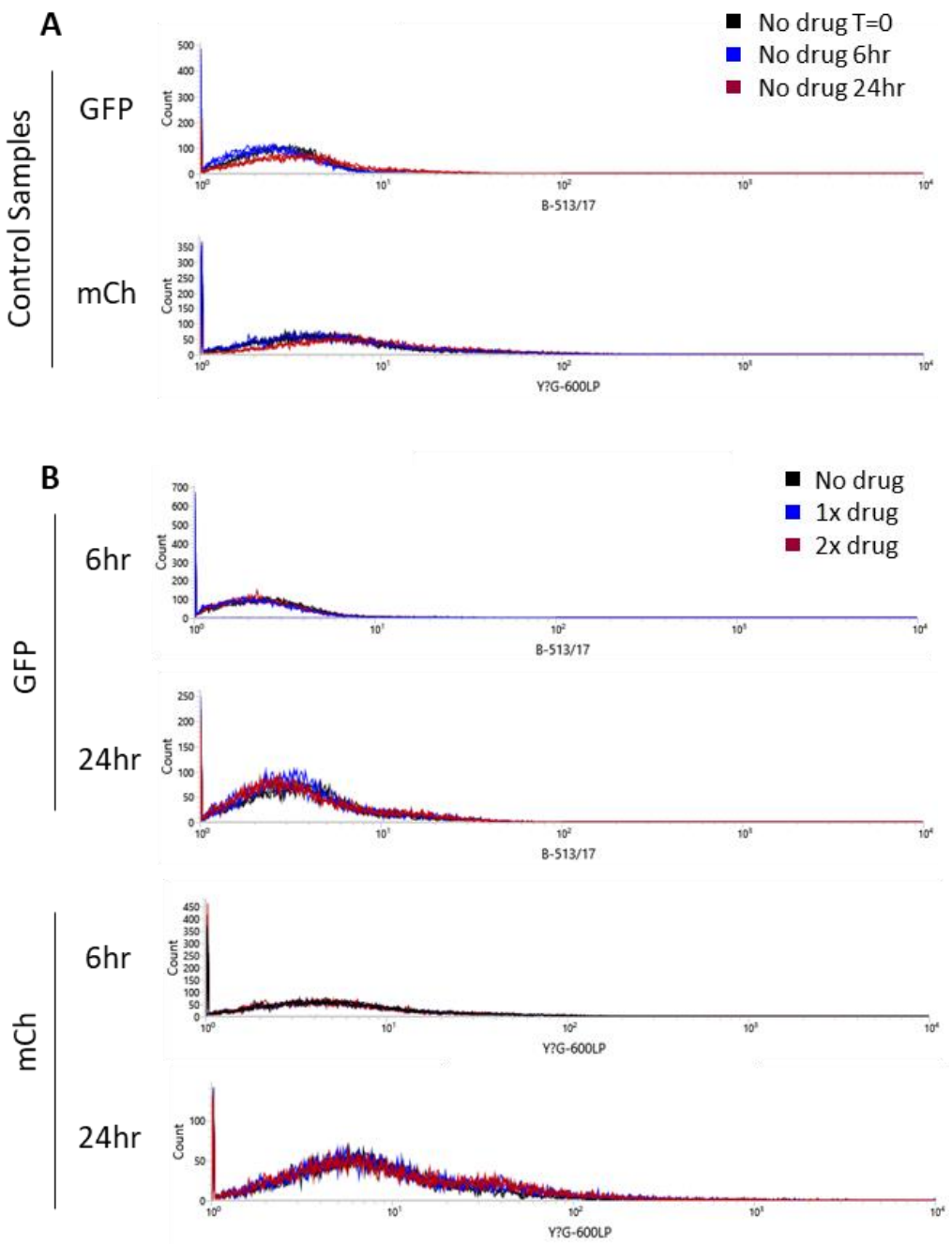

Figure 6.9: Histograms generated from flow cytometry data showing GFP and mCherry fluorescence of CHO-S cells transiently transfected with the ERSE-TATA stress reporter construct and treated with different concentrations of tunicamycin. Triplicate samples are plotted for each condition and time point. **(A)** Control samples with no drug added at T=0, 6 hour and 24-hour time points **(B)** Samples treated with 6 µM (1 x drug - blue) or 12 µM (2 x drug - red) of tunicamycin. The no drug addition samples for each time point are also overlaid (black) for comparison. Corresponding scatter plots can be found in Appendix B.

6.3.2 Validation of the ARE-SV40 and ARE-TATA Reporter Constructs

The ARE stress reporter constructs were also validated and showed a clear response to oxidative stress. Both the ARE-SV40 and ARE-TATA vectors showed an increase in GFP expression in response to treatment with t-BHQ (Figures 6.10 and 6.11). When comparing GFP histograms for samples treated with 1x and 2x t-BHQ concentrations at 6 hours, a clear difference in GFP fluorescence was observed between drug concentrations at each time point for both vectors. Distinct histogram curves were produced in response to each condition, where the 2x t-BHQ samples were shifted further to the right than histograms corresponding to 1x t-BHQ samples (see Figures 6.10 and 6.11). Furthermore, a shift in GFP expression between drug concentrations was also observed at the 24-hour time point, with samples treated with 2 x t-BHQ shifting further to the right (and hence had greater GFP expression) than those treated with 1 x drug and the corresponding control sample. Both the ARE-SV40 and ARE-TATA vectors showed similar sensitivity to t-BHQ.

The reporter gene constructs were designed with GFP downstream of the corresponding stress response element and promoter, so that GFP expression was induced in response to stress. An SV40 promoter followed by mCherry was placed further downstream, where it was assumed that mCherry expression would not be influenced by stress perception and under the control of the appropriate stress response element. In the case of the ARE-SV40 and ARE-TATA vectors, however, a shift in mCherry expression was observed at both time points for cells treated with t-BHQ, where this shift to the right was greater in samples treated with 2x drug concentrations than 1x. There was, however, no change in mCherry expression between time points of samples which were drug free. Upon preparing the t-BHQ stock solution in media and DMSO, the solution turned pink. Despite this being diluted upon addition into the corresponding well, cultures were visually pink as a result. Prior to running samples on the flow cytometer, cells were removed from their well, pelleted, washed and resuspended in PBS; however pink colouring may have still impacted the sample. A change in mCherry expression may therefore be caused by (i) pink colouring from the t-BHQ solution staining the cells and resulting in false 'mCherry' signal being detected, or (ii) there being a general increase in protein synthesis capacity in the CHO cells upon treatment with the t-BHQ agent. There was no difference in GFP and mCherry expression between untreated samples at T=0, 6-hour and 24-hour time points. This suggests that; (i) oxidative stress was not induced over this relatively short period of time, and (ii) the ARE vectors are not sensitive enough to report oxidative stress resulting from a short period of culture duration and in the absence of a large recombinant protein load.

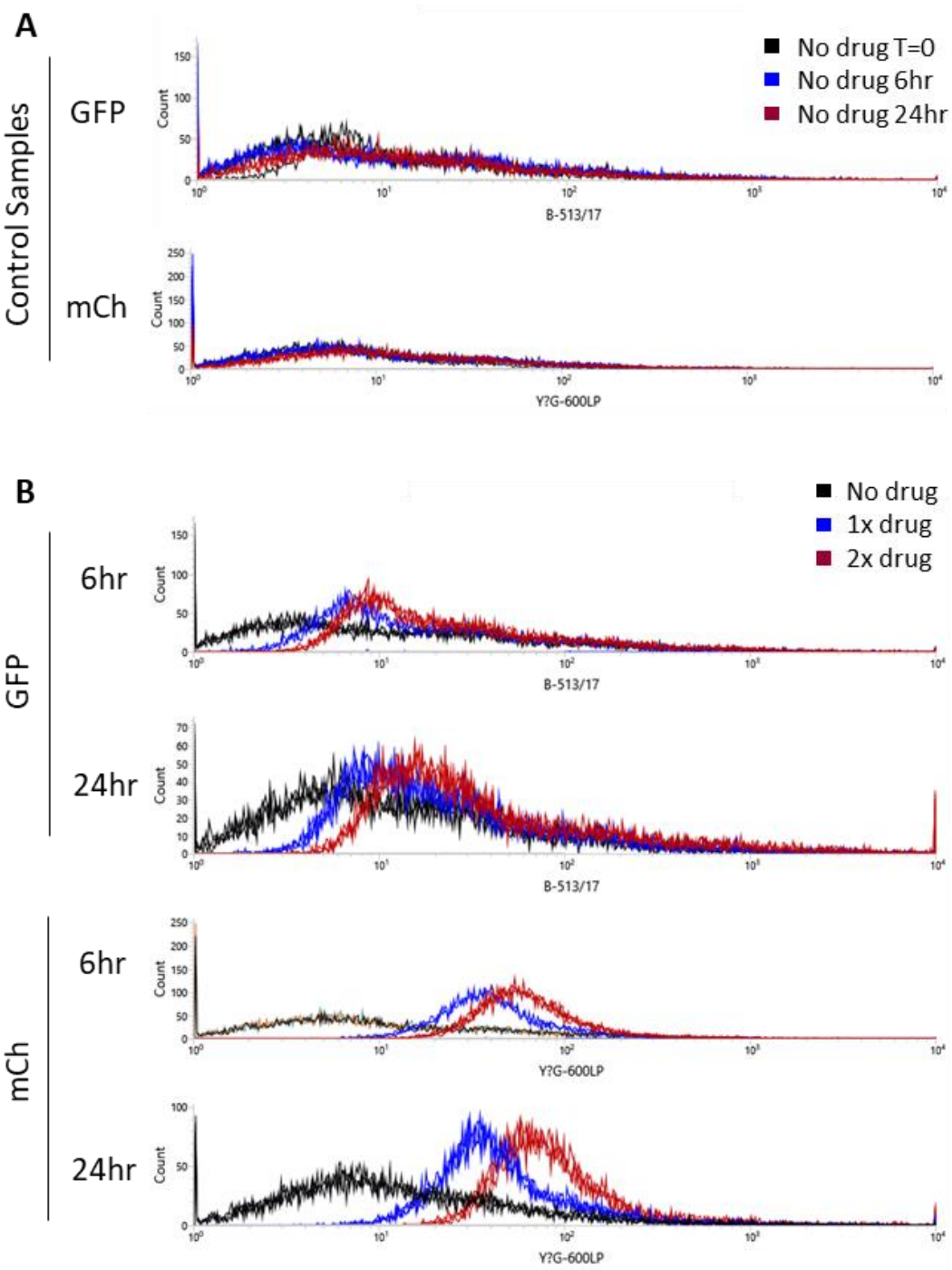

Figure 6.10: Histograms generated from flow cytometry data showing GFP and mCherry fluorescence in CHO-S cells transiently transfected with the ARE-SV40 stress reporter construct and treated with different concentrations of t-BHQ. Triplicate samples are plotted for each condition and time point. **(A)** Control samples with no drug added at T=0, 6 hour and 24-hour time points **(B)** Samples treated with 50 µM (1 x drug - blue) or 100 µM (2 x drug - red) of t-BHQ. The no drug addition samples for each time point are also overlaid (black) for comparison. Corresponding scatter plots can be found in Appendix B.

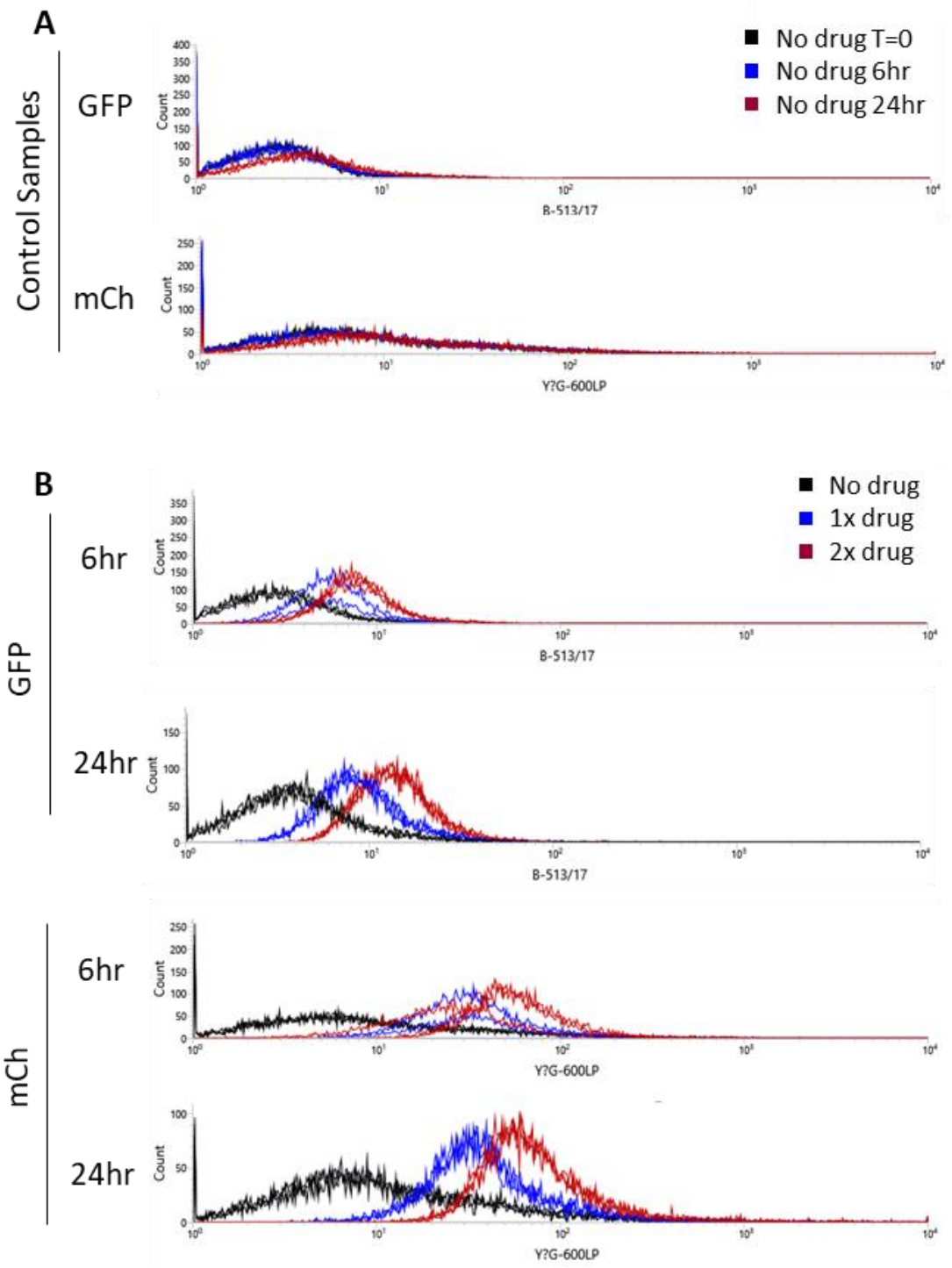

Figure 6.11: Histograms generated from flow cytometry data showing GFP and mCherry fluorescence of CHO-S cells transiently transfected with the ARE-TATA stress reporter construct and treated with t-BHQ. Triplicate samples are plotted for each condition and time point. **(A)** Control samples with no drug added at T=0, 6 hour and 24-hour time points **(B)** Samples treated with 50 µM (1 x drug - blue) or 100 µM (2 x drug - red) of t-BHQ. The no drug addition samples for each time point are also overlaid (black) for comparison. Corresponding scatter plots can be found in Appendix B.

6.4 Application of the ARE-TATA Oxidative Stress Responsive Reporter Construct in Fed-Batch Over-Grow Culture

On the basis of the initial construct testing, only the ARE-TATA reporter construct was applied in mAb producing cell lines. This reporter construct was selected as the ARE reporter showed greater sensitivity to chemically induced stress than the ERSE reporter. Through using a TATA promoter during over-grow culture, any expression of mCherry resulting from signal 'leaking' from the stress response element should be minimal, if at all, relative to using the stronger SV40 promoter.

Nine 30 mL fed-batch cultures were set up for each cell line to provide triplicate samples at each time point for transfection with the ARE-TATA GFP reporter construct. Cultures were labelled A - I for each cell line, and run for 12 days. Samples were analysed for GFP and mCherry expression using flow cytometry on days 4, 7 and 12, whereby cultures were transfected 24 hours prior to analysis on days 3, 6 and 11. To validate the ARE-TATA reporter construct at each sampling, control samples at each time point were treated with 200 µM TBHP. A commercial staining kit (Invitrogen) was also used to assess oxidative stress throughout culture, and to compare with data from ARE-TATA eGFP reporter gene transfected cells.

6.4.1 Cell Growth and Productivity Characteristics of the Cell Lines during Fed-Batch Culture

6.4.1.1 Cell Line 109

At the first time point analysed, on day 4 of culture, cells displayed identical growth profiles (Figure 6.12), with an average viable cell density of 5.4 x10^6 cells/mL and average culture viability of 97.3%. By day 7, however, cultures displayed more varied growth profiles, with cell viabilities beginning to decline and culture viabilities reduced to 93%. At this point of culture, culture 109I cell concentration peaked at 13.19 x10^6 viable cells/mL, compared to the remaining cultures, D-H, which ranged from 11.23-11.68 x10^6 cells/mL. By the final time point, on day 12 of culture, cultures had similar viable cell concentrations ranging from 7.06 – 7.13 x10^6 cells, and culture viabilities ranging from 56.3% to 59.9%.

Specific mAb productivity, as reported in Table 6.2, was lower in the 30 mL cultures for cell line 109 than during the 10 L cultures described in Chapter 4. 30 mL cultures reached an average Qp, between days 0-11, of 19.8 pg/cell/day; compared to 23.9 pg/cell/day in the disposable bioreactors. In terms of titre, cultures produced similar amounts of mAb at each time point analysed, as reported in Table 6.3, where the greatest variation in titre was seen on day 3 ,

ranging from 55 mg/L to 93.8 mg/L. At all other time points, cultures produced similar quantities of mAb. When comparing transfection time points, average titres were over 5.9-fold greater on day 6 of culture relative to day 3, and were over 3-fold greater on day 11 relative to day 6 (Table 6.2). Overall, there was >20-fold increase in titre between the first transfection time point at day 3, and the final transfection time point on day 11.

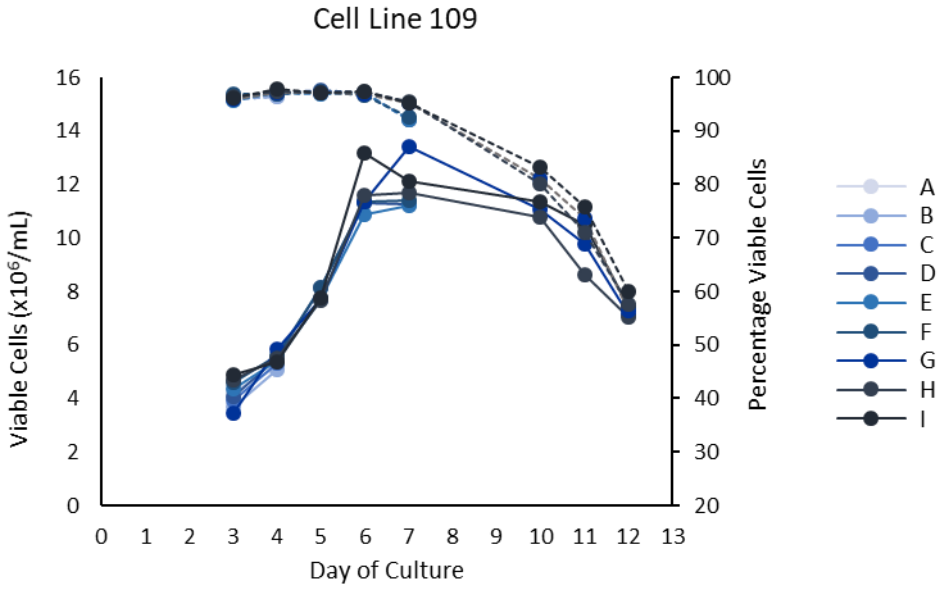

Figure 6.12: Viable cell concentration and percentage culture viability of cell line 109 fed-batch cultures. Cultures A, B and C were analysed on day 4, cultures D, E and F on day 7 and cultures G, H and I on day 12, where cultures were transfected 24 hours prior to analysis with the ARE-TATA GFP reporter construct on days 3, 6 and 11.

Table 6.2: Specific productivity (Qp) for cell line 109 cultures fed-batch cultures. Qp was established by plotting integral viable cell concentrations against titre, and was only calculated where there were 3 or more points plotted, meaning Qp data is not presented for cultures A B and C. Note that n=6 between days 0-6 of culture, and n=3 for days 0-11. Plots used to establish Qp are presented in Appendix B.

	Culture	Qp (pg/cell/day)	Average Qp (pg/cell/day)
Days 0-6	D	15.2	15.6
	E	15.7	
	F	15.8	
Days 0-11	G	19.6	19.8
	H	19.8	
	I	20.1	

Table 6.3: mAb Titre Data for Each Cell Line 109 Culture. Samples were taken on days 3, 4, 6, 7, 10 and 11 of culture for analysis of secreted mAb concentration.

Day	Culture	Titre (mg/L)	Average Titre (mg/L)
3	A	61.3	66.7
	B	61.2	
	C	61.8	
	D	55.0	
	E	74.8	
	F	56.6	
	G	63.6	
	H	93.8	
	I	71.9	
4	D	130.9	136.6
	E	135.3	
	F	137.9	
	G	138.9	
	H	137.1	
	I	139.5	
6	D	380.4	392.9
	E	396.1	
	F	400.0	
	G	397.8	
	H	388.5	
	I	394.4	
7	G	649.9	648.6
	H	641.9	
	I	654.1	
10	G	1225.0	1233.8
	H	1191.5	
	I	1284.9	
11	G	1356.6	1355.5
	H	1320.8	
	I	1389.0	

6.4.1.2 Cell Line AB001

Cell line AB001 cultures had similar growth profiles until day 7 of culture, as shown in Figure 6.13. At the first time point on day 4 of culture, cultures had obtained an average viable cell concentration of 7.2 x10^6 cells/mL, with an average culture viability of 99.3%. At the second time point, on day 7 of culture, viable cell concentrations showed more variation, with a range of 14.53 – 17.53 x10^6 cells/mL observed. Culture viability however, showed less variation, ranging from 95.6 – 98%. From this point onwards, culture viabilities substantially declined. By day 12

the average culture viability was 36%, with an average viable cell concentration of 7.1 x10^6 cells/mL.

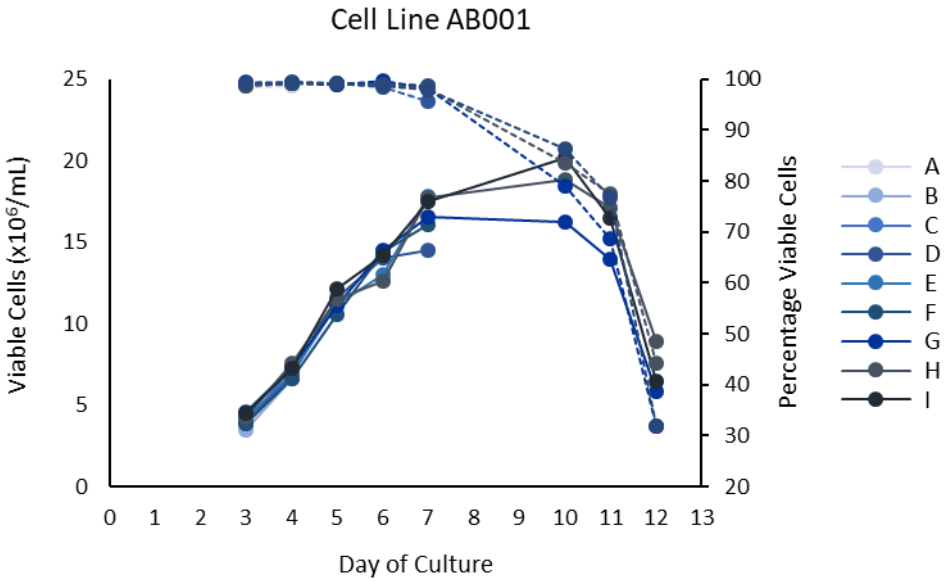

Figure 6.13: Viable cell concentration and percentage culture viability of cell line AB001 during fed-batch cultures. Cultures A, B and C were analysed on day 4, cultures D, E and F on day 7 and cultures G, H and I on day 12, where cultures were transfected 24 hours prior to analysis with the ARE-TATA GFP reporter construct on days 3, 6 and 11.

Table 6.4: Specific productivity (Qp) for cell line AB001 cultures. Qp was established by plotting integral viable cell concnetrations against titre, and was only calculated where there were 3 or more points plotted, meaning Qp data is not presented for cultures A B and C. Note that n=6 between days 0-6 of culture, and n=3 for days 0-11. Plots used to establish Qp are presented in Appendix B.

	Culture	Qp (pg/cell/day)	Average Qp (pg/cell/day)
Days 0-6	D	4.25	5.1
	E	5.53	
	F	5.47	
Days 0-11	G	11.24	10.7
	H	10.8	
	I	10.11	

Cell line AB001 obtained the highest viable cell concentrations of all the cell lines investigated in this study, but had the lowest titres, with an average Qp across culture of 10.7 pg/cell/day (Table 6.4). Average titres (Table 6.5) increased over 6-fold between the first transfection time point, on day 3, and the second transfection time point on day 6. Between days 6 and 11, titres further increased by another 6-fold, with an overall increase between the first transfection point, on day 3, and the final transfection point, on day 11, of >20-fold.

Table 6.5: mAb titre data for each cell Line AB001 culture. Samples were taken on days 3, 4, 6, 7, 10 and 11 of culture for analysis.

Day	Culture	Titre (mg/L)	Average Titre (mg/L)
3	A	27.2	25.9
	B	25.4	
	C	25.4	
	D	26.6	
	E	25.4	
	F	25.0	
	G	25.8	
	H	26.1	
	I	26.2	
4	D	42.1	41.2
	E	39.9	
	F	39.6	
	G	41.1	
	H	42.6	
	I	42.2	
6	D	140.6	166.7
	E	167.9	
	F	164.3	
	G	169.4	
	H	179.6	
	I	178.3	
7	G	342.9	353.4
	H	358.3	
	I	359.0	
10	G	836.5	878.8
	H	889.6	
	I	910.2	
11	G	1015.3	989.1
	H	1007.1	
	I	945.0	

6.4.1.3 Cell Lines 2223 and 2491

Cell lines 2223 and 2491 both produced mAb 4212, and showed the poorest growth of all the cell lines investigated in this study, reaching a maximum average viable cell concentration in fed-batch cultures of 6.7 and 6.8 x10^6 cells/mL respectively. At the first transfection time point, on day 3, cell line 2491 cultures had similar numbers of viable cells, with an average of 3.8 x10^6 cells/mL and an average culture viability of 98.6%. At this point, cell line 2223 showed greater variation in viable cell concentrations between cultures, with cell concentrations ranging from 2.58 – 4.48 x10^6 cells/mL. On day 3 culture viability ranged from 97.5 – 98.6%.

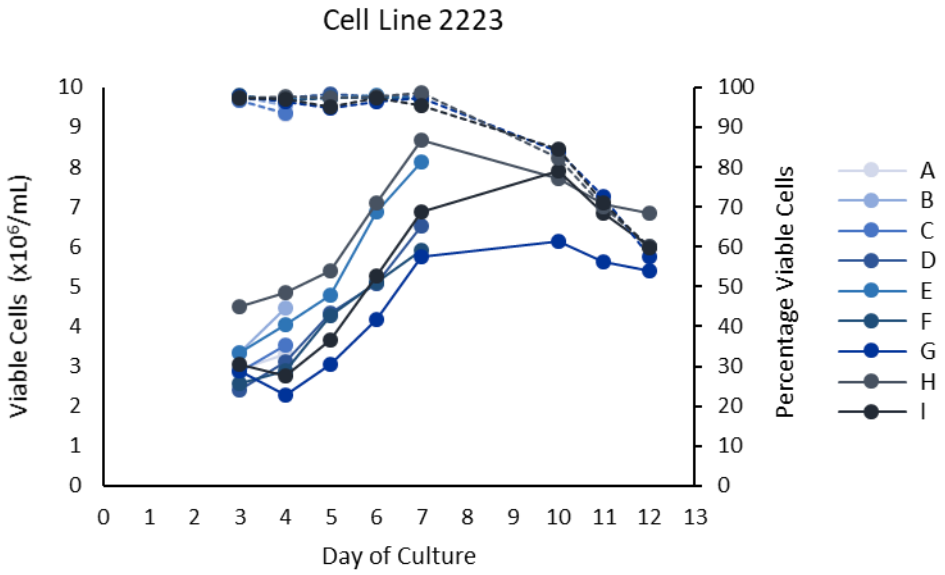

Figure 6.14: Viable cell concentration and culture viability of cell line 2223 fed-batch cultures. Cultures A, B and C were analysed on day 4 and cultures D, E and F on day 7, where cultures were transfected 24 hours prior to analysis with the ARE-TATA GFP reporter construct on days 3 and 6.

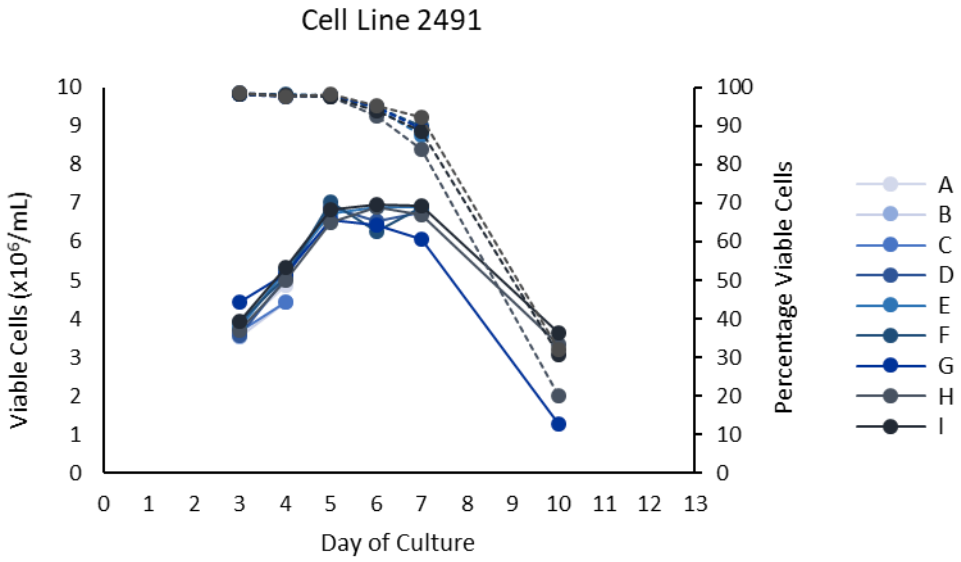

Figure 6.15: Viable cell concentration and culture viability of cell line 2491 fed-batch cultures. Cultures A, B and C were taken analysed on day 4, cultures D, E and F on day 7 and cultures G, H and I on day 12, where cultures were transfected 24 hours prior to analysis with the ARE-TATA GFP reporter construct on days 3 and 6. Note that cultures were terminated on day 11 and not transfected due to poor viabilities.

Table 6.6: Specific productivity (Qp) for cell line 2223 cultures. Qp was established by plotting integral viable cell concentrations against titre, and was only calculated where there were 3 or more points plotted, meaning Qp data is not presented for cultures A B and C. Note that n=6 between days 0-6 of culture, and n=3 for days 0-11. Plots used to establish Qp are presented in Appendix B.

	Culture	Qp (pg/cell/day)	Average Qp (pg/cell/day)
Days 0-6	D	16.8	17.5
	E	17.7	
	F	17.9	
Days 0-11	G	18.1	17.0
	H	17.6	
	I	15.3	

Table 6.7: Specific productivity (Qp) for cell line 2491 cultures. Qp was established by plotting integral viable cell densities against titre, and was only calculated where there were 3 or more points plotted, meaning Qp data is not presented for cultures A B and C. Note that n=6 between days 0-6 of culture, and n=3 for days 0-10. Plots used to establish Qp are presented in Appendix B.

	Culture	Qp (pg/cell/day)	Average Qp (pg/cell/day)
Days 0-6	D	9.2	9.2
	E	9.2	
	F	9.2	
Days 0-10	G	10.6	12.2
	H	14.1	
	I	11.9	

At the second transfection time point, on day 6 of culture, cell line 2491 viable cell concentrations remained similar between replicates, ranging from 6.25 – 6.44 $x10^6$ cells/mL, compared to cell line 2223 for which a greater range of 4.16 – 7.1 $x10^6$ was observed. From day 6 onwards, culture viabilities began to drop for cell line 2491, averaging 94.2% compared to cell line 2223 for which the average culture viability was 97.4%, and began to decrease between days 7 and 10. On day 10, viable cell concentrations for cell line 2491 ranged from 1.28 – 6.22 $x10^6$ cells, with an average culture viability of 33%. Due to low cell concentrations and poor culture viabilities, the remaining 2491 cultures, G H and I, were terminated. Cell line 2223 cultures were, however, of an appropriate cell concentration and culture viability for transfection on day 11, with an average viable cell concentration of 6.5 $x10^6$ cells/mL and an average culture viability of 71%.

Cell line 2491 achieved a lower specific productivity (Table 6.6) than cell line 2223 (Table 6.7), with a Qp of 9.2 pg/cell/day compared to 17.5 pg/cell/day between days 0-6 of culture; and 12.2 pg/cell/day compared to 17.0 pg/cell/day between days 0-11. When comparing mAb titres, cell line 2223 produced consistently higher average titres than those for 2491 throughout culture. For both cell lines, however, there was a greater than 4-fold increase in titre between days 3 and 6, and with cell line 2223 producing over 2-fold more material on day 11 compared to day 6. Overall, cell line 2223 had a 32-fold difference in titre between the first transfection time point on day 3, and final transfection on day 11.

Table 6.8A and 6.8B: mAb titre data for each cell line (A) 2223 and (B) 2491 during fed-batch culture. Samples were taken on days 3, 4, 6, 7, 10 and 11 of culture. Note that cell line 2491 cultures died on day 11, and so titre samples were not taken as transfections could not be carried out for analysis on day 12.

A

Day	Culture	Titre (mg/L)	Average Titre (mg/L)
3	A	89.7	85.5
	B	84.5	
	C	81.9	
	D	82.0	
	E	84.5	
	F	84.4	
	G	86.8	
	H	84.7	
	I	91.5	
4	D	194.2	177.4
	E	134.8	
	F	101.8	
	G	174.5	
	H	281.8	
	I	177.1	
6	D	289.1	377.6
	E	327.2	
	F	273.2	
	G	316.8	
	H	580.8	
	I	478.6	
7	G	386.4	523.4
	H	603.6	
	I	580.2	
10	G	662.3	800.7
	H	972.1	
	I	767.7	
11	G	631.3	800.3
	H	921.1	
	I	848.4	

B

Day	Culture	Titre (mg/L)	Average Titre (mg/L)
3	A	44.8	45.6
	B	42.9	
	C	46.3	
	D	45.1	
	E	46.2	
	F	46.3	
	G	46.3	
	H	46.8	
	I	45.3	
4	D	67.5	66.8
	E	65.2	
	F	68.1	
	G	66.2	
	H	67.6	
	I	66.3	
6	D	197.1	199.4
	E	199.6	
	F	199.6	
	G	191.1	
	H	195.4	
	I	213.6	
7	G	274.7	308.3
	H	314.4	
	I	335.9	
10	G	291.6	481.9
	H	449.5	
	I	704.5	
11	G	-	-
	H	-	
	I	-	

6.4.2 Comparing Oxidative Stress Responses Between Culture Time Points and Cell Lines Using the ARE-TATA GFP Stress Reporter Construct

Transfected cells were analysed on days 4, 7 and 12 to evaluate oxidative stress, as assessed using the ARE-TATA GFP stress response vector and subsequent fluorescence, throughout fed-batch over grow culture. Figure 6.16 shows the resultant histograms showing GFP expression for non-transfected, control samples and triplicate cultures transfected with the ARE-TATA vector on each sample day for cell lines 109, AB001, 2223 and 2491 as determined by flow cytometry. If the level of oxidative stress perceived by the cells reaches a sufficient threshold to activate ARE-TATA stress reporter expression, then GFP expression should increase and would be observed by a shift to the right in GFP in the resultant histogram, relative to the non-transfected control. In this case however, for all cell lines and sample days, there was no shift in GFP expression relative to the control. This suggested that any change in oxidative stress within the cell across culture was below that which was required to activate the ARE sufficiently to upregulate GFP expression via the ARE controlled construct. Figure 6.17 reports mCherry expression for the same selection of samples, for which there was also no change observed as expected.

The flow cytometry fluorescence data can also be visualised as a scatter plot, as reported in Figure 6.18, and by tabulating the percentage of events which lie in each quadrant of these plots, as reported in Table 6.9. In the event of increased GFP expression, an increase in data falling within Q1 should be observed, and an increase in mCherry expression would result in data shifting into Q3. In the event that both GFP and mCherry expression is impacted, the corresponding data would fall in Q2. For all cell lines and sample days, however, >97% of total events were plotted in Q4, meaning that there was no change in GFP or mCherry expression within any of the samples relative to the control, as shown in the histogram data.

Throughout the study, transfected samples were also taken and treated with TBHP as a positive control. Unlike the previously used t-BHQ, TBHP does not turn the media pink when dissolved. Figures 6.19, 6.20 and Table 6.10 show the data from transfected samples +/- 200 µM TBHP, where positive control samples were incubated with TBHP for an hour prior to analysis. Histograms plotting GFP fluorescence in Figure 6.19 showed a clear difference between the positive and negative control samples, with TBHP treated samples shifted to the right, indicative of higher fluorescence as a result of enhanced GFP expression. This trend was consistently observed for all cell lines across all sample days, with a greater shift in expression of TBHP treated cells observed on days 7 and 12 relative to day 4. There was no increase in mCherry

fluorescence in samples treated with TBHP, as reported in Appendix B. Scatter plots were also created (Figure 6.20) and the percentage of events within each quadrant are presented in Table 6.10.

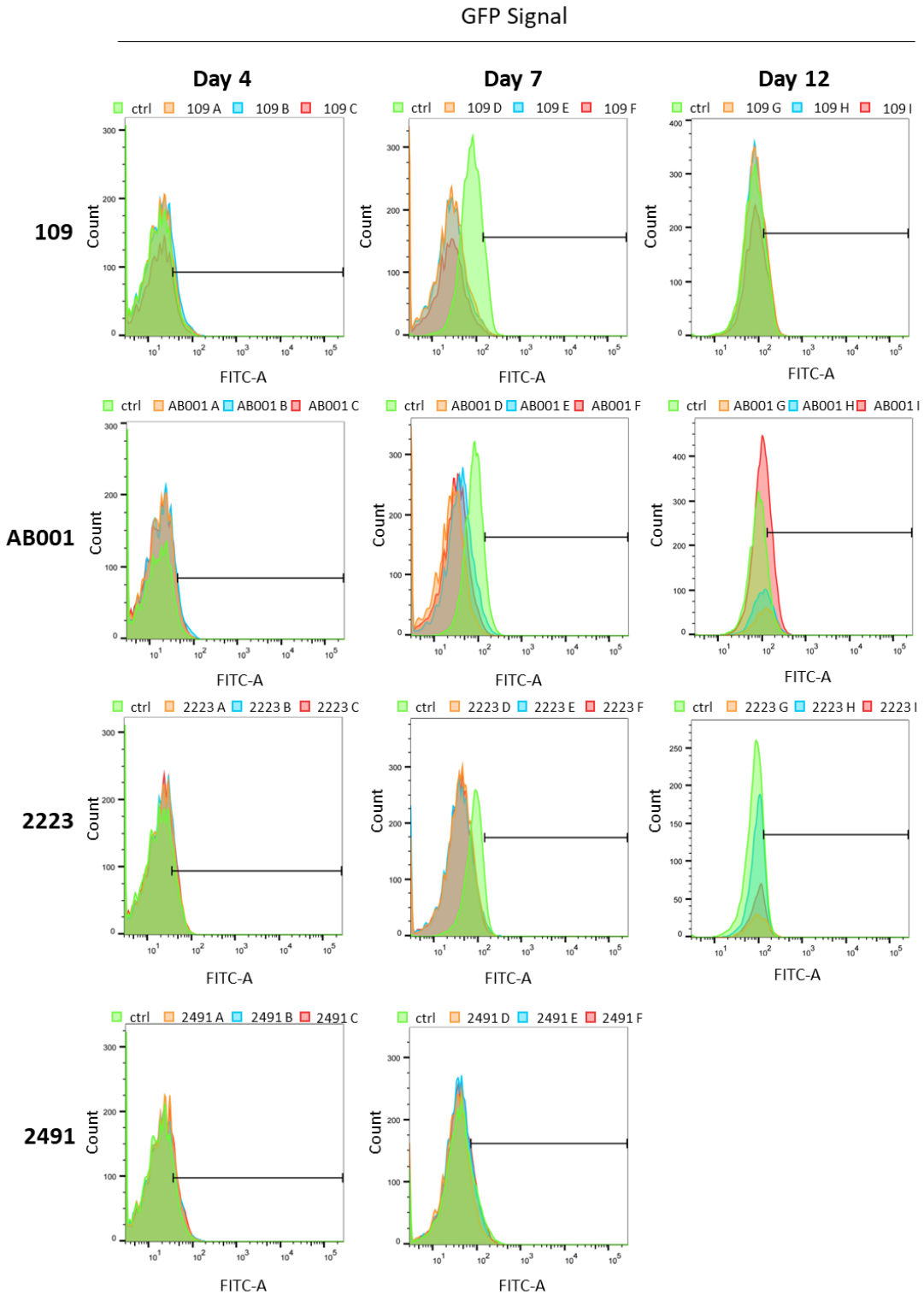

Figure 6.16: Histograms showing fluorescence of CHO cells, as determined by flow cytometry, as a result of GFP expression in samples from cell lines 109, AB001, 2223 and 2491 transfected with the ARE-TATA stress reporter construct. Control (ctrl) samples, shown in green, are non-transfected cells. Day 4 samples were transfected on day 3, day 7 transfected on day 6, and day 12 samples were transfected on day 11. Replicate cultures are shown for each time point in orange, blue and red; where the black line indicates where GFP signal of transfected samples should shift to if there is a difference between the transfected and control samples. Note that on day 12 there were not enough viable cells to reach 10,000 events for samples AB001 and 2223, and that on this day no samples were analysed for cell line 2491.

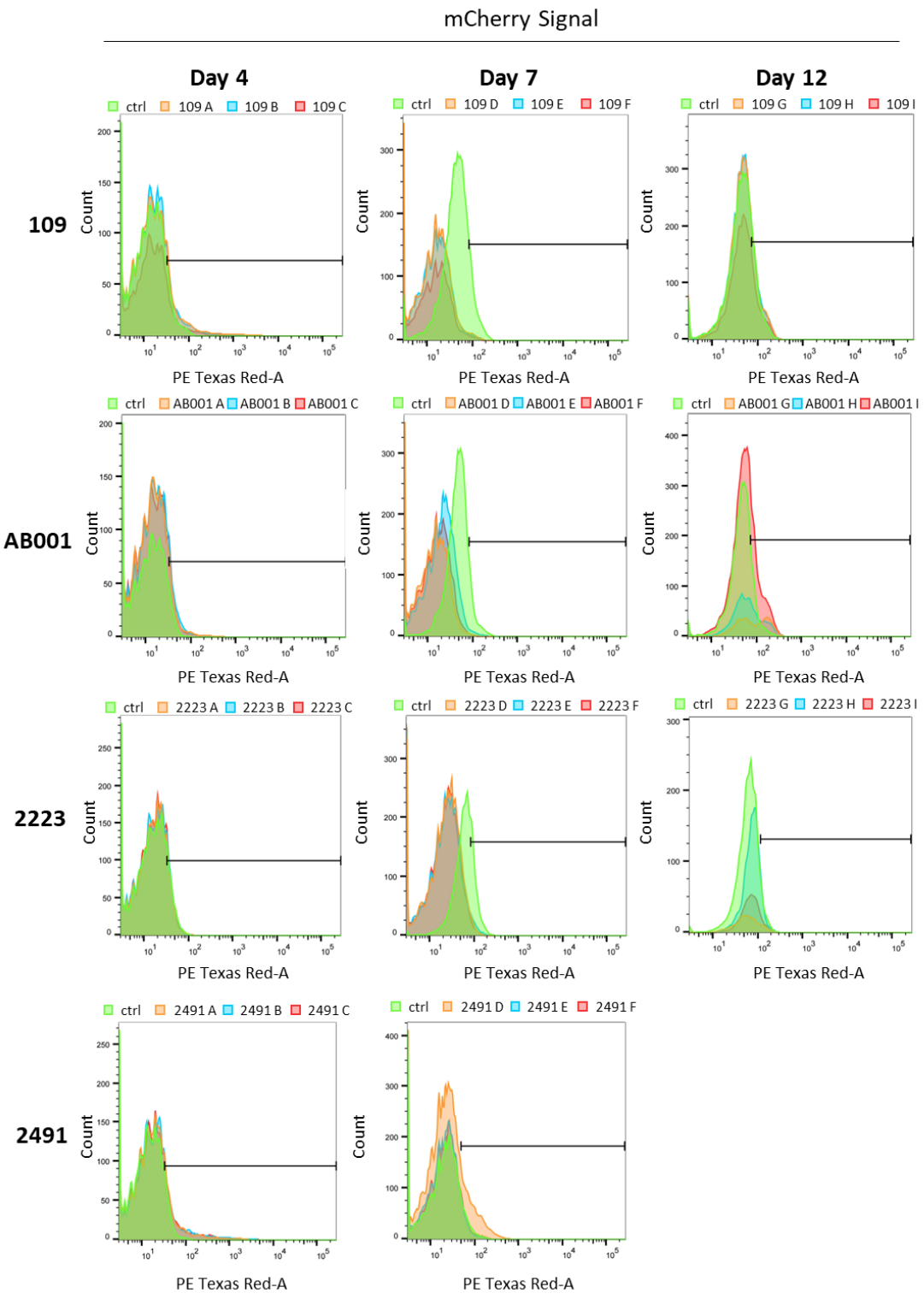

Figure 6.17: Histograms showing fluorescence of CHO cells, as determined by flow cytometry, as a result of mCherry expression in samples from cell lines 109, AB001, 2223 and 2491 transfected with the ARE-TATA stress reporter construct. Control (ctrl) samples, shown in green, are non-transfected cells. Day 4 samples were transfected on day 3, day 7 transfected on day 6, and day 12 samples were transfected on day 11. Replicate cultures are shown for each time point in orange, blue and red; where the black line indicates where GFP signal of transfected samples should shift to if there is a difference between the transfected and control samples. Note that on day 12 there were not enough viable cells to reach 10,000 events for samples AB001 and 2223, and that on this day no samples were analysed for cell line 2491.

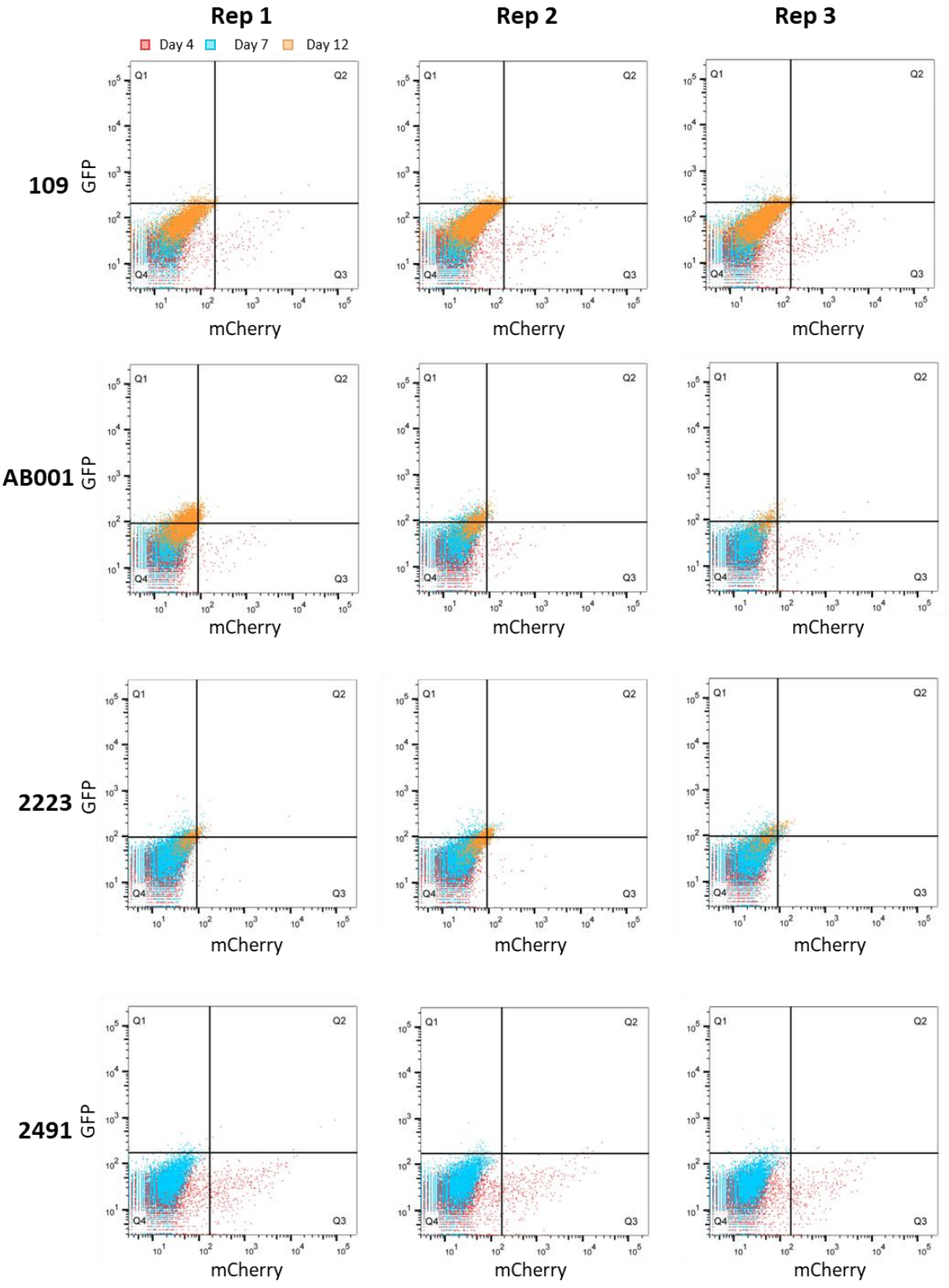

Figure 6.18: Scatter plots showing GFP and mCherry expression, as determined by flow cytometry on days 4, 7 and 12 in triplicate cultures for cell lines 109, AB001, 2223 and 2491. Top left is quadrant (Q) 1, top right Q2, bottom right Q3 and bottom left Q4, where blue plots day 4 data, red plots day 7 and orange plots day 12. Note than on day 12 there were not enough viable cells to reach 10,000 viable events for samples AB001 and 2223, and that on this day no samples were analysed for cell line 2491. The corresponding statistics can be seen in Table 6.9

Table 6.9: Percentage of events which fall into each quadrant for scatter plots presented in Figure 6.18, comparing GFP and mCherry fluorescence of ARE-TATA construct transfected samples over time. Note than on day 12 there were not enough viable cells to reach 10,000 events for samples AB001 and 2223, and that on this day no samples were analysed for cell line 2491.

		% of Viable Cells in Each Quadrant											
		Day 4				Day 7				Day 12			
		Q1	Q2	Q3	Q4	Q1	Q2	Q3	Q4	Q1	Q2	Q3	Q4
109	Rep 1	0.1	0.1	2.1	97.8	0.2	0.0	0.0	99.8	2.3	0.4	0.0	97.2
	Rep 2	0.1	0.1	2.1	97.7	0.3	0.0	0.0	99.7	2.0	0.4	0.0	97.6
	Rep 3	0.0	0.1	2.4	97.4	0.5	0.0	0.0	99.5	2.0	0.3	0.0	97.7
AB001	Rep 1	0.0	0.0	0.7	99.3	0.1	0.0	0.0	99.9	3.0	0.0	0.0	97.0
	Rep 2	0.1	0.0	0.6	99.3	0.4	0.0	0.0	99.6	2.8	0.1	0.0	97.1
	Rep 3	0.0	0.0	0.9	99.1	0.0	0.0	0.0	100	1.3	0.3	0.1	98.3
2223	Rep 1	0.0	0.0	0.1	99.9	0.3	0.0	0.0	99.7	0.3	0.0	0.0	99.7
	Rep 2	0.0	0.0	0.2	99.8	0.0	0.0	0.0	99.7	0.1	0.0	0.1	99.8
	Rep 3	0.0	0.0	0.1	99.1	0.2	0.0	0.0	99.8	1.6	0.3	0.1	98.1
2491	Rep 1	0.1	0.2	3.9	95.8	0.4	0.0	0.0	99.5	-	-	-	-
	Rep 2	0.1	0.2	3.8	95.9	0.3	0.0	0.0	99.7	-	-	-	-
	Rep 3	0.1	0.1	3.0	96.8	0.0	0.0	0.0	99.6	-	-	-	-

Table 6.10: Percentage of events which fall into each quadrant for scatter plots presented in Figure 6.20, plotting GFP and mCherry fluorescence of ARE-TATA construct transfected samples +/- TBHP. Positive control samples (+ TBHP) were incubated in 200 µM TBHP for one hour prior to analysis. – TBHP samples were transfected only.

		% of Viable Cells in Each Quadrant											
		Day 4				Day 7				Day 12			
		Q1	Q2	Q3	Q4	Q1	Q2	Q3	Q4	Q1	Q2	Q3	Q4
109	+ TBHP	19.2	1.6	1.4	77.5	38.3	0.6	0.0	61.1	35.2	0.5	0.0	64.3
	- TBHP	0.0	0.0	0.0	99.1	0.1	0.1	0.0	99.8	0.0	0.1	0.0	99.8
AB001	+ TBHP	37.2	1.2	0.4	60.7	47.5	0.7	0.0	51.7	45.3	0.7	0.0	54.2
	- TBHP	0.0	0.0	0.0	100	0.1	0.0	0.0	99.9	0.0	0.0	0.0	99.9
2223	+ TBHP	4.2	0.1	0.0	95.7	15.8	0.1	0.0	84.1	15.1	0.1	0.0	84.1
	- TBHP	0.0	0.0	0.0	99.9	0.1	0.0	0.0	99.9	0.1	0.0	0.0	99.9
2491	+ TBHP	22.9	3.3	2.8	71.0	30.8	0.9	0.0	68.3	-	-	-	-
	- TBHP	0.0	0.0	0.1	99.8	1.0	0.0	0.0	99.0	-	-	-	-

On day 4 of culture in samples with no TBHP, an average of 99.7% of events fell in Q4, compared to samples treated with THBP for which an average of 76.2% of events were in Q4 (Table 6.10). The remaining 24.8% of events were divided between Q1, Q2 and Q3; with each quadrant possessing an average 20.9%, 1.6% and 1.1% of events respectively. The majority of events shifting into Q1 therefore show an increase in GFP expression, whilst just 1.1% of events moving to Q3 demonstrates a negligible increase in mCherry expression

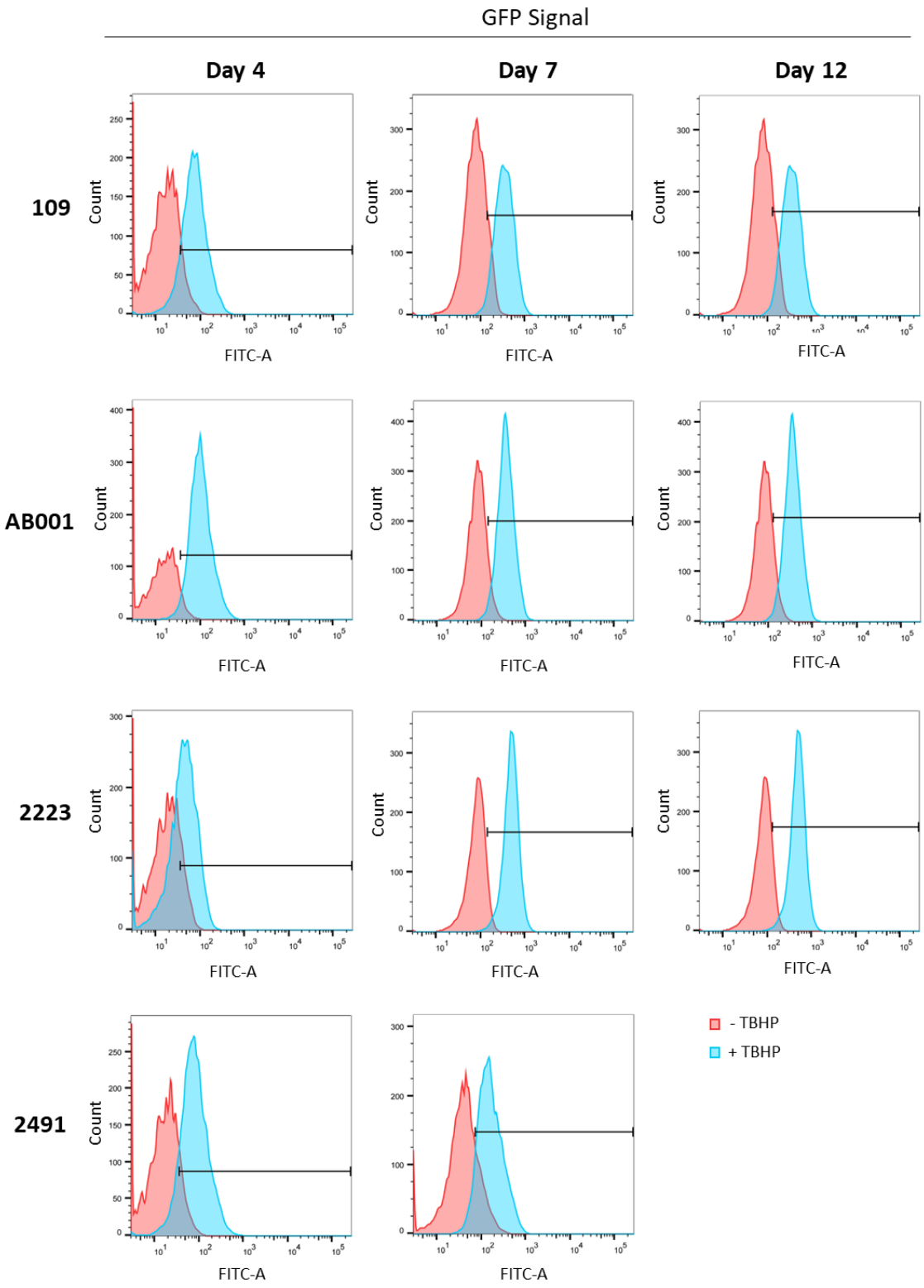

Figure 6.19: Histograms showing fluorescence representing GFP expression within samples +/- TBHP from Cell Lines 109, AB001, 2223 and 2491 transfected with the ARE-TATA Stress reporter construct. Peaks in red show transfected samples with no TBHP added, and peaks in blue show samples incubated with 200 µM TBHP for one hour prior to analysis.

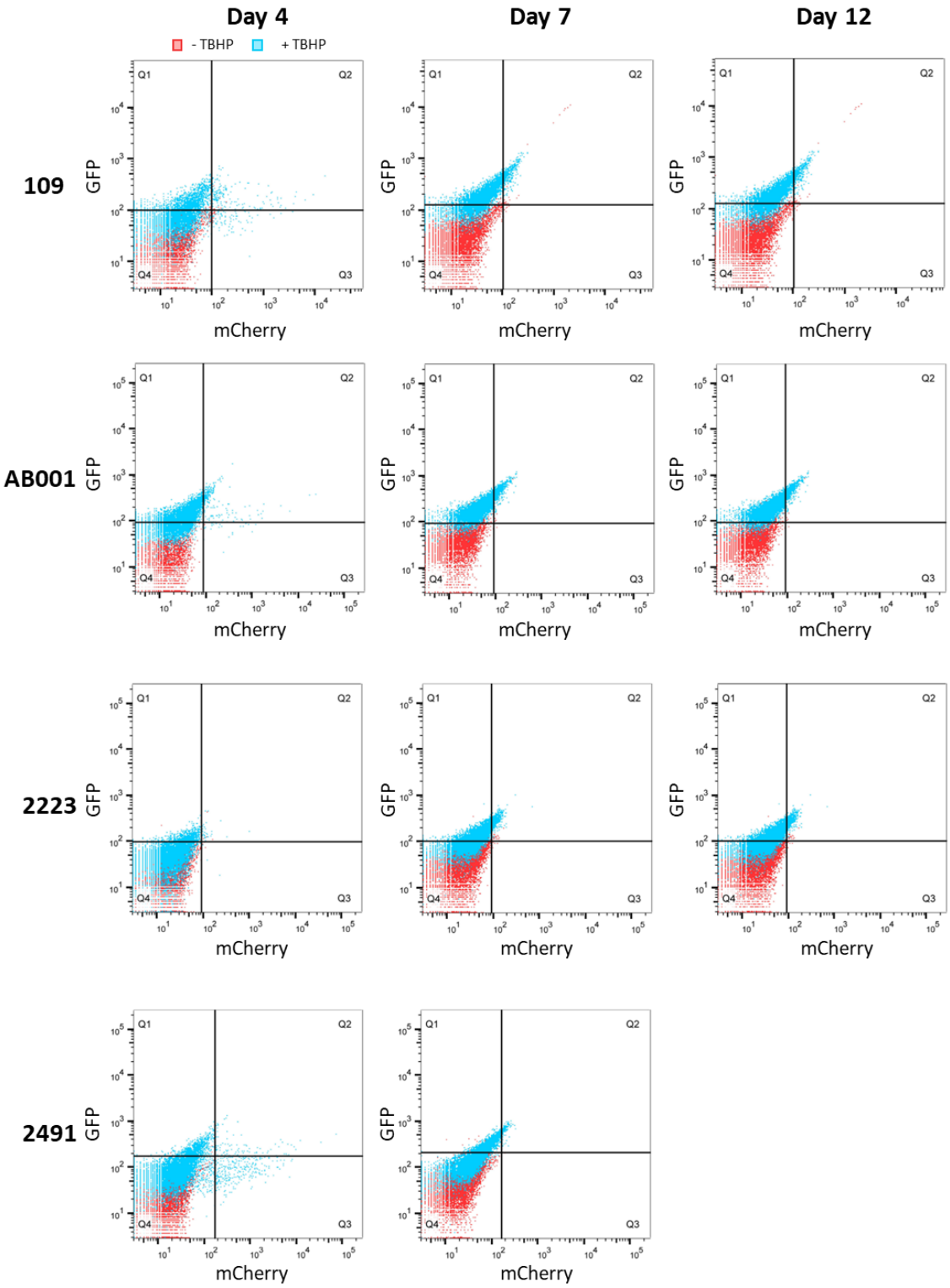

Figure 6.20: Scatter plots showing fluorescence as a result of GFP and mCherry expression on days 4, 7 and 12 in transfected Cultures +/- TBHP for cell lines 109, AB001, 2223 and 2491. The top left is quadrant (Q) 1, top right Q2, bottom right Q3 and bottom left Q4, where red plots show samples transfected with ARE-TBHP, and blue plots show transfected samples treated with 200 µM TBHP. The corresponding statistics can be seen in Table 6.10.

On day 7, samples without TBHP added had an average of 99.7% of events plotted in Q4, compared to an average of 66.3% for TBHP treated samples. As on day 4, the majority of the remaining points were observed to lie in Q1, which accounted for 33.1% of events. On day 12, the same trend was observed, with samples without TBHP having 99.9% of events in Q4 and TBHP treated samples having 67.5% with an average of 31.9% of events in Q1. GFP expression therefore increased for TBHP treated samples on days 7 and 12, demonstrating that the transfected ARE-TATA vectors do function in response to chemically induced oxidative stress once an appropriate threshold response is reached.

6.4.3 Comparing Oxidative Stress Responses Between Culture Time Points and Cell Lines Using a Commercial Cell Staining Kit

A commercial cell staining kit was also used to monitor oxidative stress in samples on days 4, 7 and 12 of culture. Unlike the ARE-TATA stress reporter construct, the cell stain provided in the kit responds to oxidative stress in its entirety through the stain itself becoming oxidised to fluoresce. Figure 6.21 shows histograms from flow cytometry data plotting fluorescence within samples prepared as per the commercial kit instructions. Samples were compared to a control, which was untreated and unstained. All samples for all cell lines on each sample day showed an increase in fluorescence as indicated by curves shifting to the right relative to the control sample.

On day 4 of fed-batch culture, cell line 109 had the greatest fluorescence, and therefore presumably was experiencing the highest oxidative stress, compared to cell lines AB001, 2223 and 2491 at this time point. AB001 and 2223 showed similar levels of signal, and therefore one assumes similar levels of oxidative stress, with cell line 2491 having the lowest fluorescence and lowest level of stress. On day 7, fluorescence signal for cell lines 109 and 2223 samples showed no change relative to day 4, indicating no change in perceived oxidative stress. Cell lines AB001 and 2491, however, showed an increase in fluorescence as denoted by histograms shifting to the right, and therefore had an increase perception of oxidative stress. Due to low culture viabilities on day 12 of culture, it was not possible to achieve 10,000 viable events during flow cytometry analysis for cell lines 109, AB001 and 2223. It would therefore be misleading to compare day 12 data between cell lines or time points.

As with the ARE-TATA construct transfected samples, positive controls treated with TBHP were also run for stained samples, as reported in Figure 6.22. TBHP treated samples also showed increased fluorescence, with peaks shifting to the right relative to untreated control samples.

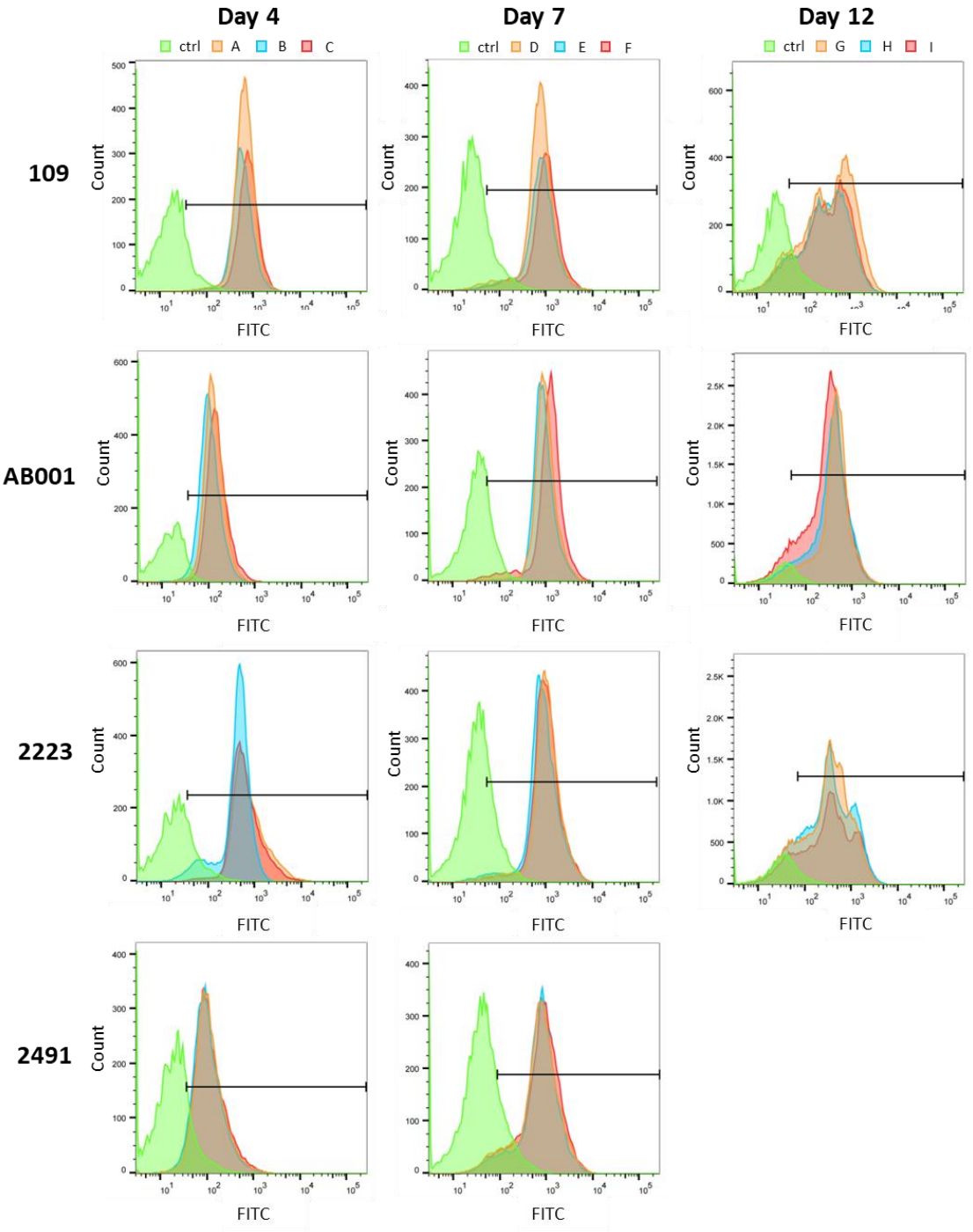

Figure 6.21: Histograms showing fluorescence as determined by flow cytometry within samples from cell lines 109, AB001, 2223 and 2491 assayed using a commercial cell staining kit. Data in green shows control (ctrl) samples consisting of unstained cells, and data in orange blue and red shows samples from replicate cultures. Note that on day 12 there were not enough viable cells to reach 10,000 events for samples AB001 and 2223, and that on this day no samples were analysed for cell line 2491.

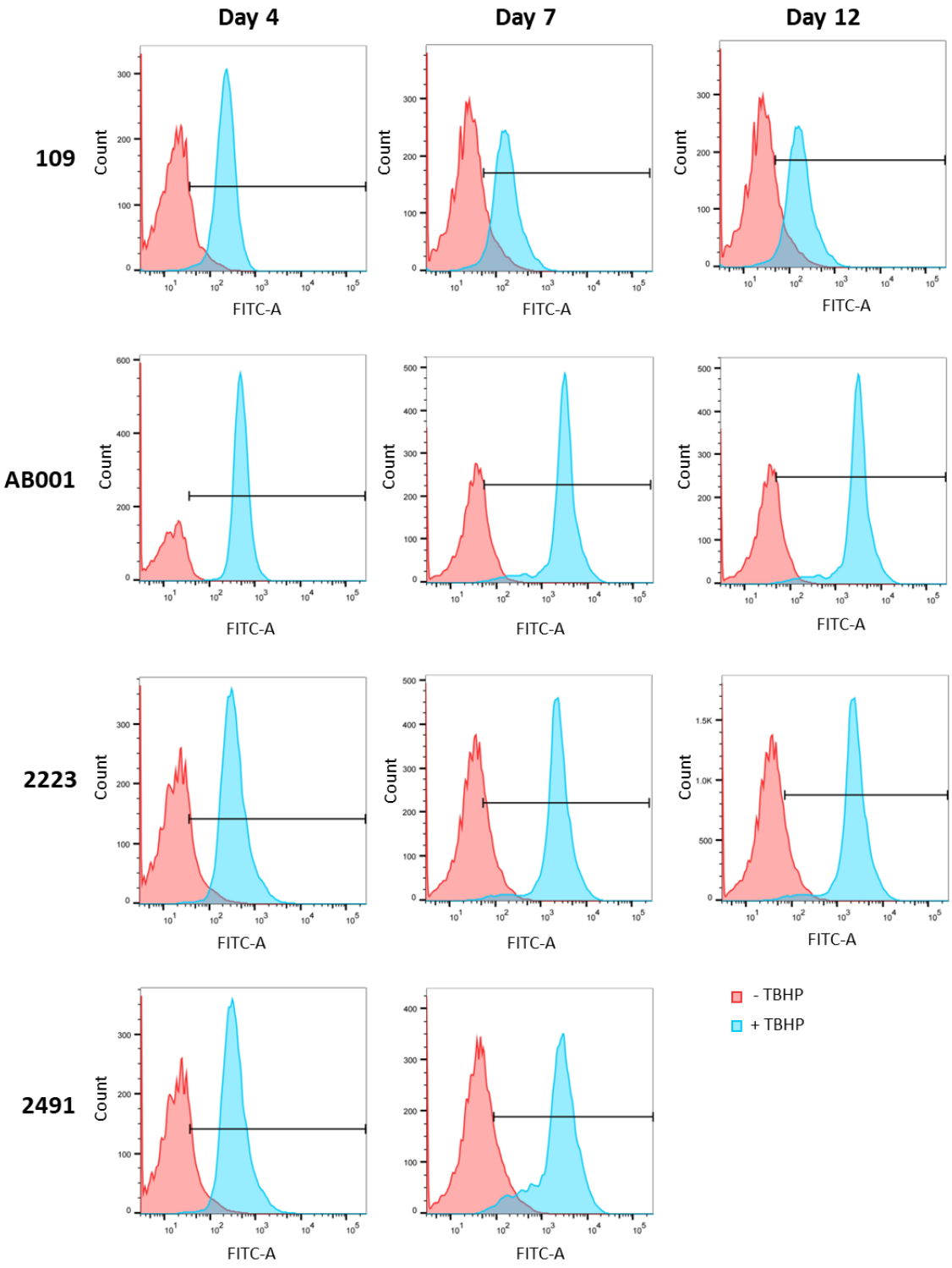

Figure 6.22: Histograms showing fluorescence as determined by flow cytometry within samples +/- TBHP for cell lines 109, AB001, 2223 and 2491 assayed using a commercial cell staining kit. Data in red shows samples without TBHP, and data in blue shows samples with 200 µM TBHP. Samples were incubated in TBHP for one hour prior to assaying.

6.5 Discussion

The aim of the work presented in this Chapter was to evaluate the use of stress reporter constructs to assess ER and oxidative stress during fed-batch culture of mAb producing CHO cell lines. Such reporter systems may present an advantage over transcriptional analysis of biomarkers for such stresses through enabling cellular stress responses to be monitored in real time in a high through-put manner, compared to RNA analysis which involves laborious sample preparation and assaying. To investigate this, 4 GFP stress reporter constructs were created; ERSE-SV40, ERSE-TATA, ARE-SV40 and ARE-TATA, where the stress response elements were taken from publications by Du *et al* (2013) and Wang *et al* (2006) respectively. Each construct was designed to drive GFP expression in response to the selected stress, with mCherry placed further downstream to function as a normaliser (Figures 6.3, 6.4 and 6.5.).

Reporter constructs were initially tested in a non-producing host CHO-S cell line, through supplementing tunicamycin and t-BHQ to chemically induce ER and oxidative stresses, with the ARE-TATA construct subsequently being taken forward for application in mAb producing cell lines. The results from preliminary testing of the vectors showed that both ERSE constructs were not responsive to ER stress induced by tunicamycin at the concentrations used. This was surprising, as in the study by Du *et al*, overnight incubation of HEK293 cells with 3 µM (compared to 6 µM and 12 µM used in this Chapter) of tunicamycin induced a 20-fold change in luciferase expression. Furthermore, the group found that stably transfected, mAb producing CHO cell lines showed a significant increase in GFP expression from day 7 of culture onwards which correlated to an increase in titre and, therefore, ER stress. When comparing the study by Du *et al* and the work presented in this Chapter, it is possible that the tunicamycin concentrations used were too high and instead of activating ER stress, caused cells to trigger cell death. This was not the case, however, as most samples and replicates (Appendix B) achieved 10,000 viable events during FACS analysis, hence cells were not dying in response to supplementation with 6 µM or 12 µM of tunicamycin. Instead, it is possible that ER stress was not great enough in the host CHO-S cell line, relative to stresses observed in mAb producing cell lines or HEK293 as used in the study by Du *et al*, to observe the impact of tunicamycin treatment on GFP expression driven by the ERSE. Another possibility is that the transient nature of expression of the reporter means that different cells will receive a varying number of plasmid DNA copies and hence there will be large heterogeneity of expression across cells. When tunicamycin is added this heterogeneity of delivery may therefore mask smaller changes in GFP expression.

To address this, further work could be undertaken to evaluate the function of the ERSE-SV40 and ERSE-TATA reporter constructs, utilising a variety of cell lines (including HEK293) and chemical inducers of ER stress, to enable more in-depth comparisons with the work by Du *et al*. Moreover, vectors to induce upregulation of ATF6 and XBP1 expression should also be transfected into cell lines to further test the sensitivity and functionality of the ERSE; and vectors should be modified to enable stable cell line construction. Ultimately, stably expressing reporter gene cell lines would need to be established to remove the variability associated with transient expression studies.

On the other hand, both ARE constructs showed a strong response to chemically induced oxidative stress, with both concentrations of t-BHQ (50 µM and 100 µM) causing a clear increase in GFP expression after 24 hours incubation with the drug, compared to 6 hours and T=0. Furthermore, an increase in GFP expression was observed in samples treated with 100 µM t-BHQ compared to those treated with 50 µM. This data demonstrated that the ARE reporter vectors were effective in relaying oxidative stress responses within the CHO-S cell lines, and were sensitive enough to enable differentiation between the two concentrations of t-BHQ used.

During this preliminary testing of the ARE vectors, it was noted that t-BHQ reagent turned the media solution pink. A shift in mCherry signal was also observed in t-BHQ treated samples only, with the higher concentration of t-BHQ also resulting in increased mCherry signal. As a result, it was unclear if these histogram shifts were due to 'leaking' of the stress response signal, or staining of the cells. In the study by Wang *et al*, t-BHQ was also used as a chemical stimulant of antioxidative responses, however, the study did not use mCherry within the construct. It is therefore possible that discolouration was observed but not considered relevant in the study as the resultant data was not impacted by this. When considering the data in this Chapter as a whole, subsequent over-grow experiments, using the ARE-TATA vector, suggested that the issue was due to colouring of the t-BHQ solution as over-grow control samples treated with TBHP (which was colourless) showed a clear shift in GFP (and therefore stress response) but no change in mCherry signal.

Although the ARE-TATA construct proved effective in detecting stress induced by treatment with tBHQ, the construct was not effective in assaying oxidative stress during over grow culture, as shown in Figures 6.16, 6.17, 6.18 and Table 6.8. Throughout all time points and cell lines, no change in GFP expression was seen, despite large fold changes in titre being observed for all cell lines and cultures over the duration of culture. There was, however, an increase in GFP expression in response to treatment with TBHP (Figures 6.19, 6.20 and Table 6.9), a chemical

oxidant which remained colourless when dissolved in media. There was also no change in mCherry expression for samples treated with TBHP, unlike t-BHQ treated samples during initial construct testing. This suggests that either the cells do not perceive an increase in oxidative stress across culture and under the conditions assayed, or that the reporter system is not sufficiently sensitive to detect more subtle changes in oxidative stress than those arising from treatment with TBHP.

Throughout the fed-batch over-grow culture study, a further control was introduced in the form of a commercial cell stain, to establish if any negative results from transfected samples were due to sensitivity issues or due to an absence of oxidative stress. Under reduced conditions, the CellROX Green reagent does not fluoresce, or is weakly fluorescent, however, under oxidising conditions the reagent itself becomes oxidised and fluoresces as a result. It should be noted that the commercial cell staining reagent responds to oxidation as a whole, compared to the ARE reporter which is activated by only one component of the cellular response to oxidative stress.

Cells stained with the CellROX Green reagent showed increased fluorescence relative to an unstained control. Unlike samples transfected with the ARE-TATA vector, differences were observed between cell lines and sample days assayed with this cell stain (Figure 6.21), indicating that cells were experiencing varying oxidative stress. On day 4 of culture, cell line 109 was under the most oxidative stress, as indicated by this cell line having the highest fluorescence peak. Cell lines AB001 and 2223 appeared to experience the second highest oxidative stress levels followed by 2491, which displayed the lowest fluorescence. On day 7 of culture there was no change in fluorescence from cell line 109 and 2223 samples, however AB001 and 2491 showed an increase in fluorescence, suggesting that by this day of culture all cell lines were experiencing a similar level of oxidative stress. Unfortunately, it is not possible to compare samples from day 12 of culture as 10,000 viable events could not be obtained during flow cytometry analysis. In combination, the results from transfected samples and those assayed using the commercial stain suggest that cells are experiencing differing levels of oxidative stress throughout culture, but that the ARE-TATA reporter construct is not sensitive enough to detect this. This is likely because the ARE itself is only bound by one component of the cellular antioxidative response (nrf2) which will limit the sensitivity of the construct. Alternatively, an increase in GFP requires time and a 24 h window after transfection may not be sufficient to allow an increase in response to perceived oxidative stress. This is because the plasmid must be delivered to the nucleus, where transcription of the gene takes places followed by translation of the gene which all takes a period of time.

Further work could be undertaken to characterise the sensitivity of both the ARE and ERSE reporter constructs, and to develop additional stress response motifs to assay ER and oxidative stress more broadly. In a previous study by Roy *et al* (2017), a stress reporter vector was used to assess UPR activation which included red fluorescent protein (RFP) to act as a normaliser, as was for mCherry in the work presented in this Chapter. The stress motif responds to inositol requiring enzyme 1 (IRE1) mediated splicing of XBP1, which is a key component of the UPR. In this study the stress response element contained the full XBP1 gene, with RFP encoded upstream and GFP further downstream but in different reading frames. Under conditions where the UPR is not activated, GFP is therefore not expressed as it is not in the correct reading frame. When cells trigger the UPR, IRE1 splices the XBP1 gene which results in RFP and GFP genes being in the same reading frame. As a result, both RFP and GFP are expressed during times of ER stress, hence cells display dual fluorescence upon triggering of the UPR. Utilising this construct, Roy *et al* (2017) created an ER stress index (ERSI) as a measure of ER stress, where ERSE = Dual fluorescence/ (RFP fluorescence + dual fluorescence). The higher the ERSI score, the more dual fluorescence and therefore the higher the UPR response within cells. Interestingly, when stably transfecting mAb producing CHO cell lines, the group reported an increase in ERSE score from day 7 of culture onwards, which coincides with an increase in titre. This observation matches that reported by Du *et al,* who utilised the ERSE motif (bound by ATF6 and XBP1) to also establish an increase in UPR within mAb producing CHO cell lines from day 7 of culture onwards when an increase in titre was observed. The work by Roy *et al* therefore presents a good example of how a dual florescence system could be used to score and compare stress responses between cell lines.

To compare stress responses in a broader manner, future work could also focus on identifying and investigating new stress response motifs, and on utilising existing sequences simultaneously. New targets, however, are limited to proteins such as transcription factors, as these need to be present in the nucleus to be able to bind to the intended stress response element.

6.5.1 Limitations

Due to time constraints, the stress reporter constructs described throughout this chapter were not tested and troubleshooted extensively. When using the ARE and ERSE within a host CHO-S cell line, the ERSE showed no response to chemical stress however the ARE did. With more time, the ERSE vectors would have been tested more extensively, with a small panel of mAb producing cell lines used (as in the study by Du *et al*) in combination with tunicamycin to establish if

recombinant protein production was able to induce enough cellular stress to see a change in GFP expression driven by the ER stress response element.

Another variable which warrants further investigation is the impact of the transfection technique on cellular stress as measured by the ERSE and ARE vectors. During initial studies in the host CHO-S cell line, cells were transfected using electroporation; however, when the ARE-TATA vector was taken forward for use in mAb producing cell lines, cells were chemically transfected. Whilst any transfection method places cells under increased stress, and causes cell death, electroporation methods are documented to cause increased stress compared to chemical methods (Kim and Eberwine 2010). In the case of the ARE-TATA vector, it is therefore possible that the use of electroporation to transfect host CHO-S samples was the cause of the stress response observed in these samples. Future studies should ideally use chemical transfection methods, with either choice of technique used consistently throughout all studies to minimise the likelihood of transfection methods impacting on any variation in GFP expression between cell lines and conditions.

Time points analysed when utilising the ARE-TATA vector within 2223, 2491, AB001 and 109 cell lines should also be evaluated. Samples were analysed for GFP and mCherry expression 24 hours after chemical transfection, however it is possible that leaving more time post transfection would better represent cellular stress during mAb production. Transfection places cells under increased stress, and it is therefore possible that in response to this stress, cells reduced or halted recombinant protein expression to alleviate some of this stress. Such a response to transfection may explain why the ARE-TATA was responsive within the CHO-S samples but not the panel of mAb producing cell lines. To investigate this a variety of time points, post transfection should be analysed. To ultimately address this point, however, stress response vectors should be modified to contain an appropriate selection marker (such as hygromycin) to produce stable cell lines. In this way transfection methods would be eliminated from impacting on GFP expression, and would not factor into sampling time-points.

To fully address the issue of mCherry expression during initial studies of the ARE-TATA and ARE-SV40 vectors in CHO-S samples, reporter constructs should be re-engineered to reverse the orientation of the SV40-mCherry portion. Through this alteration, any leakage form the SRE-SV40/TATA – GFP portion would not be able to impact on mCherry expression. Without this change, it is not possible to conclusively say if mCherry expression observed during the CHO-S studies was due to the colouring of the t-BHQ reagent.

Chapter 7

Discussion

7.1 Overall Discussion

Understanding the stability profile of a mAb, and establishing an appropriate formulation to mitigate issues such as aggregation and SVP formation, is essential to ensure product safety and efficacy and can also influence the drug format and dosing (Daugherty and Mrsny, 2006; Wang *et al.*, 2007; Manning *et al.*, 2010). The quality, and therefore stability, of a mAb is continuously impacted throughout bioprocessing however, with the molecule encountering a multitude of stresses such as concentration, temperature, and pH changes, and shear stresses. During cell culture, cells may be placed under elevated ER stress as a result of high recombinant protein production (Ruggiano *et al.*, 2014; Cudna and Dickson, 2003), which can impact on the quality of the secreted protein. No studies to date, however, have investigated the impact of cell culture stresses on the stability of formulated mAbs.

The work described in this thesis investigated the relationship between cellular stress responses, culture harvest day and formulated mAb stability. Throughout this work cell lines 109, 4212 and 184, producing model therapeutic mAbs, were used to explore this relationship. These cell lines have been cultured in two formats, using 400 mL roller bottle cultures (Chapter 3) and 10 L disposable bioreactors (Chapter 4) to gain industrially relevant insights into cellular stress profiles during recombinant protein production. qRT-PCR was used to monitor biomarker profiles of ER stress responses throughout culture, by assessing the change in expression of a panel of genes involved in UPR and ERAD pathways. Furthermore, RNA seq was also utilised to further understand transcriptional profiles within cells at varying points of culture (Chapter 5), and to analyse the statistical significance of differentially expressed gene profiles and pathway enrichment.

To study the relationship between harvest day and product stability, mAb material was harvested and purified at what was considered an early (day 9 in roller bottle work and day 8 in bioreactors) and late (day 13) harvest day; purified by Protein A affinity chromatography, and then formulated and subjected to routine stability analysis under accelerated storage conditions of 40^{o}C (Chapters 3 and 4). Throughout all stability studies, samples were assessed for visible degradation, aggregate/fragment/monomeric content and SVP formation, using visual inspection, SEC-HPLC and MFI methods respectively, to compare the stability of material from the two harvest days. AFM was also deployed to study the morphology of aggregates at the nanometre level in samples from stability studies, and used to further compare material from biological replicate cultures, between harvest days and between cell lines/mAbs. Finally, the use of stress reporter constructs to monitor ER and oxidative stress throughout culture was also

investigated (Chapter 6) for a further panel of cell lines (109, AB001, 2223 and 2491). Whilst the vectors created for this thesis did not show sufficient sensitivity during fed-batch culture to detect changes in ER or oxidative stress, studies utilising reporter constructs to assess ER and oxidative stresses throughout mAb synthesis (Oslowski and Urano, 2011; Roy *et al.*, 2017; Wang *et al.*, 2006; Du *et al.*, 2013) have shown great promise to monitor such cellular stresses in real time.

Overall, the data presented in this thesis demonstrates a dynamic relationship between cell culture processes, cellular stresses and SVP formation within formulated mAbs. Moreover, this work shows significant transcriptional differences within the cell throughout culture, and presents the use of stress reporter constructs to assess cellular stresses in real time. Such observations provide the foundations for further investigations into the relationship between cell culture processes, cellular stress and mAb stability, as discussed below in more detail.

One of the focuses of the work presented in Chapters 3 and 4 was to profile ER stress throughout culture in cell lines 4212, 184 (Chapter 3) and 109 (Chapter 4), where the work described in Chapter 3 was carried out using fed-batch and batch 400 mL roller bottle cultures, and that described in Chapter 4 used fed-batch 10 L disposable bioreactors. In the studies described in both chapters, ER stress was assessed using qRT-PCR for a panel of 11 genes (summarised in Chapter 3, Table 3.1). In Chapter 3, linear regression analysis showed significant differences in biomarker profiles between batch and fed-batch culture conditions, with transcript expression, productivity and growth similar between the two cell lines when cultured under batch conditions; but significant differences observed between cell lines under fed-batch conditions. Such data agrees with comparisons between fed-batch and batch conditions in other studies (Prashad and Mehra, 2015), and highlights how cell lines may elicit growth, productivity and transcriptional differences depending upon existing culture stresses. This data demonstrates the importance of using industrially relevant fed-batch conditions throughout cell line development processes to ensure that studies are as representative as possible of a cell line's manufacturing characteristics.

As described above, during roller bottle fed-batch culture, cell lines 4212 and 184 had very different specific productivities, where 4212 had a Qp almost half that of 184 (Chapter 3 supplementary Table 3.2), which was reflected in the biomarker profiles. Linear regression analysis showed different combinations of genes significantly changing between the two cell lines, matching with observations made in previous studies comparing the expression of genes relating to ER stress between cell lines with varying productivities (Roy *et al.*, 2017; Prashad and

Mehra, 2015). When comparing cell lines under fed-batch conditions, cell line 4212 had elevated *bip* and *hsp90b* expression, and HC:LC mRNA and protein ratios. BiP and Hsp90b sequentially bind the HC in the ER, to keep the polypeptide soluble until the LC polypeptide is available for assembly. This data therefore suggested that cell line 4212 was under increased ER stress as a result of excess HC production.

When carrying out qRT-PCR analysis on the same panel of genes for cell lines 4212, 184 and 109 cultured in fed-batch 10 L disposable bioreactors (Chapter 4), there was no significant change in expression observed for any of the 11 genes analysed for all three cell lines. Cell line 4212, still demonstrated high *HC:LC* ratios which, in the case of the 10 L disposable bioreactors, did not appear to impact on ER stress relative to the panel of genes analysed. During 10 L bioreactor culturing, cell line 4212 also achieved a higher average Qp of 19.8 pg/cell/day, compared to 8.3 pg/cell/day during roller bottle culture, suggesting that HC:LC ratios were not impacting on productivity as much during large scale culture as they perhaps were when the cell line was cultured in roller bottles. The data presented in Chapters 3 and 4, relating to ER biomarker profiling and HC:LC mRNA/protein ratios, therefore showed that cells were under less stress during culture in disposable bioreactors, where parameters such as DO and pH were tightly regulated, compared to roller bottle culture (400 mL) when such conditions were not regulated.

Previous studies (Jiang *et al.*, 2006; Ho *et al.*, 2015b) have established a link between high HC:LC ratios and mAb aggregation in culture, as well as linking high ratios to decreased productivity. These studies assessed mAb material straight from culture or after protein A purification, and therefore did not study the stability profile extensively within a formulated product. Moreover, these studies also used small scale culture techniques, during which key parameters such as pH and DO are not well regulated. It is therefore possible that HC:LC ratios impact mAb quality more severely during culturing conditions when cellular stress is elevated, and that a high ratio is not as detrimental to a cell line/product if existing cellular stress is at a manageable level. In the case of 4212 material produced during 10 L bioreactor culturing, it is likely that the cell line was better able to cope with any stresses induced as a result of high HC:LC ratios when cultured under regulated conditions, and that the ratios were not high enough to impact on productivity, or to induce a significant increase in *bip* and *hsp90b* expression.

The mAb stability data presented in Chapters 3 and 4 showed a link between culture harvest day and SVP formation of formulated mAb material across multiple buffers. There were, however, differences in stability profiles between harvest days of the same cell lines/mAbs cultured in roller bottles and 10 L bioreactors. As such, it is important to note differences between each

culture process. During roller bottle culture cells were incubated and shaken at 70% humidity and 4% CO_2, however parameters such as pH and DO were not monitored or adjusted throughout culture. During disposable bioreactor culture, DO, CO_2, pH, glucose and rocking speeds were continuously monitored and adjusted for each individual culture as required. Bioreactor culturing therefore offered a far more regulated environment for cell growth compared to roller bottle culturing, which is likely to result in cells being under increased stress during roller bottle culture compared to bioreactor conditions.

When cultured in roller bottles, mAb 4212 material from day 9 of culture produced fewer SVPs than that from day 13, however, stability data for the same mAb harvested at an early and late time point from 10 L bioreactor cultures showed no obvious difference in the stability of the material. mAb 184 material from roller bottle cultures showed no harvest day trend, however, when mAb 184 was produced in 10 L bioreactors, a strong harvest day trend was observed; with material from day 8 of culture producing fewer SVPs and appearing less opalescent than that harvested on day 13. Cell line 4212 appeared to be under greater ER stress than cell line 184 during roller bottle culture as determined from monitoring of ER biomarkers, however during bioreactor culture neither cell line appeared to be under elevated ER stress with respect to the original panel of 11 biomarker genes analysed. Whilst it has been shown that different biotherapeutic products can cause varying degrees of stress within a host cell line (Alves and Dobrowsky, 2017), this observation, in combination with the change in impact of harvest day on mAb stability for the two cell lines between culture systems, suggests that previously observed stress in chapter 3 was induced by the culturing process itself. Thus, the culture format can impact on (i) the ER stress experienced by the cell, and (ii) the stability profile of the formulated product. This stability data, in combination with previously discussed biomarker profiling suggests that cellular stress is a factor which can contribute to SVP formation; and that this relationship is dynamic and heavily influenced by a number of parameters during culture as well as 'molecular variables' such as HC:LC ratios.

To further investigate particle formation, AFM was used to visualise the morphology of aggregates/SVPs at the nanometre level from samples from the 10 L bioreactor cultures. AFM has been reportedly used for assessing mAb aggregate mechanisms, self-assembly and orientation at solid/solution interfaces (Andersen *et al.*, 2010; Xu *et al.*, 2006; Kominami *et al.*, 2018), hence AFM was deployed here to further compare samples stored in different formulations from early and late harvests (Figures 4.25, 4.26 and Appendix A). No differences were observed between samples of mAb 109 or 184 material, however, there were visible differences between biological replicate mAb 4212 samples. Material from replicate 4212A

produced fibrillose networks of material, compared to 4212 B and C for which small, punctate areas of aggregates were seen. These observations at the nanometre level matched with other differences between 4212A culture material compared to B and C culture material, with culture 4212A achieving a far greater titre and Qp than B and C, and showing a different visual stability profile and CD spectra. Collectively these data suggest a relationship between productivity, mAb conformation and aggregate formation. CD spectroscopy also revealed conformational differences between mAb 184 samples from day 8 and day 13 harvests (Figure 4.38A, 4.38B, 4.38C and 4.38D). Furthermore, conformational differences were also observed between material formulated in 80 mM Arg and that in 190 mM Arg and 120 mM sucrose.

As cell line/mAb 184 showed a strong relationship between harvest day and formulated mAb stability during 10 L bioreactor culturing, samples from days 6, 8 and 13 of these cultures were sent for total RNA seq analysis (Chapter 5). Although KEGG and GO pathway enrichment analysis of this data did not highlight any pathways relating to ER or oxidative stress as significantly changing, pathways such as DNA replication, cell cycle and lysosome pathways were shown to be enriched across the samples. This agrees with observations from previous studies (Reinhart *et al.*, 2018; Tamosaitis and Smales, 2018), which link such pathways to CHO cell lines with increased cellular growth and productivity. Based on such literature, RNA seq data for cell line 184 samples were therefore indicative of a 'typical' high producing cell line with robust growth characteristics, and provides evidence that, as a result, cells within these cultures could have been placed under elevated stress due to high recombinant protein production and rapid cellular growth. Furthermore, PCA analysis showed that the profile of differentially expressed genes was similar between biological replicate samples, but was significantly different between all time points analysed. As such, between the two harvest days (day 8 and 13) there were significant differences in transcriptional profiles within the cells as culture progressed. This RNA seq data, in combination with published literature, further reinforces the concept that molecular changes were occurring within the cell throughout culture in response to stress, and that such changes are dynamic and can ultimately impact on formulated mAb stability.

Finally, in Chapter 6, GFP stress reporter constructs (termed the ERSE and ARE) were created to quantify ER and oxidative stress during culture in real time. Both ERSE constructs did not prove responsive to chemically induced ER stress; however, both the ARE-TATA and ARE-SV40 vectors did prove sensitive when oxidative stress was chemically induced in transfected cells. Both stress response element sequences were obtained from previous studies (Wang *et al.*, 2006; Du *et al.*, 2013), which utilised the same chemical stimulants (tunicamycin and t-BHQ respectively) for each respective stress. It was therefore surprising that the ERSE did not prove sensitive to

chemical stress within the initial CHO-S host cell line, however studies utilising other stress response elements to measure ER stress (Oslowski and Urano, 2011; Roy *et al.*, 2017) have successfully applied such an approach to mAb producing CHO cell lines. Both previous studies used their respective constructs to show an increase in cellular UPR responses, which also coincided with an increase in titre on day 7 of fed-batch culture. These studies have demonstrated the potential of reporter constructs in quantifying stresses in real time, and in combination with the biomarker profiling techniques used throughout this thesis, offer the potential to be powerful tools to further understand the impact of culture processes on the cell, and on recombinant protein stability.

7.2 Future Work

To further understand the relationship between cell culture processes, cellular stress, harvest day and formulated mAb stability, it would be beneficial for future work to incorporate the use of additional cell lines producing a range of recombinant mAbs with a wide variety of stability issues. It would also be advantageous to use a number of cell lines producing the same molecule but with varying productivities. Through investigating products with a range of stability problems, such as phase separation and reversible self-association, qRT-PCR and RNA seq techniques could be further applied to identify transcript targets which relate to productivity and/or specific stability issues. To further utilise such molecular techniques, cell lines producing 'stable' molecules and non-producing cell lines should also be analysed to provide a 'baseline', and to work towards understanding what genes and pathways may relate to cell culture processes, and which may relate to the specific product and/or cell line itself. Future studies should also be conducted using a range of cell culture methodologies, such as re-usable bioreactors, ambr™ systems and well plate formats to work towards understanding how culture conditions throughout industrial cell line development, and scaling studies, may influence a cells transcriptional biomarker profile; and how this may in turn impact on the stability of the product.

To build on the stability studies presented here, recombinant material from further harvest days should also be assessed; and the subsequent material formulated in different buffers. Such studies would enable an understanding of which specific stresses and/or points of culture result in an improved or worsened stability profile for the secreted product, and would work towards understanding if formulation development could be coupled to biomarker profiles during culture. Moreover, to fully understand the impact of harvest day on product stability, in a fully relevant context, stability studies should be conducted over longer periods of time, with 5^{o}C and

25°C time points also introduced as per ICH guidelines over a time period of 6 months to a year. Throughout future stability studies it would also be advantageous to deploy further methods to assess the structure and function of material between cell lines, culture processes and harvest days. Mass spectrometry would be a powerful tool to provide detailed information on chemical modifications and glycan profiles to be obtained and compared. Such data would provide further insights into the cause of stability differences between harvest days and biological replicates, as well as providing more detailed comparisons between formulation compositions. Moreover, another interesting aspect to explore within this work would be to compare the efficacy of mAbs between harvest days, replicates and formulations. Such comparisons may be made by using commercially available ELISA kits or cell-based assays; and would have significant industrial relevance.

Previous studies have reported on how HCP content may impact on protein A purification of mAbs (Bracewell *et al.*, 2015; Hogwood *et al.*, 2014; Hogwood *et al.*, 2013), and have also been linked to SVP formation in formulated mAb material (Bee *et al.*, 2015). To further work towards understanding the impact of the bioprocess in its entirety on formulated mAb stability, HCP profiles should also be analysed in future studies, through using commercially available western blotting and ELISA kits to analyse cell culture supernatant samples. Moreover, material in future studies should be purified using additional polishing steps after protein A purification to remove further impurities and to eliminate viruses, endotoxins and aggregate/structural variations of the mAb. Through a more stringent purification process, results generated will have further industrial relevance.

Despite the stress reporter vectors created and presented in this thesis proving unsuccessful in quantifying ER and oxidative stresses during fed-batch over-grow culture, future work could also look to develop such reporter systems and carry out further testing across a range of cell lines and culture conditions. As previously mentioned, other published work has successfully used such vectors to quantify stresses during mAb production, hence there is justifiable potential in ERSE and ARE vectors for quantifying cellular stress under the right conditions. To further trouble-shoot these systems, reporter constructs should be modified to contain an appropriate selection marker to enable stable cell lines to be produced. Through using reporter constructs in stable expression systems, further work utilising ERSE and ARE response elements will be more comparable to the studies where these sequences originate (Du *et al.*, 2013; Wang *et al.*, 2006), and would eliminate the heterogeneity associated with transient transfection methods.

7.3 Conclusions

Overall, the work in this thesis demonstrates a relationship between cell culture processes, cellular stress and SVP formation within formulated mAbs. It also shows that this relationship is complex and dynamic, and that several approaches are required to understand it in its entirety. Specifically, conclusions presented from data within this thesis are as follows:

1. Fed-batch cell culture conditions should be used throughout cell line development processes to fully characterise productivity, growth and molecular differences between cell lines.
2. Different cell lines elicit varying mRNA biomarker profiles relating to ER stress, which may be linked to productivity, HC:LC ratios, growth and/or cell culture processes; and such relationships are complex and closely related.
3. Harvest day, and therefore culture duration/cellular stress, can have an impact on visual degradation and SVP formation of formulated mAbs in a cell line and/or culture process and/or product specific manner As such, harvest day could be used as a tool for improving formulated mAb stability on a case by case basis.
4. Product stability may also be linked to the productivity of a culture, and can show variation between biological replicate cultures which have similar growth characteristics.
5. qRT-PCR and RNA seq are powerful tools if used in combination with high sample numbers for working towards understanding pathway enrichment and differentially expressed genes which may relate to culture processes and mAb stability.
6. In combination with transcriptional techniques, stress reporter constructs could offer an effective method for quantifying cellular stresses throughout culture to understand how such stresses may fluctuate with productivity and culture duration in real time; and to determine how this relates to the stability of the subsequent harvested mAb material.

Together, these conclusions and their associated data presents a comprehensive and detailed study into the implications of upstream cell culture processes on formulation development. This work also presents harvest day as a potential tool in improving the stability of a product, as despite losing material as a result of terminating cultures earlier in the bioprocess; harvesting cultures earlier on a case-by-case basis offers the potential to increase a product's stability, and to therefore reduce formulation development timelines. Moreover, this work highlights the importance of bioprocess linking, and presents novel insights into how each step of the bioprocess may influence another. Subsequently, decisions throughout product development

and manufacturing should be considered collaboratively to ensure that the safety and quality of the final biotherapeutic product is optimised.

References

ABE, A., TAKAHASHI-NIKI, K., TAKEKOSHI, Y., SHIMIZU, T., KITAURA, H., MAITA, H., IGUCHI-ARIGA, S. M. & ARIGA, H. 2013. Prefoldin plays a role as a clearance factor in preventing proteasome inhibitor-induced protein aggregation. *J Biol Chem,* 288**,** 27764-76.

ALVES, C. S. & DOBROWSKY, T. M. 2017. Strategies and Considerations for Improving Expression of "Difficult to Express" Proteins in CHO Cells. *Methods Mol Biol,* 1603**,** 1-23.

ANDERSEN, C. B., MANNO, M., RISCHEL, C., THÓRÓLFSSON, M. & MARTORANA, V. 2010. Aggregation of a multidomain protein: a coagulation mechanism governs aggregation of a model IgG1 antibody under weak thermal stress. *Protein science : a publication of the Protein Society,* 19**,** 279-290.

ARAKAWA, T., EJIMA, D., LI, T. & PHILO, J. S. 2010. The critical role of mobile phase composition in size exclusion chromatography of protein pharmaceuticals. *J Pharm Sci,* 99**,** 1674-92.

ARAKAWA, T., PHILO, J. S., TSUMOTO, K., YUMIOKA, R. & EJIMA, D. 2004. Elution of antibodies from a Protein-A column by aqueous arginine solutions. *Protein Expr Purif,* 36**,** 244-8.

AWWAD, S. & ANGKAWINITWONG, U. 2018. Overview of Antibody Drug Delivery. *Pharmaceutics,* 10.

BAEK, Y., SINGH, N., ARUNKUMAR, A. & ZYDNEY, A. L. 2017. Effects of Histidine and Sucrose on the Biophysical Properties of a Monoclonal Antibody. *Pharm Res,* 34**,** 629-639.

BAYNES, B. M., WANG, D. I. & TROUT, B. L. 2005. Role of arginine in the stabilization of proteins against aggregation. *Biochemistry,* 44**,** 4919-25.

BECK, R., DEJEANS, N., GLORIEUX, C., CRETON, M., DELAIVE, E., DIEU, M., RAES, M., LEVÊQUE, P., GALLEZ, B., DEPUYDT, M., COLLET, J.-F., CALDERON, P. B. & VERRAX, J. 2012. Hsp90 Is Cleaved by Reactive Oxygen Species at a Highly Conserved N-Terminal Amino Acid Motif. *PLOS ONE,* 7**,** e40795.

BEE, J. S., TIE, L., JOHNSON, D., DIMITROVA, M. N., JUSINO, K. C. & AFDAHL, C. D. 2015. Trace levels of the CHO host cell protease cathepsin D caused particle formation in a monoclonal antibody product. *Biotechnol Prog,* 31**,** 1360-9.

BIRBEN, E., SAHINER, U. M., SACKESEN, C., ERZURUM, S. & KALAYCI, O. 2012. Oxidative stress and antioxidant defense. *World Allergy Organ J,* 5**,** 9-19.

BOLTON, G. R. & MEHTA, K. K. 2016. The role of more than 40 years of improvement in protein A chromatography in the growth of the therapeutic antibody industry. *Biotechnol Prog,* 32**,** 1193-1202.

BOYCE, M., BRYANT, K. F., JOUSSE, C., LONG, K., HARDING, H. P., SCHEUNER, D., KAUFMAN, R. J., MA, D., COEN, D. M., RON, D. & YUAN, J. 2005. A selective inhibitor of eIF2alpha dephosphorylation protects cells from ER stress. *Science,* 307**,** 935-9.

BRACEWELL, D. G., FRANCIS, R. & SMALES, C. M. 2015. The future of host cell protein (HCP) identification during process development and manufacturing linked to a risk-based management for their control. *Biotechnol Bioeng,* 112**,** 1727-37.

BRAVO, R., PARRA, V., GATICA, D., RODRIGUEZ, A. E., TORREALBA, N., PAREDES, F., WANG, Z. V., ZORZANO, A., HILL, J. A., JAIMOVICH, E., QUEST, A. F. & LAVANDERO, S. 2013. Endoplasmic reticulum and the unfolded protein response: dynamics and metabolic integration. *Int Rev Cell Mol Biol,* 301**,** 215-90.

BREMS, D. N., ALTER, L. A., BECKAGE, M. J., CHANCE, R. E., DIMARCHI, R. D., GREEN, L. K., LONG, H. B., PEKAR, A. H., SHIELDS, J. E. & FRANK, B. H. 1992. Altering the association properties of insulin by amino acid replacement. *Protein Eng,* 5**,** 527-33.

BROSTROM, C. O. & BROSTROM, M. A. 1998. Regulation of translational initiation during cellular responses to stress. *Prog Nucleic Acid Res Mol Biol,* 58**,** 79-125.

BRUNNER, M., FRICKE, J., KROLL, P. & HERWIG, C. 2017. Investigation of the interactions of critical scale-up parameters (pH, pO2 and pCO2) on CHO batch performance and critical quality attributes. *Bioprocess Biosyst Eng,* 40**,** 251-263.

CARPENTER, J. F., RANDOLPH, T. W., JISKOOT, W., CROMMELIN, D. J., MIDDAUGH, C. R., WINTER, G., FAN, Y. X., KIRSHNER, S., VERTHELYI, D., KOZLOWSKI, S., CLOUSE, K. A., SWANN, P. G., ROSENBERG, A. & CHERNEY, B. 2009. Overlooking subvisible particles in therapeutic protein products: gaps that may compromise product quality. *J Pharm Sci,* 98**,** 1201-5.

CHAKRABARTI, A., CHEN, A. W. & VARNER, J. D. 2011. A review of the mammalian unfolded protein response. *Biotechnol Bioeng,* 108**,** 2777-93.

CHEN, B., BAUTISTA, R., YU, K., ZAPATA, G. A., MULKERRIN, M. G. & CHAMOW, S. M. 2003. Influence of histidine on the stability and physical properties of a fully human antibody in aqueous and solid forms. *Pharm Res,* 20**,** 1952-60.

CHEN, K., LI, D., LI, H., LI, B., LI, J., HUANG, L., LI, R., XU, X., JIANG, L., JIANG, C., GU, H. & FANG, J. 2017. Genetic analysis of heterogeneous sub-clones in recombinant Chinese hamster ovary cells. *Appl Microbiol Biotechnol,* 101**,** 5785-5797.

CHI, E. Y., KRISHNAN, S., RANDOLPH, T. W. & CARPENTER, J. F. 2003. Physical stability of proteins in aqueous solution: mechanism and driving forces in nonnative protein aggregation. *Pharm Res,* 20**,** 1325-36.

COCK, P. J. A., FIELDS, C. J., GOTO, N., HEUER, M. L. & RICE, P. M. 2010. The Sanger FASTQ file format for sequences with quality scores, and the Solexa/Illumina FASTQ variants. *Nucleic acids research,* 38**,** 1767-1771.

CONNELL-CROWLEY, L., NGUYEN, T., BACH, J., CHINNIAH, S., BASHIRI, H., GILLESPIE, R., MOSCARIELLO, J., HINCKLEY, P., DEHGHANI, H., VUNNUM, S. & VEDANTHAM, G. 2012. Cation exchange chromatography provides effective retrovirus clearance for antibody purification processes. *Biotechnol Bioeng,* 109**,** 157-65.

CORVARI, V., NARHI, L. O., SPITZNAGEL, T. M., AFONINA, N., CAO, S., CASH, P., CECCHINI, I., DEFELIPPIS, M. R., GARIDEL, P., HERRE, A., KOULOV, A. V., LUBINIECKI, T., MAHLER, H. C., MANGIAGALLI, P., NESTA, D., PEREZ-RAMIREZ, B., POLOZOVA, A., ROSSI, M., SCHMIDT, R., SIMLER, R., SINGH, S., WEISKOPF, A. & WUCHNER, K. 2015. Subvisible (2-100 mum) particle analysis during biotherapeutic drug product development: Part 2, experience with the application of subvisible particle analysis. *Biologicals,* 43**,** 457-73.

CUDNA, R. E. & DICKSON, A. J. 2003. Endoplasmic reticulum signaling as a determinant of recombinant protein expression. *Biotechnology and Bioengineering,* 81**,** 56-65.

DARAMOLA, O., STEVENSON, J., DEAN, G., HATTON, D., PETTMAN, G., HOLMES, W. & FIELD, R. 2014. A high-yielding CHO transient system: coexpression of genes encoding EBNA-1 and GS enhances transient protein expression. *Biotechnol Prog,* 30**,** 132-41.

DAS, T. K. 2012. Protein particulate detection issues in biotherapeutics development--current status. *AAPS PharmSciTech,* 13**,** 732-46.

DAUGHERTY, A. L. & MRSNY, R. J. 2006. Formulation and delivery issues for monoclonal antibody therapeutics. *Advanced Drug Delivery Reviews,* 58**,** 686-706.

DAVIS, G. C. 1993. Protein stability: impact upon protein pharmaceuticals. *Biologicals,* 21**,** 105.

DHARA, V. G., NAIK, H. M., MAJEWSKA, N. I. & BETENBAUGH, M. J. 2018. Recombinant Antibody Production in CHO and NS0 Cells: Differences and Similarities. *BioDrugs,* 32**,** 571-584.

DOESSEGGER, L., MAHLER, H. C., SZCZESNY, P., ROCKSTROH, H., KALLMEYER, G., LANGENKAMP, A., HERRMANN, J. & FAMULARE, J. 2012. The potential clinical relevance of visible particles in parenteral drugs. *J Pharm Sci,* 101**,** 2635-44.

DU, Z. M., TREIBER, D., MCCOY, R. E., MILLER, A. K., HAN, M., HE, F., DOMNITZ, S., HEATH, C. & REDDY, P. 2013. Non-invasive UPR monitoring system and its applications in CHO production cultures. *Biotechnology and Bioengineering,* 110**,** 2184-2194.

DYSON, M. R. 2016. Fundamentals of Expression in Mammalian Cells. *Adv Exp Med Biol,* 896**,** 217-24.

FAN, Y., JIMENEZ DEL VAL, I., MULLER, C., WAGTBERG SEN, J., RASMUSSEN, S. K., KONTORAVDI, C., WEILGUNY, D. & ANDERSEN, M. R. 2015. Amino acid and glucose metabolism in fed-batch CHO cell culture affects antibody production and glycosylation. *Biotechnol Bioeng,* 112**,** 521-35.

FAN, Y., LEY, D. & ANDERSEN, M. R. 2018. Fed-Batch CHO Cell Culture for Lab-Scale Antibody Production. *Methods Mol Biol,* 1674**,** 147-161.

FEIGE, M. J. & BUCHNER, J. 2014. Principles and engineering of antibody folding and assembly. *Biochim Biophys Acta,* 1844**,** 2024-2031.

FEIGE, M. J., HENDERSHOT, L. M. & BUCHNER, J. 2010a. How antibodies fold. *Trends Biochem Sci,* 35**,** 189-98.

FEIGE, M. J., HENDERSHOT, L. M. & BUCHNER, J. 2010b. How antibodies fold. *Trends in Biochemical Sciences,* 35**,** 189-198.

GENG, X., KONG, X., HU, H., CHEN, J., YANG, F., LIANG, H., CHEN, X. & HU, Y. 2015. Research and development of therapeutic mAbs: An analysis based on pipeline projects. *Human vaccines & immunotherapeutics,* 11**,** 2769-2776.

GERVASI, V., DALL AGNOL, R., CULLEN, S., MCCOY, T., VUCEN, S. & CREAN, A. 2018. Parenteral protein formulations: An overview of approved products within the European Union. *European Journal of Pharmaceutics and Biopharmaceutics,* 131**,** 8-24.

GIKANGA, B., EISNER, D. R., OVADIA, R., DAY, E. S., STAUCH, O. B. & MAA, Y. F. 2017. Processing Impact on Monoclonal Antibody Drug Products: Protein Subvisible Particulate Formation Induced by Grinding Stress. *PDA J Pharm Sci Technol,* 71**,** 172-188.

GILLE, J. J. & JOENJE, H. 1992. Cell culture models for oxidative stress: superoxide and hydrogen peroxide versus normobaric hyperoxia. *Mutat Res,* 275**,** 405-14.

GOMEZ, N., SUBRAMANIAN, J., OUYANG, J., NGUYEN, M. D., HUTCHINSON, M., SHARMA, V. K., LIN, A. A. & YUK, I. H. 2012. Culture temperature modulates aggregation of recombinant antibody in cho cells. *Biotechnol Bioeng,* 109**,** 125-36.

GOWTHAM, Y. K., SASKI, C. A. & HARCUM, S. W. 2017. Low glucose concentrations within typical industrial operating conditions have minimal effect on the transcriptome of recombinant CHO cells. *Biotechnol Prog,* 33**,** 771-785.

GRILO, A. L. & MANTALARIS, A. 2019. The Increasingly Human and Profitable Monoclonal Antibody Market. *Trends in Biotechnology,* 37**,** 9-16.

GRONEMEYER, P., DITZ, R. & STRUBE, J. 2014. Trends in Upstream and Downstream Process Development for Antibody Manufacturing. *Bioengineering,* 1**,** 188.

GUAN, B.-J., KROKOWSKI, D., MAJUMDER, M., SCHMOTZER, C. L., KIMBALL, S. R., MERRICK, W. C., KOROMILAS, A. E. & HATZOGLOU, M. 2014. Translational control during endoplasmic reticulum stress beyond phosphorylation of the translation initiation factor eIF2α. *The Journal of biological chemistry,* 289**,** 12593-12611.

GUO, S., KIEFER, H., ZHOU, D., GUAN, Y. H., WANG, S., WANG, H., LU, Y. & ZHUANG, Y. 2016. A scale-down cross-flow filtration technology for biopharmaceuticals and the associated theory. *Journal of Biotechnology,* 221**,** 25-31.

HA, T. K., HANSEN, A. H., KOL, S., KILDEGAARD, H. F. & LEE, G. M. 2018. Baicalein Reduces Oxidative Stress in CHO Cell Cultures and Improves Recombinant Antibody Productivity. *Biotechnol J,* 13**,** e1700425.

HALLIWELL, B. 2014. Cell culture, oxidative stress, and antioxidants: avoiding pitfalls. *Biomed J,* 37**,** 99-105.

HARDING, H. P., NOVOA, I., ZHANG, Y., ZENG, H., WEK, R., SCHAPIRA, M. & RON, D. 2000. Regulated translation initiation controls stress-induced gene expression in mammalian cells. *Mol Cell,* 6**,** 1099-108.

HARDING, H. P., ZHANG, Y., ZENG, H., NOVOA, I., LU, P. D., CALFON, M., SADRI, N., YUN, C., POPKO, B., PAULES, R., STOJDL, D. F., BELL, J. C., HETTMANN, T., LEIDEN, J. M. & RON, D. 2003. An integrated stress response regulates amino acid metabolism and resistance to oxidative stress. *Mol Cell,* 11**,** 619-33.

HAUPTMANN, A., PODGORŠEK, K., KUZMAN, D., SRČIČ, S., HOELZL, G. & LOERTING, T. 2018. Impact of Buffer, Protein Concentration and Sucrose Addition on the Aggregation and Particle Formation during Freezing and Thawing. *Pharmaceutical research,* 35**,** 101-101.

HEAL, R. & MCGIVAN, J. 1998. Induction of calreticulin expression in response to amino acid deprivation in Chinese hamster ovary cells. *Biochem J,* 329 (Pt 2)**,** 389-94.
HERNANDEZ BORT, J. A., HACKL, M., HOFLMAYER, H., JADHAV, V., HARREITHER, E., KUMAR, N., ERNST, W., GRILLARI, J. & BORTH, N. 2012. Dynamic mRNA and miRNA profiling of CHO-K1 suspension cell cultures. *Biotechnol J,* 7**,** 500-15.
HETZ, C. 2012. The unfolded protein response: controlling cell fate decisions under ER stress and beyond. *Nat Rev Mol Cell Biol,* 13**,** 89-102.
HO, S. C., KOH, E. Y., VAN BEERS, M., MUELLER, M., WAN, C., TEO, G., SONG, Z., TONG, Y. W., BARDOR, M. & YANG, Y. 2013. Control of IgG LC:HC ratio in stably transfected CHO cells and study of the impact on expression, aggregation, glycosylation and conformational stability. *J Biotechnol,* 165**,** 157-66.
HO, S. C., WANG, T., SONG, Z. & YANG, Y. 2015a. IgG Aggregation Mechanism for CHO Cell Lines Expressing Excess Heavy Chains. *Mol Biotechnol,* 57**,** 625-34.
HO, S. C. L., WANG, T., SONG, Z. & YANG, Y. 2015b. IgG Aggregation Mechanism for CHO Cell Lines Expressing Excess Heavy Chains. *Molecular Biotechnology,* 57**,** 625-634.
HOGWOOD, C. E., BRACEWELL, D. G. & SMALES, C. M. 2013. Host cell protein dynamics in recombinant CHO cells: impacts from harvest to purification and beyond. *Bioengineered,* 4**,** 288-91.
HOGWOOD, C. E., BRACEWELL, D. G. & SMALES, C. M. 2014. Measurement and control of host cell proteins (HCPs) in CHO cell bioprocesses. *Curr Opin Biotechnol,* 30**,** 153-60.
HUANG, C. T., SHARMA, D., OMA, P. & KRISHNAMURTHY, R. 2009. Quantitation of protein particles in parenteral solutions using micro-flow imaging. *J Pharm Sci,* 98**,** 3058-71.
HUANG, Y.-M., HU, W., RUSTANDI, E., CHANG, K., YUSUF-MAKAGIANSAR, H. & RYLL, T. 2010. Maximizing productivity of CHO cell-based fed-batch culture using chemically defined media conditions and typical manufacturing equipment. *Biotechnology Progress,* 26**,** 1400-1410.
ICH 1995. Stability Testing of Biotechnological/Biological Products Q5C.
ICH 2003. Guidance for Industry: Q1A(R2) Stability Testing of New Drug Substances and Products.
IONESCU, R. & VLASAK, J. 2010. Kinetics of Chemical Degradation in Monoclonal Antibodies: Relationship between Rates at the Molecular and Peptide Levels. *Analytical Chemistry,* 82**,** 3198-3206.
IRANI, V., GUY, A. J., ANDREW, D., BEESON, J. G., RAMSLAND, P. A. & RICHARDS, J. S. 2015. Molecular properties of human IgG subclasses and their implications for designing therapeutic monoclonal antibodies against infectious diseases. *Mol Immunol,* 67**,** 171-82.
ISHII, Y., MURAKAMI, J., SASAKI, K., TSUKAHARA, M. & WAKAMATSU, K. 2014. Efficient folding/assembly in Chinese hamster ovary cells is critical for high quality (low aggregate content) of secreted trastuzumab as well as for high production: stepwise multivariate regression analyses. *J Biosci Bioeng,* 118**,** 223-30.
JEFFERIS, R. 2007. Antibody therapeutics: isotype and glycoform selection. *Expert Opin Biol Ther,* 7**,** 1401-13.
JIANG, Z., HUANG, Y. & SHARFSTEIN, S. T. 2006. Regulation of recombinant monoclonal antibody production in chinese hamster ovary cells: a comparative study of gene copy number, mRNA level, and protein expression. *Biotechnol Prog,* 22**,** 313-8.
JORGENSEN, L., HOSTRUP, S., MOELLER, E. H. & GROHGANZ, H. 2009. Recent trends in stabilising peptides and proteins in pharmaceutical formulation - considerations in the choice of excipients. *Expert Opin Drug Deliv,* 6**,** 1219-30.
JOSHI, V., SHIVACH, T., KUMAR, V., YADAV, N. & RATHORE, A. 2014. Avoiding antibody aggregation during processing: establishing hold times. *Biotechnol J,* 9**,** 1195-205.
KADOWAKI, H., NAGAI, A., MARUYAMA, T., TAKAMI, Y., SATRIMAFITRAH, P., KATO, H., HONDA, A., HATTA, T., NATSUME, T., SATO, T., KAI, H., ICHIJO, H. & NISHITOH, H. 2015. Pre-

emptive Quality Control Protects the ER from Protein Overload via the Proximity of ERAD Components and SRP. *Cell Rep,* 13**,** 944-56.

KELLY, S. M. & PRICE, N. C. 2000. The Use of Circular Dichroism in the Investigation of Protein Structure and Function. *Current Protein & Peptide Science,* 1**,** 349-384.

KHEDDO, P., TRACKA, M., ARMER, J., DEARMAN, R. J., UDDIN, S., VAN DER WALLE, C. F. & GOLOVANOV, A. P. 2014. The effect of arginine glutamate on the stability of monoclonal antibodies in solution. *Int J Pharm,* 473**,** 126-33.

KHODABANDEHLOO, A. & CHEN, D. D. 2017. Particle sizing methods for the detection of protein aggregates in biopharmaceuticals. *Bioanalysis,* 9**,** 313-326.

KIM, T. K. & EBERWINE, J. H. 2010. Mammalian cell transfection: the present and the future. *Anal Bioanal Chem,* 397**,** 3173-8.

KIM, Y. J., BAEK, E., LEE, J. S. & LEE, G. M. 2013. Autophagy and its implication in Chinese hamster ovary cell culture. *Biotechnol Lett,* 35**,** 1753-63.

KINCAID, M. M. & COOPER, A. A. 2007. ERADicate ER stress or die trying. *Antioxid Redox Signal,* 9**,** 2373-87.

KIYOSHI, M., SHIBATA, H., HARAZONO, A., TORISU, T., MARUNO, T., AKIMARU, M., ASANO, Y., HIROKAWA, M., IKEMOTO, K., ITAKURA, Y., IWURA, T., KIKITSU, A., KUMAGAI, T., MORI, N., MURASE, H., NISHIMURA, H., ODA, A., OGAWA, T., OJIMA, T., OKABE, S., SAITO, S., SAITOH, S., SUETOMO, H., TAKEGAMI, K., TAKEUCHI, M., YASUKAWA, H., UCHIYAMA, S. & ISHII-WATABE, A. 2019. Collaborative Study for Analysis of Subvisible Particles Using Flow Imaging and Light Obscuration: Experiences in Japanese Biopharmaceutical Consortium. *Journal of Pharmaceutical Sciences,* 108**,** 832-841.

KOMINAMI, H., KOBAYASHI, K., IDO, S., KIMIYA, H. & YAMADA, H. 2018. Immunoactivity of self-assembled antibodies investigated by atomic force microscopy. *RSC Advances,* 8**,** 29378-29384.

KONITZER, J. D., MULLER, M. M., LEPARC, G., PAUERS, M., BECHMANN, J., SCHULZ, P., SCHAUB, J., ENENKEL, B., HILDEBRANDT, T., HAMPEL, M. & TOLSTRUP, A. B. 2015. A global RNA-seq-driven analysis of CHO host and production cell lines reveals distinct differential expression patterns of genes contributing to recombinant antibody glycosylation. *Biotechnol J,* 10**,** 1412-23.

KRAYUKHINA, E., TSUMOTO, K., UCHIYAMA, S. & FUKUI, K. 2015. Effects of syringe material and silicone oil lubrication on the stability of pharmaceutical proteins. *Journal of pharmaceutical sciences,* 104**,** 527-535.

KRISHNAMURTHY, A. & JIMENO, A. 2018. Bispecific antibodies for cancer therapy: A review. *Pharmacol Ther,* 185**,** 122-134.

KRISHNAMURTHY, R. & MANNING, M. C. 2002. The stability factor: importance in formulation development. *Curr Pharm Biotechnol,* 3**,** 361-71.

LAEMMLI, U. K. 1970. Cleavage of Structural Proteins during the Assembly of the Head of Bacteriophage T4. *Nature,* 227**,** 680.

LAI, T., YANG, Y. & NG, S. 2013. Advances in Mammalian Cell Line Development Technologies for Recombinant Protein Production. *Pharmaceuticals,* 6**,** 579.

LAPTOŠ, T. & OMERSEL, J. 2018. The importance of handling high-value biologicals: Physico-chemical instability and immunogenicity of monoclonal antibodies. *Experimental and therapeutic medicine,* 15**,** 3161-3168.

LEE, C. J., SETH, G., TSUKUDA, J. & HAMILTON, R. W. 2009a. A clone screening method using mRNA levels to determine specific productivity and product quality for monoclonal antibodies. *Biotechnology and bioengineering,* 102**,** 1107-1118.

LEE, C. J., SETH, G., TSUKUDA, J. & HAMILTON, R. W. 2009b. A clone screening method using mRNA levels to determine specific productivity and product quality for monoclonal antibodies. *Biotechnol Bioeng,* 102**,** 1107-18.

LEE, J. S. & LEE, G. M. 2012. Monitoring of autophagy in Chinese hamster ovary cells using flow cytometry. *Methods,* 56**,** 375-82.

LI, J., ZHANG, C., JOSTOCK, T. & DUBEL, S. 2007. Analysis of IgG heavy chain to light chain ratio with mutant Encephalomyocarditis virus internal ribosome entry site. *Protein Eng Des Sel,* 20**,** 491-6.

LIU, H. & MAY, K. 2012. Disulfide bond structures of IgG molecules: structural variations, chemical modifications and possible impacts to stability and biological function. *mAbs,* 4**,** 17-23.

LIU, H. F., MA, J., WINTER, C. & BAYER, R. 2010. Recovery and purification process development for monoclonal antibody production. *mAbs,* 2**,** 480-499.

LOVE, M. I., HUBER, W. & ANDERS, S. 2014. Moderated estimation of fold change and dispersion for RNA-seq data with DESeq2. *Genome Biology,* 15**,** 550.

MACMANES, M. D. 2014. On the optimal trimming of high-throughput mRNA sequence data. *Frontiers in genetics,* 5**,** 13-13.

MAHLER, H.-C., FRIESS, W., GRAUSCHOPF, U. & KIESE, S. 2009. Protein aggregation: Pathways, induction factors and analysis. *Journal of Pharmaceutical Sciences,* 98**,** 2909-2934.

MALDONADO-AGURTO, R. & DICKSON, A. J. 2018. Multiplexed digital mRNA expression analysis profiles system-wide changes in mRNA abundance and responsiveness of UPR-specific gene expression changes during batch culture of recombinant Chinese Hamster Ovary cells. *Biotechnol J*.

MANNING, M. C., CHOU, D. K., MURPHY, B. M., PAYNE, R. W. & KATAYAMA, D. S. 2010. Stability of protein pharmaceuticals: an update. *Pharm Res,* 27**,** 544-75.

MANNING, M. C., PATEL, K. & BORCHARDT, R. T. 1989. Stability of protein pharmaceuticals. *Pharm Res,* 6**,** 903-18.

MASON, B. D., ZHANG, L., REMMELE, R. L., JR. & ZHANG, J. 2011. Opalescence of an IgG2 monoclonal antibody solution as it relates to liquid-liquid phase separation. *J Pharm Sci,* 100**,** 4587-96.

MATHONET, S., MAHLER, H. C., ESSWEIN, S. T., MAZAHERI, M., CASH, P. W., WUCHNER, K., KALLMEYER, G., DAS, T. K., FINKLER, C. & LENNARD, A. 2016. A Biopharmaceutical Industry Perspective on the Control of Visible Particles in Biotechnology-Derived Injectable Drug Products. *PDA J Pharm Sci Technol,* 70**,** 392-408.

MATUCCI, A., NENCINI, F., PRATESI, S., MAGGI, E. & VULTAGGIO, A. 2016. An overview on safety of monoclonal antibodies. *Curr Opin Allergy Clin Immunol,* 16**,** 576-581.

MAZZER, A. R., PERRAUD, X., HALLEY, J., O'HARA, J. & BRACEWELL, D. G. 2015. Protein A chromatography increases monoclonal antibody aggregation rate during subsequent low pH virus inactivation hold. *J Chromatogr A,* 1415**,** 83-90.

MEAD, E. J., MASTERTON, R. J., FEARY, M., OBREZANOVA, O., ZHANG, L., YOUNG, R. & SMALES, C. M. 2015. Biological insights into the expression of translation initiation factors from recombinant CHOK1SV cell lines and their relationship to enhanced productivity. *Biochemical Journal,* 472**,** 261-273.

MELCHORE, J. A. & BERDOVICH, D. 2012. Considerations for design and use of container challenge sets for qualification and validation of visible particulate inspection. *PDA J Pharm Sci Technol,* 66**,** 273-84.

MIESEGAES, G. R., LUTE, S., STRAUSS, D. M., READ, E. K., VENKITESHWARAN, A., KREUZMAN, A., SHAH, R., SHAMLOU, P., CHEN, D. & BRORSON, K. 2012. Monoclonal antibody capture and viral clearance by cation exchange chromatography. *Biotechnol Bioeng,* 109**,** 2048-58.

MORRISON, C. 2018. Fresh from the biotech pipeline—2017. *Nature Biotechnology,* 36**,** 131.

NAIDOO, N. 2009. ER and aging-Protein folding and the ER stress response. *Ageing Res Rev,* 8**,** 150-9.

NARHI, L. O., CORVARI, V., RIPPLE, D. C., AFONINA, N., CECCHINI, I., DEFELIPPIS, M. R., GARIDEL, P., HERRE, A., KOULOV, A. V., LUBINIECKI, T., MAHLER, H. C., MANGIAGALLI, P., NESTA, D., PEREZ-RAMIREZ, B., POLOZOVA, A., ROSSI, M., SCHMIDT, R., SIMLER, R., SINGH, S., SPITZNAGEL, T. M., WEISKOPF, A. & WUCHNER, K. 2015. Subvisible (2-100 mum) Particle

Analysis During Biotherapeutic Drug Product Development: Part 1, Considerations and Strategy. *J Pharm Sci,* 104**,** 1899-908.
NARHI, L. O., JIANG, Y., CAO, S., BENEDEK, K. & SHNEK, D. 2009. A critical review of analytical methods for subvisible and visible particles. *Curr Pharm Biotechnol,* 10**,** 373-81.
ODA, Y., OKADA, T., YOSHIDA, H., KAUFMAN, R. J., NAGATA, K. & MORI, K. 2006. Derlin-2 and Derlin-3 are regulated by the mammalian unfolded protein response and are required for ER-associated degradation. *J Cell Biol,* 172**,** 383-93.
ORELLANA, C. A., MARCELLIN, E., PALFREYMAN, R. W., MUNRO, T. P., GRAY, P. P. & NIELSEN, L. K. 2018. RNA-Seq Highlights High Clonal Variation in Monoclonal Antibody Producing CHO Cells. *Biotechnology Journal,* 13**,** 1700231.
OSLOWSKI, C. M. & URANO, F. 2011. Measuring ER stress and the unfolded protein response using mammalian tissue culture system. *Methods in enzymology,* 490**,** 71-92.
PARK, J. H., JIN, J. H., LIM, M. S., AN, H. J., KIM, J. W. & LEE, G. M. 2017. Proteomic Analysis of Host Cell Protein Dynamics in the Culture Supernatants of Antibody-Producing CHO Cells. *Sci Rep,* 7**,** 44246.
PATEL, J., MCLEOD, L. E., VRIES, R. G. J., FLYNN, A., WANG, X. & PROUD, C. G. 2002. Cellular stresses profoundly inhibit protein synthesis and modulate the states of phosphorylation of multiple translation factors. *European Journal of Biochemistry,* 269**,** 3076-3085.
PATRO, R., DUGGAL, G., LOVE, M. I., IRIZARRY, R. A. & KINGSFORD, C. 2017. Salmon provides fast and bias-aware quantification of transcript expression. *Nature Methods,* 14**,** 417.
PAUL, A. J., HANDRICK, R., EBERT, S. & HESSE, F. 2018. Identification of process conditions influencing protein aggregation in Chinese hamster ovary cell culture. *Biotechnol Bioeng,* 115**,** 1173-1185.
PHILO, J. S. 2009. A critical review of methods for size characterization of non-particulate protein aggregates. *Curr Pharm Biotechnol,* 10**,** 359-72.
PHILO, J. S. & ARAKAWA, T. 2009. Mechanisms of protein aggregation. *Curr Pharm Biotechnol,* 10**,** 348-51.
PLATTS, L., DARBY, S. J. & FALCONER, R. J. 2016. Control of Globular Protein Thermal Stability in Aqueous Formulations by the Positively Charged Amino Acid Excipients. *J Pharm Sci,* 105**,** 3532-3536.
PRASHAD, K. & MEHRA, S. 2015. Dynamics of unfolded protein response in recombinant CHO cells. *Cytotechnology,* 67**,** 237-54.
RAJENDRA, Y., PEERY, R. B. & BARNARD, G. C. 2016. Generation of stable Chinese hamster ovary pools yielding antibody titers of up to 7.6 g/L using the piggyBac transposon system. *Biotechnol Prog,* 32**,** 1301-1307.
RATANJI, K. D., DERRICK, J. P., DEARMAN, R. J. & KIMBER, I. 2014. Immunogenicity of therapeutic proteins: influence of aggregation. *J Immunotoxicol,* 11**,** 99-109.
RATHORE, A. S., KUMAR SINGH, S., PATHAK, M., READ, E. K., BRORSON, K. A., AGARABI, C. D. & KHAN, M. 2015. Fermentanomics: Relating quality attributes of a monoclonal antibody to cell culture process variables and raw materials using multivariate data analysis. *Biotechnol Prog,* 31**,** 1586-99.
RAUT, A. S. & KALONIA, D. S. 2015. Opalescence in monoclonal antibody solutions and its correlation with intermolecular interactions in dilute and concentrated solutions. *J Pharm Sci,* 104**,** 1263-74.
RAUT, A. S. & KALONIA, D. S. 2016. Pharmaceutical Perspective on Opalescence and Liquid-Liquid Phase Separation in Protein Solutions. *Mol Pharm,* 13**,** 1431-44.
REINHART, D., DAMJANOVIC, L., CASTAN, A., ERNST, W. & KUNERT, R. 2018. Differential gene expression of a feed-spiked super-producing CHO cell line. *J Biotechnol,* 285**,** 23-37.
RITACCO, F. V., WU, Y. & KHETAN, A. 2018. Cell culture media for recombinant protein expression in Chinese hamster ovary (CHO) cells: History, key components, and optimization strategies. *Biotechnol Prog,* 34**,** 1407-1426.

ROBERTS, C. J. 2014. Protein aggregation and its impact on product quality. *Current Opinion in Biotechnology,* 30**,** 211-217.

ROY, G., ZHANG, S., LI, L., HIGHAM, E., WU, H., MARELLI, M. & BOWEN, M. A. 2017. Development of a fluorescent reporter system for monitoring ER stress in Chinese hamster ovary cells and its application for therapeutic protein production. *PLOS ONE,* 12**,** e0183694.

RUGGIANO, A., FORESTI, O. & CARVALHO, P. 2014. ER-associated degradation: Protein quality control and beyond. *The Journal of Cell Biology,* 204**,** 869-879.

RUTKOWSKI, D. T., ARNOLD, S. M., MILLER, C. N., WU, J., LI, J., GUNNISON, K. M., MORI, K., SADIGHI AKHA, A. A., RADEN, D. & KAUFMAN, R. J. 2006. Adaptation to ER Stress Is Mediated by Differential Stabilities of Pro-Survival and Pro-Apoptotic mRNAs and Proteins. *PLoS Biology,* 4**,** e374.

RUTKOWSKI, D. T. & KAUFMAN, R. J. 2004. A trip to the ER: coping with stress. *Trends Cell Biol,* 14**,** 20-8.

SALINAS, B. A., SATHISH, H. A., BISHOP, S. M., HARN, N., CARPENTER, J. F. & RANDOLPH, T. W. 2010. Understanding and modulating opalescence and viscosity in a monoclonal antibody formulation. *J Pharm Sci,* 99**,** 82-93.

SANO, R. & REED, J. C. 2013a. ER stress-induced cell death mechanisms. *Biochimica et biophysica acta,* 1833**,** 10.1016/j.bbamcr.2013.06.028.

SANO, R. & REED, J. C. 2013b. ER stress-induced cell death mechanisms. *Biochim Biophys Acta,* 1833**,** 3460-3470.

SCHLATTER, S., STANSFIELD, S. H., DINNIS, D. M., RACHER, A. J., BIRCH, J. R. & JAMES, D. C. 2005. On the optimal ratio of heavy to light chain genes for efficient recombinant antibody production by CHO cells. *Biotechnol Prog,* 21**,** 122-33.

SCHNEIDER, C. A., RASBAND, W. S. & ELICEIRI, K. W. 2012. NIH Image to ImageJ: 25 years of image analysis. *Nature Methods,* 9**,** 671.

SCHRODER, K. C. 2015. *Characterization of Chinese Hamster Ovary Cells Producing Coagulation Factor VIII Using Multi-omics Tools.* PhD, Technical University of Denmark.

SCHRODER, M. 2006. The unfolded protein response. *Mol Biotechnol,* 34**,** 279-90.

SCHRODER, M. 2008. Endoplasmic reticulum stress responses. *Cell Mol Life Sci,* 65**,** 862-94.

SCHRÖDER, M. & KAUFMAN, R. J. 2005. The Mammalian Unfolded Protein Response. *Annual Review of Biochemistry,* 74**,** 739-789.

SCHUMOCK, G. T., STUBBINGS, J., HOFFMAN, J. M., WIEST, M. D., SUDA, K. J., RIM, M. H., TADROUS, M., TICHY, E. M., CUELLAR, S., CLARK, J. S., MATUSIAK, L. M., HUNKLER, R. J. & VERMEULEN, L. C. 2019. National trends in prescription drug expenditures and projections for 2019. *Am J Health Syst Pharm*.

SEDYKH, S. E., PRINZ, V. V., BUNEVA, V. N. & NEVINSKY, G. A. 2018. Bispecific antibodies: design, therapy, perspectives. *Drug Des Devel Ther,* 12**,** 195-208.

SHA, S., BHATIA, H. & YOON, S. 2018. An RNA-seq based transcriptomic investigation into the productivity and growth variants with Chinese hamster ovary cells. *Journal of Biotechnology,* 271**,** 37-46.

SHAH, M. 2018. Commentary: New perspectives on protein aggregation during Biopharmaceutical development. *Int J Pharm,* 552**,** 1-6.

SHARMA, D. K., KING, D., OMA, P. & MERCHANT, C. 2010a. Micro-flow imaging: flow microscopy applied to sub-visible particulate analysis in protein formulations. *The AAPS journal,* 12**,** 455-464.

SHARMA, D. K., OMA, P., POLLO, M. J. & SUKUMAR, M. 2010b. Quantification and characterization of subvisible proteinaceous particles in opalescent mAb formulations using micro-flow imaging. *J Pharm Sci,* 99**,** 2628-42.

SHENG, S. & KONG, F. 2012. Separation of antigens and antibodies by immunoaffinity chromatography. *Pharm Biol,* 50**,** 1038-44.

SHUKLA, D., SCHNEIDER, C. P. & TROUT, B. L. 2011. Complex Interactions between Molecular Ions in Solution and Their Effect on Protein Stability. *Journal of the American Chemical Society,* 133**,** 18713-18718.

SIDDIQI, M. K., ALAM, P., CHATURVEDI, S. K., SHAHEIN, Y. E. & KHAN, R. H. 2017. Mechanisms of protein aggregation and inhibition. *Front Biosci (Elite Ed),* 9**,** 1-20.

SINGH, S. K., AFONINA, N., AWWAD, M., BECHTOLD-PETERS, K., BLUE, J. T., CHOU, D., CROMWELL, M., KRAUSE, H.-J., MAHLER, H.-C., MEYER, B. K., NARHI, L., NESTA, D. P. & SPITZNAGEL, T. 2010. An Industry Perspective on the Monitoring of Subvisible Particles as a Quality Attribute for Protein Therapeutics. *Journal of Pharmaceutical Sciences,* 99**,** 3302-3321.

SOMASUNDARAM, B., PLEITT, K., SHAVE, E., BAKER, K. & LUA, L. H. L. 2018. Progression of continuous downstream processing of monoclonal antibodies: Current trends and challenges. *Biotechnol Bioeng,* 115**,** 2893-2907.

STEVENSON, J., HUANG, E. Y. & OLZMANN, J. A. 2016. Endoplasmic Reticulum–Associated Degradation and Lipid Homeostasis. *Annual Review of Nutrition,* 36**,** 511-542.

STRAUSS, D. M., GORRELL, J., PLANCARTE, M., BLANK, G. S., CHEN, Q. & YANG, B. 2009. Anion exchange chromatography provides a robust, predictable process to ensure viral safety of biotechnology products. *Biotechnol Bioeng,* 102**,** 168-75.

SUKUMAR, M., DOYLE, B. L., COMBS, J. L. & PEKAR, A. H. 2004. Opalescent appearance of an IgG1 antibody at high concentrations and its relationship to noncovalent association. *Pharm Res,* 21**,** 1087-93.

SZEGEZDI, E., LOGUE, S. E., GORMAN, A. M. & SAMALI, A. 2006. Mediators of endoplasmic reticulum stress-induced apoptosis. *EMBO Rep,* 7**,** 880-5.

TAMOSAITIS, L. & SMALES, C. M. 2018. Meta-Analysis of Publicly Available Chinese Hamster Ovary (CHO) Cell Transcriptomic Datasets for Identifying Engineering Targets to Enhance Recombinant Protein Yields. *Biotechnol J***,** e1800066.

TORKASHVAND, F. & VAZIRI, B. 2017. Main Quality Attributes of Monoclonal Antibodies and Effect of Cell Culture Components. *Iran Biomed J,* 21**,** 131-141.

TORKASHVAND, F., VAZIRI, B., MALEKNIA, S., HEYDARI, A., VOSSOUGHI, M., DAVAMI, F. & MAHBOUDI, F. 2015. Designed Amino Acid Feed in Improvement of Production and Quality Targets of a Therapeutic Monoclonal Antibody. *PLOS ONE,* 10**,** e0140597.

USP 2012. <788> Particulate Matter in Injections.

VAGENENDE, V., HAN, A. X., MUELLER, M. & TROUT, B. L. 2013. Protein-associated cation clusters in aqueous arginine solutions and their effects on protein stability and size. *ACS Chem Biol,* 8**,** 416-22.

VANHOVE, M., USHERWOOD, Y. K. & HENDERSHOT, L. M. 2001. Unassembled Ig heavy chains do not cycle from BiP in vivo but require light chains to trigger their release. *Immunity,* 15**,** 105-114.

VELUGULA-YELLELA, S. R., WILLIAMS, A., TRUNFIO, N., HSU, C. J., CHAVEZ, B., YOON, S. & AGARABI, C. 2018. Impact of media and antifoam selection on monoclonal antibody production and quality using a high throughput micro-bioreactor system. *Biotechnol Prog,* 34**,** 262-270.

VIDARSSON, G., DEKKERS, G. & RISPENS, T. 2014. IgG subclasses and allotypes: from structure to effector functions. *Front Immunol,* 5**,** 520.

VIJAYASANKARAN, N., VARMA, S., YANG, Y., MUN, M., AREVALO, S., GAWLITZEK, M., SWARTZ, T., LIM, A., LI, F., ZHANG, B., MEIER, S. & KISS, R. 2013. Effect of cell culture medium components on color of formulated monoclonal antibody drug substance. *Biotechnol Prog,* 29**,** 1270-7.

WANG, C., YAMNIUK, A., DAI, J., CHEN, S., STETSKO, P., DITTO, N. & ZHANG, Y. 2015. Investigation of a Degradant in a Biologics Formulation Buffer Containing L-Histidine. *Pharm Res,* 32**,** 2625-35.

WANG, W. 2005. Protein aggregation and its inhibition in biopharmaceutics. *Int J Pharm,* 289**,** 1-30.

WANG, W. 2015. Advanced protein formulations. *Protein science : a publication of the Protein Society,* 24**,** 1031-1039.

WANG, W., SINGH, S., ZENG, D. L., KING, K. & NEMA, S. 2007. Antibody structure, instability, and formulation. *J Pharm Sci,* 96**,** 1-26.

WANG, W. R., J. C. 2010. *Aggregation of Therapeutic Proteins*, John Wiley and Sons.

WANG, X. J., HAYES, J. D. & WOLF, C. R. 2006. Generation of a stable antioxidant response element-driven reporter gene cell line and its use to show redox-dependent activation of nrf2 by cancer chemotherapeutic agents. *Cancer Res,* 66**,** 10983-94.

WANG, X. Z., HARDING, H. P., ZHANG, Y., JOLICOEUR, E. M., KURODA, M. & RON, D. 1998. Cloning of mammalian Ire1 reveals diversity in the ER stress responses. *The EMBO journal,* 17**,** 5708-5717.

WIJESURIYA, S. D., PONGO, E., TOMIC, M., ZHANG, F., GARCIA-RODRIQUEZ, C., CONRAD, F., FARR-JONES, S., MARKS, J. D. & HORWITZ, A. H. 2018. Antibody engineering to improve manufacturability. *Protein Expression and Purification,* 149**,** 75-83.

WURM, F. M. 2004. Production of recombinant protein therapeutics in cultivated mammalian cells. *Nat Biotechnol,* 22**,** 1393-8.

XU, H., ZHAO, X., GRANT, C., LU, J. R., WILLIAMS, D. E. & PENFOLD, J. 2006. Orientation of a Monoclonal Antibody Adsorbed at the Solid/Solution Interface: A Combined Study Using Atomic Force Microscopy and Neutron Reflectivity. *Langmuir,* 22**,** 6313-6320.

YANG, Y., VELAYUDHAN, A., THORNHILL, N. F. & FARID, S. S. 2017. Multi-criteria manufacturability indices for ranking high-concentration monoclonal antibody formulations. *Biotechnol Bioeng,* 114**,** 2043-2056.

ZHANG, J., WOODS, C., HE, F., HAN, M., TREUHEIT, M. J. & VOLKIN, D. B. 2018. Structural Changes and Aggregation Mechanisms of Two Different Dimers of an IgG2 Monoclonal Antibody. *Biochemistry,* 57**,** 5466-5479.

ZOLLS, S., TANTIPOLPHAN, R., WIGGENHORN, M., WINTER, G., JISKOOT, W., FRIESS, W. & HAWE, A. 2012. Particles in therapeutic protein formulations, Part 1: Overview of analytical methods. *Journal of Pharmaceutical Sciences,* 101**,** 914-935.

Appendix A

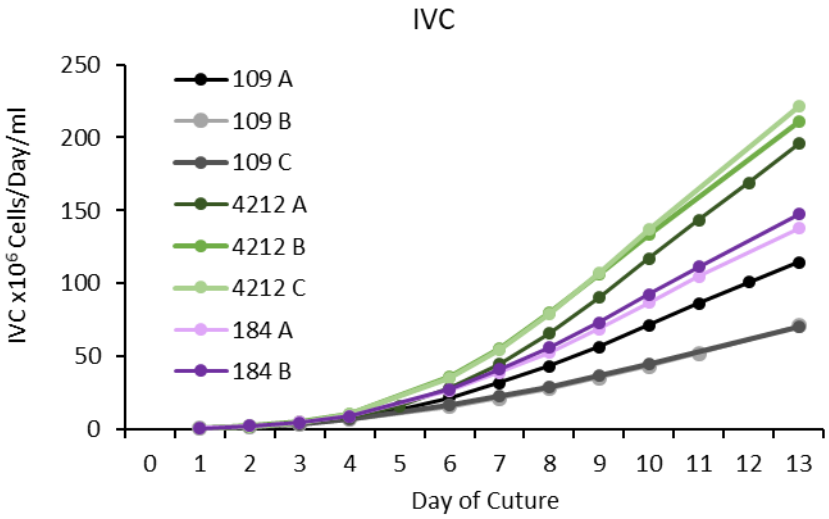

Appendix A.1: Integral viable cell (IVC) densities for all biological replicates of cell line 109, 4212 and 184.

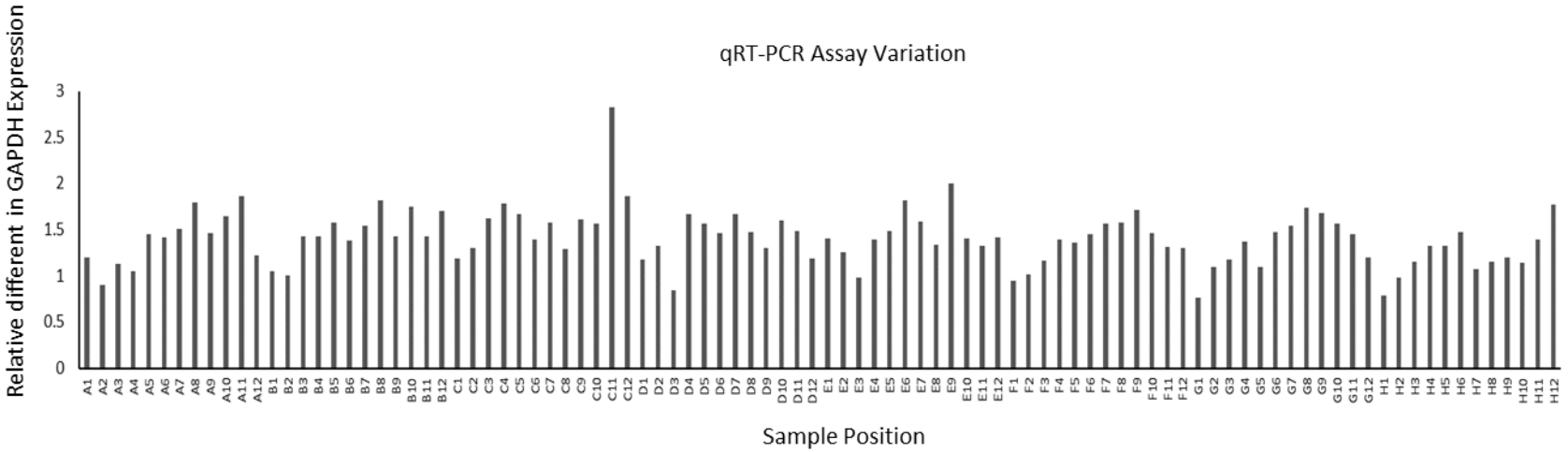

Appendix A.2: qRT-PCR assay variation determined by analysing the fold change in GAPDH expression of a single sample across the entire 96 well plate. All gene expression was made relative to that in well B2, ensuring not to use an outer well as the normaliser as evaporation is known to occur in these positions. A fold change as high as 2.5 is observed, therefore any change in GOI expression below 2.5 is not considered real based on this data.

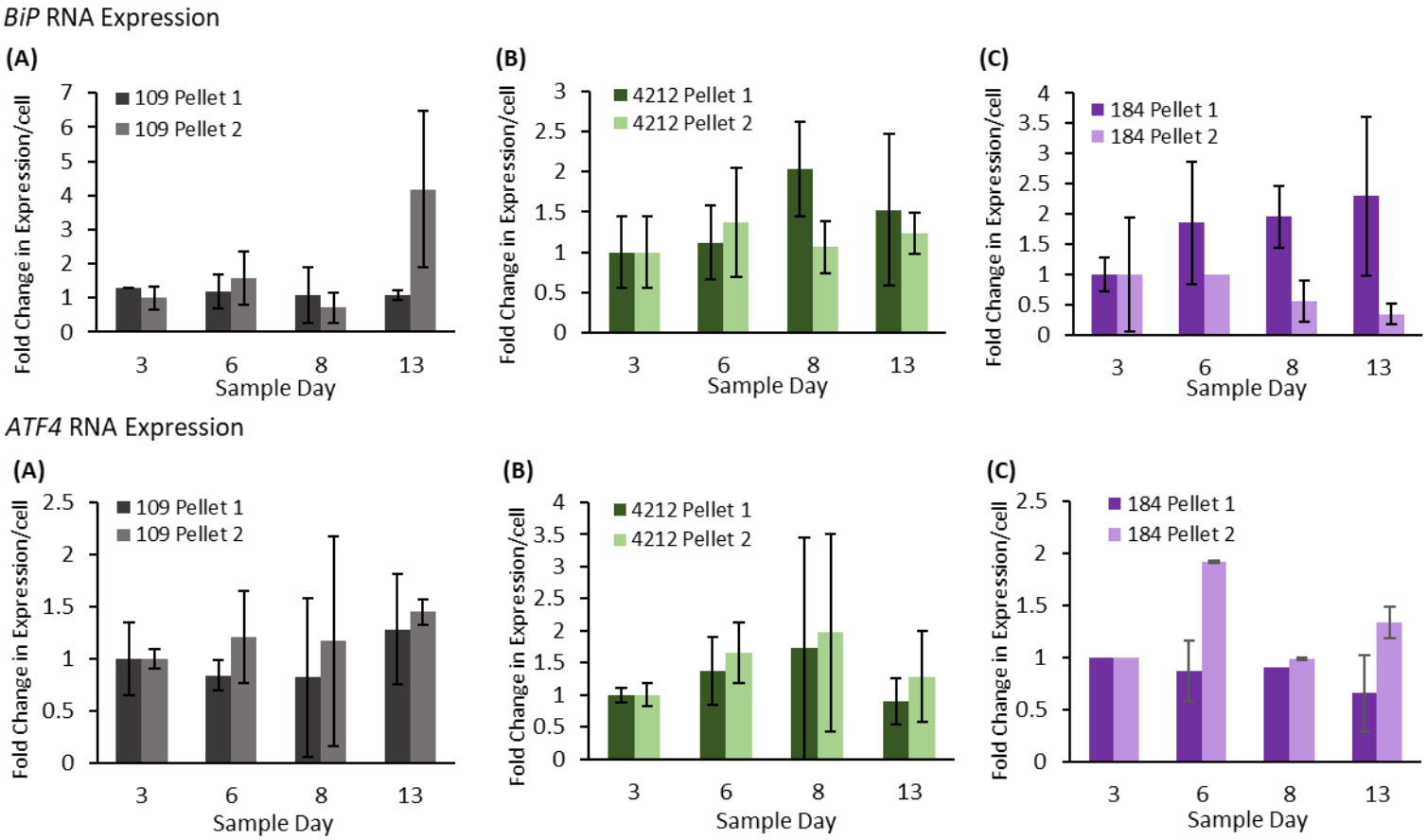

Appendix A.3: Relative fold change of BiP and ATF4 RNA expression for cell lines 109, 4212 and 184 determined by qRT-PCR. Pellet 1 and pellet 2 denote technical replicate RNA samples which were extracted from separate cell pellets collected during culture sampling. Gene expression was relative to that of GAPDH. Fold change was established relative to day 3 of culture. Error bars represent the average relative difference across biological replicates +/- one standard deviation.

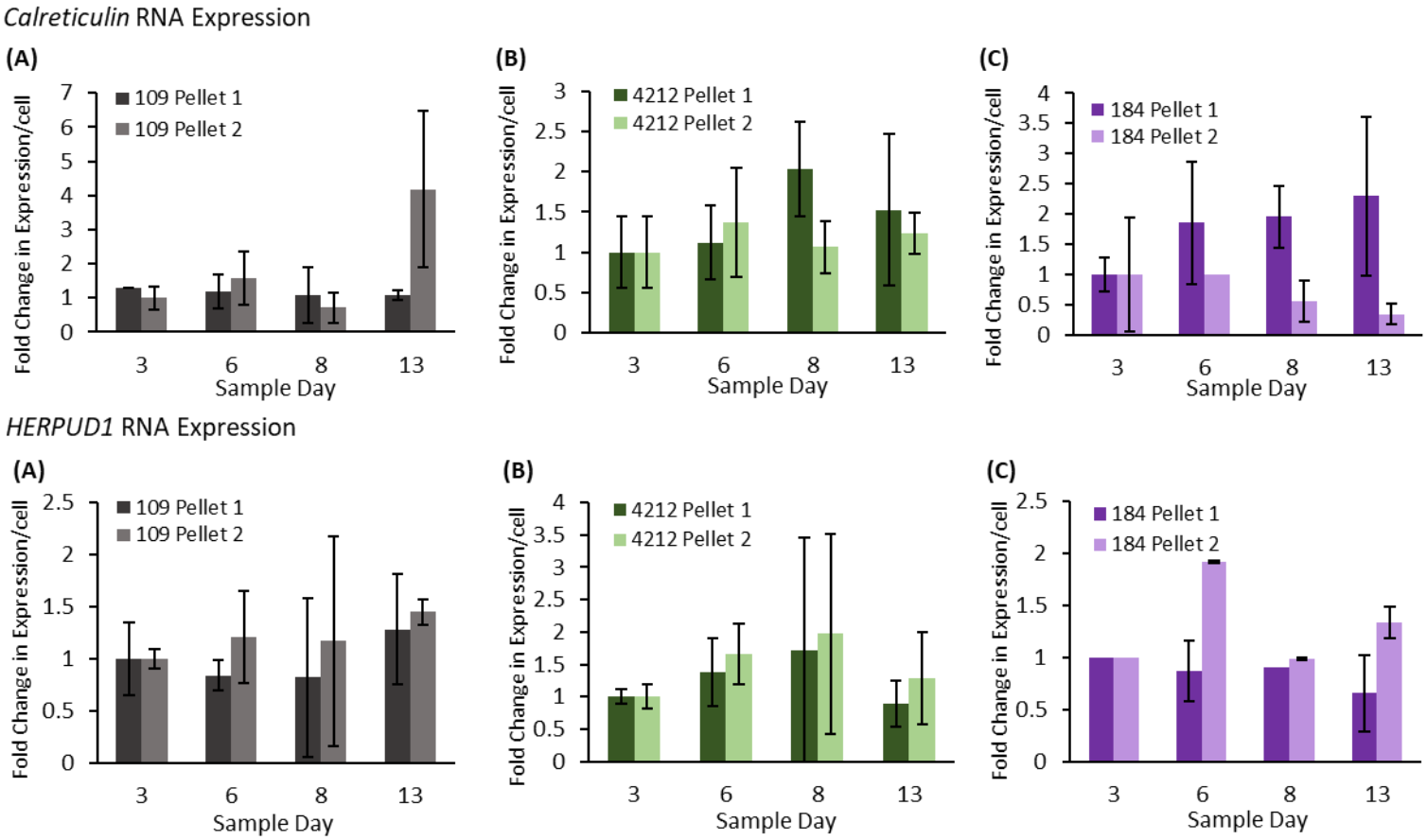

Appendix A.4: Relative fold change of Calreticulin and HERPUD1 RNA expression for cell lines 109, 4212 and 184 determined by qRT-PCR. Pellet 1 and pellet 2 denote technical replicate RNA samples which were extracted from separate cell pellets collected during culture sampling. Gene expression was relative to that of GAPDH. Fold change was established relative to day 3 of culture. Error bars represent the average relative difference across biological replicates +/- one standard deviation.

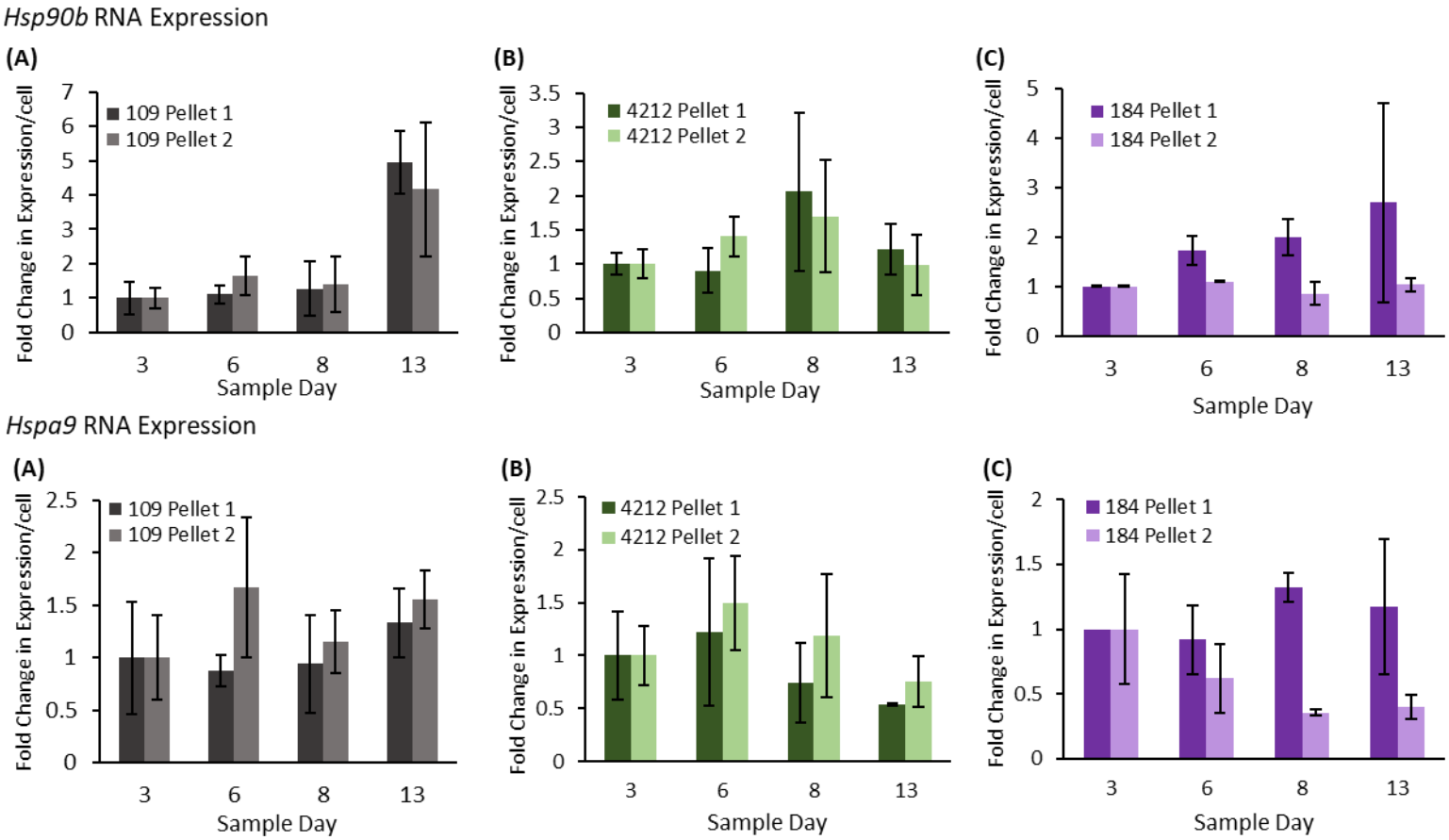

Appendix A.5: Relative fold change of Hsp90b and Hspa9 RNA expression for cell lines 109, 4212 and 184 determined by qRT-PCR. Pellet 1 and pellet 2 denote technical replicate RNA samples which were extracted from separate cell pellets collected during culture sampling. Gene expression was relative to that of GAPDH. Fold change was established relative to day 3 of culture. Error bars represent the average relative difference across biological replicates +/- one standard deviation.

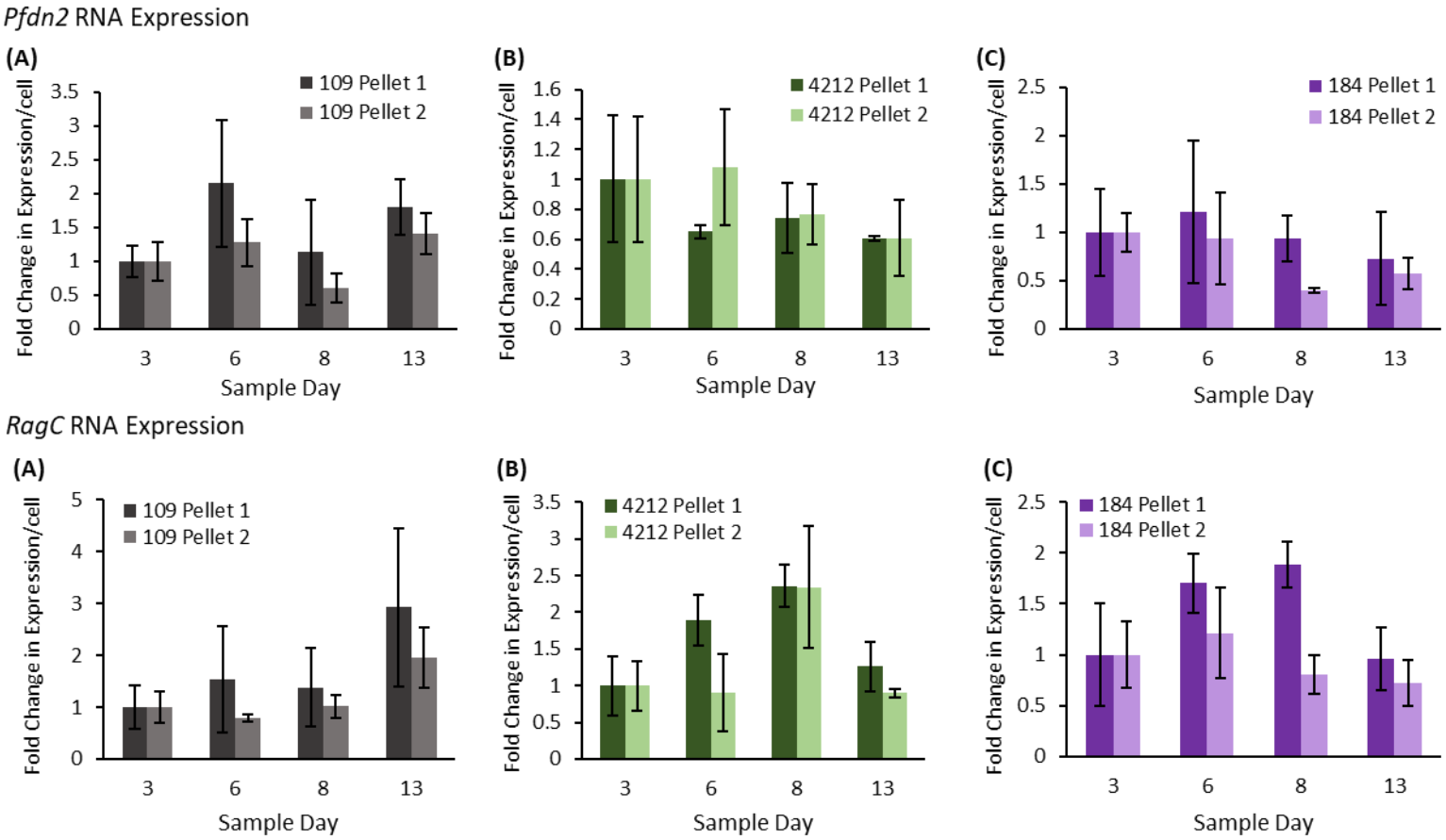

Appendix A.6: Relative fold change of Pfdn2 and RagC RNA expression for cell lines 109, 4212 and 184 determined by qRT-PCR. Pellet 1 and pellet 2 denote technical replicate RNA samples which were extracted from separate cell pellets collected during culture sampling. Gene expression was relative to that of GAPDH. Fold change was established relative to day 3 of culture. Error bars represent the average relative difference across biological replicates +/- one standard deviation.

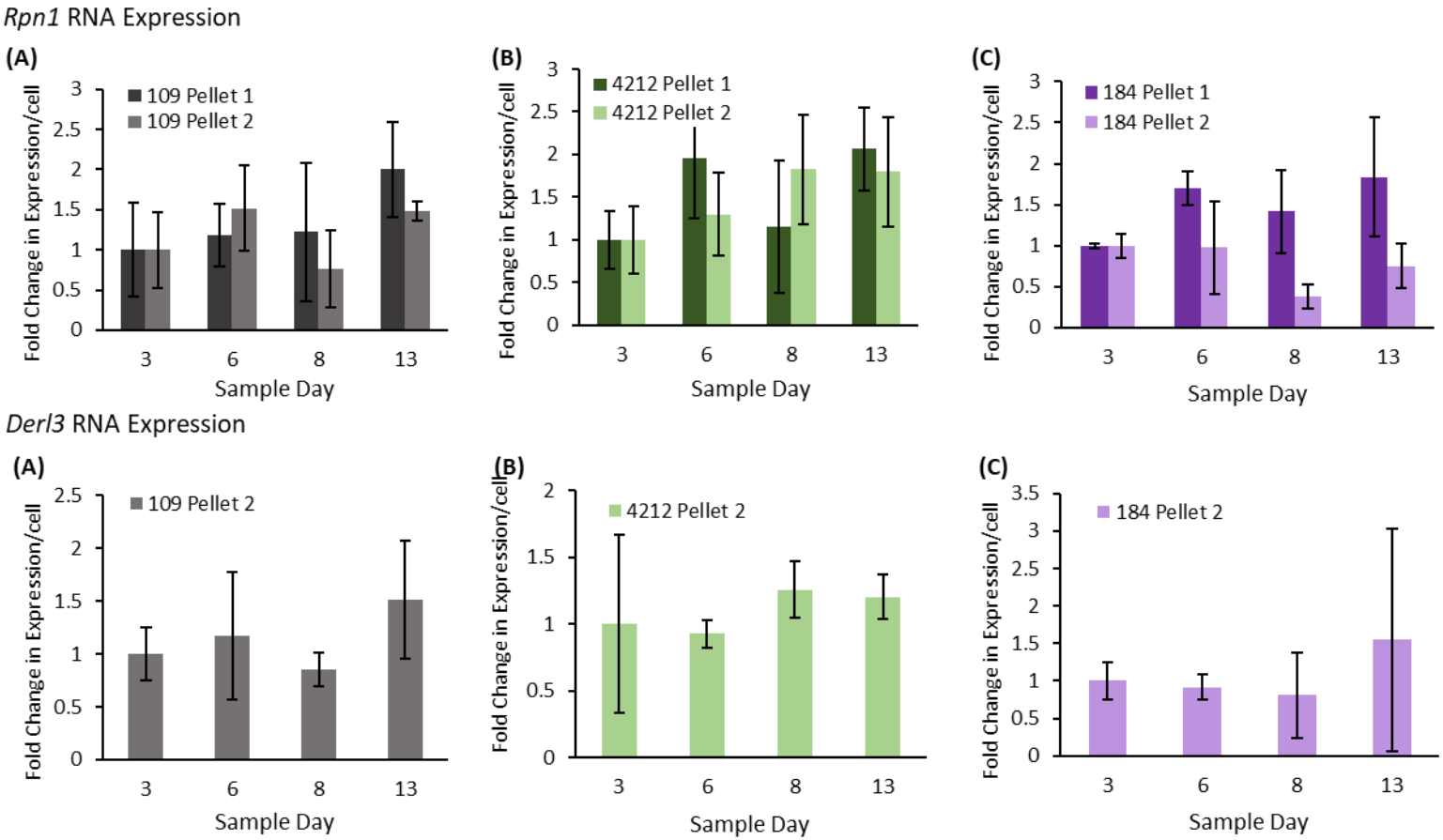

Appendix A.7: Relative fold change of RPn1 and Derl3 RNA expression for cell lines 109, 4212 and 184 determined by qRT-PCR. Pellet 1 and pellet 2 denote technical replicate RNA samples which were extracted from separate cell pellets collected during culture sampling. Gene expression was relative to that of GAPDH. Fold change was established relative to day 3 of culture. Error bars represent the average relative difference across biological replicates +/- one standard deviation. Note that only pellet 2 samples were analysed for Derl3 expression due to limited stocks of the corresponding primer.

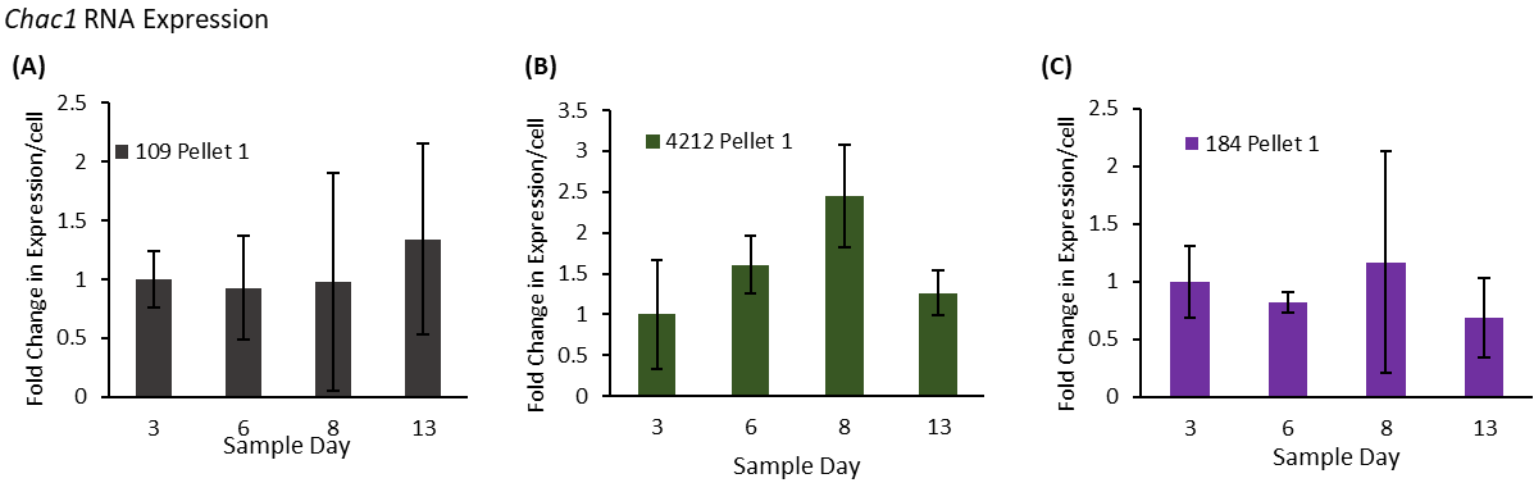

Appendix A.8: Relative fold change of RPn1 and Derl3 RNA expression for cell lines (A) 109, (B) 4212 and (C) 184 determined by qRT-PCR. Pellet 1 and pellet 2 denote technical replicate RNA samples which were extracted from separate pellets collected during culture sampling. Gene expression was relative to that of GAPDH. Fold change was established relative to day 3 of culture. Error bars represent the average relative difference across biological replicates +/- one standard deviation. Note that only pellet 1 samples were analysed for Chac1 expression due to limited stocks of the corresponding primer.

Appendix Table A.1: Opalescence, particle and yellowing scores for mAb 109 samples incubated at 40°C for up to 3 months. Scores were determined by comparing vials to pre-made standards.

A 80mM Arg 120mM Sucrose

Sample	T=0			T=1 mth 40°C			T=3 mth 40°C		
	Opalescence	Particles	Yellow	Opalescence	Particles	Yellow	Opalescence	Particles	Yellow
109A D8	0	0	0	II	2	Y5/Y6	III	2-3	Y4
109A D13	0	0	0	II	3	Y5/Y6	III	3	Y4
109B D8	0	0	0	II	2 to 3	Y5/Y6	III	2-3	Y4
109B D13	0	0	0	II	2 to 3	Y5/Y6	III	3	Y4
109C D8	0	0	0	II	2 to 3	Y5/Y6	III	2-3	Y4
109C D13	0	0	0	II	3 to 4	Y5/Y6	III	3	Y4

B 190mM Arg

Sample	T=0			T=1 mth 40°C			T=3 mth 40°C		
	Opalescence	Particles	Yellow	Opalescence	Particles	Yellow	Opalescence	Particles	Yellow
109A D8	0	0	0	III	2	Y5/Y6	III	2-3	Y4
109A D13	0	0	0	III	3	Y5/Y6	III	3	Y4
109B D8	0	0	0	II	2	Y5/Y6	III	2-3	Y4
109B D13	0	0	0	II	3	Y5/Y6	III	3	Y4
109C D8	0	0	0	II	3	Y5/Y6	III	2-3	Y4
109C D13	0	0	0	II	3	Y5/Y6	III	3	Y4

Appendix Table A.2: Opalescence, particle and yellowing scores for mAb 4212 samples incubated at 40°C for up to 3 months. Scores were determined by comparing vials to pre-made standards. * indicates samples for which visible particles could not be assessed.

A 80mM Arg 120mM Sucrose

Sample	T=0			T=1 mth 40°C			T=3 mth 40°C		
	Opalescence	Particles	Yellow	Opalescence	Particles	Yellow	Opalescence	Particles	Yellow
4212A D8	VI	0	-	VII	2	-	VI	1-2	-
4212A D13	III	0	-	V	2	-	VI	1-2	-
4212B D8	IV	0	-	V	2	-	VI	1-2	-
4212B D13	IV-V	0	-	IV	2	-	V-VI	2-3	-
4212C D8	IV	0	-	V	2	-	V-VI	1-2	-
4212C D13	VI	0	-	IV	3 to 4	-	VII	1-2	-

B 190mM Arg

Sample	T=0			T=1 mth 40°C			T=3 mth 40°C		
	Opalescence	Particles	Yellow	Opalescence	Particles	Yellow	Opalescence	Particles	Yellow
4212A D8	V	0	-	V	3	-	V	3	-
4212A D13	VI	0	-	VI	3	-	VI	1-2	-
4212B D8	VI	0	-	VII	*	-	VI-VII	1-2	-
4212B D13	IV	0	-	V	2	-	VI-VII	1-2	-
4212C D8	IV	0	-	VI	2	-	V	1-2	-
4212C D13	IV	0	-	VI	3	-	V	3	-

Appendix Table A.3: Opalescence, particle and yellowing scores for mAb 184 samples incubated at 40°C for up to 3 months. Scores were determined by comparing vials to pre-made standards. * indicates samples for which visible particles could not be assessed.

A 80mM Arg 120mM Sucrose

Sample	T=0			T=1 mth 40°C			T=3 mth 40°C		
	Opalescence	Particles	Yellow	Opalescence	Particles	Yellow	Opalescence	Particles	Yellow
184A D8	IV	0	>D8	IV	3	Y5	V-VI	4	Y3
184A D13	VI	0		VIII	*	Y4	VIII	*	Y2
184B D8	VI	0		VIII	2 to 3	Y5	VIII	3	Y3
184B D13	VI	0		VII	3	Y4	VIII	*	Y2

B 190mM Arg

Sample	T=0			T=1 mth 40°C			T=3 mth 40°C		
	Opalescence	Particles	Yellow	Opalescence	Particles	Yellow	Opalescence	Particles	Yellow
184A D8	II	0	>D8	IV	2 to 3	Y5	IV-V	4	Y3
184A D13	V	0		VI	3	Y5	VII	*	Y2
184B D8	IV	0		IV	2 to 3	Y4	VI-VII	4	Y3
184B D13	V	0		VI	2 to 3	Y4	VIII	*	Y2

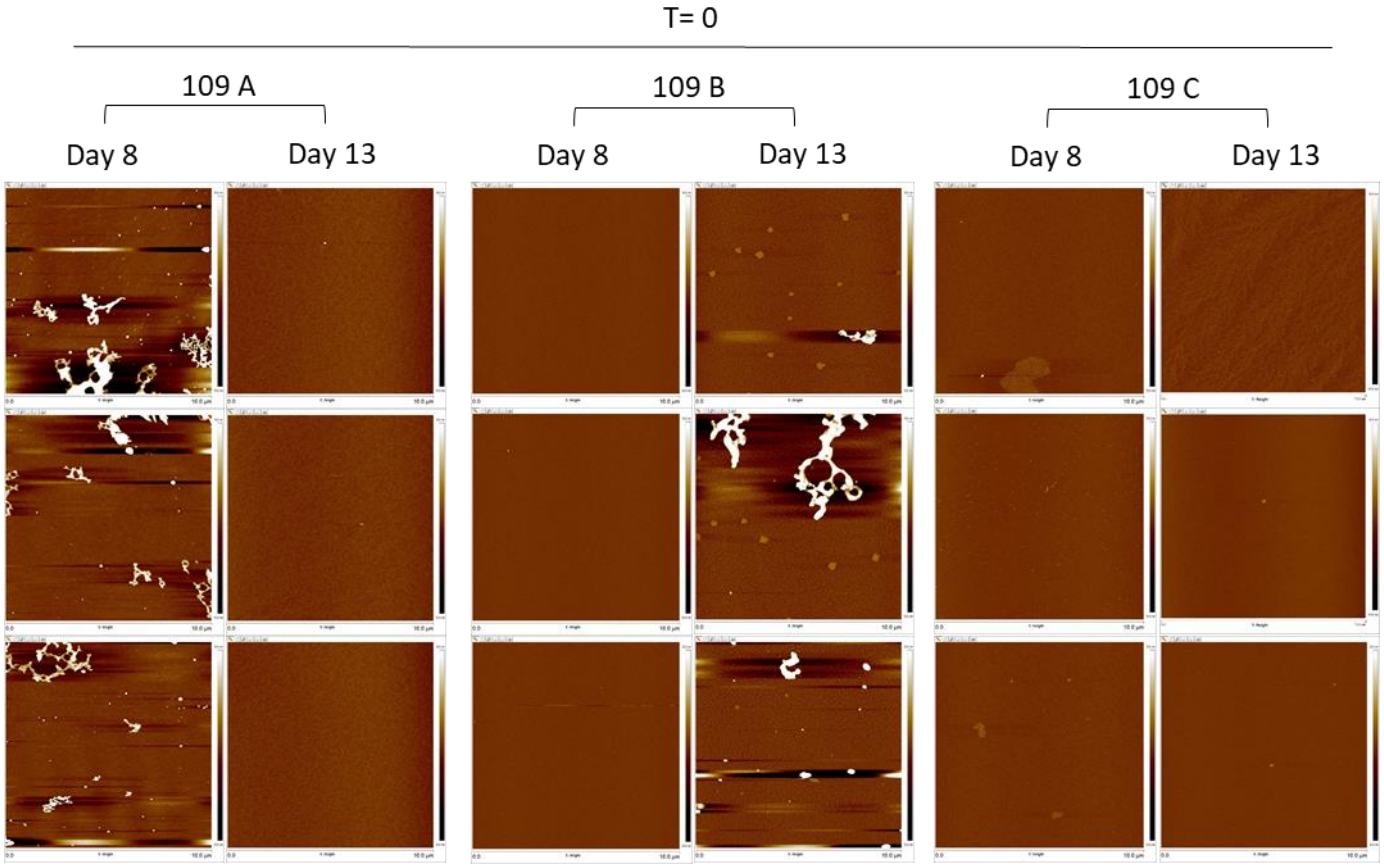

Appendix A.9: AFM analysis of mAb 109 material from samples formulated in 80 mM arginine-HCl, 120 mM sucrose and 20 mM histidine at T=0. 'Leftover' samples from stability studies were diluted with sterile filtered ddH_2O to 0.002 mg/mL to enable imaging.

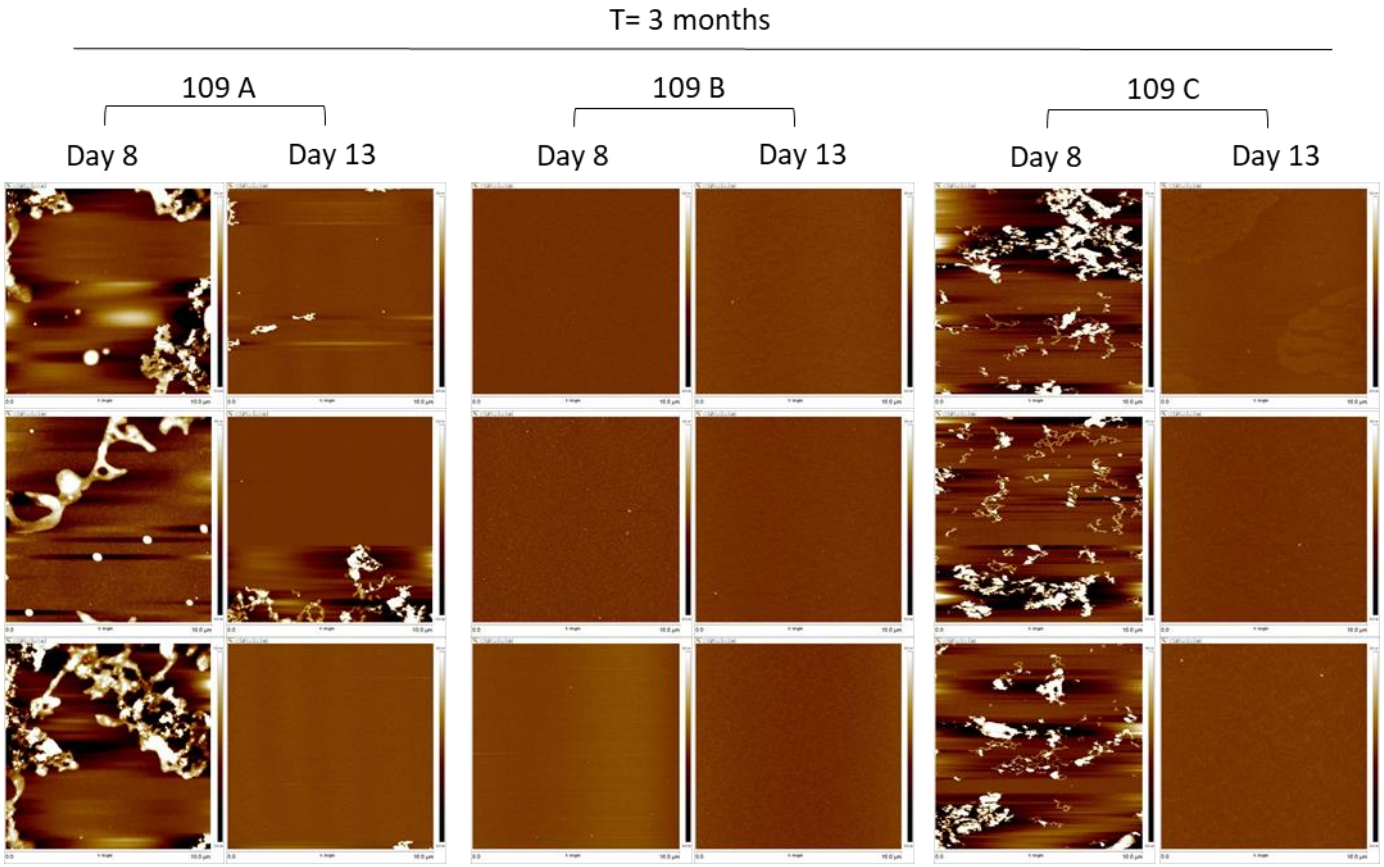

Appendix A.10: AFM analysis of mAb 109 material from samples formulated in 80 mM arginine-HCl, 120 mM sucrose and 20 mM histidine after incubation at 40°C for 3 months. 'Leftover' samples from stability studies were diluted with sterile filtered ddH_2O to 0.002 mg/mL to enable imaging.

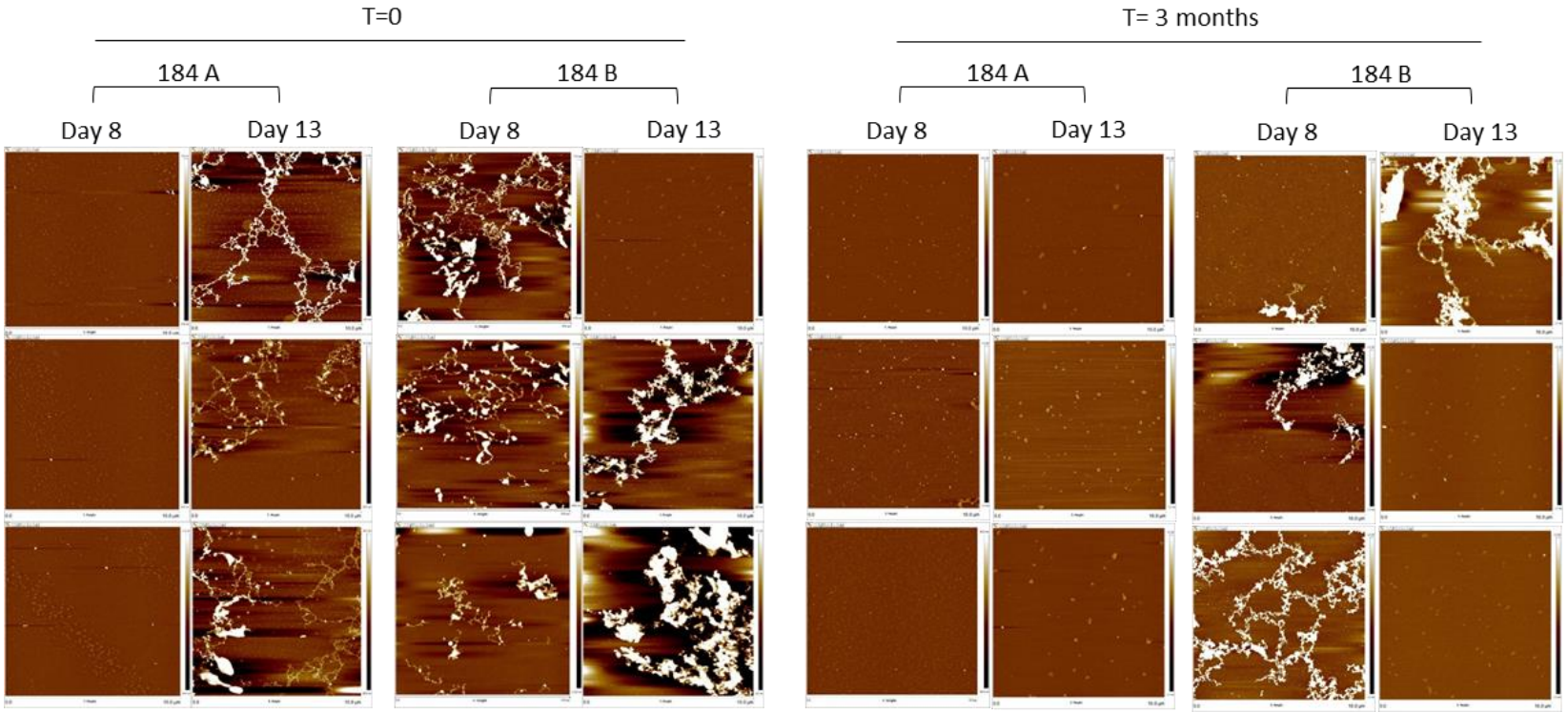

Appendix A.11: AFM analysis of mAb 184 material from samples formulated in 80 mM arginine-HCl, 120 mM sucrose and 20 mM histidine at T=0 and after incubation at 40°C for 3 months. Day 8 'Leftover' samples from stability studies were diluted with sterile filtered ddH_2O to 0.002 mg/mL to enable imaging; dat 13 samples were diluted to 0.0002 mg/mL.

Appendix Table A.4: Concentration, quantity, purity and recovery quantities for mAb material purified from harvests of 10 L disposable bioreactor cultures. % purity was determined using SEC-HPLC where % purity equates to the proportion of the total chromatogram area represented under the monomeric peak for each sample. Eluates were analysed after pH adjustment and filtration.

Sample		Conc (mg/ml)	Total Material (g)	% Purity	% recovery
109 A	Day 8	9.63	2.2	99.7	94
	Day 13	6.34	8.9	97.8	93
109 B	Day 8	9.61	2.2	99.18	93
	Day 13	9.54	8.8	99.01	97
109 C	Day 8	10.07	2.3	99.3	99
	Day 13	9.82	8.7	99	93
4212 A	Day 8	7.62	5.3	99.2	83
	Day 13	8.41	17.7	99.5	85
4212 B	Day 8	14.39	3.8	98.9	93
	Day 13	9.66	6.4	99.1	86
4212 C	Day 8	12.92	3.1	98.5	88
	Day 13	9.34	13.3	98.9	87
184 A	Day 8	6.87	4.2	98.3	83
	Day 13	10.95	16.1	96.19	84
184 B	Day 8	6.73	4.1	98.3	86
	Day 13	12.03	15.8	96.36	76

Appendix B

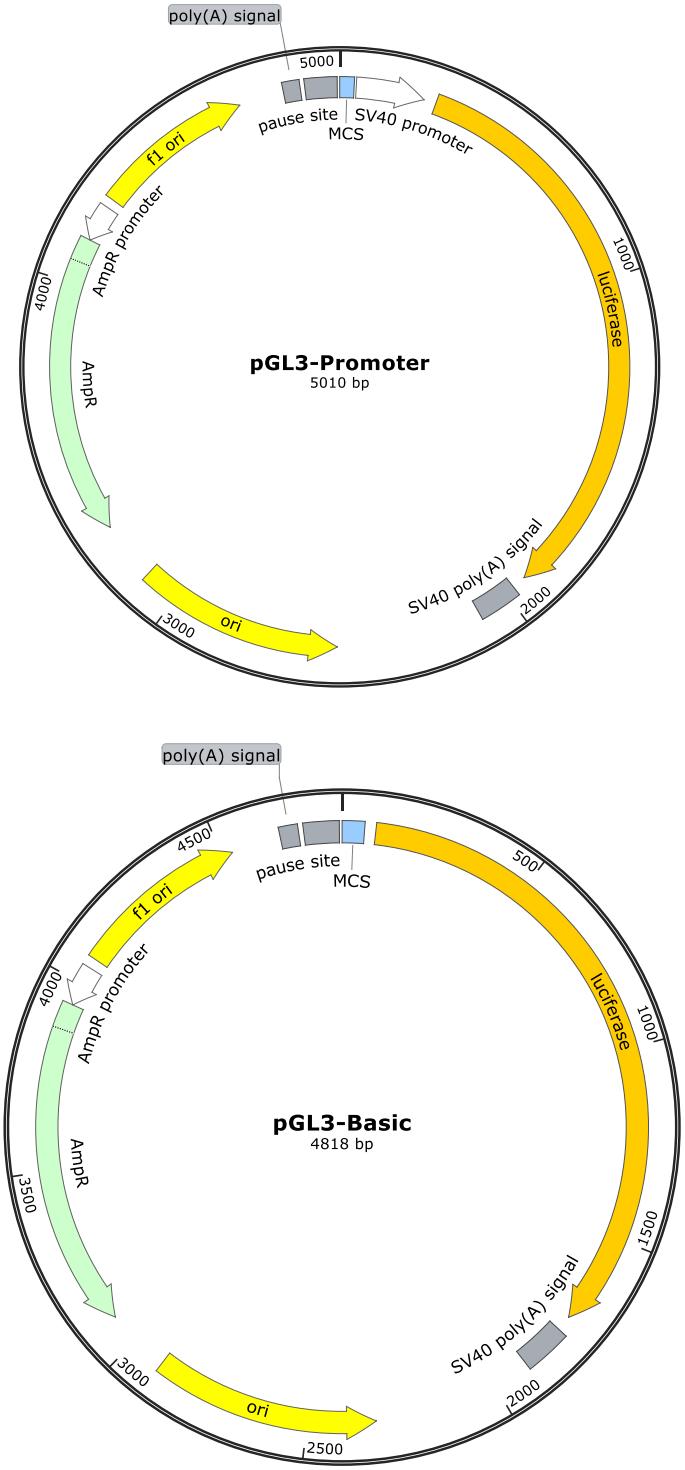

Figure B.1: PGL3P and PGL3 basic vector maps.

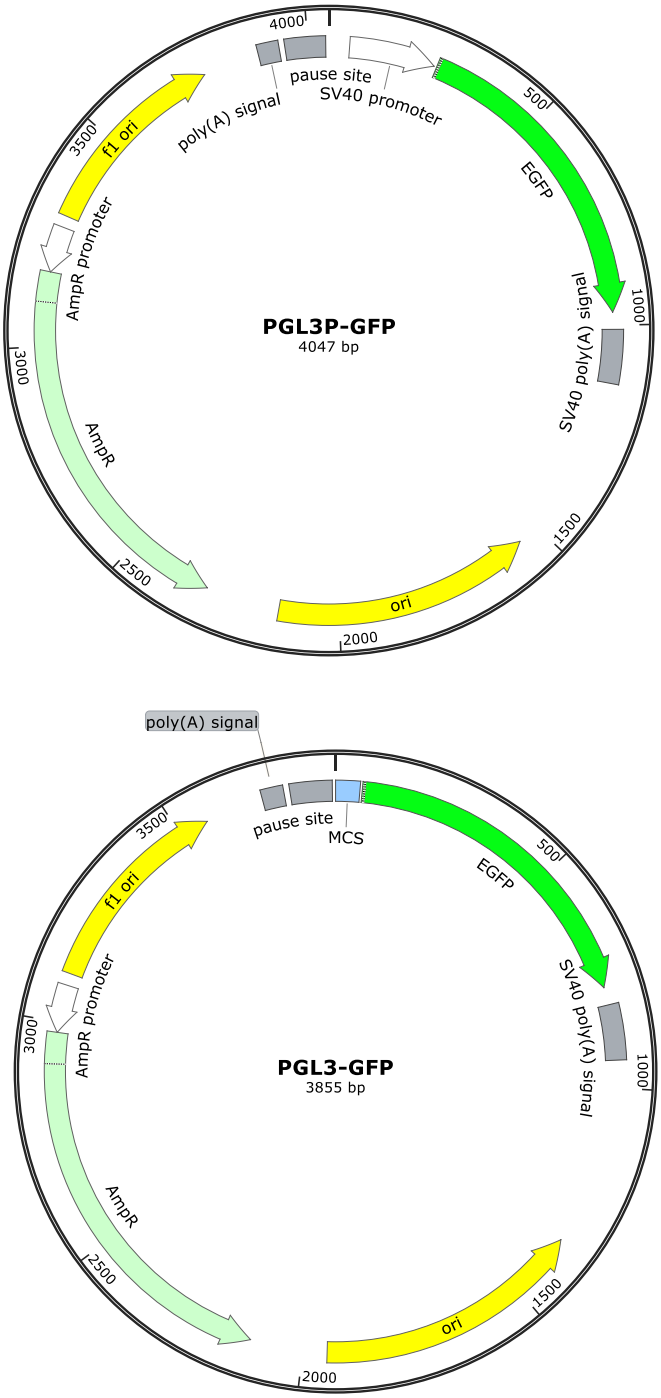

Figure B.2: PGL3P-GFP and PGL3-GFP vector maps.

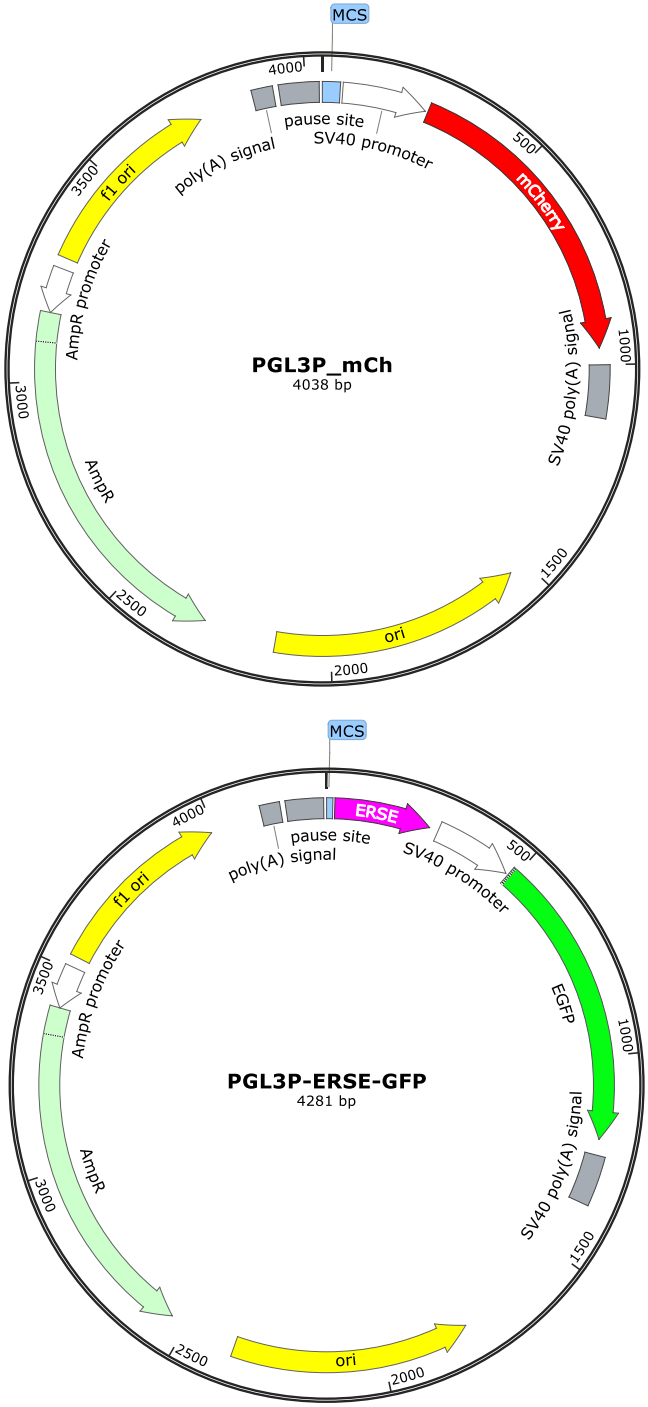

Figure B.3: PGL3P-mCh and PGL3-ERSE-GFP vector maps.

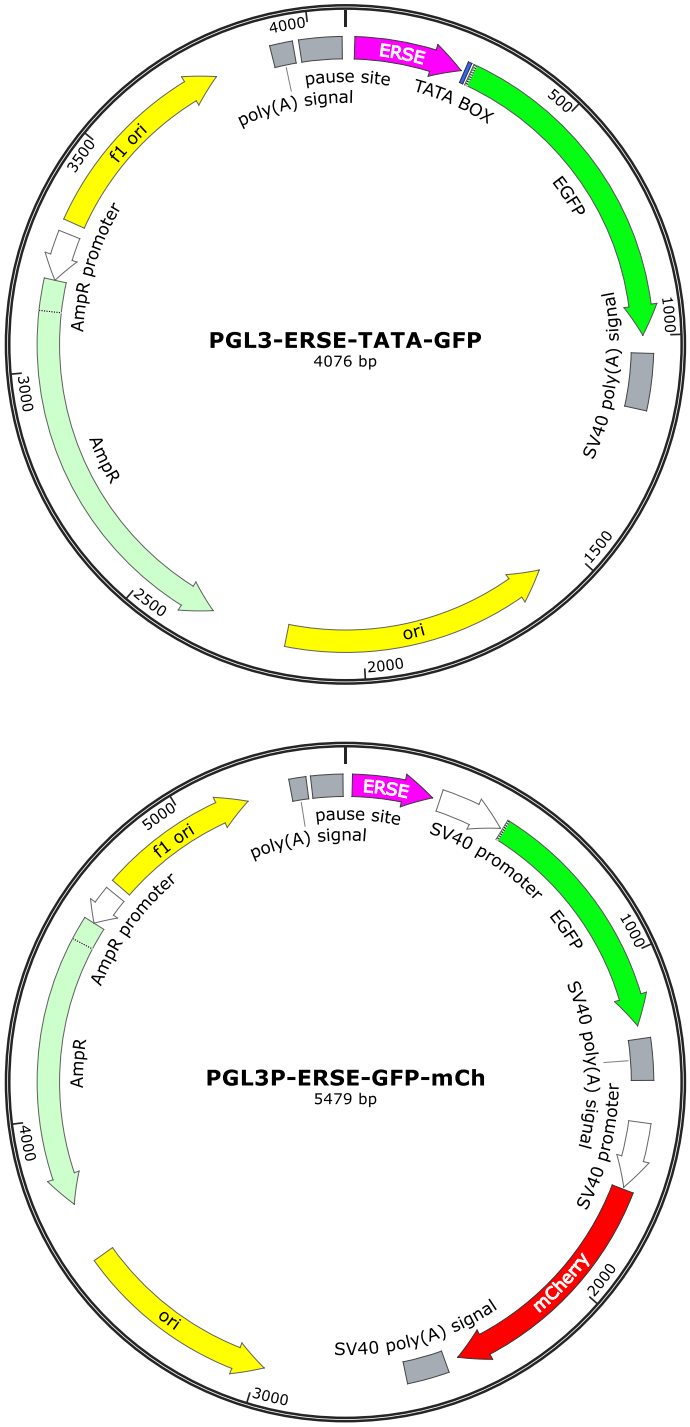

Figure B.4: PGL3-ERSE-TATA-GFP and PGL3P-ERSE-GFP-mCh vector maps.

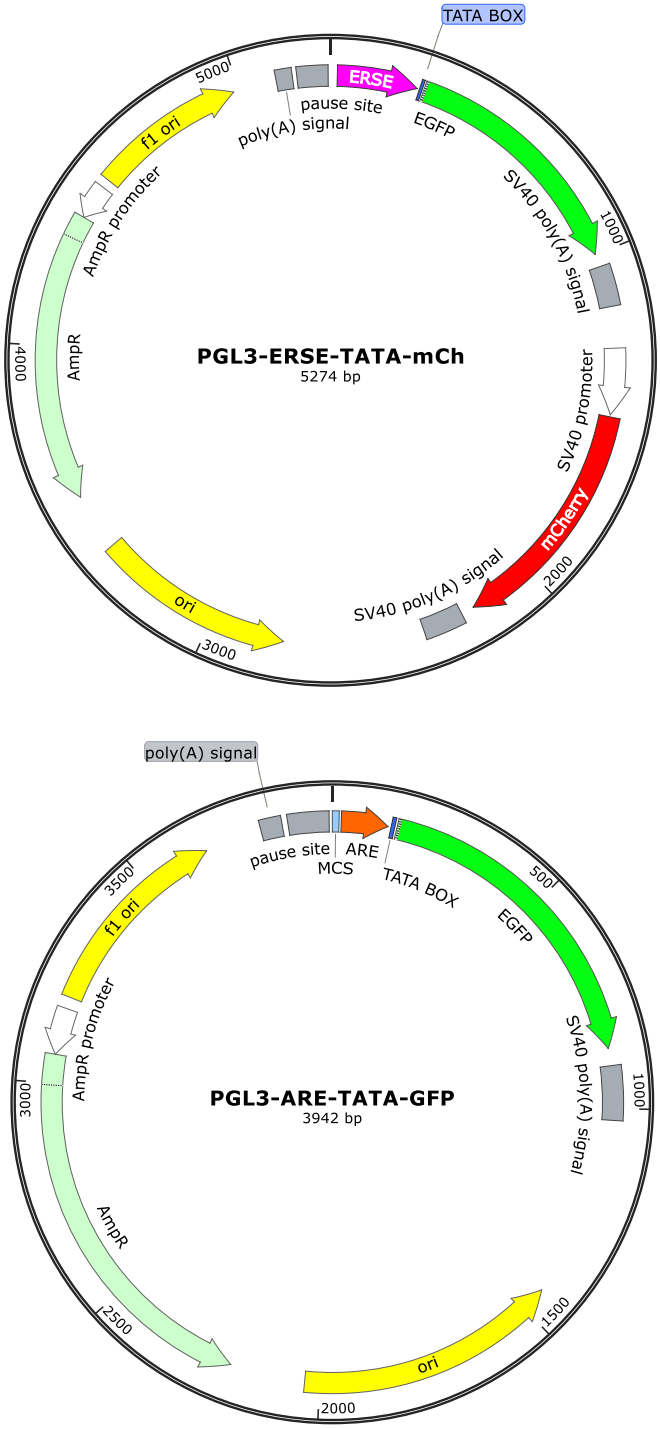

Figure B.5: PGL3-ERSE-TATA-mCh and PGL3-ARE-TATA-GFP vector maps.

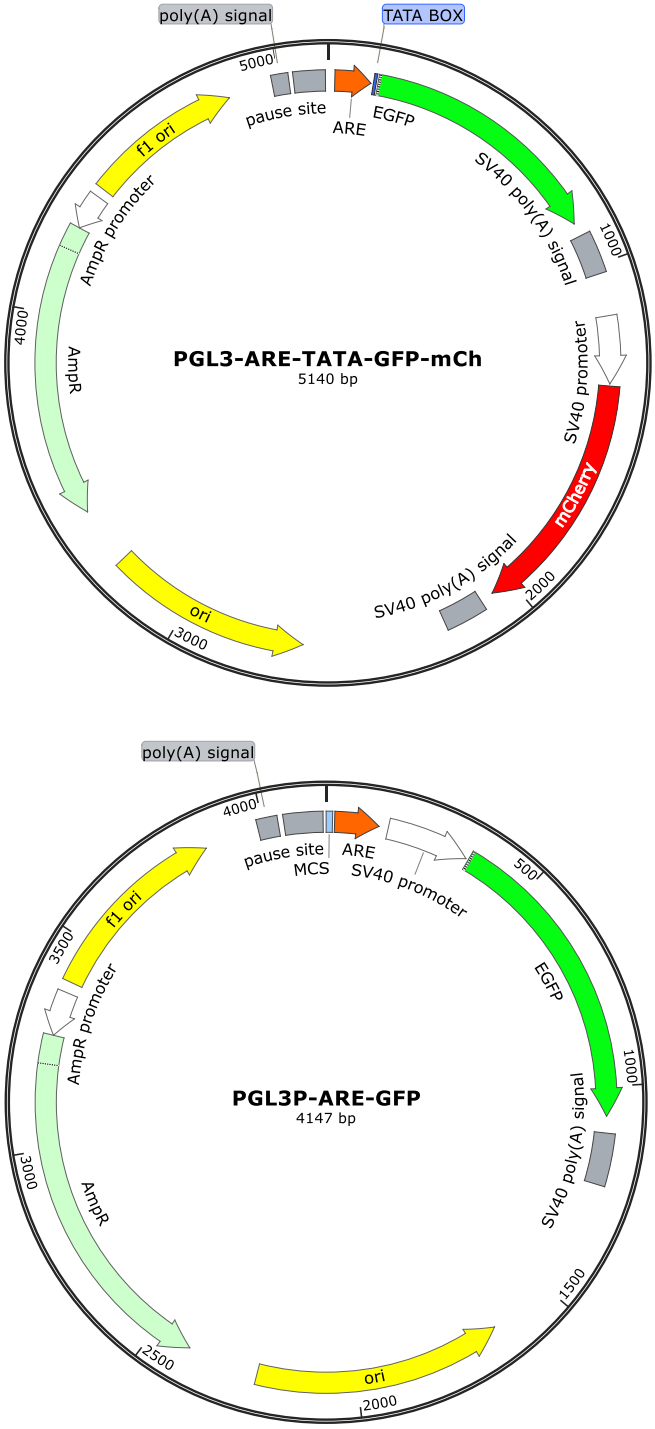

Figure B.6: PGL3-ARE-TATA-GFP-mCh and PGL3P-ARE-GFP vector maps.

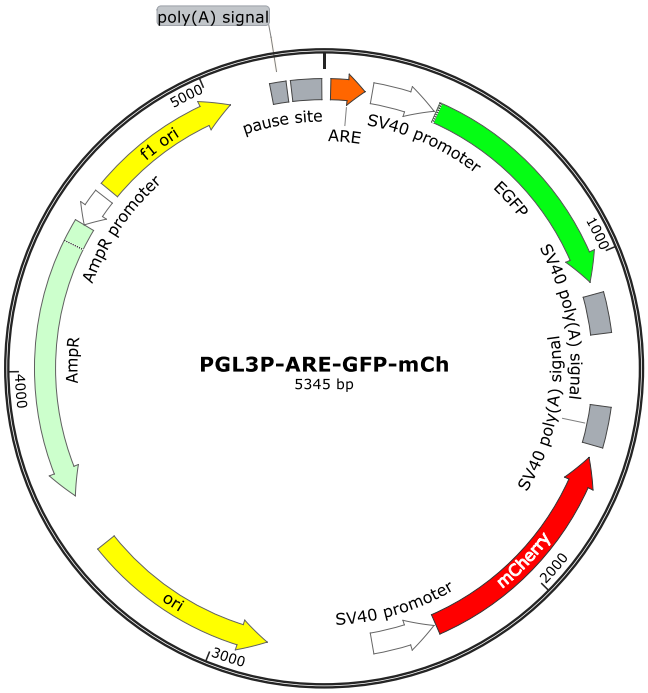

Figure B.7: PGL3P-ARE-GFP-mCh vector map.

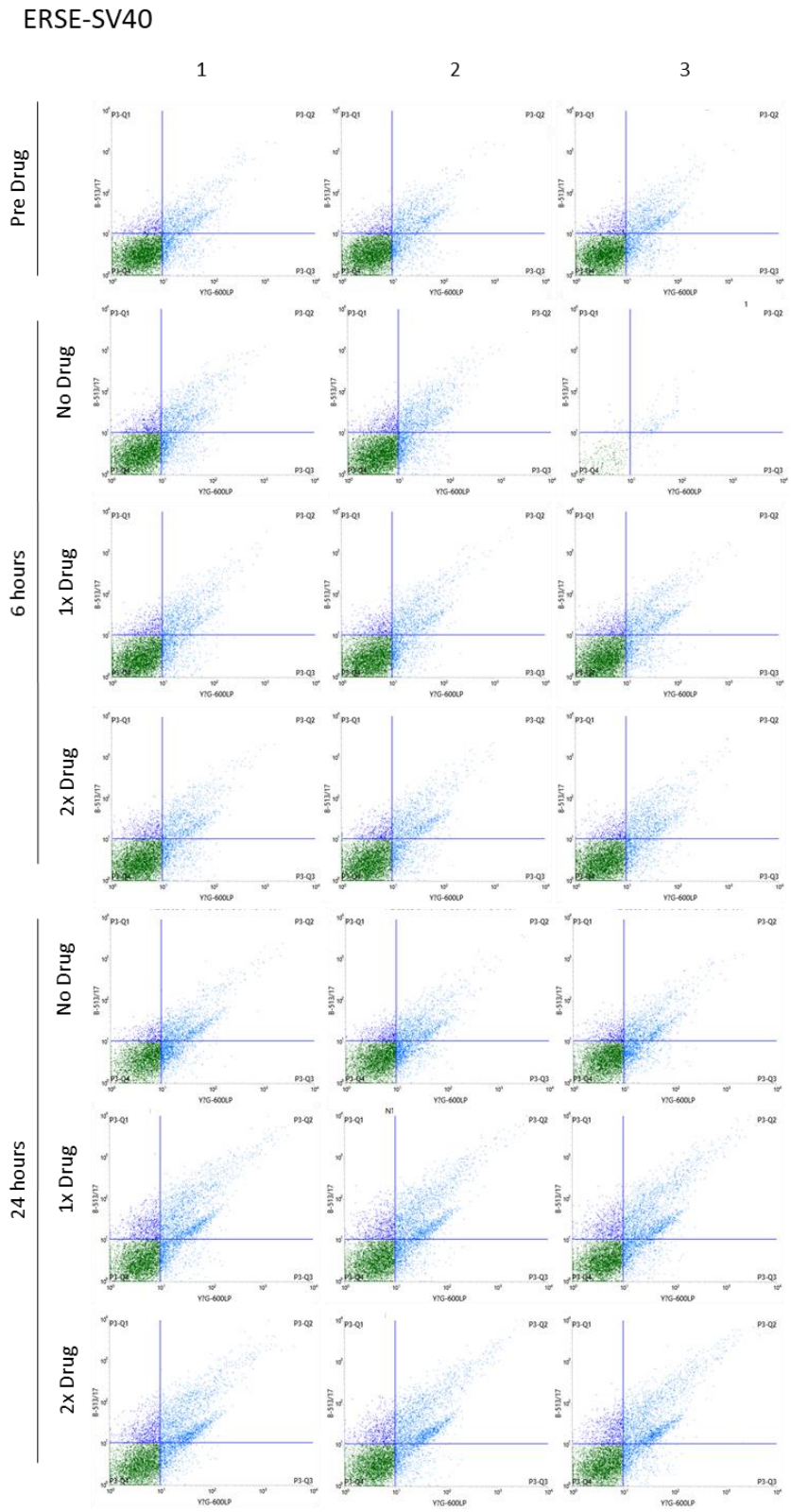

Appendix B.8: Scatter Graphs from Flow Cytometry Data Showing GFP and mCherry Flourescence of CHO-S Cells Transiently Transfected with ERSE-SV40. X axis shows mCherry expression, and Y axis shows GFP expression. Corresponding histograms in Chapter 5, Figure 6.8.

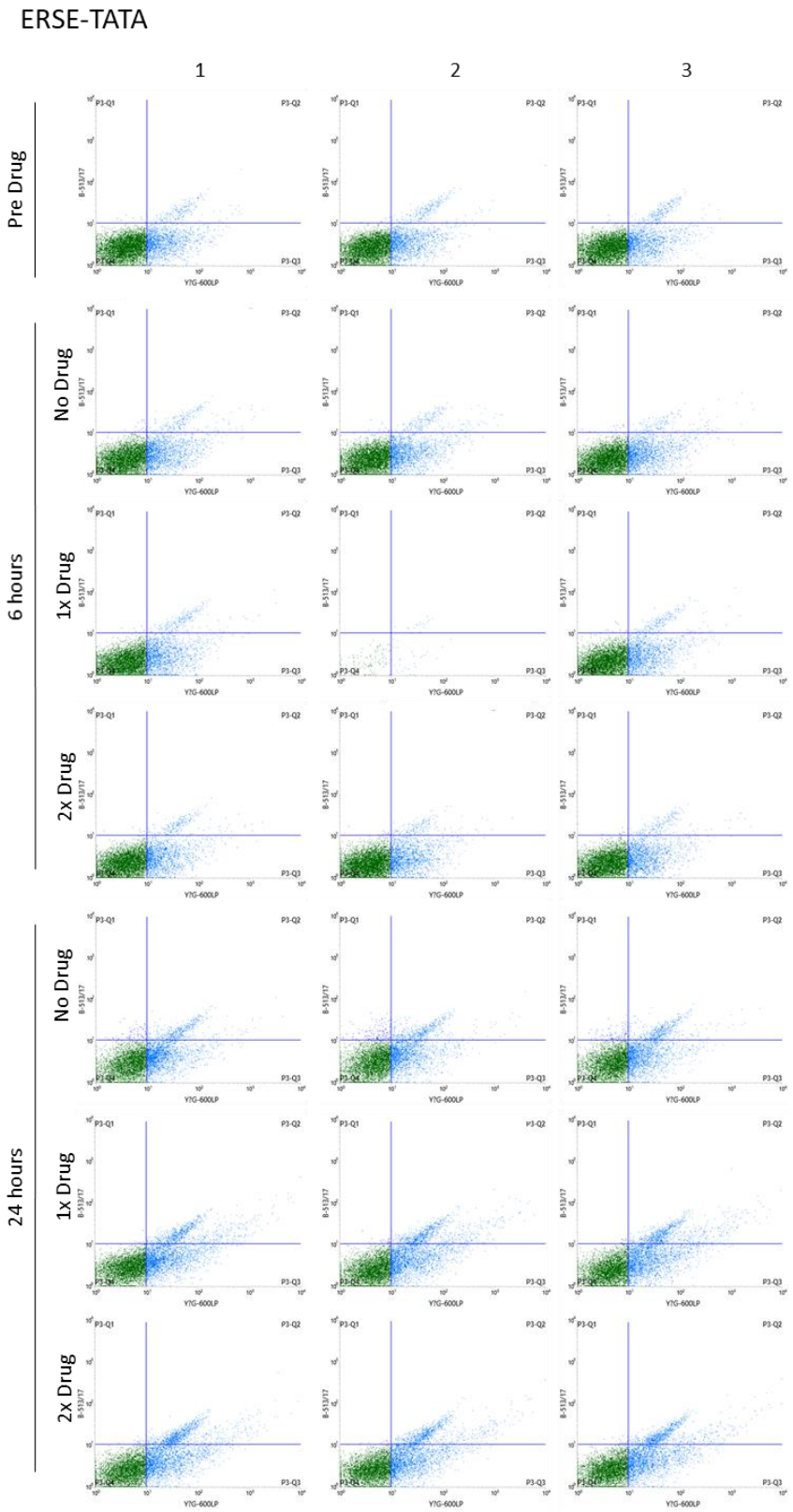

Appendix B.9: Scatter Graphs from Flow Cytometry Data Showing GFP and mCherry Flourescence of CHO-S Cells Transiently Transfected with ERSE-TATA. X axis shows mCherry expression, and Y axis shows GFP expression. Corresponding histograms in Chapter 5, Figure 6.9.

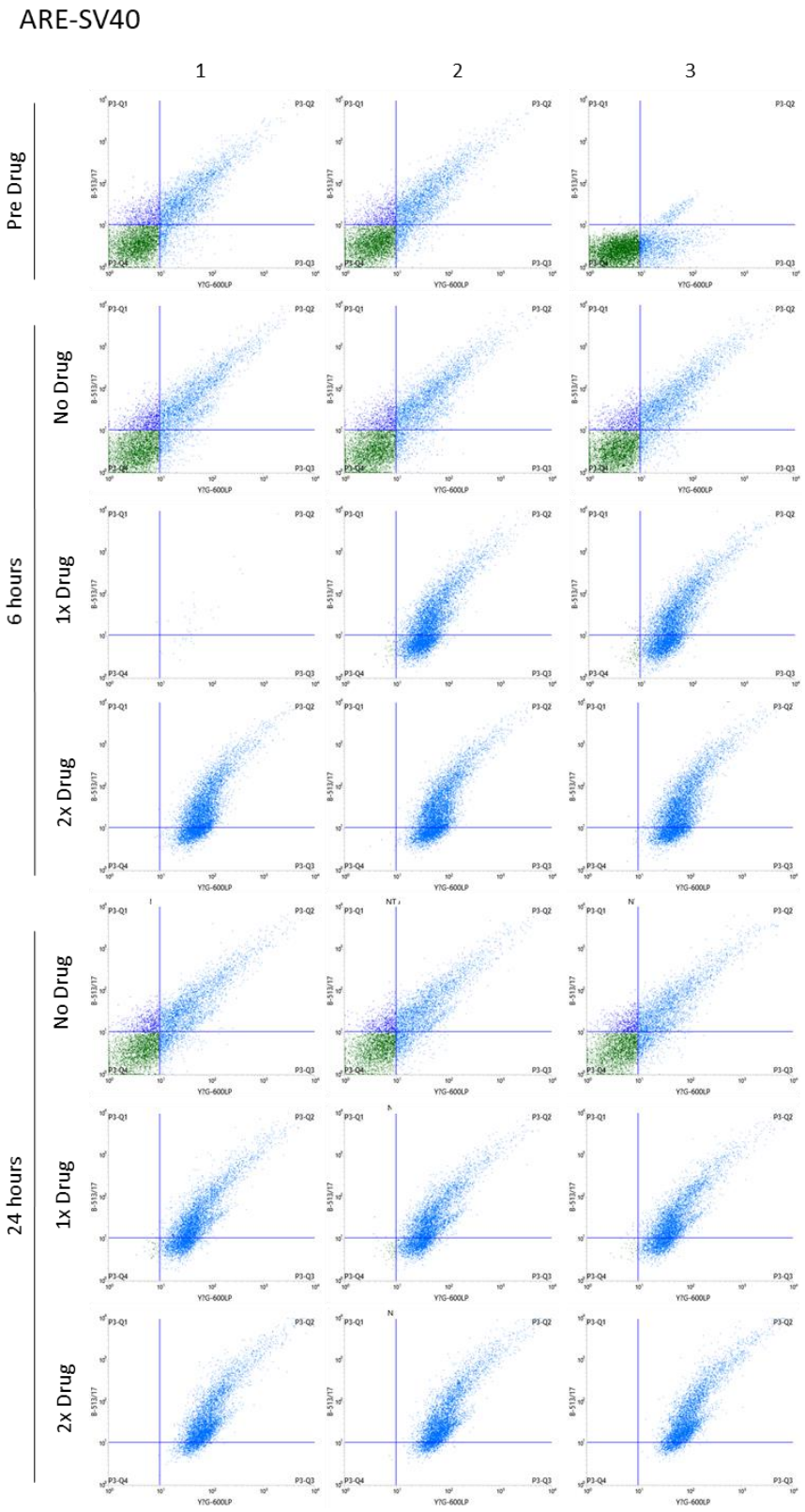

Appendix B.10: Scatter Graphs from Flow Cytometry Data Showing GFP and mCherry Flourescence of CHO-S Cells Transiently Transfected with ARE-SV40. X axis shows mCherry expression, and Y axis shows GFP expression. Corresponding histograms in Chapter 5, Figure 6.10.

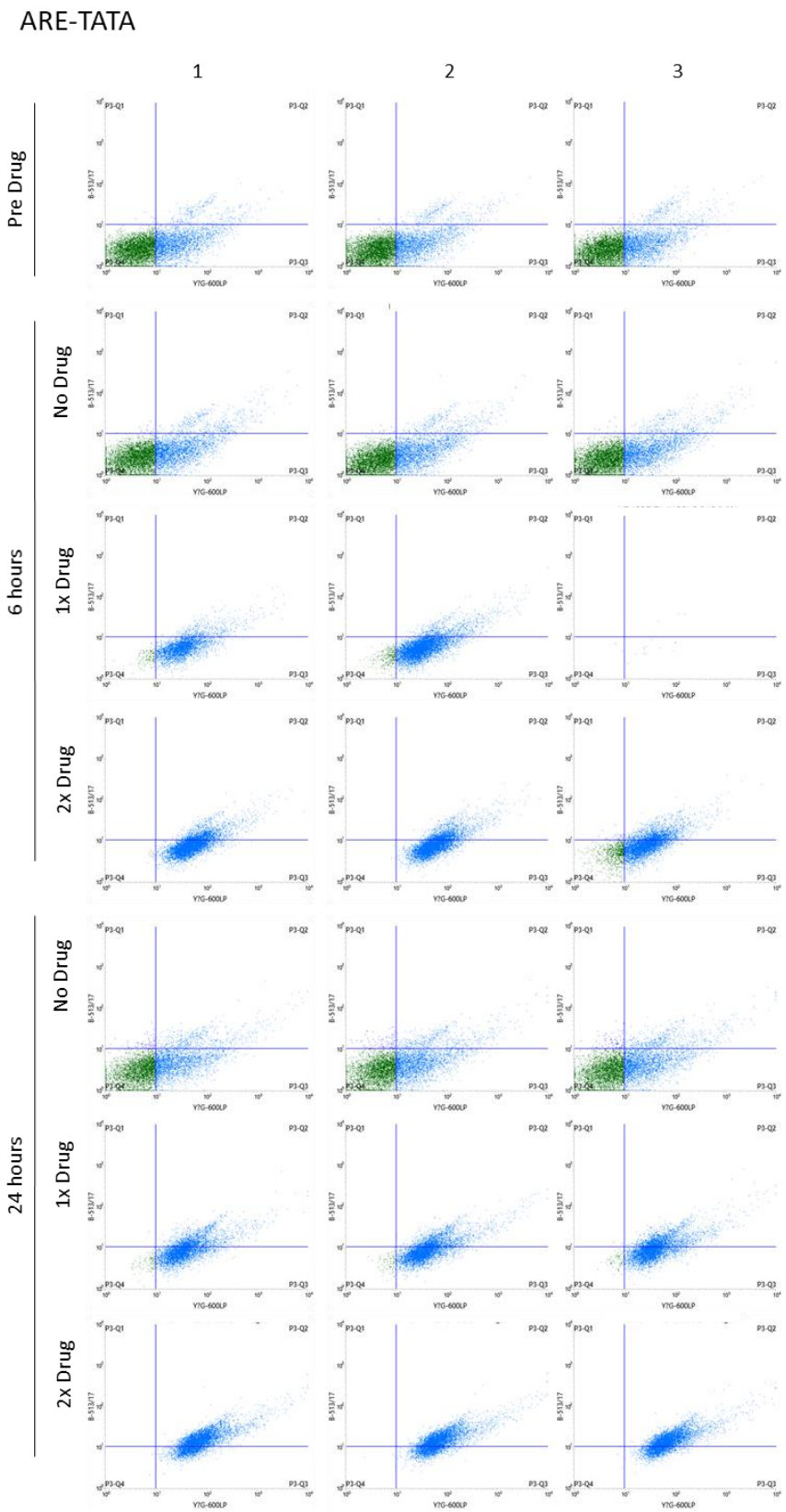

Appendix B.11: Scatter Graphs from Flow Cytometry Data Showing GFP and mCherry Flourescence of CHO-S Cells Transiently Transfected with ARE-TATA. X axis shows mCherry expression, and Y axis shows GFP expression. Corresponding histograms in Chapter 5, Figure 6.11.

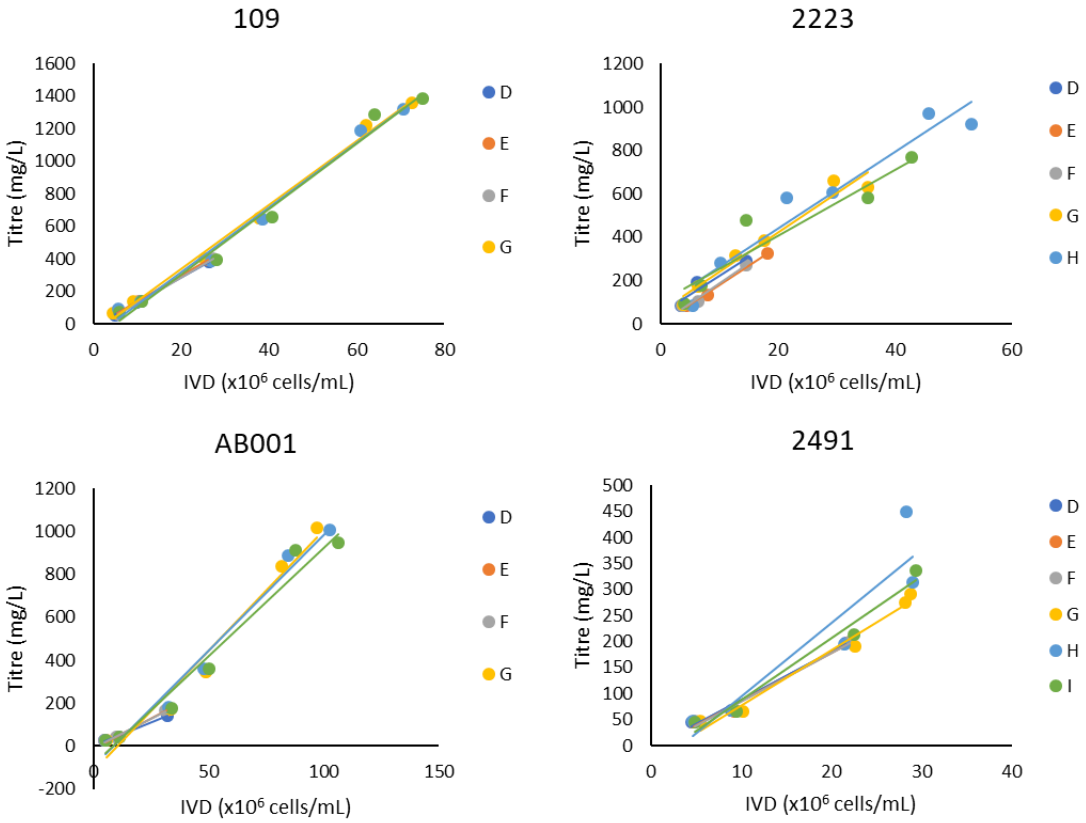

Appendix B.12: Scatter Plots of Culture IVCD Against Titre for Cell Lines 109, AB001, 2223 and 2491. Plots were used to calculate specific productivities (Qp), where the equations for each line of best fit can be seen in Appendix Table B.1

Table B.1: Equations of the Line of Best Fit for Plots of Titre Against IVCD Used to Establish Specific Productivity.

Cell Line	Time Period	Culture	Equation
109	Days 0-6	D	y = 4.2513x + 2.2181
		E	y = 5.5326x - 10.345
		F	y = 5.4735x - 7.6468
	Days 0 -11	G	y = 11.241x - 116.25
		H	y = 10.825x - 95.782
		I	y = 10.11x - 86.644
AB001	Days 0-6	D	y = 15.212x - 20.88
		E	y = 15.731x - 17.031
		F	y = 15.787x - 31.482
	Days 0 -11	G	y = 19.624x - 53.801
		H	y = 19.822x - 78.113
		I	y = 20.112x - 97.943
2223	Days 0-6	D	y = 16.801x + 53.149
		E	y = 17.709x + 1.3382
		F	y = 17.978x + 6.4265
	Days 0 -11	G	y = 18.19x + 56.177
		H	y = 17.619x + 88.158
		I	y = 15.286x + 100.98
2491	Days 0-6	D	y = 9.2335x - 4.5232
		E	y = 9.2139x - 7.4656
		F	y = 9.2228x - 7.3982
	Days 0 -11	G	y = 10.59x - 27.915
		H	y = 14.133x - 47.07
		I	y = 11.861x - 31.559